7th Enigma Meeting
8-10 May 2006, Hydra, Greece

Final Program

As during the last meeting, we have tried to arrange talks on similar topics in a group which is followed by a discussion for the entire topic immediately after the talks. These sessions are highlighted by a shaded box.

Monday, 8th May

time	activity
9:00 - 9:15	Welcome, Announcements
9:15 - 10:30	Session 1 Jose Gracia (Athens): 20+5 min, Synchrotron emission from simple MHD jet configurations Andreas Papageorgiou (Cork): 20+5 min, Helical magnetic fields in jets: a simple statistical model Vladislavs Bezrukovs (Cork): 20+5 min, Analysis of the multi-wavelength polarization VLBI observations of BL Lac objects
10:30-11:00	coffee break
11:00-13:00	Session 1, continued Nadia Kudryavtseva (Bonn): 20+5 min, A rotating jet in 1803+784? Ivan Agudo (Bonn): 30+5 min, Polarimetric radio and mm observational studies of blazars Discussion: 35 min, "Radio maps"
13:00 - 14:30	lunch break
14:30 - 16:00	Young researcher training session Kanaris Tsinganos (Athens): 30 min, Lecture: Enigma and the Sphinx Stavros Dimitrakoudis (Athens): 30 min, Lecture: The Sphinx in ancient civilizations Team leader session

Tuesday, 9th May

time	activity
9:00 - 10:45	Session 5 Stefano Ciprini (Tuorla/Torino): 20+5 min, OJ 287: XMM-Newton & WEBT Campaign Jochen Heidt (Heidelberg): 20+5 min, The OJ 287 polarization monitoring programme on Calar Alto - an update Lars Fuhrmann (Torino): 20+5 min, The large broad band campaign on OJ 287: First results in terms of short-term variability Discussion: 30 min, "OJ 287"
10:45-11:15	coffee break
11:15-13:00	Session 2 Dimitrios Emmanoulopoulos (Heidelberg): 20+5 min, Multi-wavelength observations of PKS2155-304 during 2004 Uwe Bach (Torino): 20+5 min, Multi-frequency monitoring of gamma-ray blazars Discussion 45 min, The extended 0716 campaign
13:00 - 15:00	lunch break
15:00 - 16:30	Session 3 Stefan Wagner (Heidelberg): 20+5 min, Gamma-ray properties of XBLs Lukasz Stawarz (Heidelberg): 20+5 min, High-energy gamma-ray emission in M87 Discussion 20 min, High-energy emission from AGNs Discussion session 30 min, "Post-ENIGMA activities"
16:30 -17:00	coffee break
17:00 - 18:30	Session 4 Gabriele Ghisellini (Merate): 20+5 min, Bulk Comptonization spectra in powerful blazars Krzysztof Katarzynski (Merate): 20+5 min, The synchrotron boiler and the high-energy emission of

	the low-energy peak BL Lac objects Lukasz Stawarz (Heidelberg): 20+5 min, High-energy gamma-ray emission in Centaurus A radio galaxy Discussion 15 min, Radiation processes

Wednesday, 10th May

time	activity
9:00 - 10:45	Session 6 Kari Nilsson (Tuorla): 15+5 min, Host galaxies and aperture photometry of AGN Marcus Hauser (Heidelberg): 15+5 min, Automatic Telescope for Optical Monitoring (ATOM) - a status report Discussion: 15 min, "Robotic telescopes, fast photometry, etc" Final discussion and conclusions
10:45 -11:15	coffee break
11:15 - 13:15	Young researcher training session Presentation skills
13:30 - late evening	Excursion to Mycenae and Nafplio with conference dinner

Last modified: 12 May 2006

Synthetic synchrotron emission maps from simple MHD jet configurations

José Gracia, IASA Athens
Nektarios Vlahakis, IASA Athens
Kanaris Tsinganos, IASA Athens

7th Enigma Meeting, 8-10 May 2006, Ydra

Outline

How does our MHD model for M87 "look like"?

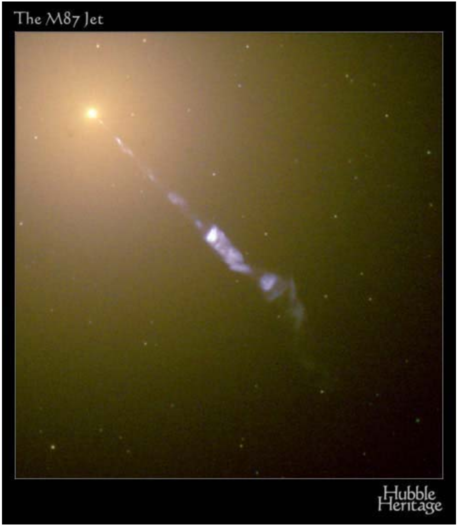

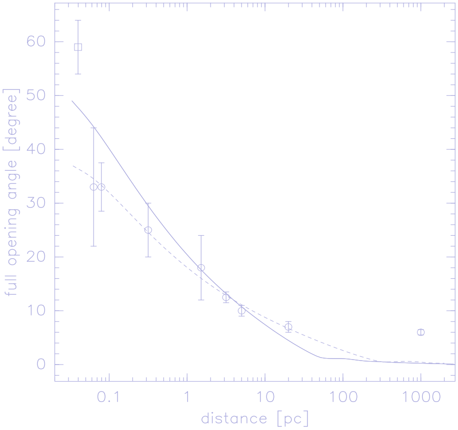

Gracia et al (2005)

How to define the jet width?

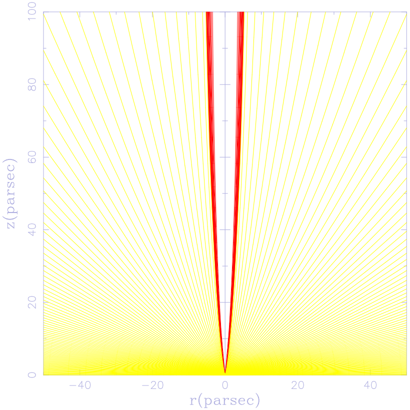

- Biretta et al measure the jet width/opening angle directly from the observational maps
- we defined the jet width through a particular magnetic field line *assuming* that this traces the intensity contours well enough
- better: create a synthetic emission map and measure the jet width directly

Intensity and polarization maps

A. Papageorgiou, thesis

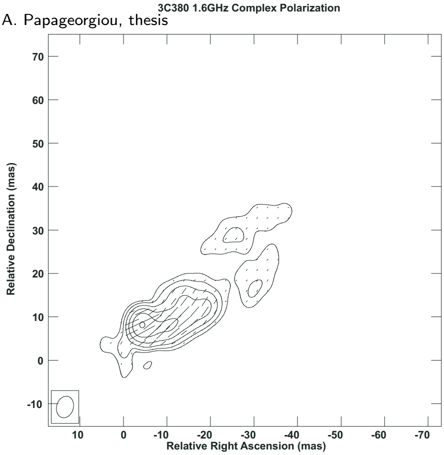

The localized emissivity is a function of density, magnetic field strength and orientation. After integration along the line-of-sight:

- total intensity: $I(\rho, |\vec{B}_{\rm a}|)$
- polarization angle: $\chi(\vec{B}_{\rm a})$
- rotation measure: $RM(\rho, |\vec{B}_{||}|)$

radio maps contain information on MHD structure

$\rightarrow$ test/constrain models!

Intensity and polarization across the jet

A. Papageorgiou, thesis

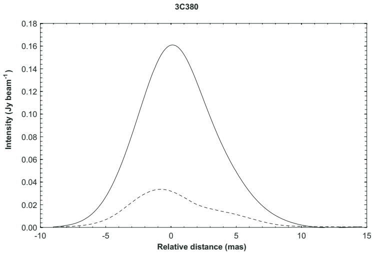

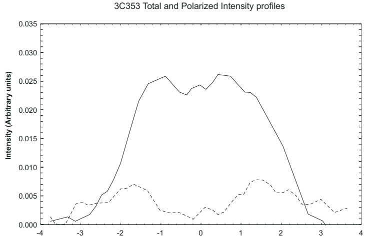

Intensity and polarization profiles across the jet may show:

- non-negligible polariation fraction
- centrally peaked profiles
- edge brightened profiles
- displacements between unpolarized and polarized light
- magnetic field either transverse or along jet axis, or even both

What magnetic field structure can produce this features?

Synchrotron emission

bild: mgn feld, elektron, photon

Assume:

- uniform and isotropic electron distribution
  $N(E) \propto E^{-(2\alpha+1)}$
- optically thin radiating region
  $S(\nu) \propto \nu^{-\alpha}$
- ordered, large-scale magnetic field only

Synchrotron emissivity: $\epsilon \propto \rho \, |\vec{B} \times \vec{n}_{\mathrm{los}}|^{\alpha+1}$

$\rightarrow$ emissivity is not sensitive to the magnetic field along the line of sight!!

Polarization

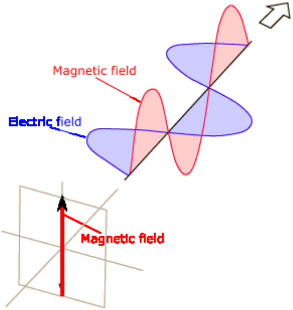

- Synchtrotron radiation is linearly polarized
- The magnetic field of the electro-magnetic wave oscillates in the plane spawned by the line-of-sight and the magnetic field of the plasma.
- Stokes vectors q,u:
  $q = \epsilon \cos 2\chi, u = \epsilon \sin 2\chi$
  where χ is the polarization angle with respect to a given "north" direction

Line-of-sight integration

- The observed radiation is a superposition of the emission along the line-of-sight:
  $I = \int \epsilon \, ds$
  $Q = \int q \, ds, \qquad U = \int u \, ds$
- The apparent/integrated polarization angle is:
  $\chi_{\rm a} = \frac{1}{2} \arctan \frac{U}{Q}$
- cylindrically symmetric configurations:
  $U = 0 \rightarrow \chi_{\rm a} = 0^\circ$ or $\chi_{\rm a} = 90^\circ$
- $\rightarrow$ the apparent magnetic field is either tranverse or parallel to the jet axis

Rotation measure

contains info on $B_{||}$

Relativistic Effects/Aberration

Doppler factor:

$$\mathcal{D} = \frac{1}{\Gamma(1 - \beta \sin\theta)}$$

Two main effects:

- Doppler Beaming by factor $\mathcal{D}^{\alpha+3}$, most efficient for $\theta \sim 1/\Gamma$
- relativistic aberration, ie rotation of the polarization angle

Note: this will result in a very complicated structure for rotating jets, since $\beta \sin\theta$ varies strongly within the source.

Clipping

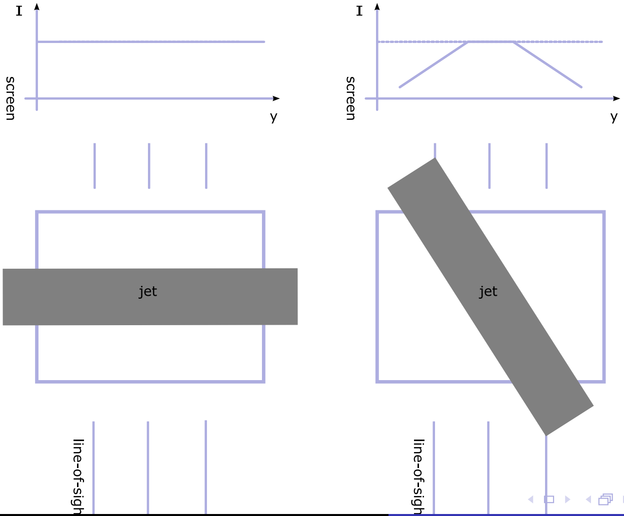

Convolution

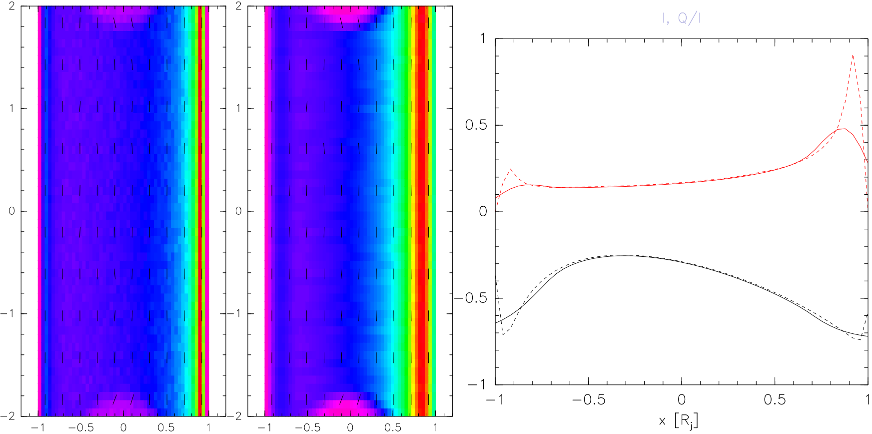

Convolution with gaussian beam of width $\sigma = R_\mathrm{j}/5$

Helical models

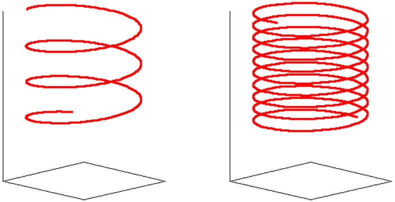

- constant density
- helical magnetic field $\tan\psi = B_\phi / B_{\mathrm{R}}$
- viewing angle $0^\circ \leq \theta \leq 90^\circ$
- velocity given by Lorentz-factor Γ

Shell versus slab:

- shell: only thin cylindrical shell around jet axis emits radiation
- slab: all the volume emits

Viewing angle variation

$$\psi = 30^\circ, \quad \Gamma = 1$$

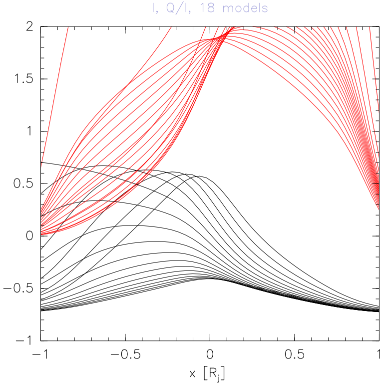

slab

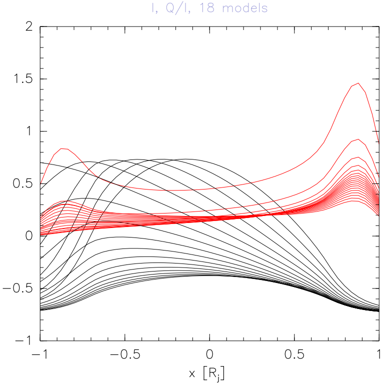

shell

Pitch angle variation

$$\theta = 90^\circ, \quad \Gamma = 1$$

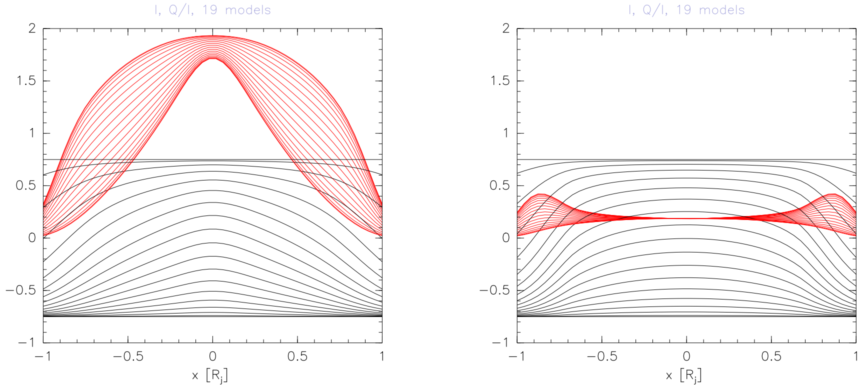

slab shell

Relativistic outflows 1

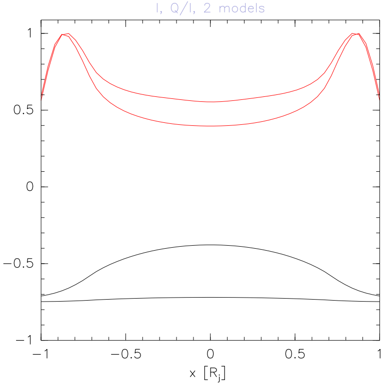

It is often stated, that a relativistic flow ($\Gamma \gg 1$) at an viewing angle $\theta \sim 1/\Gamma$ looks exactly the same as an non-relativistic flow ($\Gamma = 1$) at $\theta = 90°$.

This is true only if the relativistic corrections to the polarization angle are not taken into account. Otherwise, the relativistic flow shows higher (close to maximum) polarization.

Relativistic outflows 2

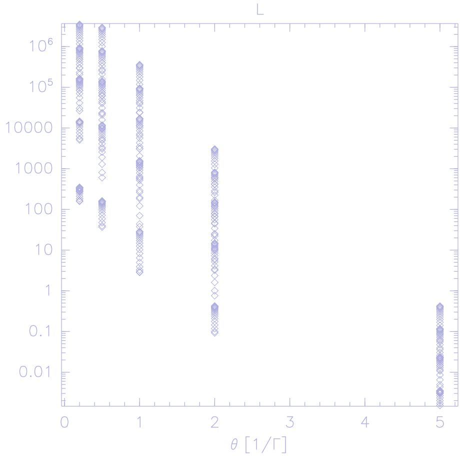

- Doppler boosting most efficient for $\theta \sim 1/\Gamma$
- luminosity of source can vary by more the 6 orders of magnitude due to doppler boosting

The jet of M87

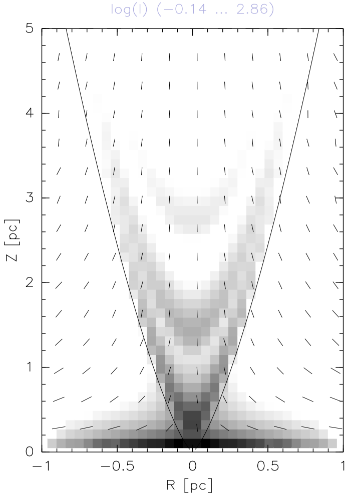

very, *very* preliminary! Just an internal proof of concept!

Assumes:

- $B_\phi = 0$
- $\rho = const$
- $V = 0$

Basically, only B_R, B_Z components. So far, the brightness contours seem to be traced well by our "particular" field line.

Outlook

- Episode 5: emission maps, polarization (thermal electrons)?
- Episode 6: non-thermal electron distribution (?)

- Episode 1-3: including the underlying accretion disk, origin of magnetic field, coupling

ENIGMA Meeting, Hydra, Greece

Polarization behaviour predictions from helical magnetic field models of AGN jets

A simple statistical model

Andreas Papageorgiou

Cork Institute of Technology

Quick Reminder

- Helical magnetic field model
  - Cylinder at an angle δ to l.o.s
  - Helical M. Field of constant pitch angle (γ)
  - Emission from the entire cylinder (const. emissivity throughout)
  - Polarization based solely on M.Field geometry
- Predictions
    - Among others, 4 BVPA behaviours across the jet

BVPA behaviour across jet

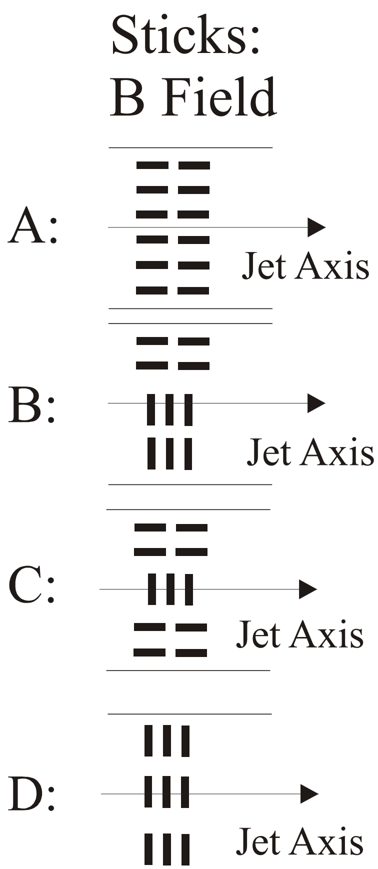

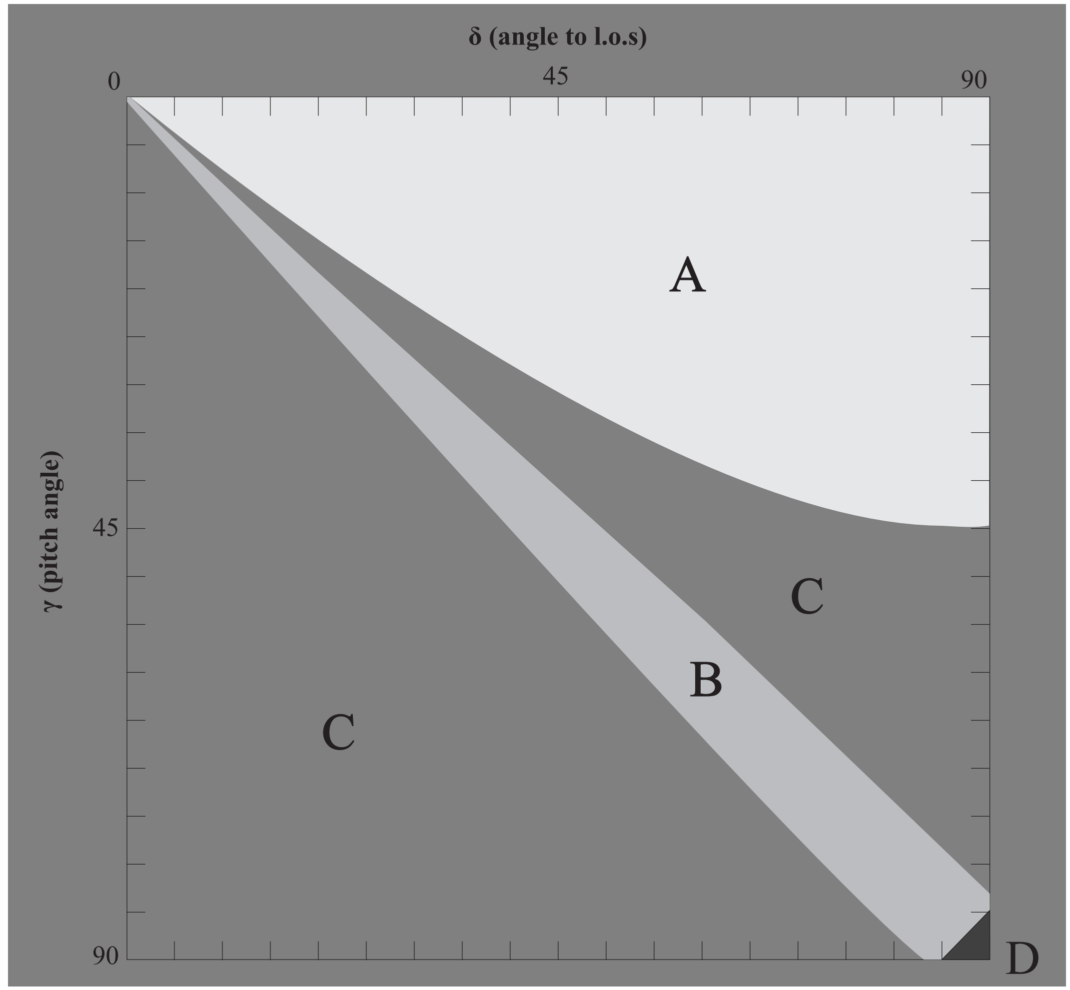

Effect of convolution

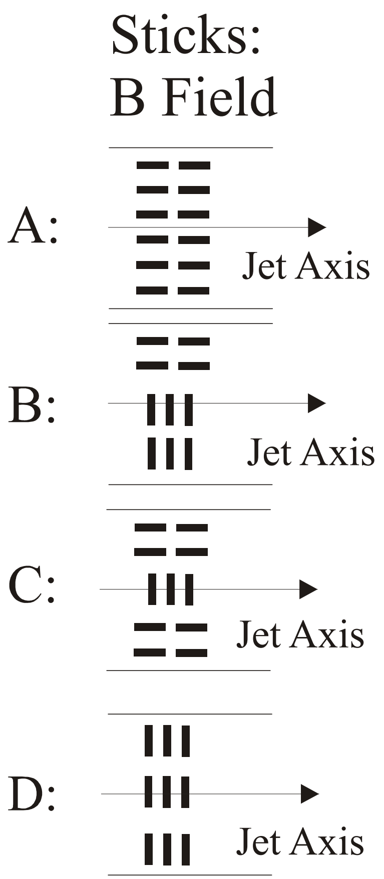

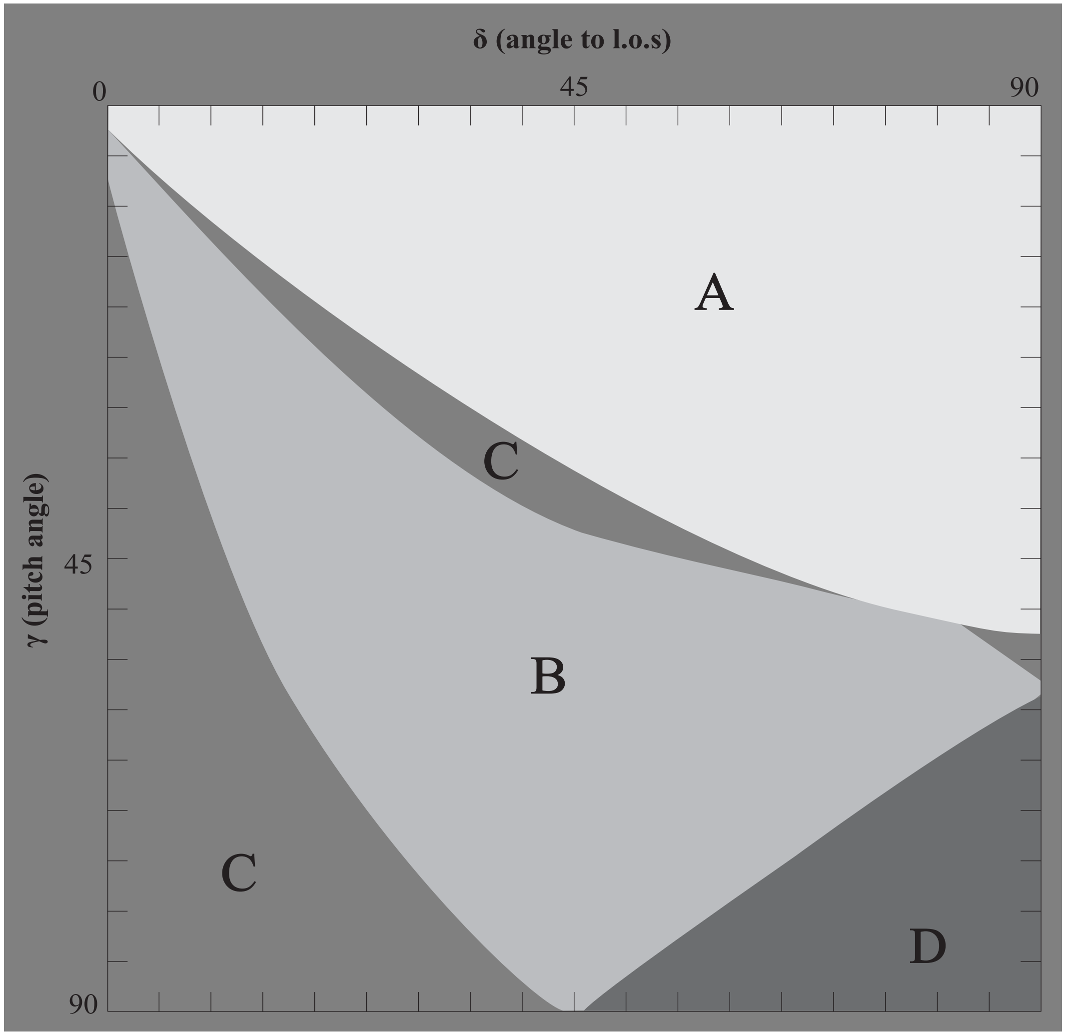

Example of previous effect

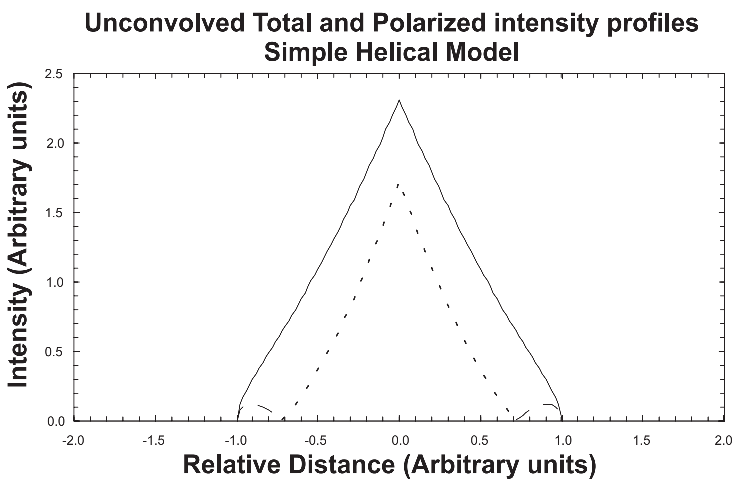

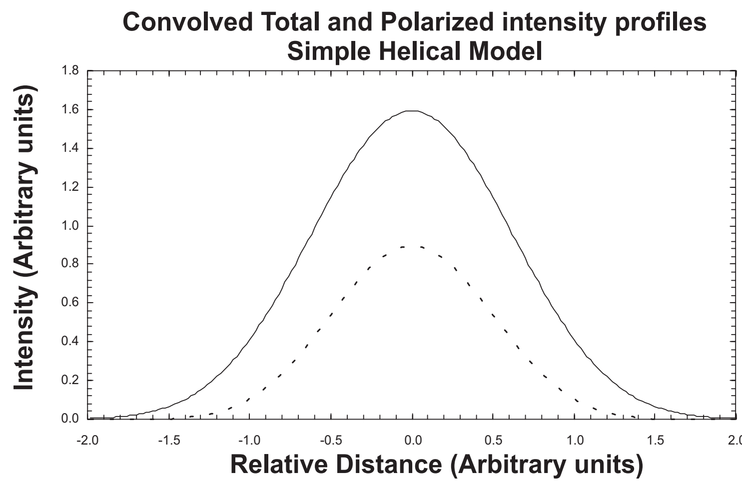

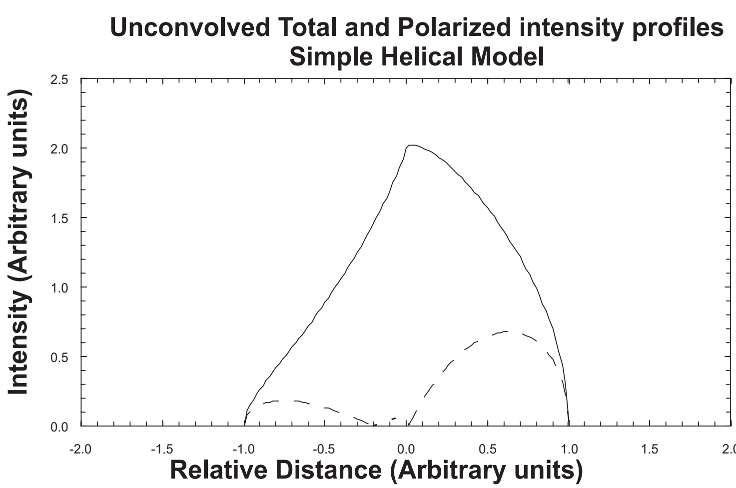

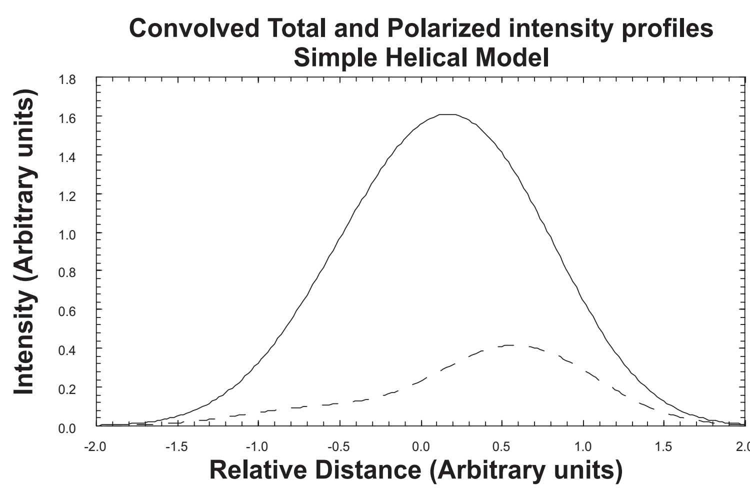

What is the likelihood of observation?

- The diagram can be misleading: Behaviours B and C seem to take a lot of space in the diagram, but are not usually observed

- Results in diagram are in jet frame

- Find likelihood of observing behaviours by creating a simple statistical model

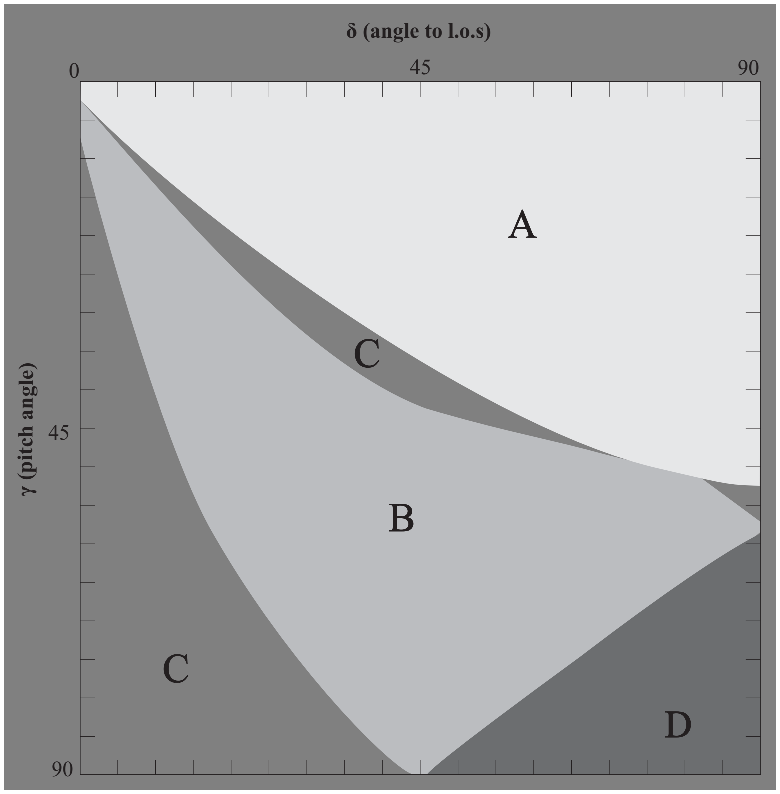

The statistical model

- Fun Part: Assumptions!!
  - Uniform distribution of jets in the sky
  - Uniform distribution of jet orientation
  - All sources in sample are at same distance
  - All jets have the same speed
  - Uniform distribution of helix pitch angles (each jet can have one pitch angle)
  - Power-law distribution of intrinsic (unbeamed) radio luminosity

Probability of observation

$$P_{\gamma,\delta} = F_{\delta}\, W_{\gamma,\delta}$$

F is the fraction of sources that lie in the interval δ, δ+dδ (jet frame)

W is the fraction of F that is bright enough to be observed

Probability of observation

Assuming uniform distribution of δ in the observer's frame:

$$F=\cos(\delta+d\delta) - \cos(\delta) \text{ (obs. frame)}$$

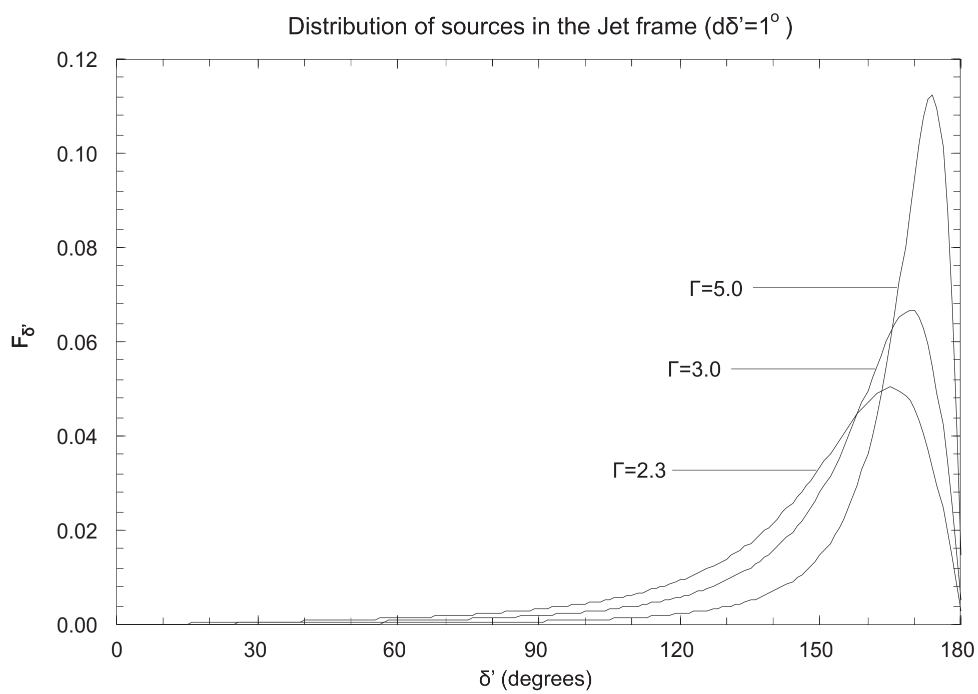

Probability of observation

- Calculating W
- Helical model predicts a range of intensities for different γ and δ ($S_{\gamma\delta}$)
- Introduce rest frame brightness factor B, so that total integrated flux is: B $S_{\gamma\delta}$
- $dN/dB = cB^{-\varepsilon}$

$$N_{\delta} = \int cB^{-\varepsilon} dB = F_{\delta}$$

$$B_{min} = S'_{min} / (D_{\delta}\, S_{\gamma\delta})$$

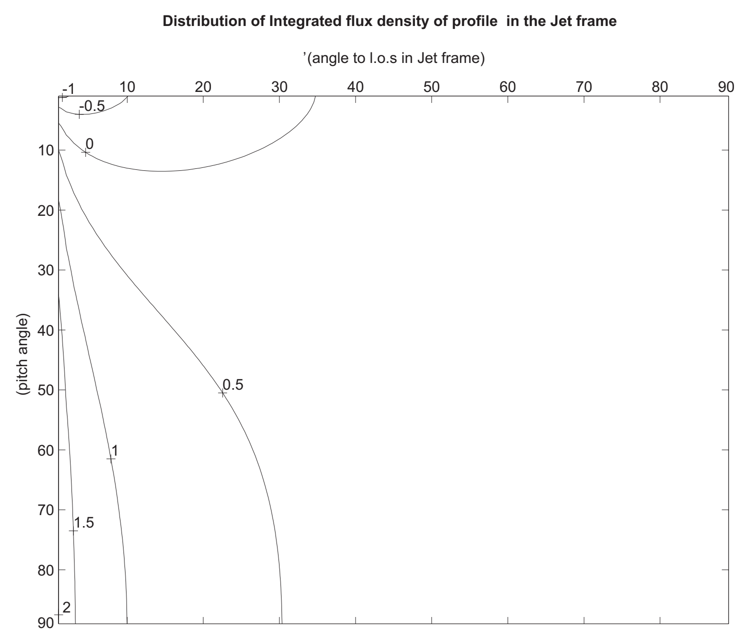

Results

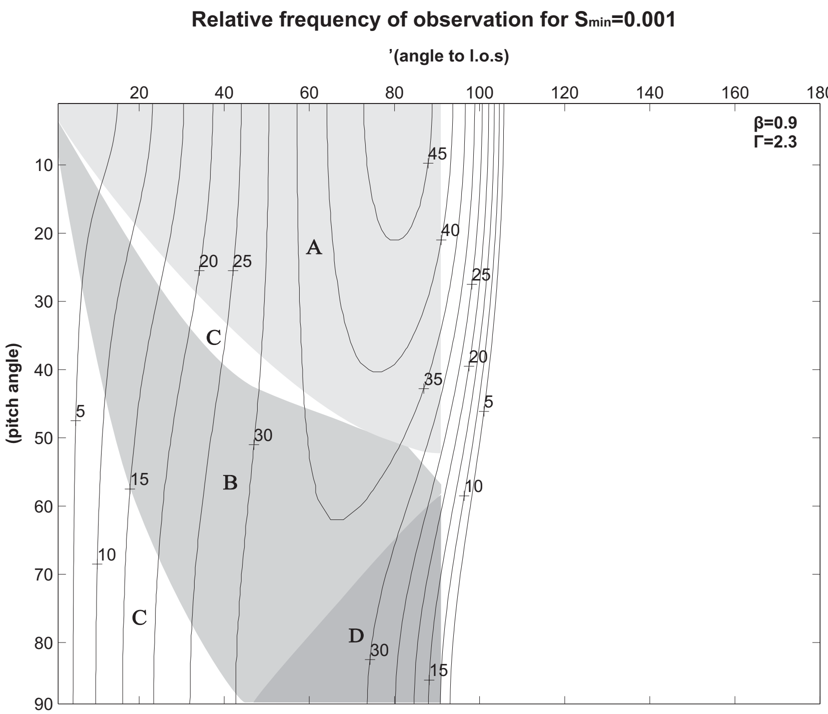

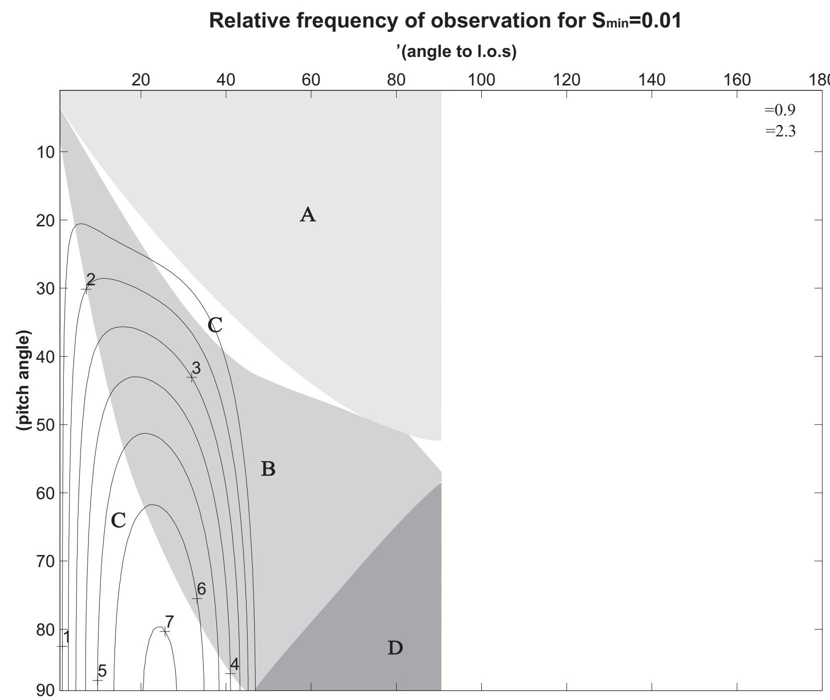

Behaviour	$S_{min}=10^{-3}$	$S_{min}=10^{-2}$
A	50%	0%
B	30%	46%
C	10%	54%
D	10%	0%

Results

Fraction of behaviours vs Pitch Angle

$S_{min}=10^{-3}$

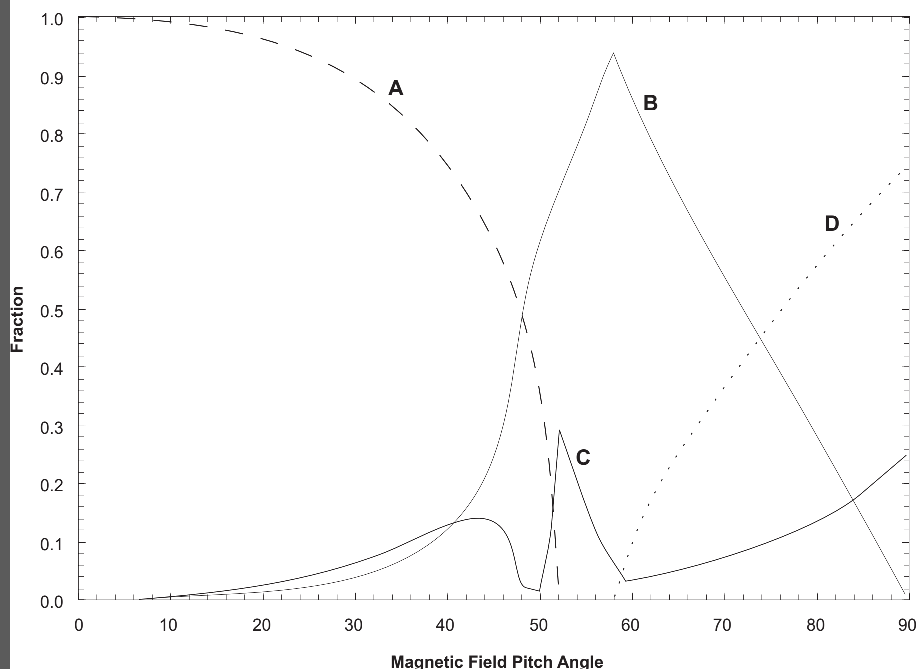

$S_{min}=10^{-2}$

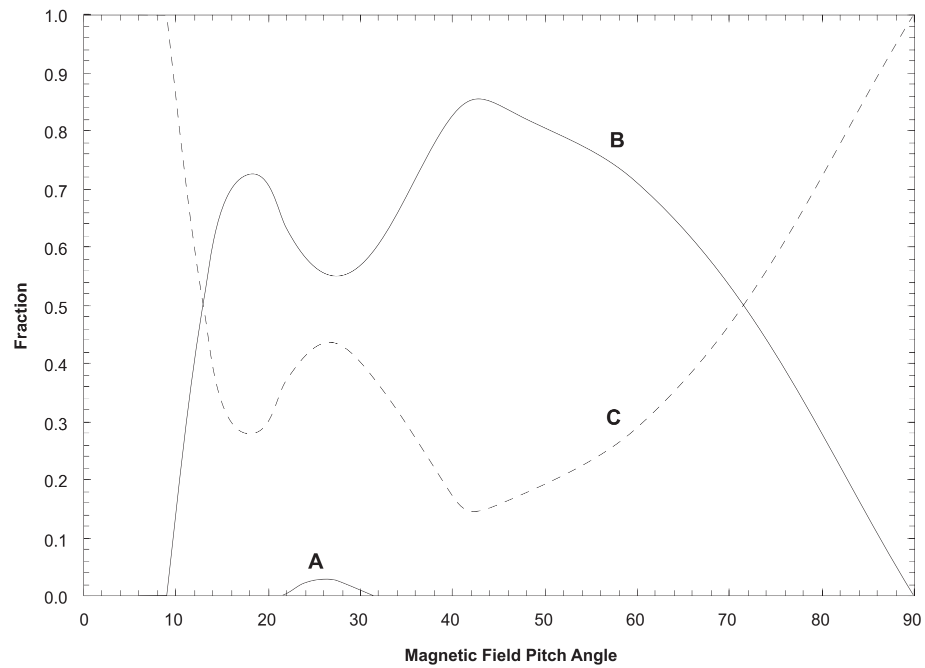

Summary

- Created a simple statistical model to check whether predictions from helical model agree with current observations (low frequency of behaviours B and C).
- Model predicts quite a high frequency of behaviour B (30%), unlike observations.
- Disagreement could be attributed to the possibility that certain helix pitch angles are more preferred by others.
  - In that case, the model suggests that helix pitch angles in the region of 30^o to 70^o, where behaviours B and C dominate, are not common place in jets.

ENIGMA 7th meeting
8 – 10 May, 2006
Hydra

Analysis of the multi-wavelength polarization VLBI observations of BL Lac objects (Task 4)

Vladislavs Bezrukovs
Cork Institute of Technology,
Irish team

Cork Institute of technology

•My project:

To analyze VLBA data from Kuhr and Schmidt sample of BL Lac objects > 1 Jy at 43 GHz, 22 GHz and 15 GHz (May 2002, August 2002, November 2004)

BG121A May 2002	BG121B August 2002	BG121C November 2004
0003-066	0119+115	0814+453
0235+164	0454+844	0828+453
0745+241	0954+658	**0851+202(OJ287)**
1147+245	1308+326	1156+245
1334+127	1803+784	
1749+096	1807-698	
2155-152	2007+777	

- Preliminary calibration and D-term calibration finished for all epoch (May 2002, August 2002, November 2004) at all 3 frequencies;
- Polarization angle calibration made for all sources;
- Maps made for all sources at 15, 22 and 43 GHz;
- Fractional polarization made for all sources at all frequencies;
- Spectral indexes made for all sources, combined from 15 and 22 Ghz and 22 and 43 Ghz intensity maps;
- Rotation measure made for all sources, combined all three frequencies
- Model fitting made for 11 sources at 3 frequencies;

CORK INSTITUTE OF TECHNOLOGY
Institiúid Teicneolaíochta Chorcaí

- All sources are weakly polarized in the core at all frequencies;

- In all sources, polarisation degree in jets is around 5 -20 %

- All sources have typical behavior in spectral index (optically thick core, optically thin jets)

- All sources reveal high RM in their cores with typical values of ~ 1000 rad/m^2

Model fitting program

- Program authors: D. Gabuzda, Roberts (Brandeis University);

+ Program fits models and polarisation;

+ Allows get model fit intensity and polarisation together;

+ Unique program which fits polarisation directly;

- Written on FORTRAN, has text interface;

- Difficult to operate.

Fractional poloraziation:

core: 1 – 3%

jet: 10 – 20%

Spectral index:

core: ~ 0

jet: ~ - 1

Rotation measure:

-1000 – 1000 rad/m^2

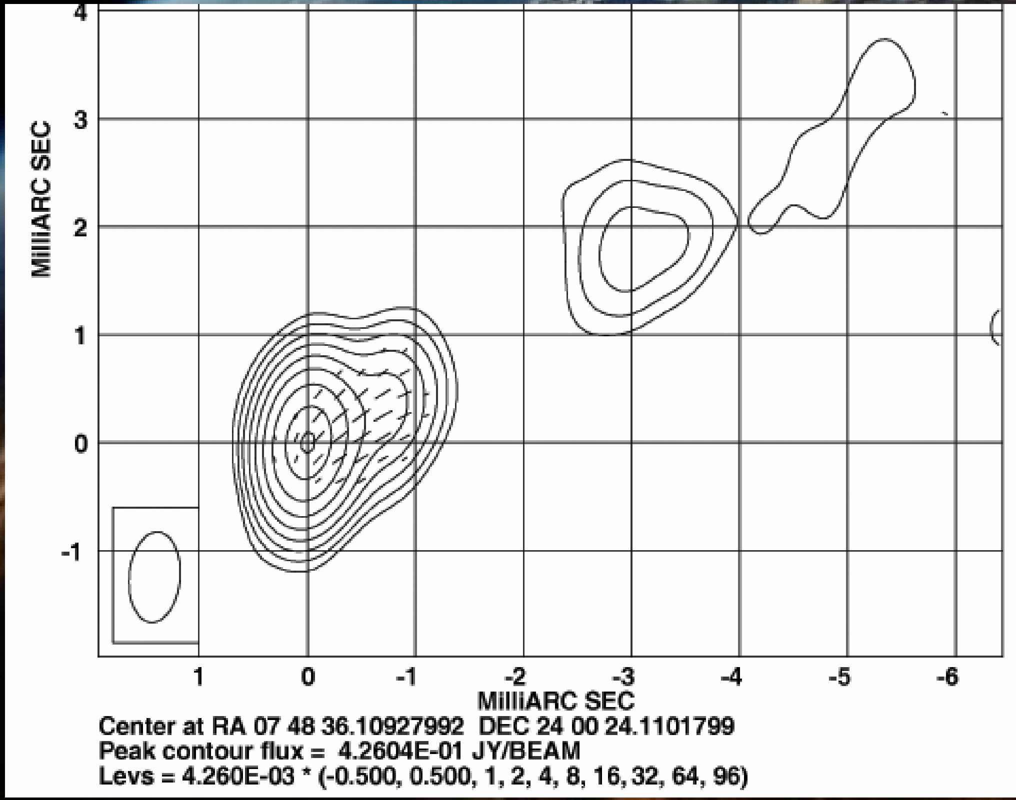

15285.459 MHZ (May 2002)

0745+241 (May 2002)

Model fitting components

22235.459 MHZ (May 2002)

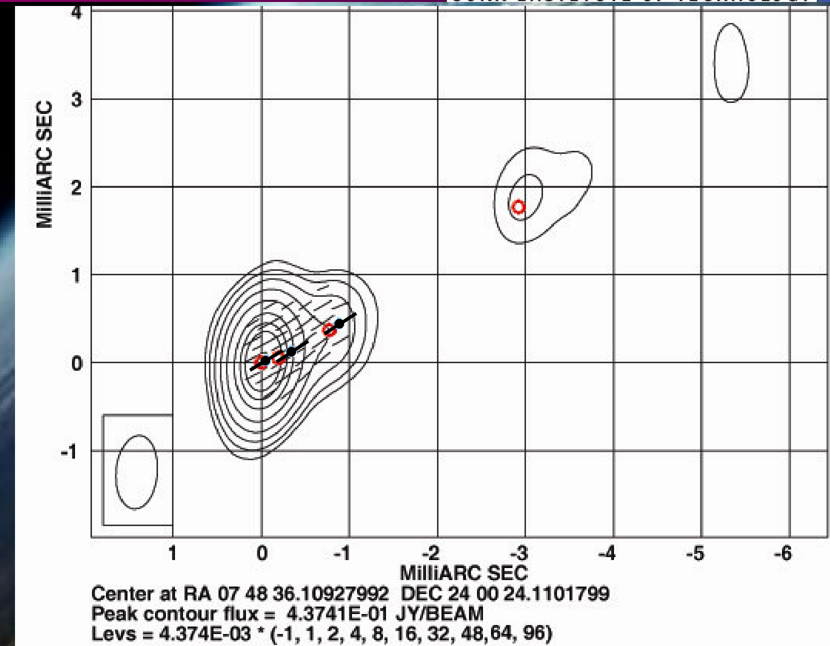

15285.459 MHZ (May 2002)

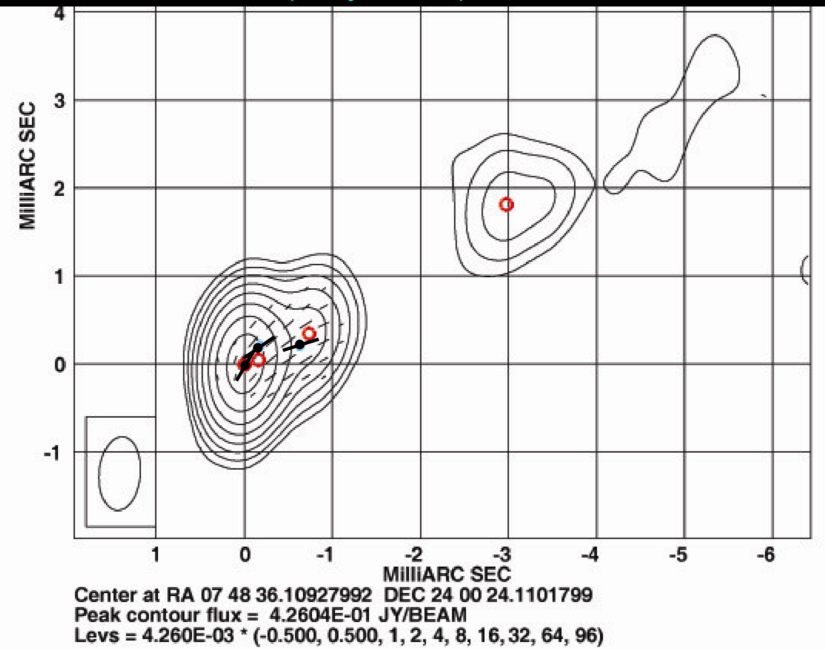

43135.459 MHZ (May 2002)

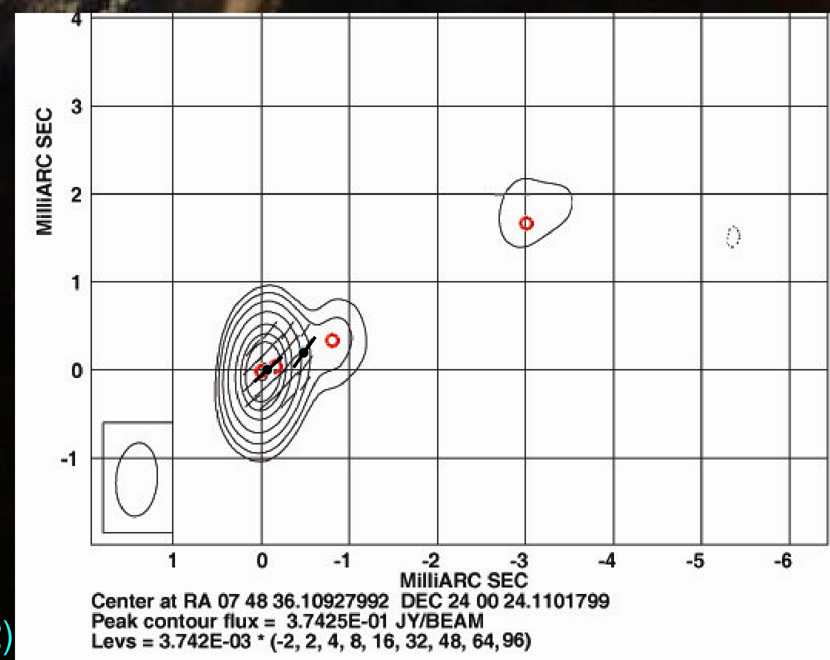

Model fitting components

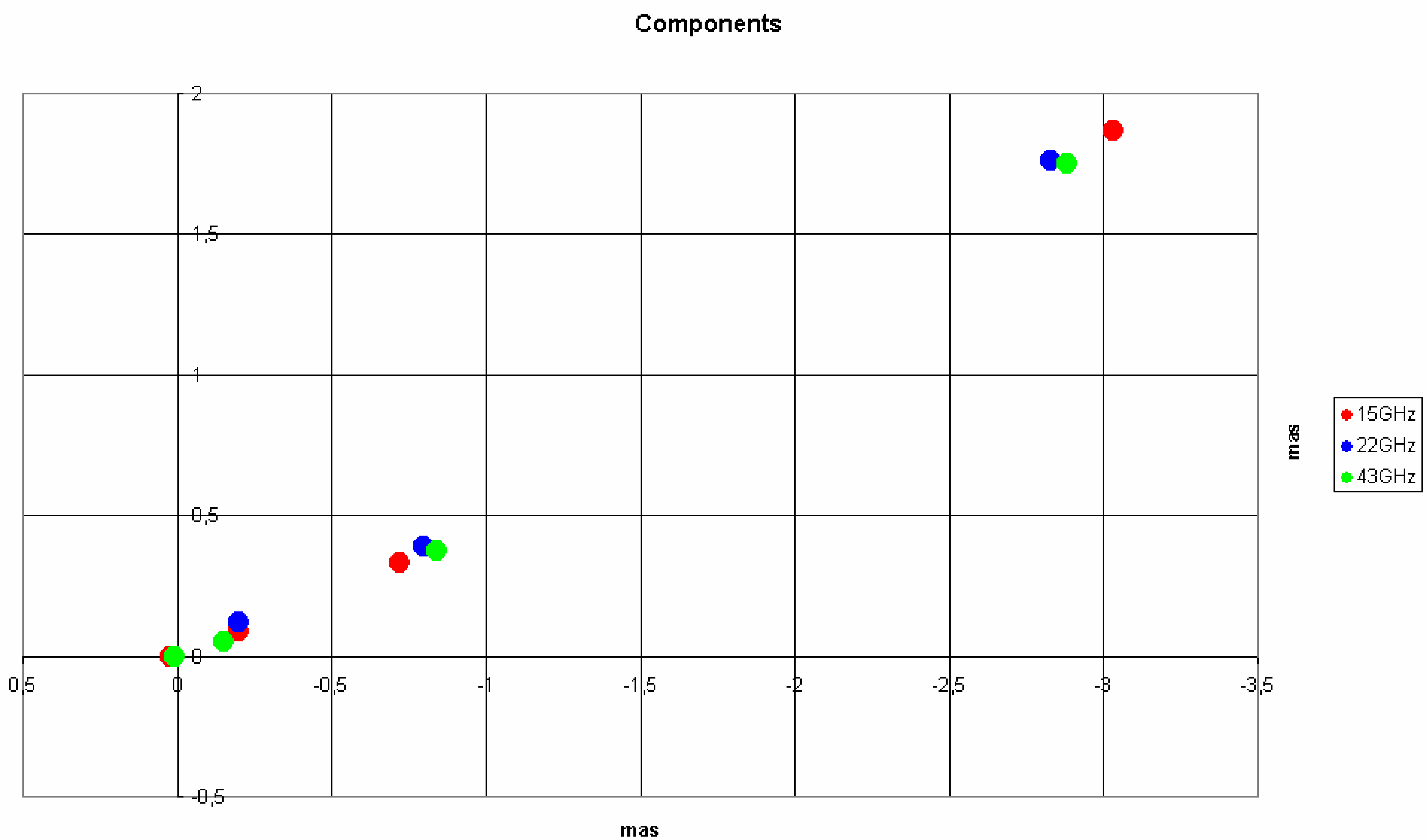

Fractional poloraziation:
- core: 1 – 8%
- jet: 10 – 15%

Spectral index:
- core: ~ 0.5 – 0.8
- jet: ~ - 1 – - 0.8

Rotation measure:
- -1000 – 1000 rad/m^2

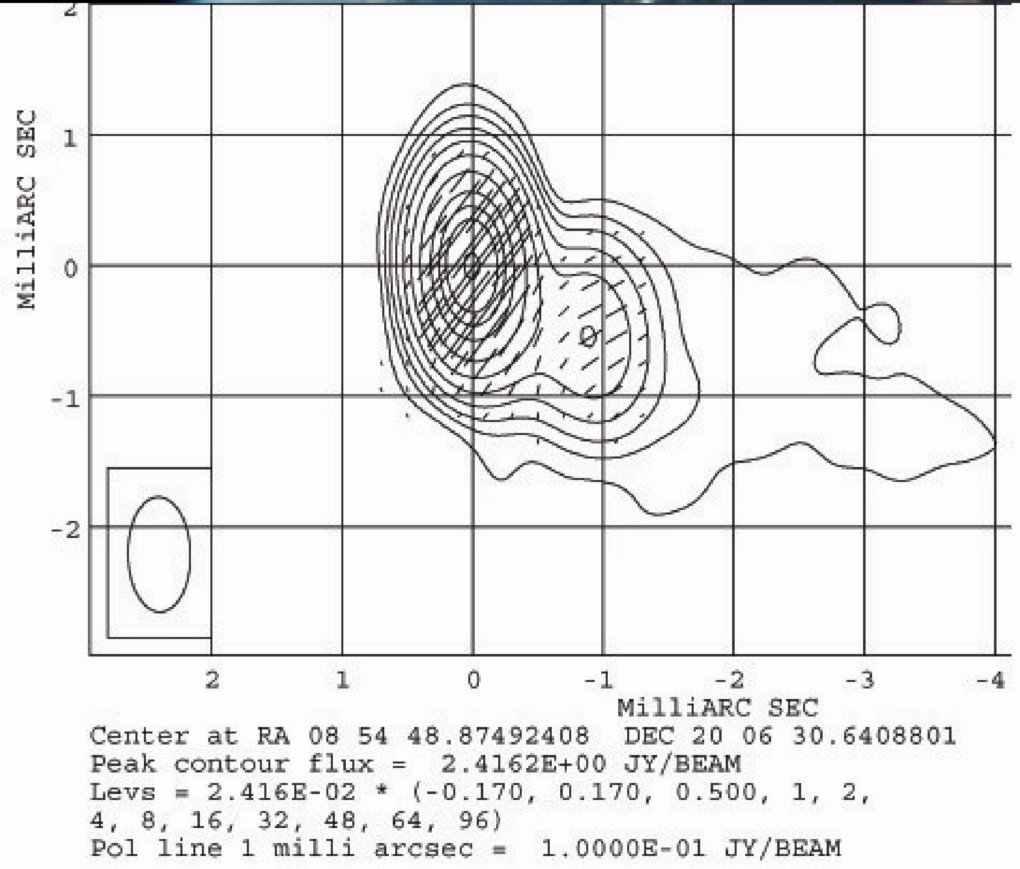

15285.459 MHZ

OJ287 (0851+202, August 2002)

Model fitting components

15285.459 MHZ (May 2002)

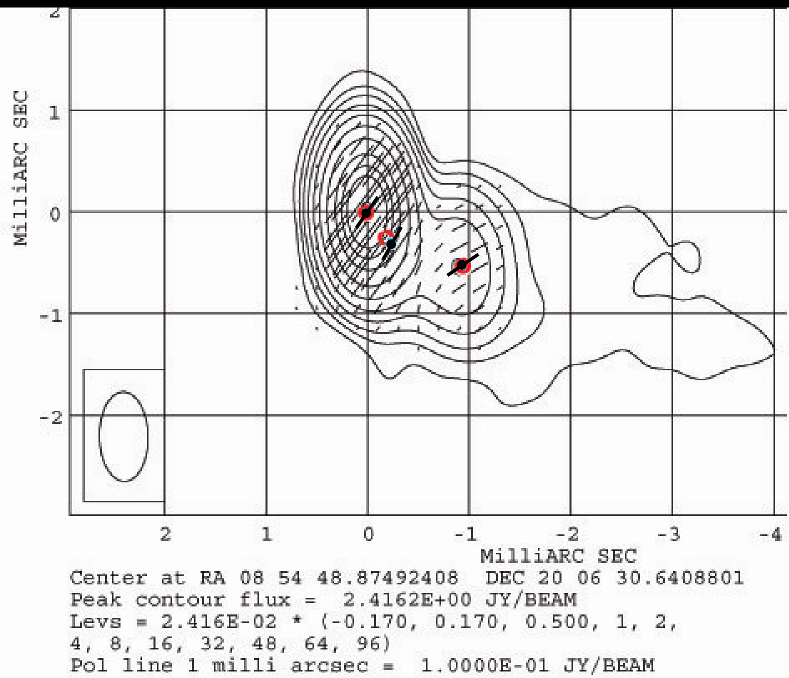

22235.459 MHZ (May 2002)

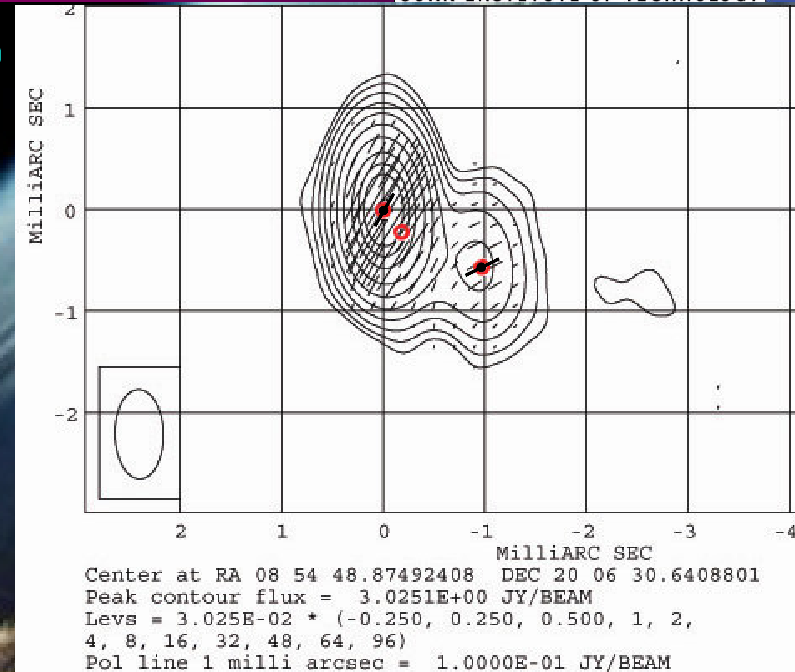

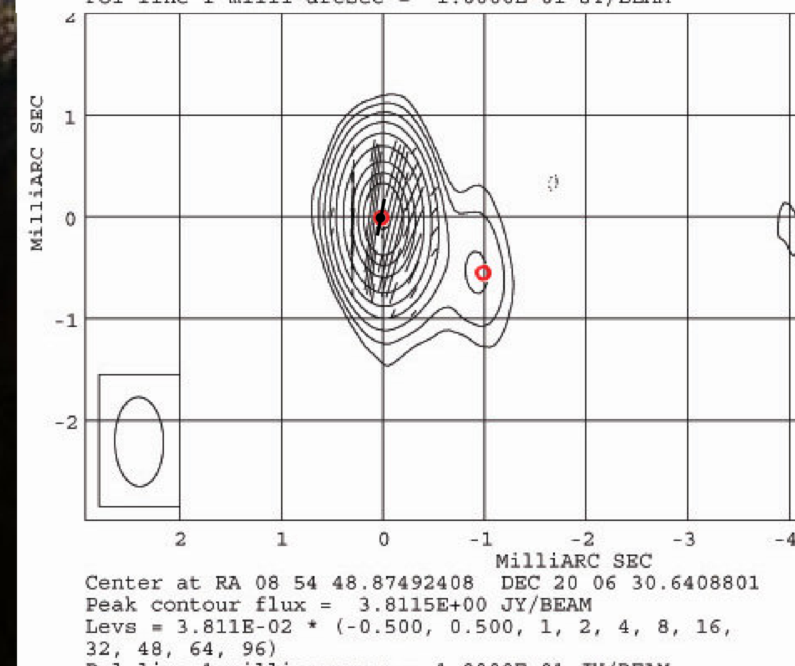

43135.459 MHZ (May 2002)

Institiúid Teicneolaíochta Chorcaí
CORK INSTITUTE OF TECHNOLOGY

Model fitting components

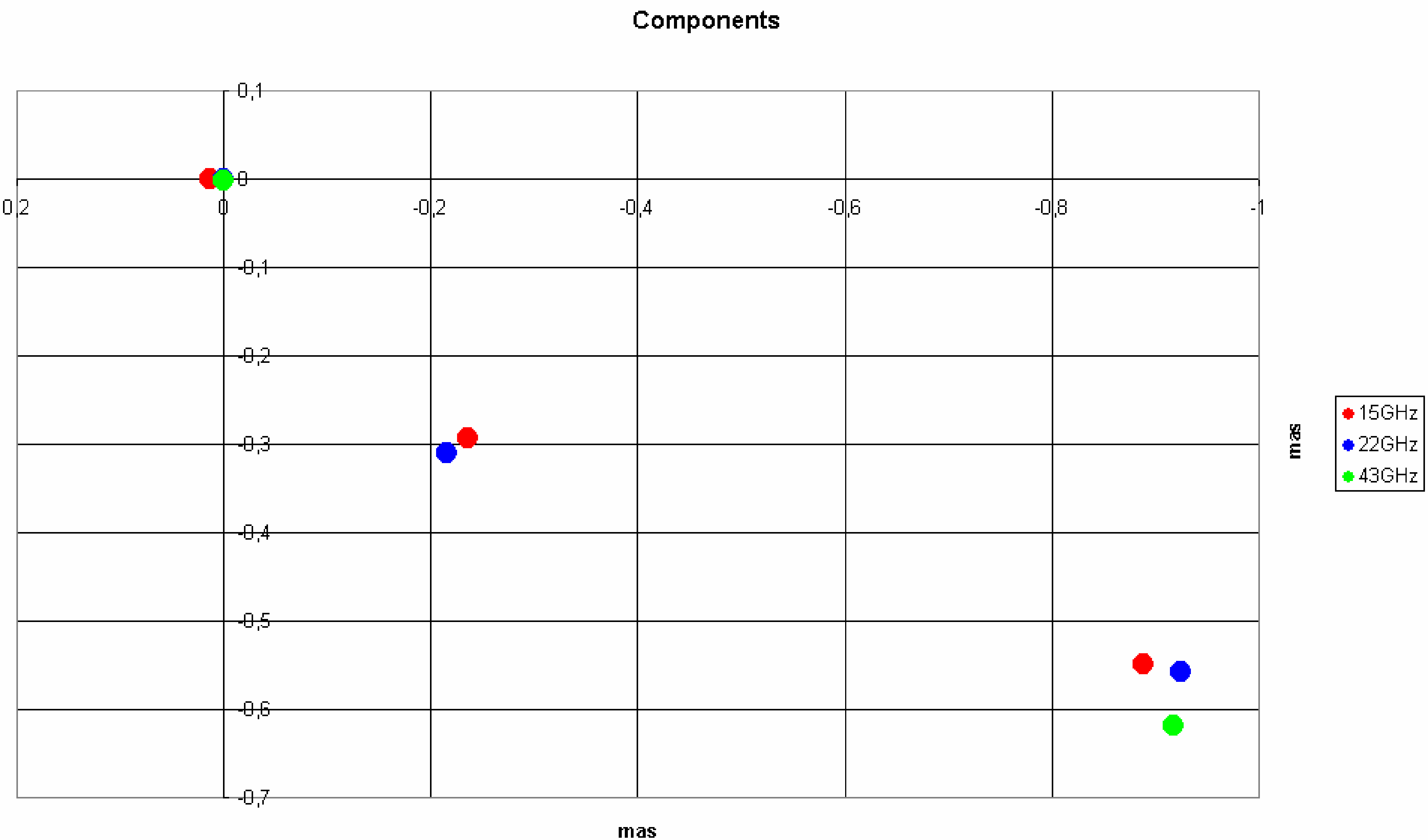

2155-152 (November 2004)

Fractional poloraziation:

core – 1 – 4%

jet – 6 – 18%

Spectral index:

core: 0.5 – 0.7

jet: -1 – -1.1

Rotation measure:

-1000 – 1000 rad/m^2

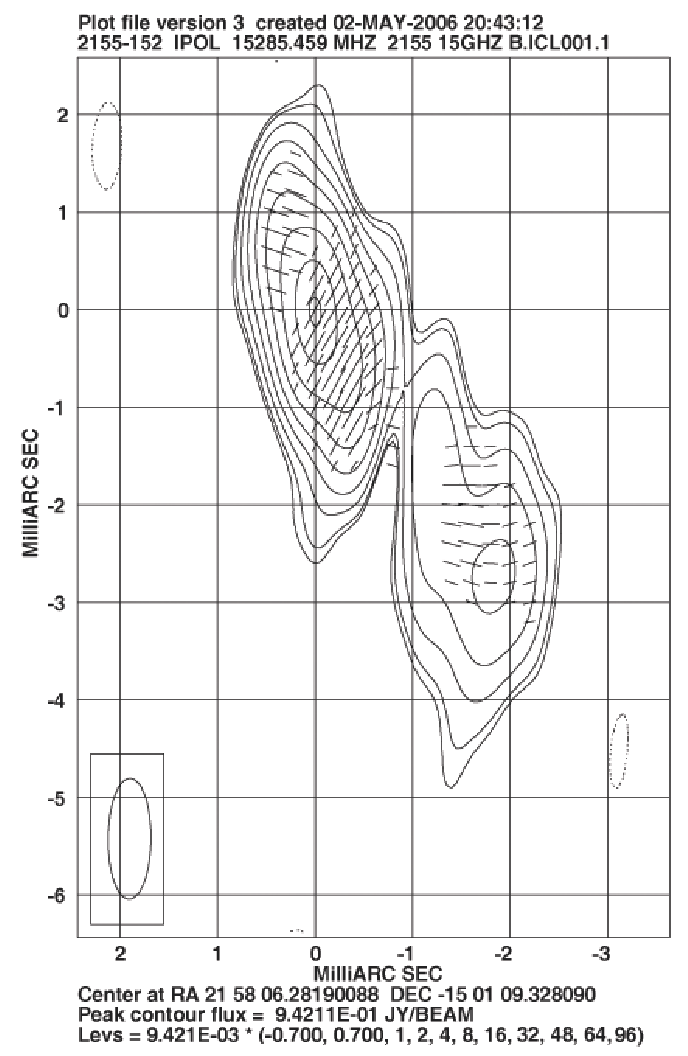

15285.459 MHZ

2155-152 (November 2004)

Model fitting components

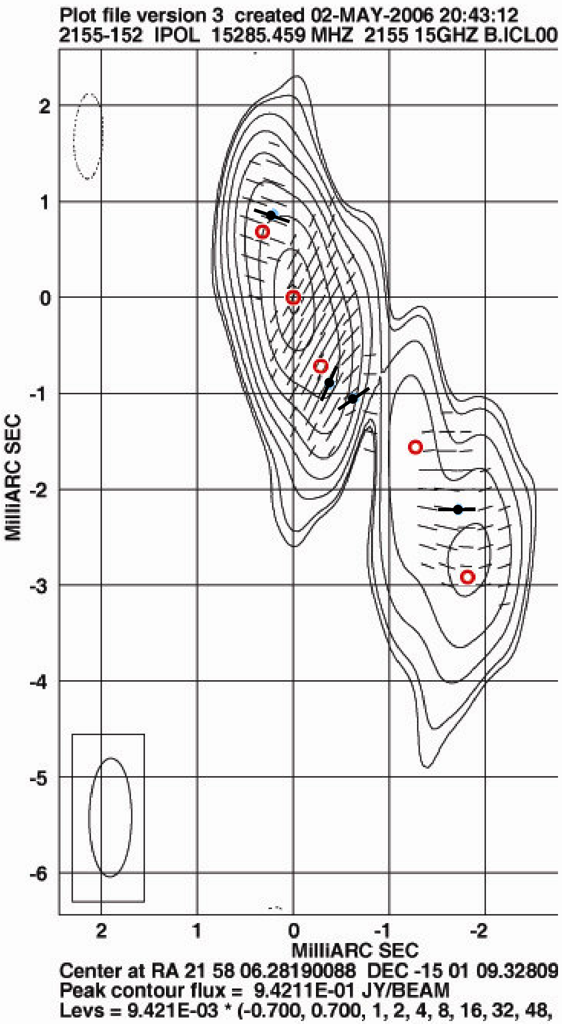

15285.459 MHZ (May 2002)

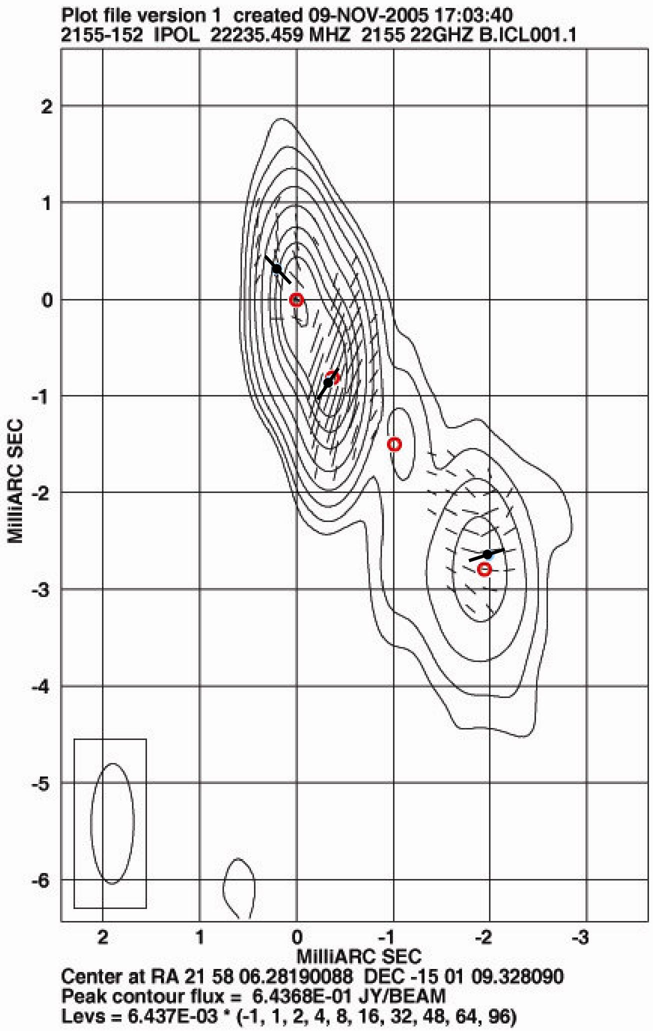

22235.459 MHZ (May 2002)

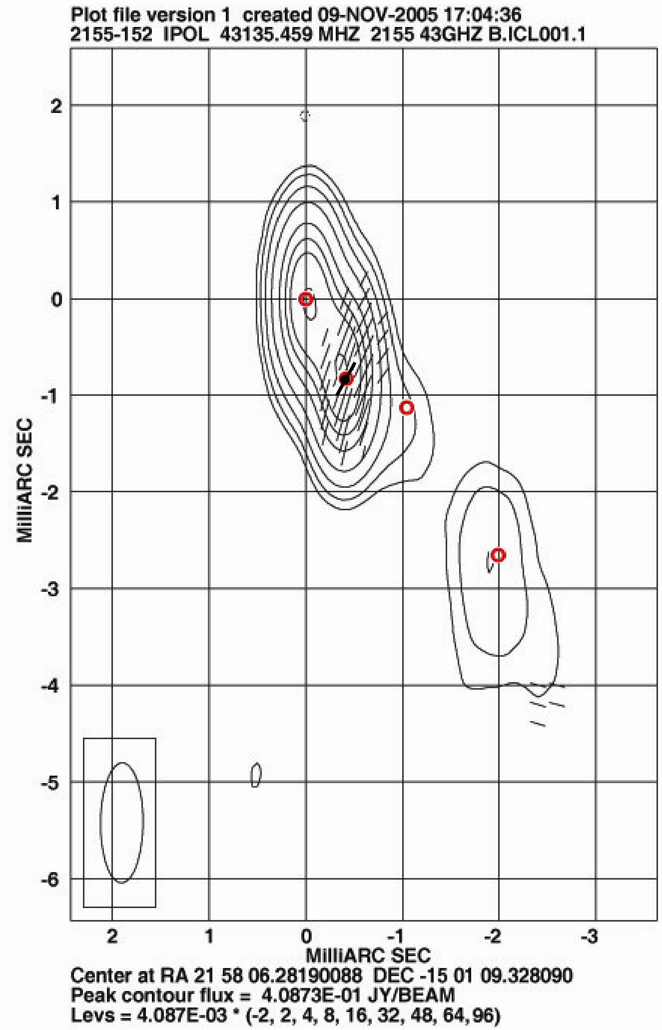

43135.459 MHZ (May 2002)

2155-152 (November 2004)

Fractional polarization maps

22235.459 MHZ
map cut off at 0.0025 Jy

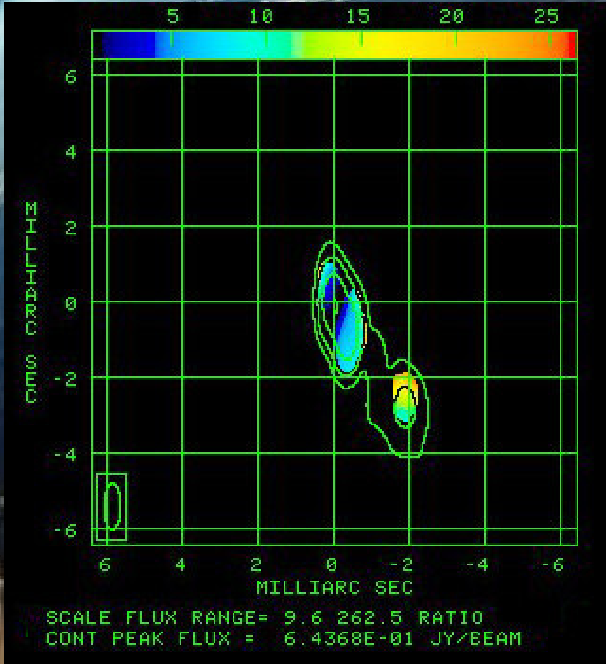

15285.459 MHZ
map cut off at 0.002 Jy

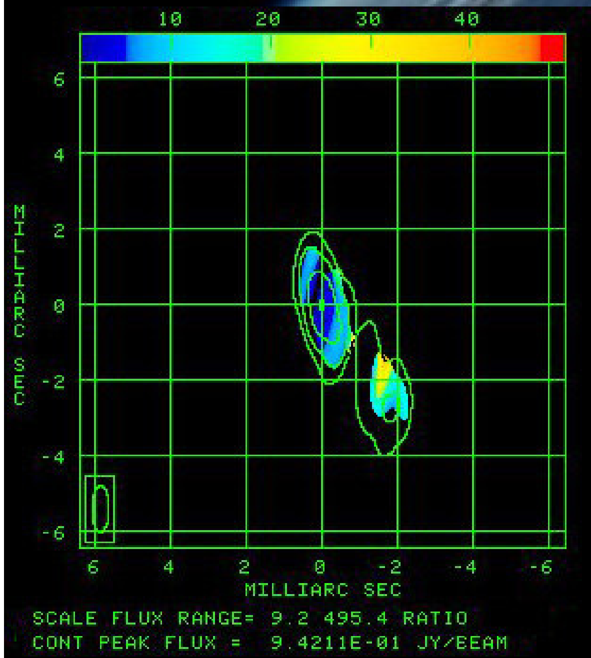

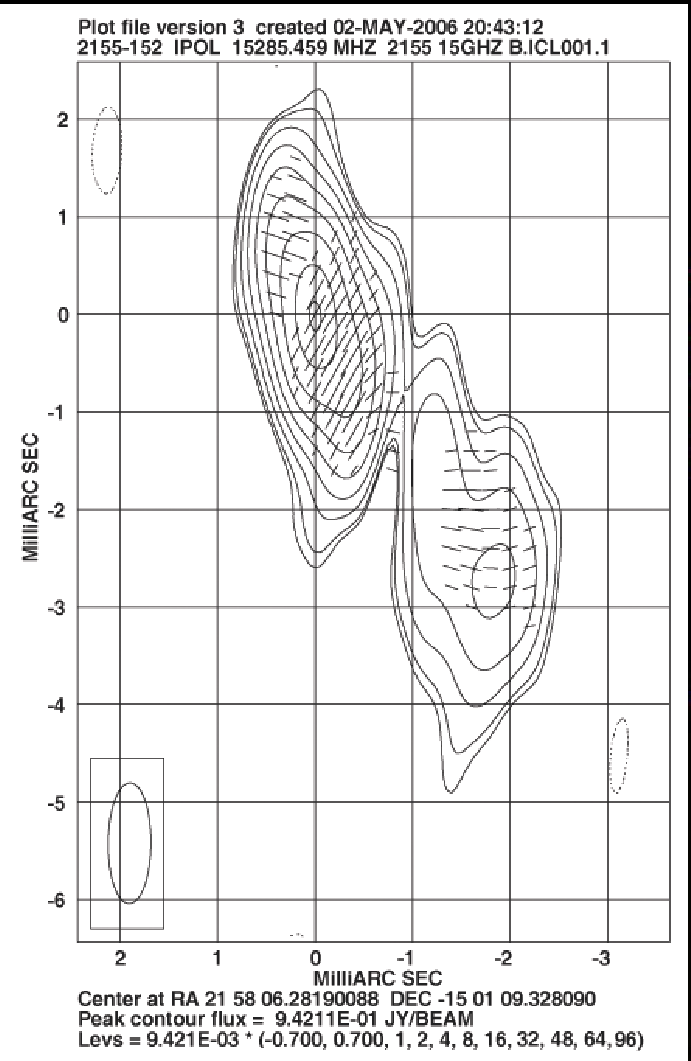

43135.459 MHZ
map cut off at 0.002 Jy

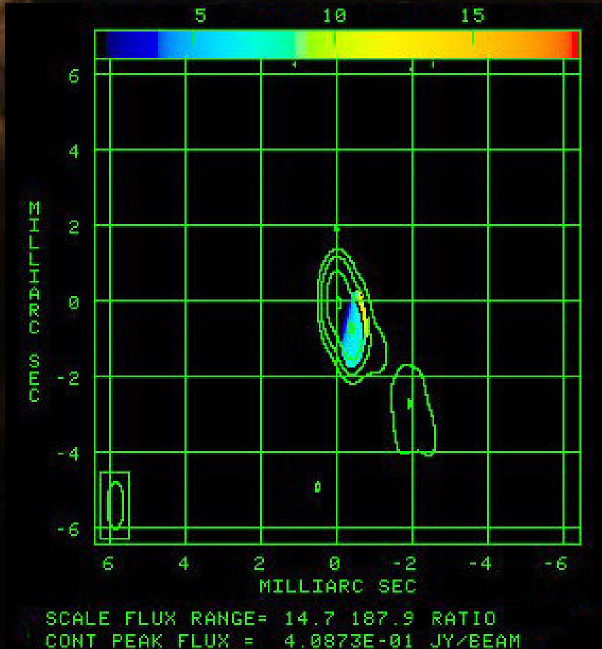

Model fitting components

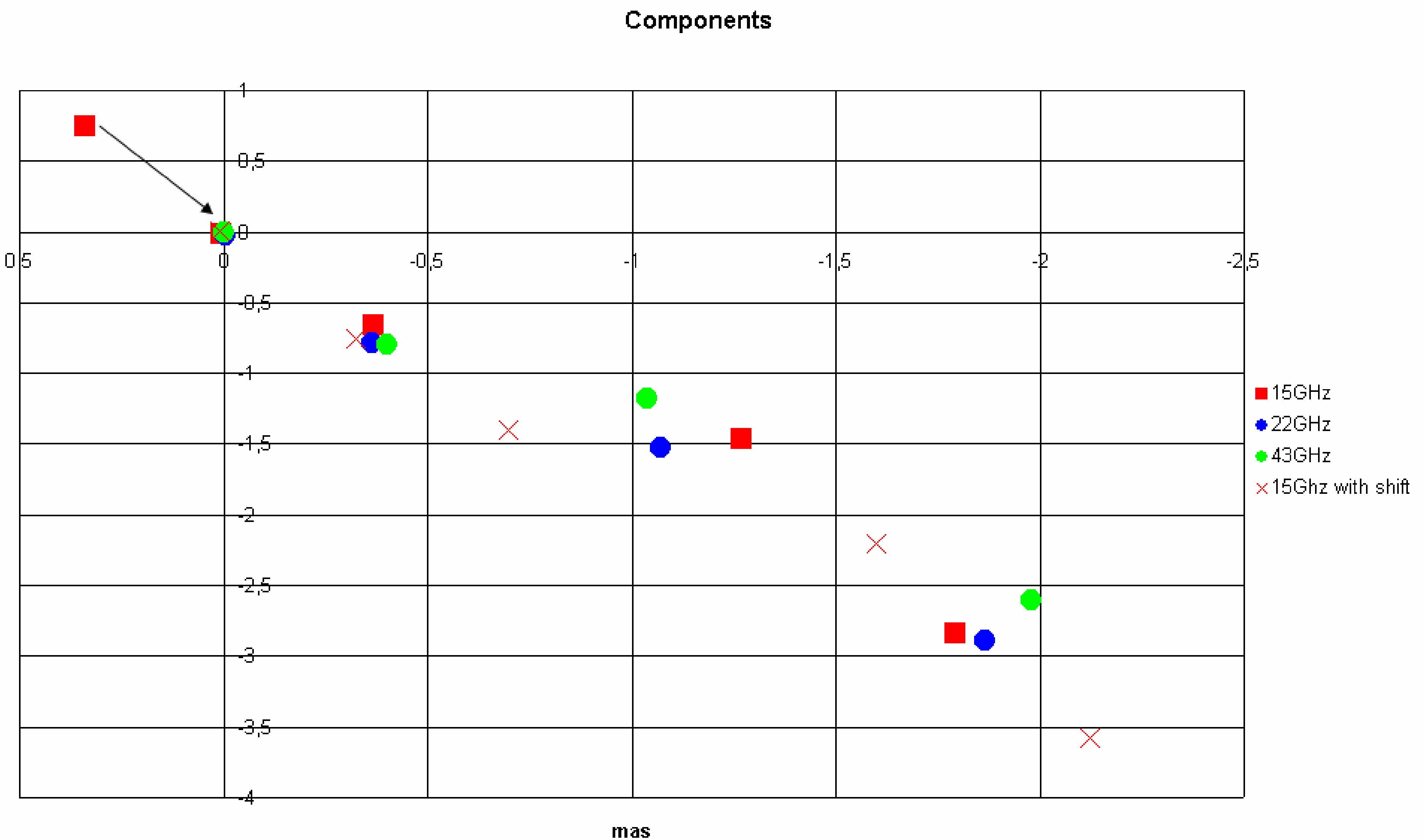

Summary / Future work

- Version of model fitting program VISFIT adapted for LINUX tested, intensity and polarisation models obtained;

- Improve model fitting program VISFIT.

- Finishing model fitting for all sources, frequencies

- Analyse properties of BL Lac sample as whole
  - core and jet polarisation
  - core Faradey Rotation

Acknowledgements

Dr. Denise Gabuzda

Radio Astronomy Lab at UCC

Enigma, Irish Group

Polarimetric radio and mm observational studies of blazars

Iván Agudo

Max-Planck-Institut für Radioastronomie

MAX-PLANCK-GESELLSCHAFT

Overview of the talk

- 3mm obs. of 0716+714 during Core campaign
- VLBA obs. of 0716+714 during Core campaign
- Bimodal behaviour in the jet of 0735+178
- Wobbling jet in NRAO 150
- Wobbling jets in OJ287, 3C273 and 3C345
- 3mm polarimetric monitoring of OJ287

- Summary and conclusions

3mm obs. of 0716+714 during the Core campaign

Collaborators:

T. Krichbaum, H. Ungerechts, A. Kraus, A. Witzel, E. Angelakis, L. Fuhrmann, U. Bach, S. Britzen, A. Zensus, S.J. Wagner, L. Ostorero, E. Ferrero, J. Gracia, M. Grewing

Results:

- Calibration accuracy better than 1.2%!!! (unprecedented)
- No clear IDV pattern in 0716+714
- Increase in flux density of ΔI≈34% (~1.5 Jy) in 4 days
- Variability should be intrinsic to the source (not ISS)
- First time that such abrupt variability has been observed for a blazar at 3mm

3mm

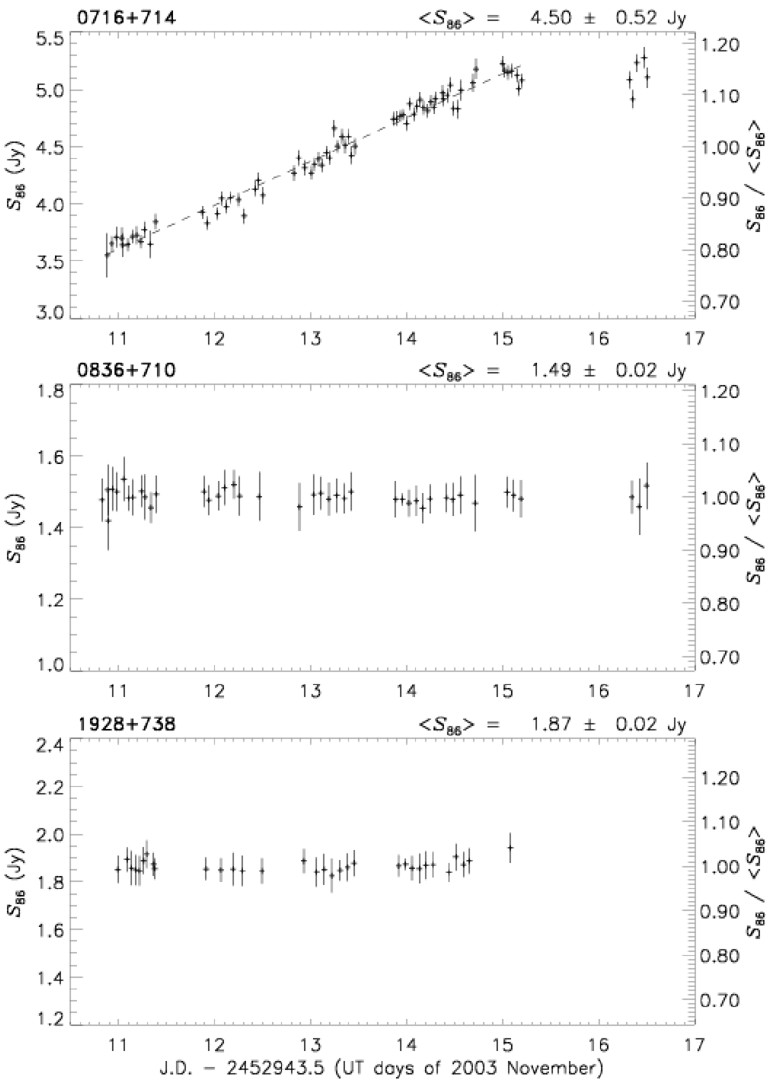

Agudo et al. A&A, submitted

3mm obs. of 0716+714 during the Core campaign

Results:

• 3mm IDV polarimetric evolution of the source measured for the first time

• Larger ever observed (at radio-mm λ) polarization degree 15%

• Evidence for P variability at 3mm on inter-day and intra-day (weaker)

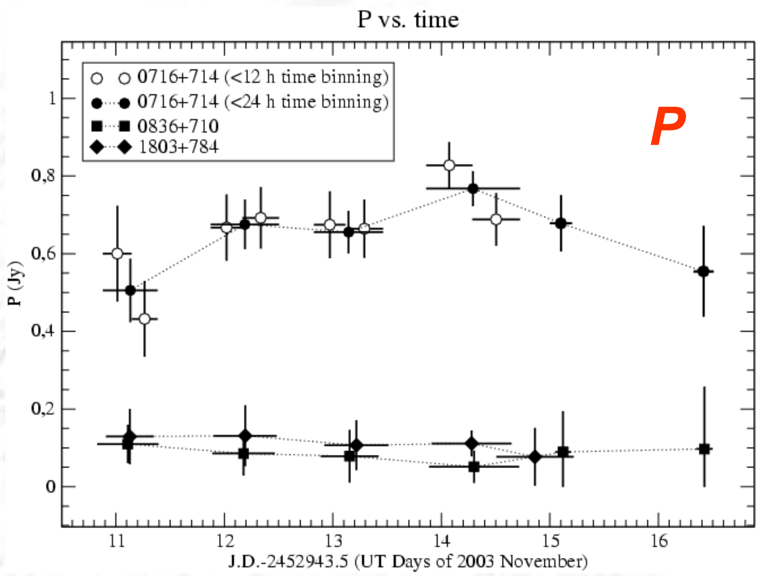

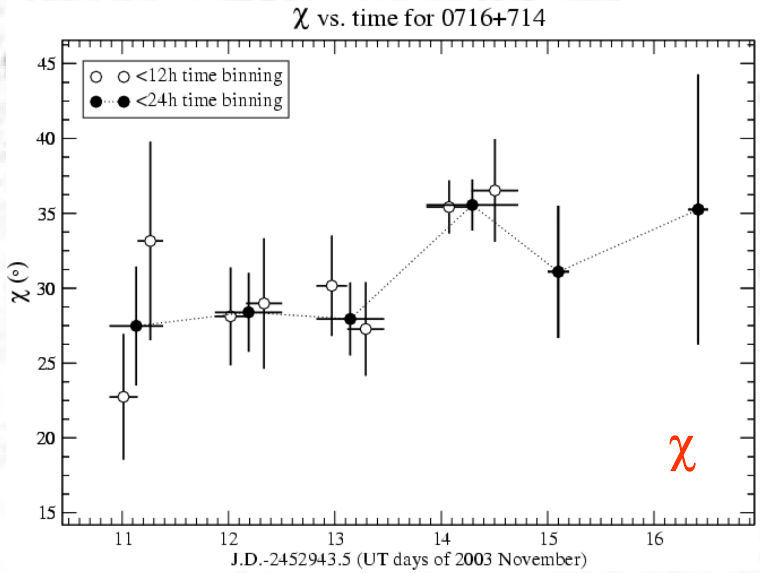

Agudo et al. A&A, submitted

3mm obs. of 0716+714 during the Core campaign

Results:

From modeling of the 3mm variability and comparison with the INTEGRAL gamma ray flux (upper limits) we obtain:

- 3mm corresponds to the turnover frequency of the source
- Apparent brightness temperature at the turn-over= 1.4×10^{14} K
- Exceeds by more than two orders of magnitude the IC limit
- Doppler factor of the source >14 from comparison of 3mm and gamma-ray flux densities (upper limits)
- This Doppler factors are fully consistent with those reported from VLBI measurements (Bach et al. 2006)
- This explains the “apparent” violation of the IC-limit
- This also explains that no “IC-catastrophe” was observed by INTEGRAL (Ostorero et al. A&A, accepted)

VLBA obs. of 0716+714 during the Core campaign

Collaborators:

T. Krichbaum et al.

- 6 VLBI runs of 12 hours each from Nov. 11 to Nov. 16 2003
- 4 λ coverage: 1.6, 5, 22 and 43 GHz
- In dual polarization mode
- Data at 22 & 43 GHz is fully reduced and calibrated

- Contours ⇒ total intensity
- Color scale ⇒ linearly polarized intensity
- Short sticks ⇒ electric vector position angle

0716+714
43 GHz
VLBA

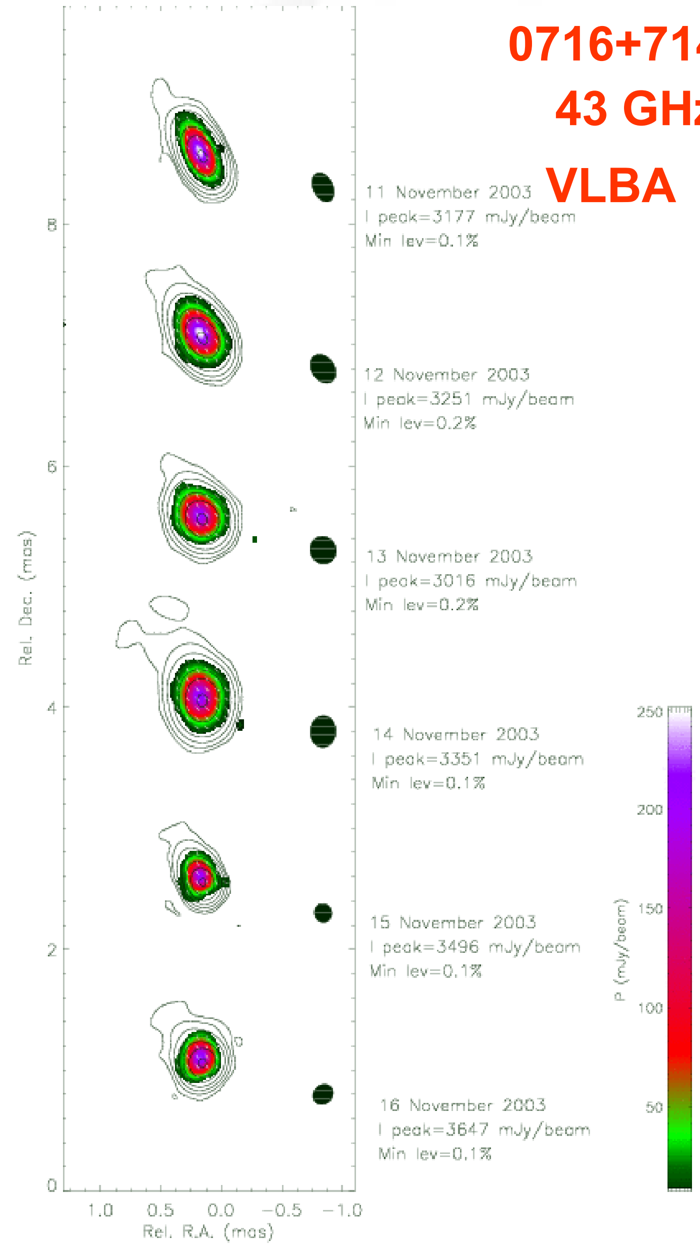

Agudo et al., in preparation

VLBA obs. of 0716+714 during the Core campaign

Collaborators:

T. Krichbaum et al.

- 6 VLBI runs of 12 hours each from Nov. 11 to Nov. 16 2003
- 4 λ coverage: 1.6, 5, 22 and 43 GHz
- In dual polarization mode
- Data at 22 & 43 GHz is fully reduced and calibrated

- Contours ⇒ total intensity
- Color scale ⇒ linearly polarized intensity
- Short sticks ⇒ electric vector position angle

0716+714
22 GHz
VLBA

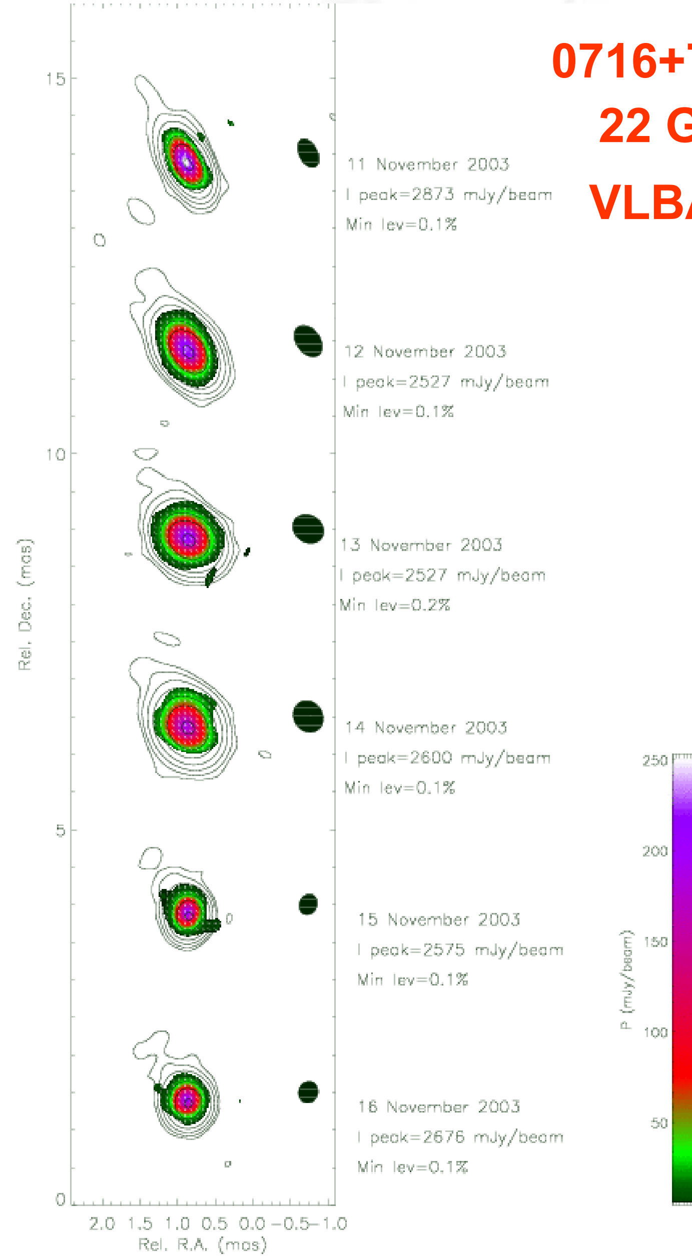

Agudo et al., in preparation

VLBA obs. of 0716+714 during the Core campaign

0716+714 @ 22 GHz (≈0.35 mas resolution)

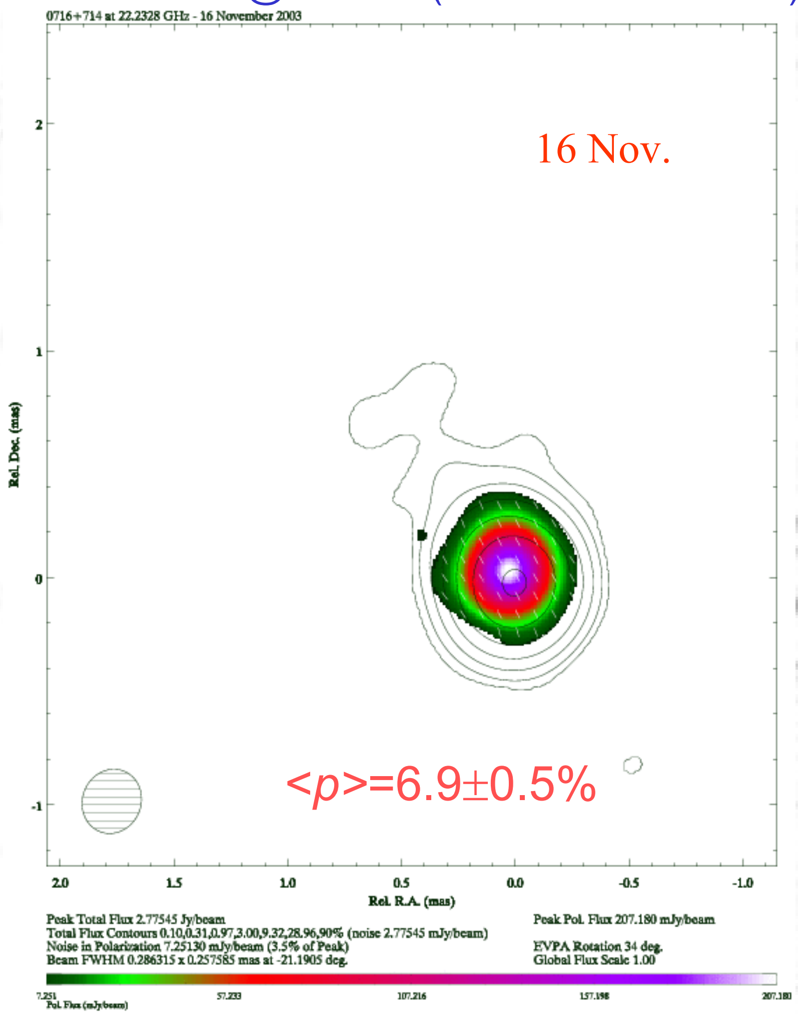

0716+714 @ 43 GHz (≈0.17 mas resolution)

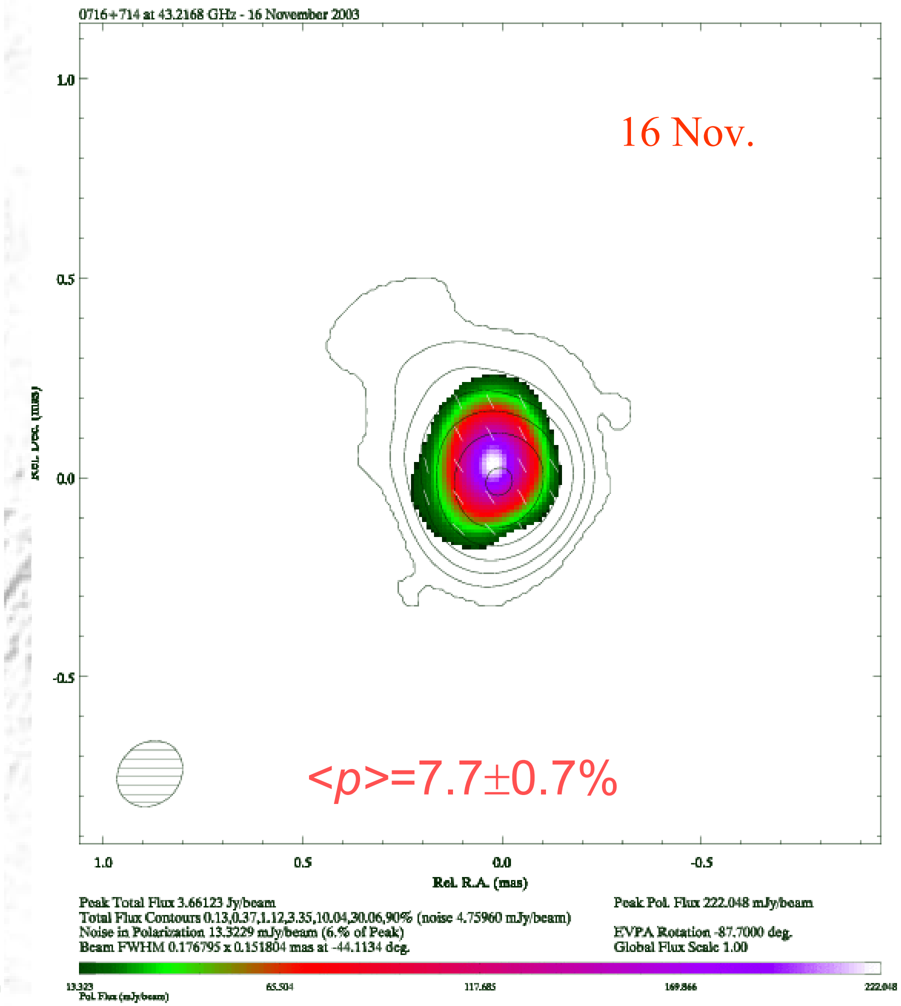

Agudo et al., in preparation

- Very compact structure at both 22 and 43 GHz
- Weak jet at PA≈30º

•The electric vector polarization angle was parallel to the jet direction

VLBA obs. of 0716+714 during the Core campaign

- Fits of the jet structure to sets of Gaussian components:
  - Total flux density of the core 80-90% total flux density of the source
  - Core governs total flux density evolution of the source

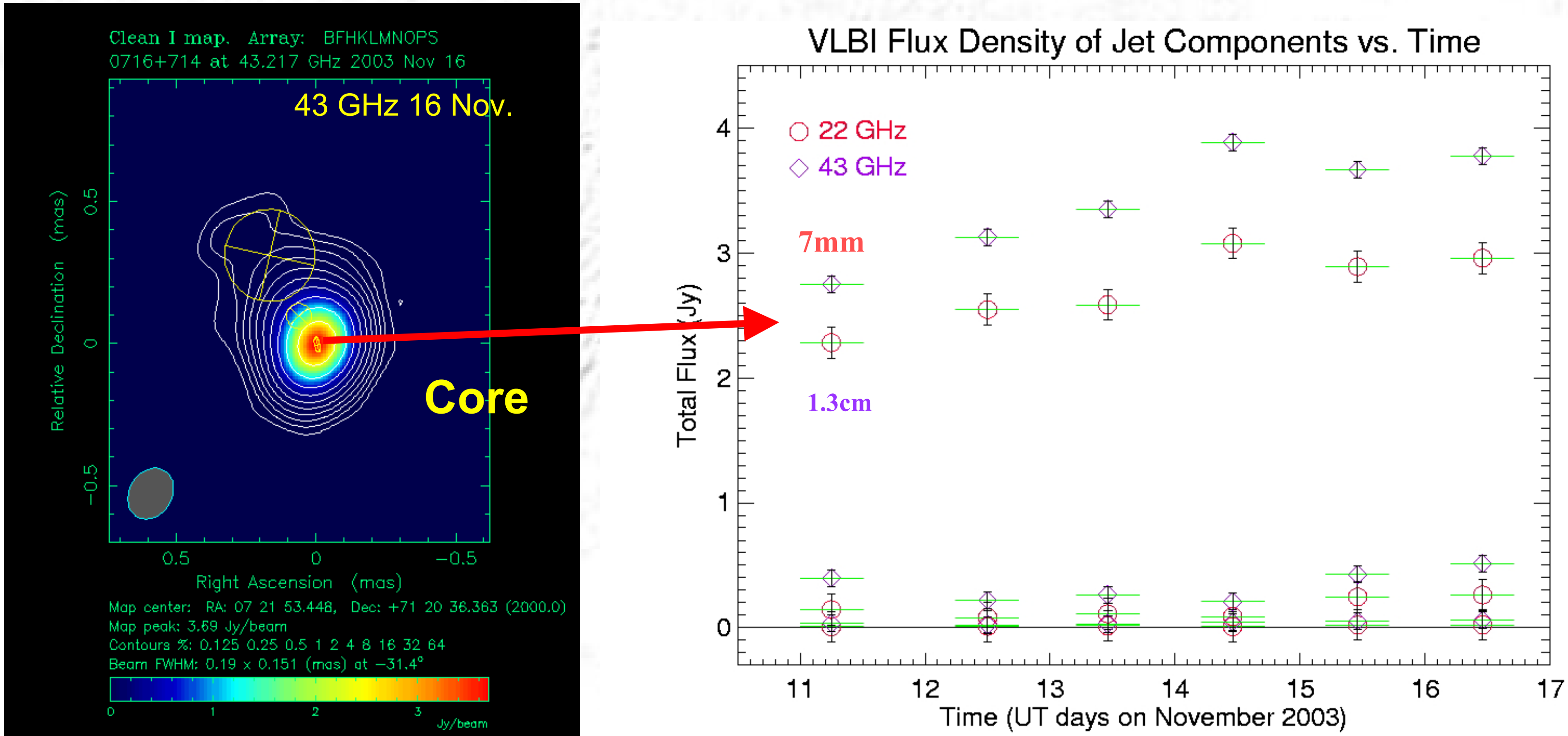

Agudo et al., in preparation

Bimodal behavior in the jet of 0735+178

Collaborators:

J. L. Gómez, D.C. Gabuzda, A.P. Marscher, S. G. Jorstad, A. Alberdi

- 0735+178 is a bright EGRET detected BL Lac object
- Observed during PhD
- 7 VLBI runs of 12 hours each from March 1996 to May 2000
- Observations at 5, 8.4, 15, 22 and 43 GHz
- In dual polarization mode
- Typical double bent structure (at 15-22 GHz)

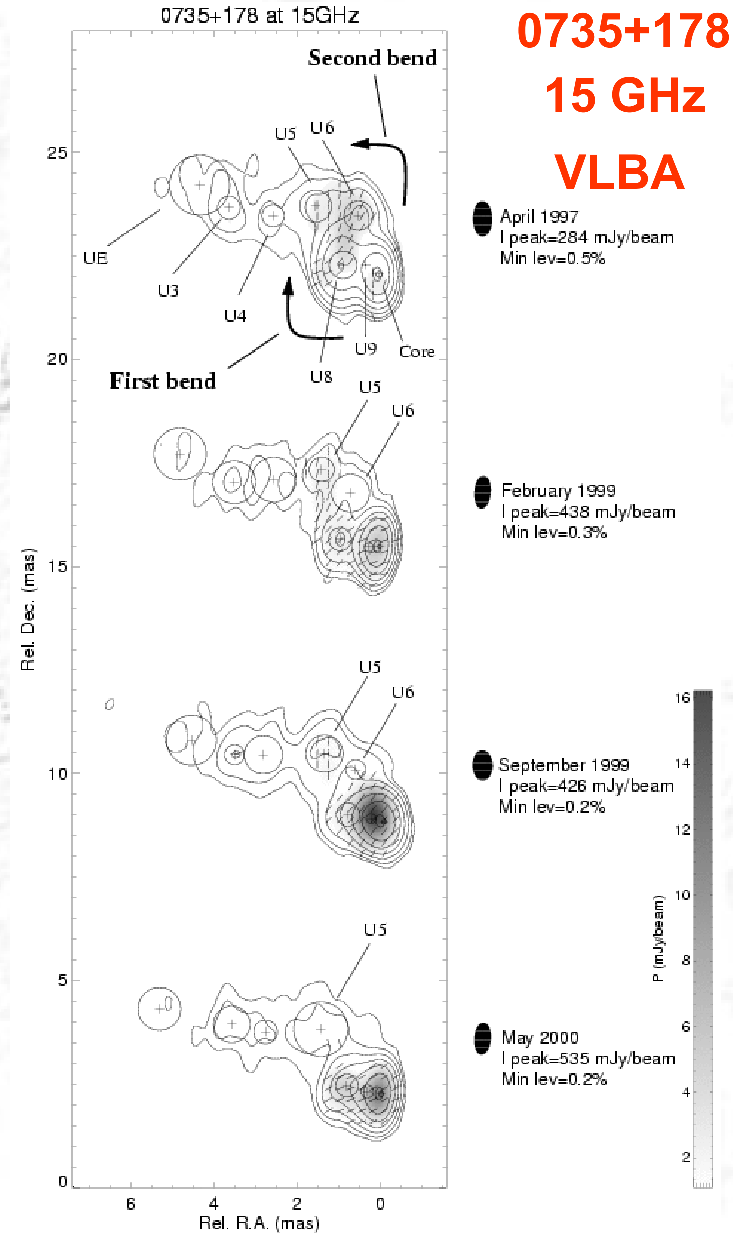

0735+178
15 GHz
VLBA

Agudo et al. A&A, accepted (astro-ph/0604543)

Bimodal behavior in the jet of 0735+178

Comparison with other observations => kinematic and structural properties of the jet influenced by the activity of the source

Time intervals of emission quiescence (from 1993 to 2000) => subluminal or slow superluminal jet features propagating through a twisted jet with two sharp bends of about 90°

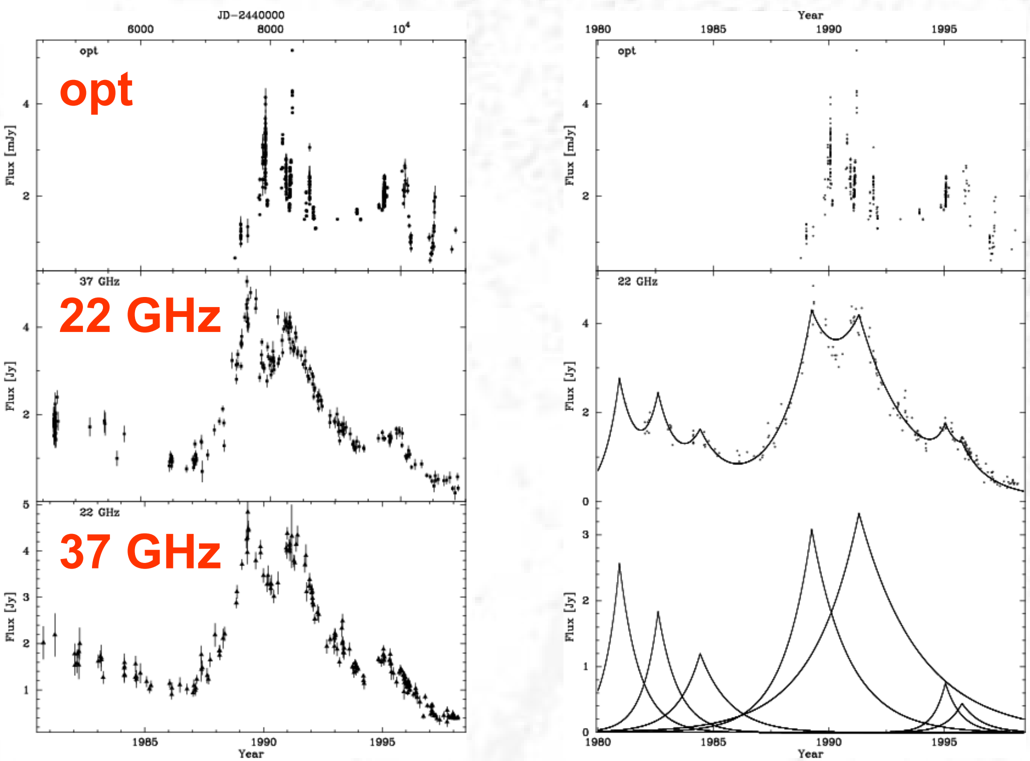

Hanski, Takalo, Valtaoja (2002)

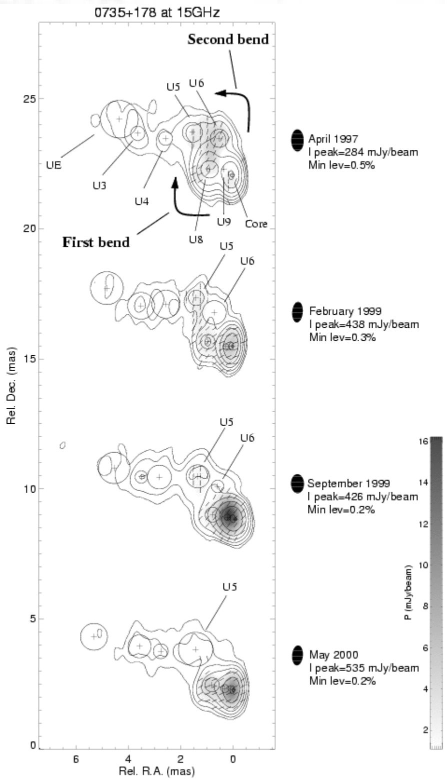

Agudo et al. (astro-ph/0604543)

Bimodal behavior in the jet of 0735+178

Time intervals of enhanced activity/emission (before 1993 and after 2000) => fast superluminal motion along a rectilinear jet.

Ciprini et al., A&A, submitted

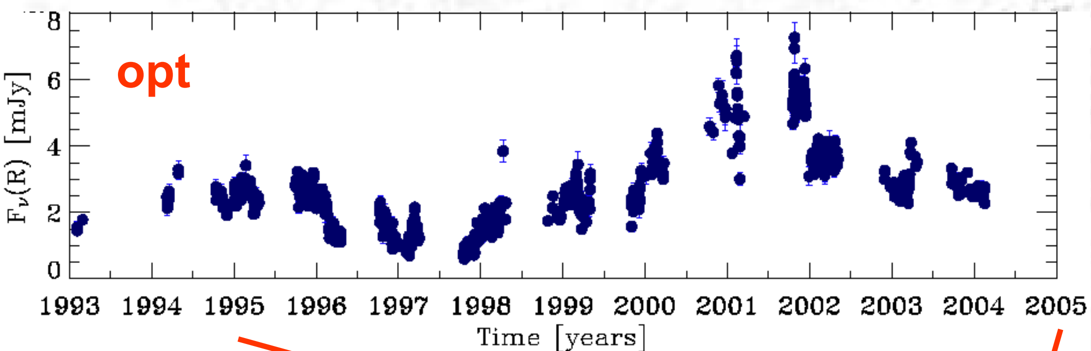

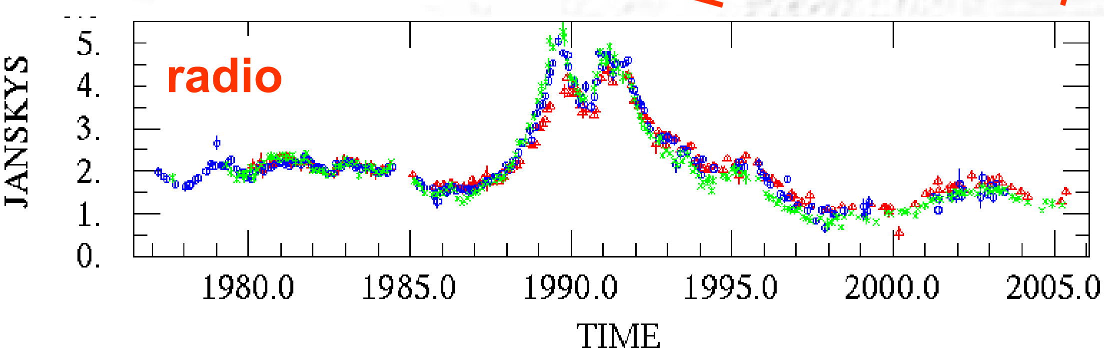

M. Aller, private communication

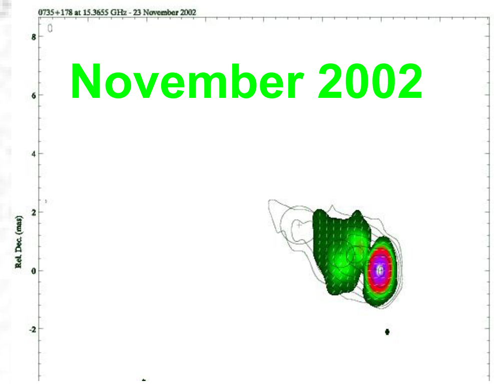

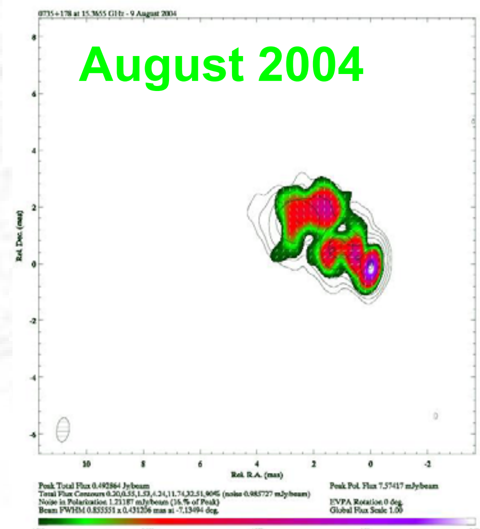

MOJAVE survey

0735+178

15 GHz

VLBA

Lister & Homan (2005)

Bimodal behavior in the jet of 0735+178

Evidence:

Low activity + weak emission + curved structure + slow motions

High activity + strong emission + linear structure + superluminal motions

Proposed interpretation:

A) Period of high activity => ejection of superluminal components (strong shocks)

Increase of the broad band emission (radio to optical)

Increase in momentum of the component

more rectilinear, quasi-ballistic, motion

B) Low activity periods => reveal the quiescent highly twisted jet => requires changing direction of ejection of the jet (otherwise we would expect the quiescent jet to follow the straight funnel left by the previous period of high activity)

Wobbling jet in NRAO 150

Collaborators:

J.A. Acosta, R. Barrena, P. Rodríguez-Gil

- Bright AGN
- Densely monitored in the radio-mm bands since the 70's
- Has been recently identified as a quasar at z=1.51 through NIR spectroscopy

NRAO 150 LIRIS on the 4.2m WHT 26th March 2005

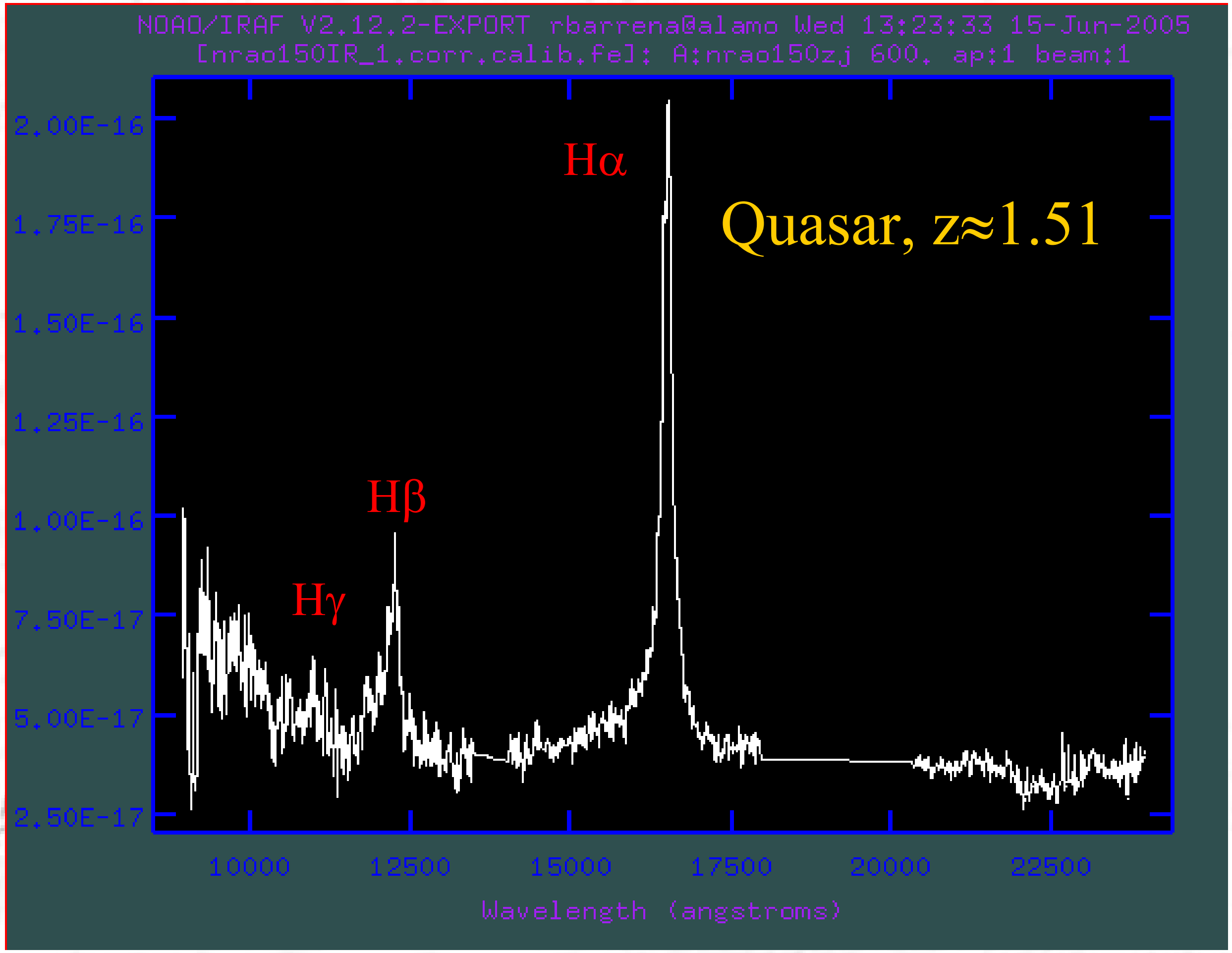

J.A. Acosta, I. Agudo, R. Barrena, P. Rodríguez-Gil, in preparation

Wobbling jet in NRAO 150

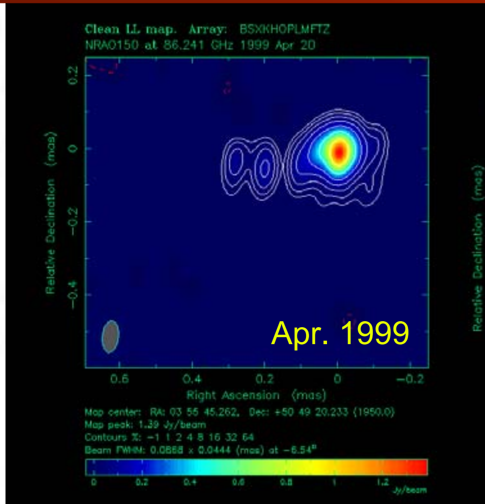

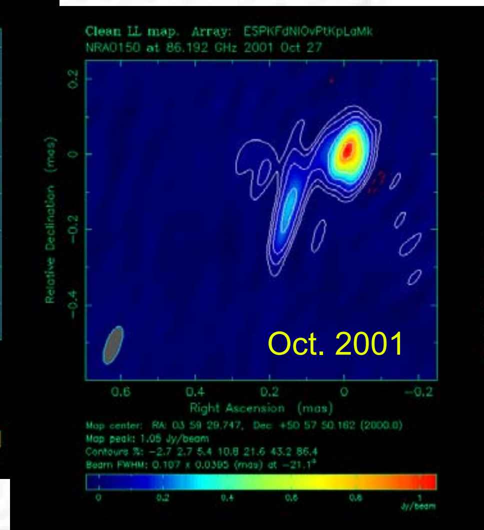

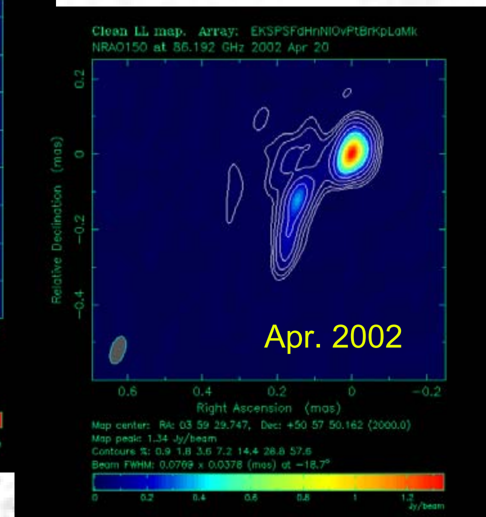

3 mm-VLBI images GMVA and CMVA

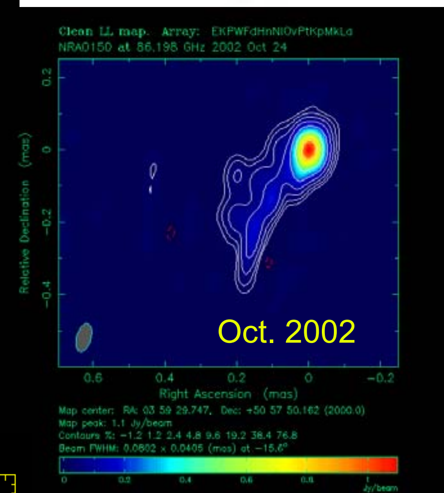

Collaborators:

T.P. Krichbaum, U. Bach, D. Graham, W. Alef, A. Pagels, A. Witzel, J.A. Zensus, M. Bremer, M. Grewing,

- Rotation at an angular speed of ~10º/yr
- The larger observed for an AGN jet up to now

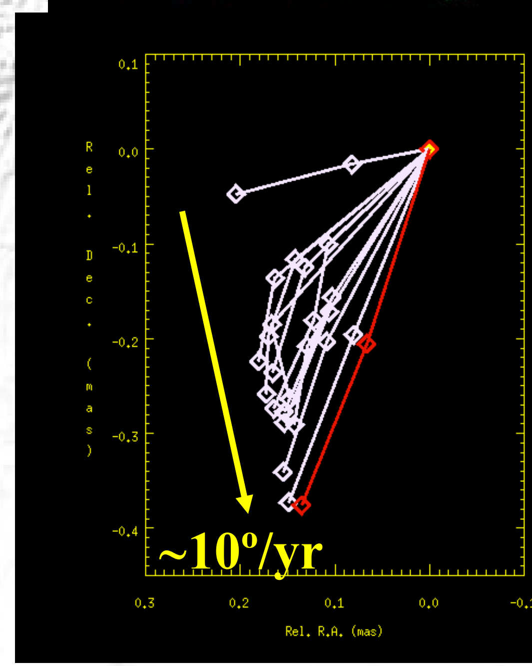

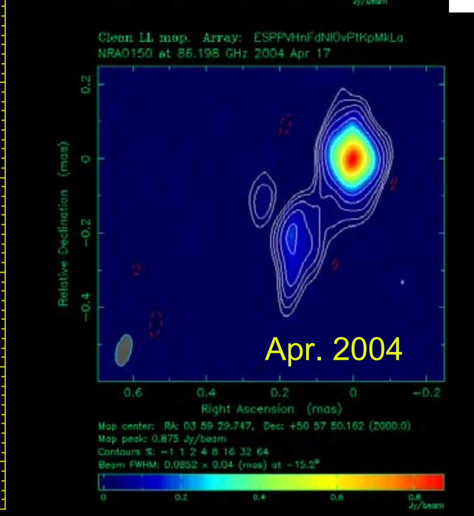

Agudo et al., in preparation

Wobbling jets in OJ287, 3C273, 3C345

Other famous blazars show clear evidence of inner jet wobbling

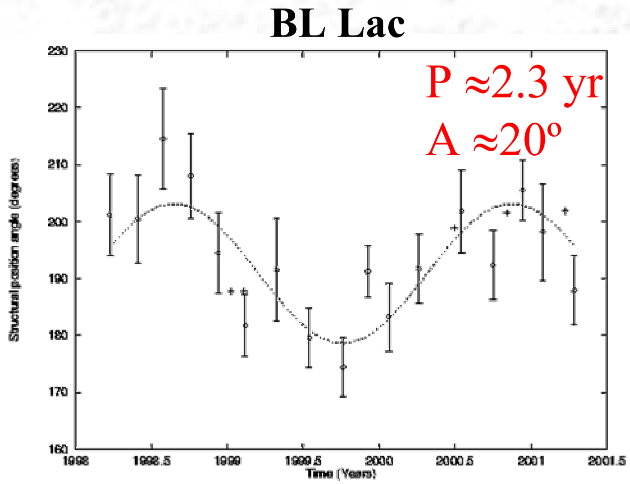

Stirling et al. (2003)

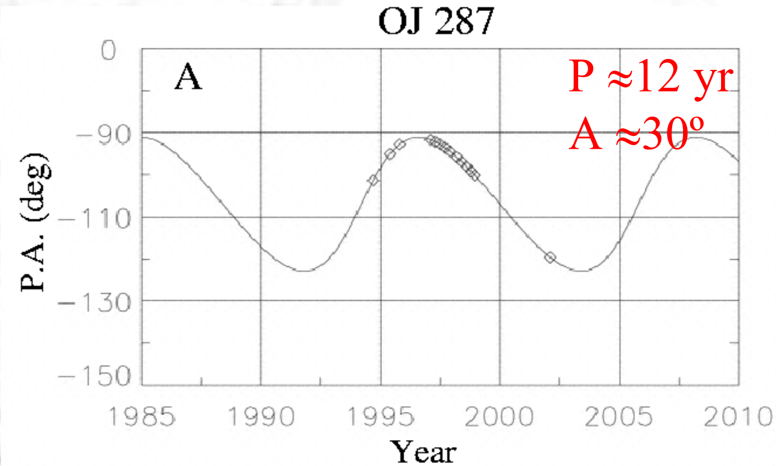

Tateyama & Kingham (2004)

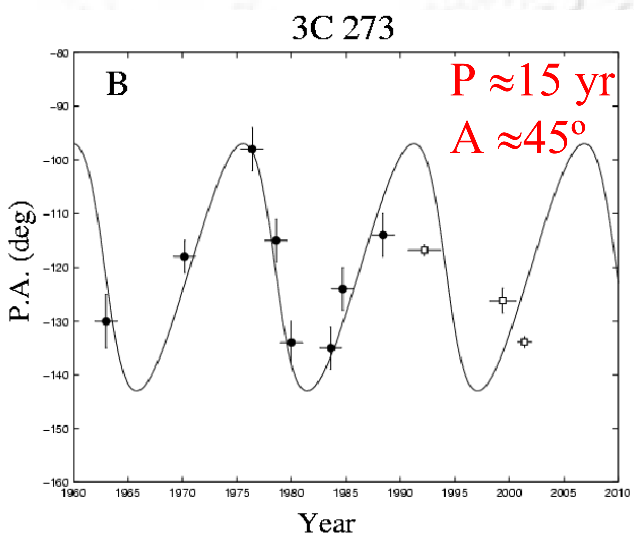

Savolainen et al. (2006)

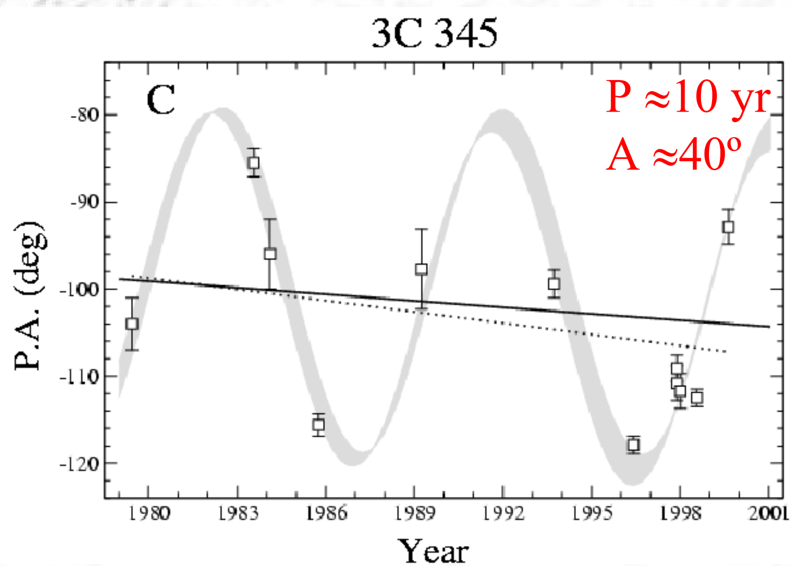

Lobanov & Roland (2005)

Wobbling jets in OJ287, 3C273, 3C345

- Wobbling is observed to be triggered in the innermost regions of the AGN (accretion disk or base of the jet)

- Can be caused by:

  A) disk precession

  B) orbital motion of the accretion system

  C) other kind of disk-jet instabilities (perturbed rotation of the jet flow around its axis)

- Disk precession driven by the presence of a massive companion is the preferred cause to model the source behaviour.

- But the other two causes are still valid and there is still no reason to rule out them

- Their triggering perturbations should related to fundamental parameters of the accretion system (a, disk ang. mom., density…)

Wobbling jets in OJ287, 3C273, 3C345

Collaborators:

A. Roy, J.L. Gómez, A. Lobanov, M. Perucho, A. Marscher, S. Jorstad, M. Roca-Sogorb, J. M. Martí

Study of the phenomenon can enhance our knowledge of SMBHs and their environments

We have proposed a monitoring of OJ287, 3C273 and 3C345 as part of a joint theoretical-numerical and observational program.

43 GHz polarimetric VLBA observations

Every 3-4 months

Astrometric mode (to identify possible absolute motions of the jet cores, which are usually assumed to be stationary)

The absolute position information should provide important clues about the cause of the wobbling

Proposal has been granted with the first 3 observing epochs

Wobbling jet in NRAO 150

Collaborators:

T.P. Krichbaum, U. Bach, A. Roy, J.L. Gómez, A. Witzel

- 3-5 % polarized
- Spot of no polarization emission close to the core
- Electric vector position angle perpendicular at opposite sides of the spot
- There is a clear polarization cancellation region close to the core

NRAO 150 at 43 GHz, VLBA

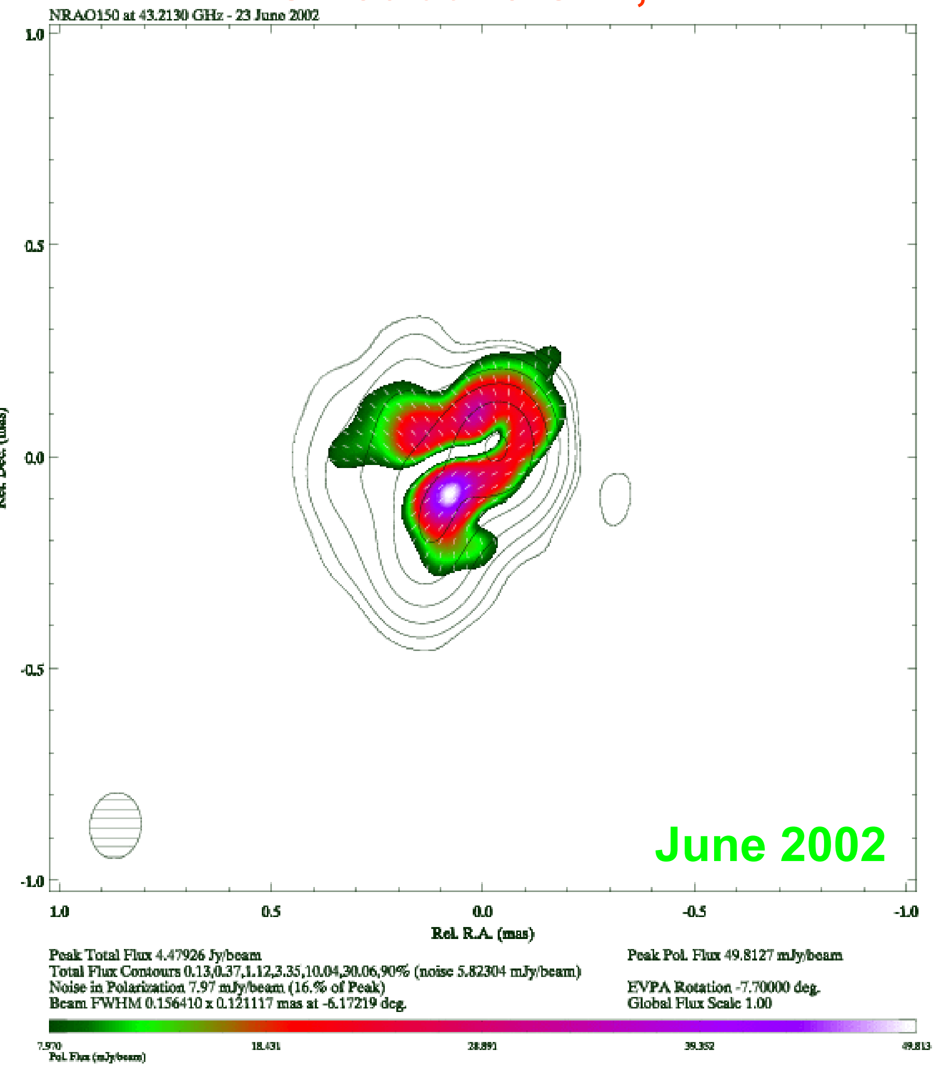

Agudo et al. in preparation

Wobbling jet in NRAO 150

Collaborators:

T.P. Krichbaum, U. Bach, A. Roy, J.L. Gómez, A. Witzel

- 3-5 % polarized
- Spot of no polarization emission close to the core
- Electric vector position angle perpendicular at opposite sides of the spot
- There is a clear polarization cancellation region close to the core

NRAO 150 at 43 GHz, VLBA

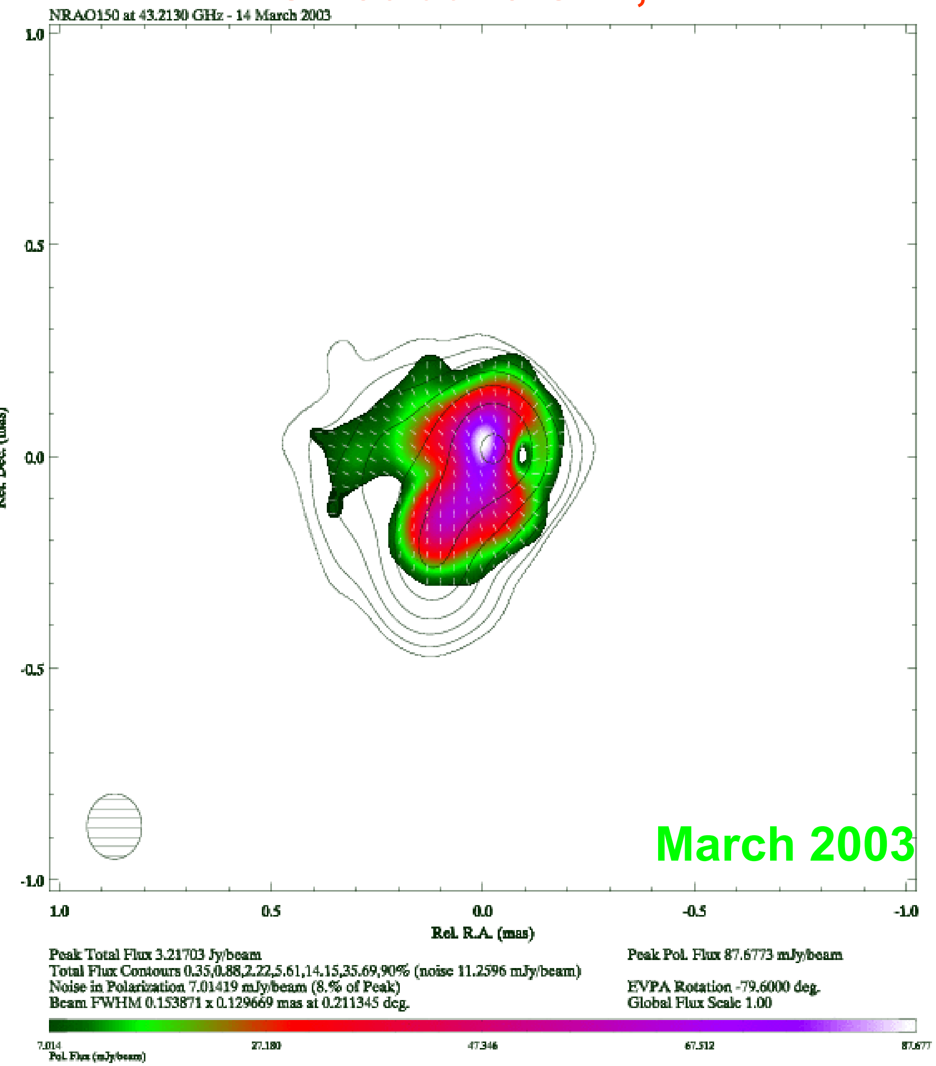

Agudo et al. in preparation

Wobbling jet in NRAO 150

Collaborators:

T.P. Krichbaum, U. Bach, A. Roy, J.L. Gómez, A. Witzel

- 3-5 % polarized
- Spot of no polarization emission close to the core
- Electric vector position angle perpendicular at opposite sides of the spot
- There is a clear polarization cancellation region close to the core

NRAO 150 at 43 GHz, VLBA

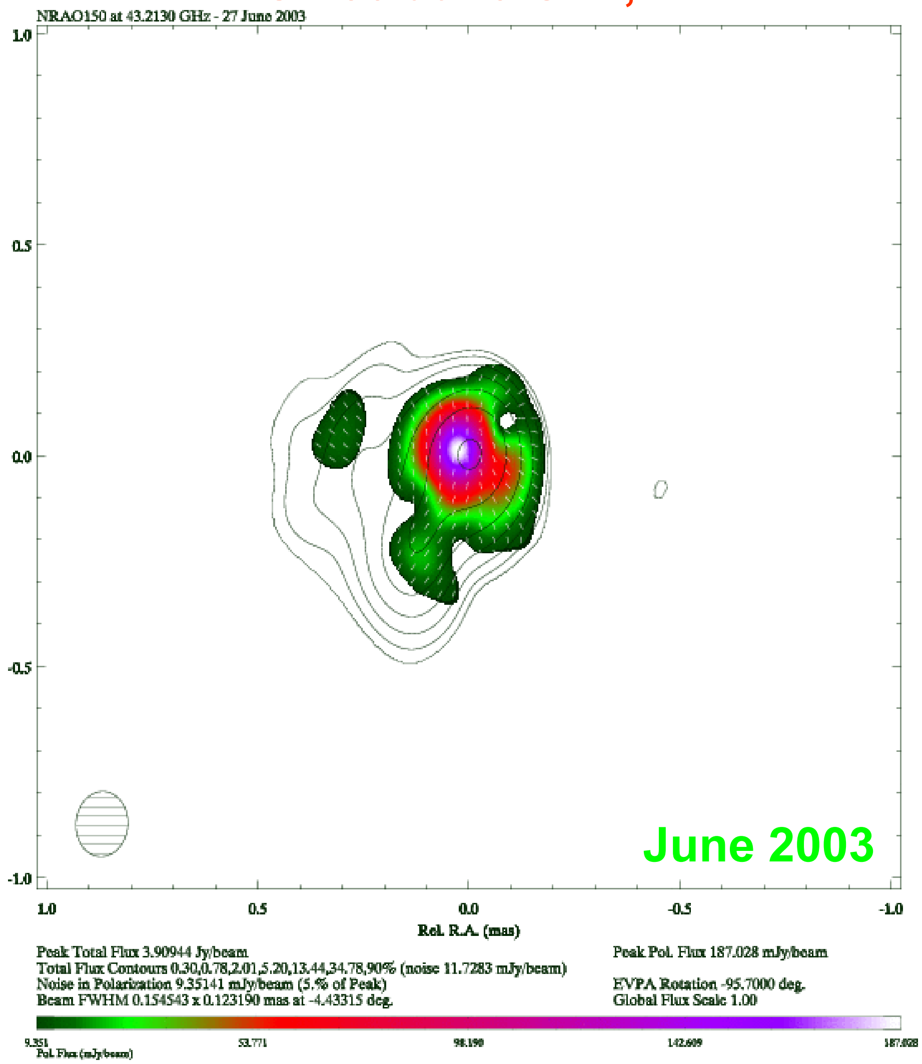

Agudo et al. in preparation

Wobbling jet in NRAO 150

Collaborators:

T.P. Krichbaum, U. Bach, A. Roy, J.L. Gómez, A. Witzel

- 3-5 % polarized
- Spot of no polarization emission close to the core
- Electric vector position angle perpendicular at opposite sides of the spot
- There is a clear polarization cancellation region close to the core

NRAO 150 at 43 GHz, VLBA

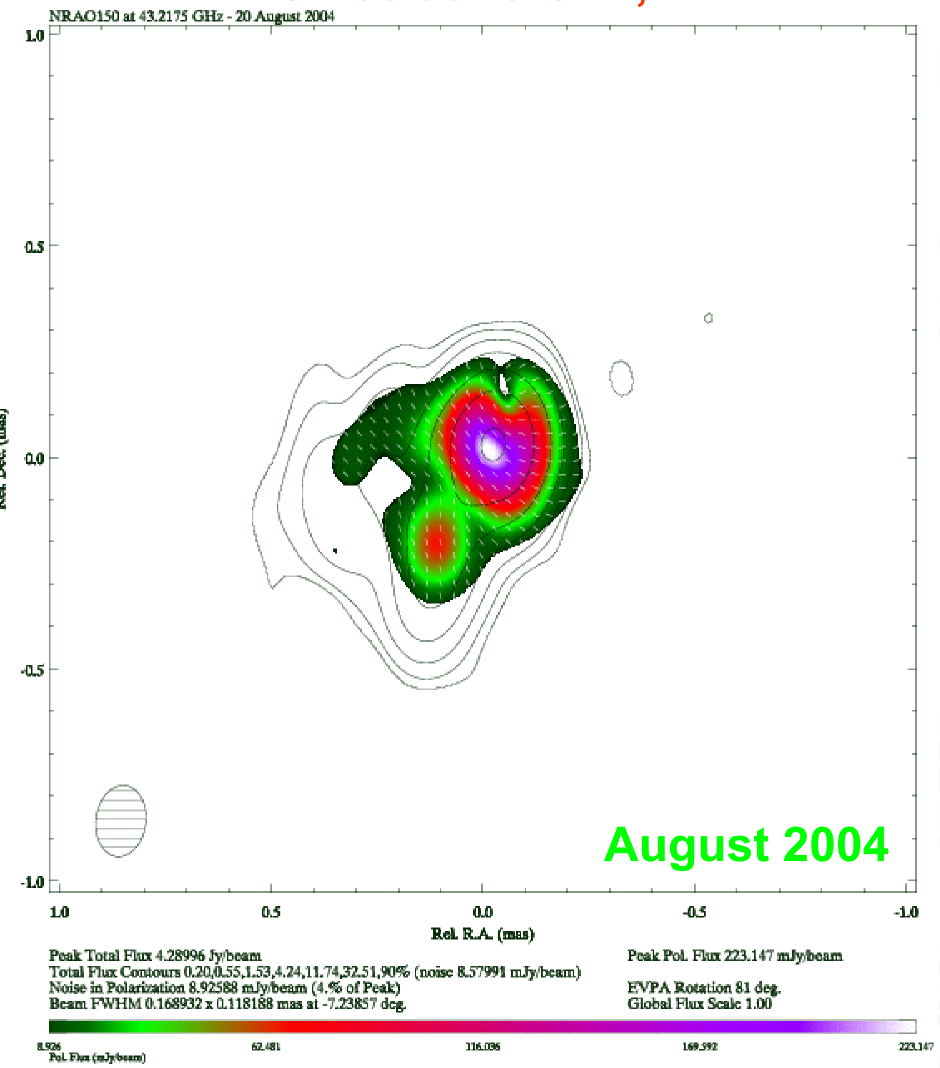

August 2004

Agudo et al. in preparation

Wobbling jet in NRAO 150

Collaborators:

T.P. Krichbaum, U. Bach, A. Roy, J.L. Gómez, A. Witzel

- 3-5 % polarized
- Spot of no polarization emission close to the core
- Electric vector position angle perpendicular at opposite sides of the spot
- There is a clear polarization cancellation region close to the core

NRAO 150 at 43 GHz, VLBA

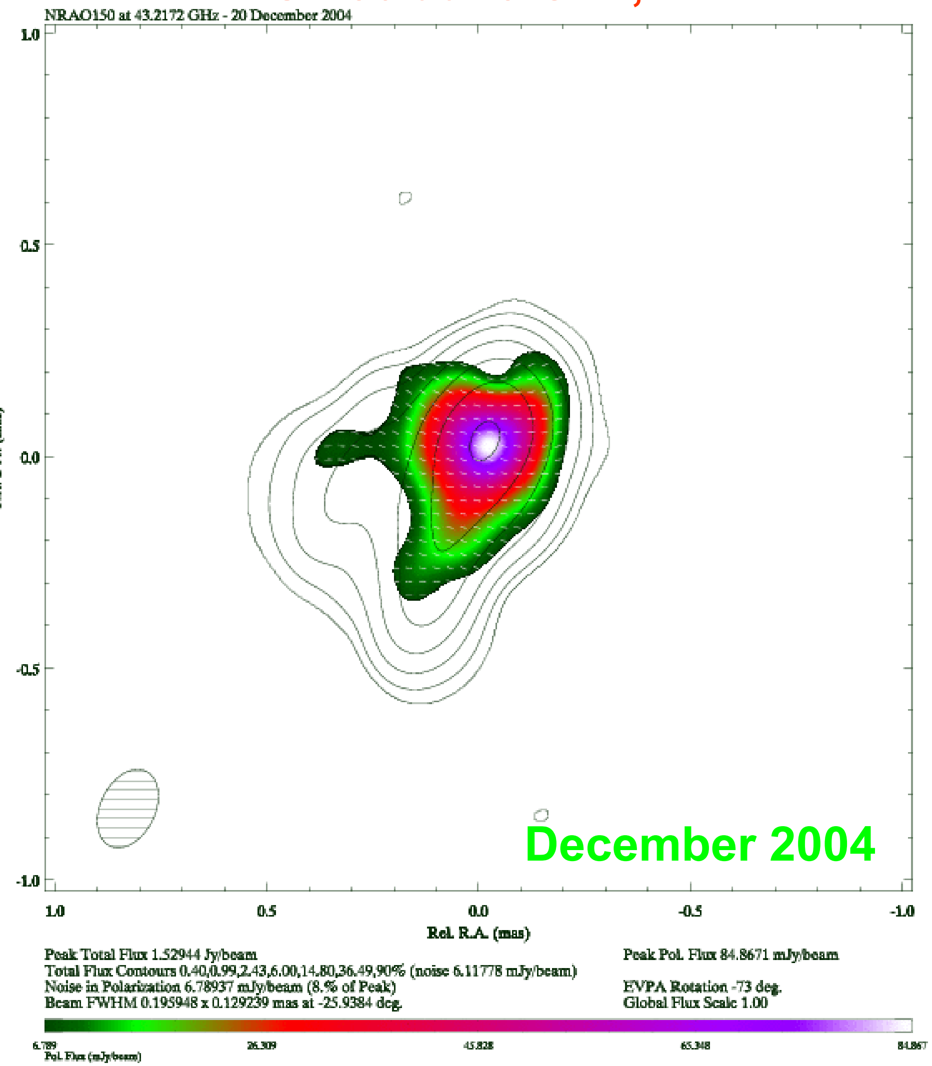

Agudo et al. in preparation

Wobbling jet in NRAO 150

Collaborators:

T.P. Krichbaum, U. Bach, A. Roy, J.L. Gómez, A. Witzel

- 3-5 % polarized
- Spot of no polarization emission close to the core
- Electric vector position angle perpendicular at opposite sides of the spot
- There is a clear polarization cancellation region close to the core

NRAO 150 at 43 GHz, VLBA

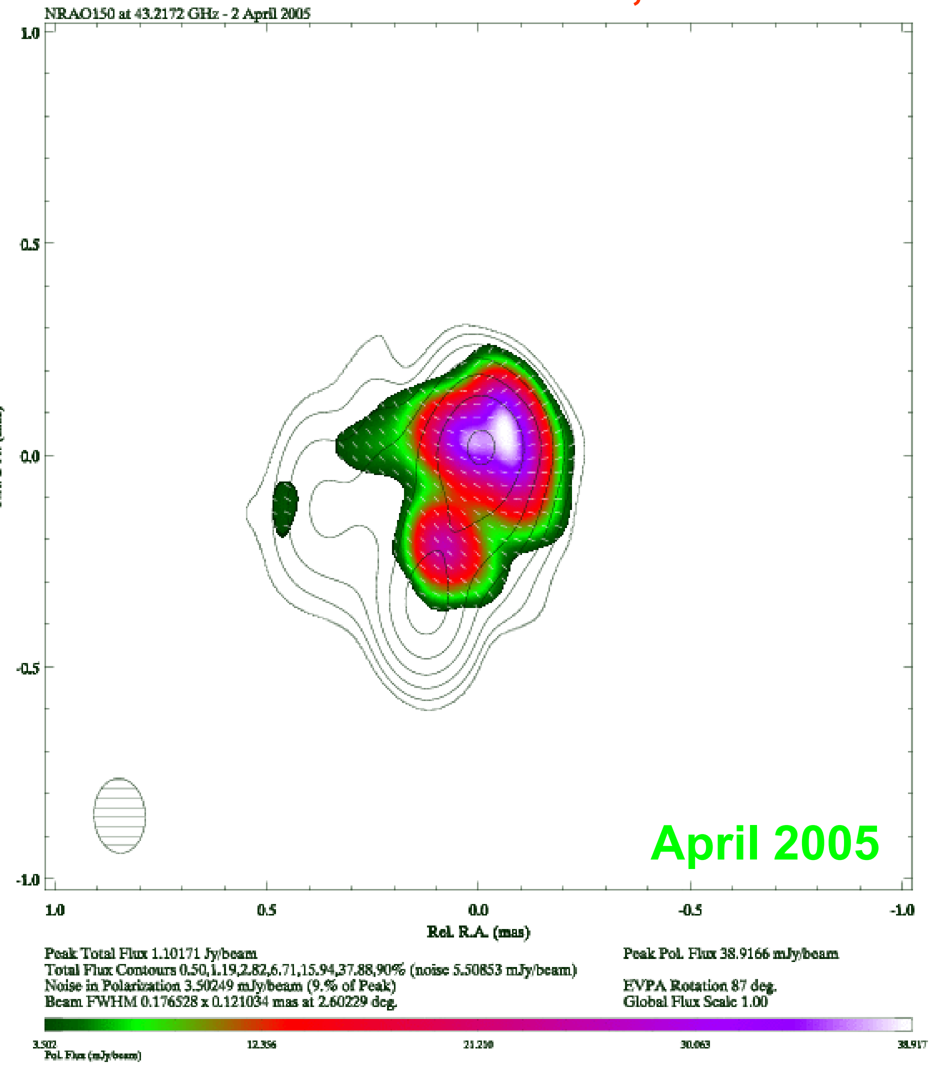

Agudo et al. in preparation

Wobbling jet in NRAO 150

Collaborators:

T.P. Krichbaum, U. Bach, A. Roy, J.L. Gómez, A. Witzel

- Rapid rotation of the polarization cancellation region with regard to the core

- 360º turn in 3-5 yr

- Possible causes for the rotation of the cancellation region are:

  - Time dependent twisting of the inner jet structure (preferred)

  - Motion of a strong wave on a twisted path with the **B** perpendicular to the one of the jet

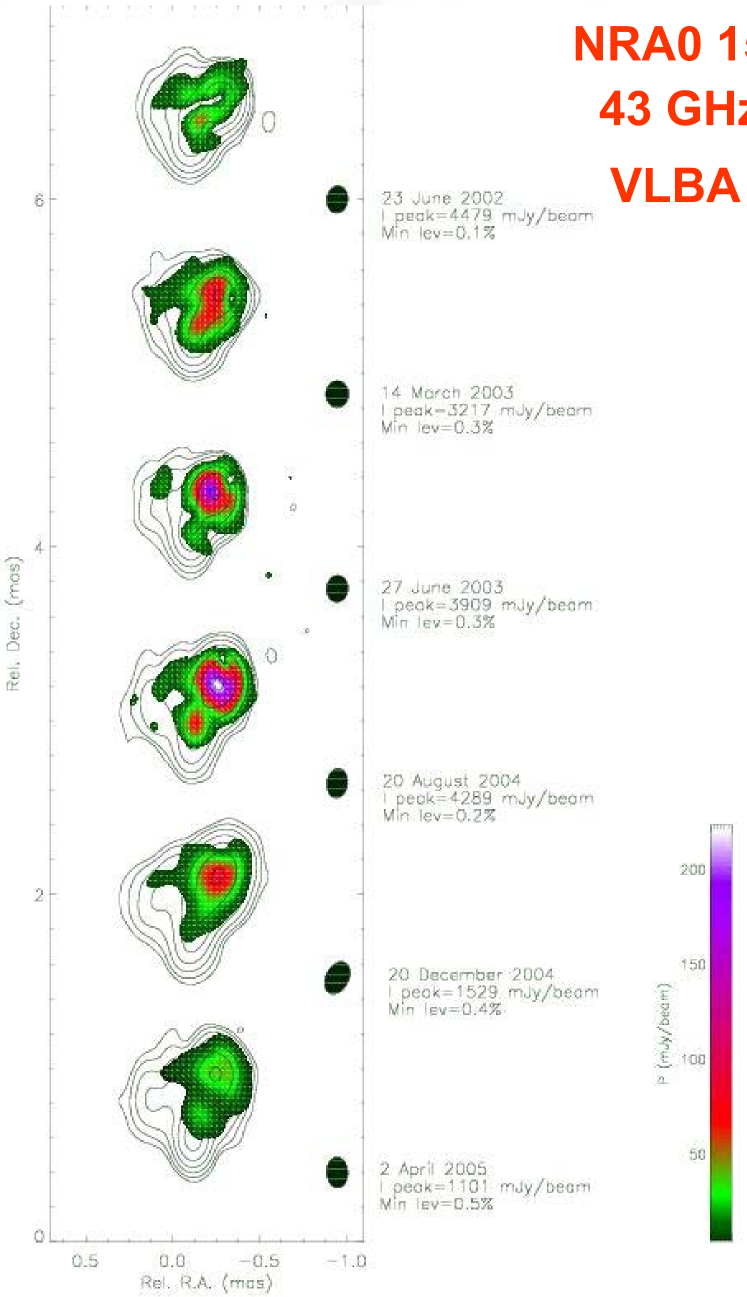

NRA0 150
43 GHz
VLBA

3mm polarimetric monitoring of OJ287

Collaborators:

T. Krichbaum, C. Thum, H. Ungerechts, H. Wiesemeyer

- New observations of OJ287

- OJ287 has shown "almost" periodic double flares every 11.6 to 11.8 yr during the last 100 yr

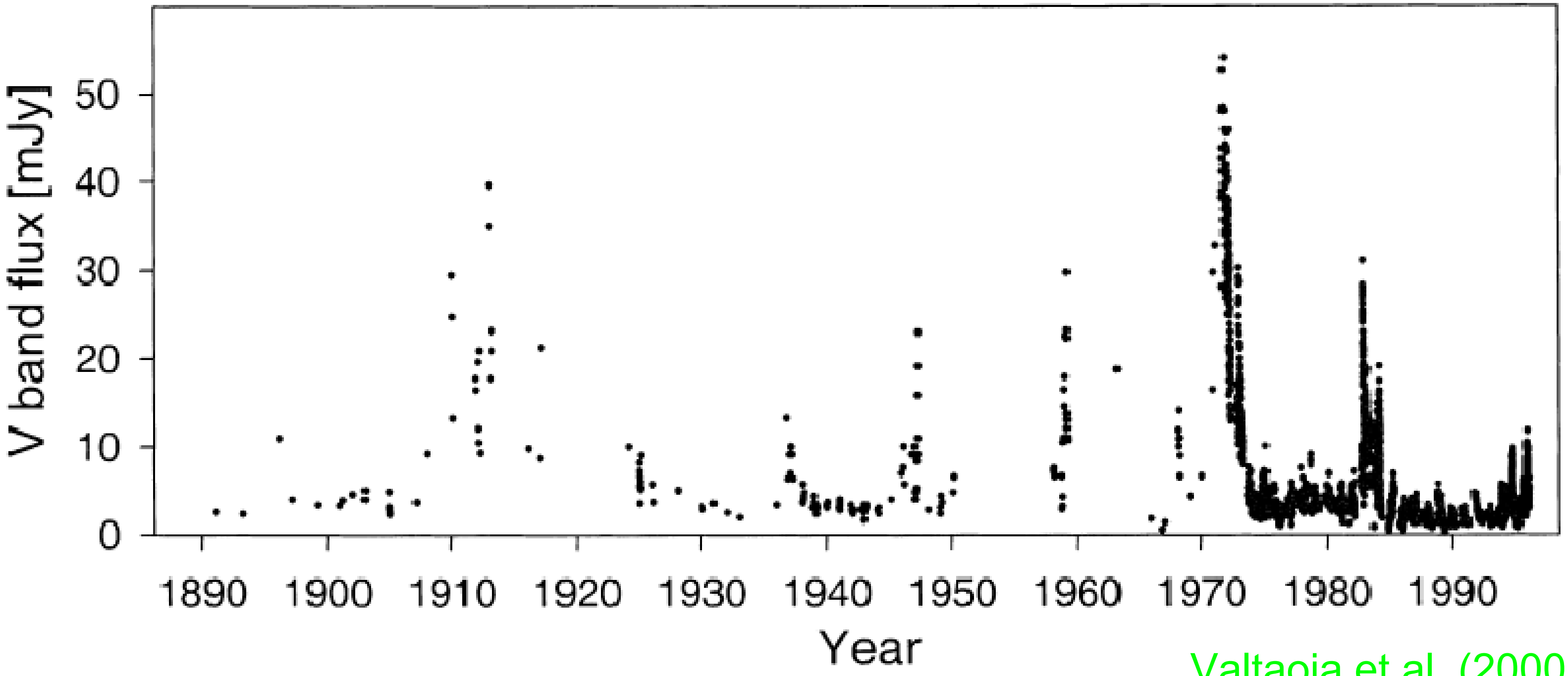

Valtaoja et al. (2000)

3mm polarimetric monitoring of OJ287

Collaborators:

T. Krichbaum, C. Thum, H. Ungerechts, H. Wiesemeyer

- New observations of OJ287

- First optical flare not matched to the radio behaviour but the second is

- Evidences of this during last two double flares, but not good correlation

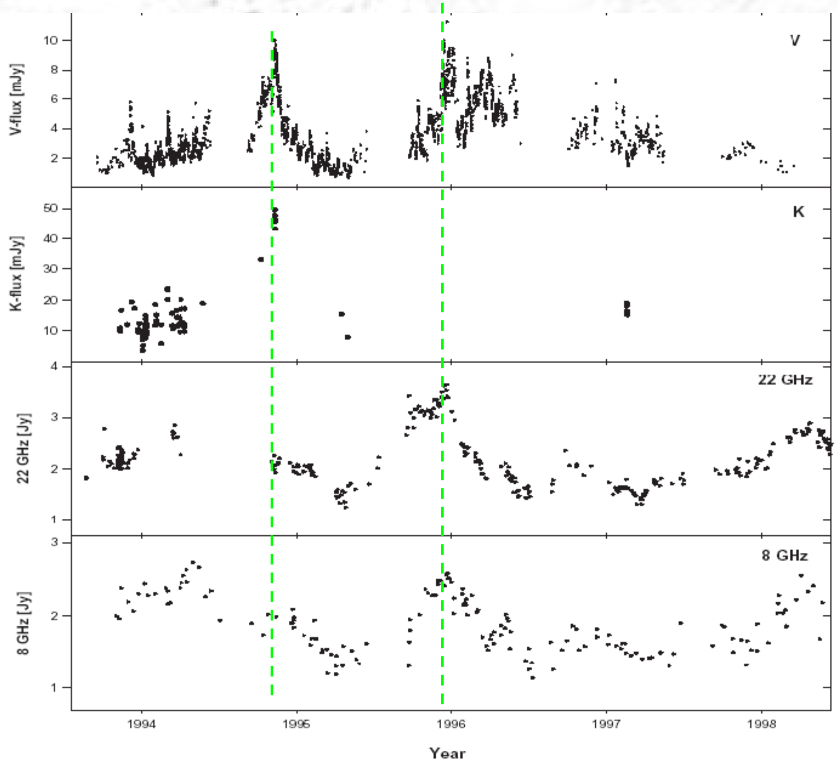

Pursimo et al. (2000)

3mm polarimetric monitoring of OJ287

Collaborators:

T. Krichbaum, C. Thum, H. Ungerechts, H. Wiesemeyer

- New observations of OJ287

- Linear polarization weak (<5%) and weakly variable during both last flares

- Polarization angle swing by 90º at radio and R band in 94-95 flare, but not on 83-84

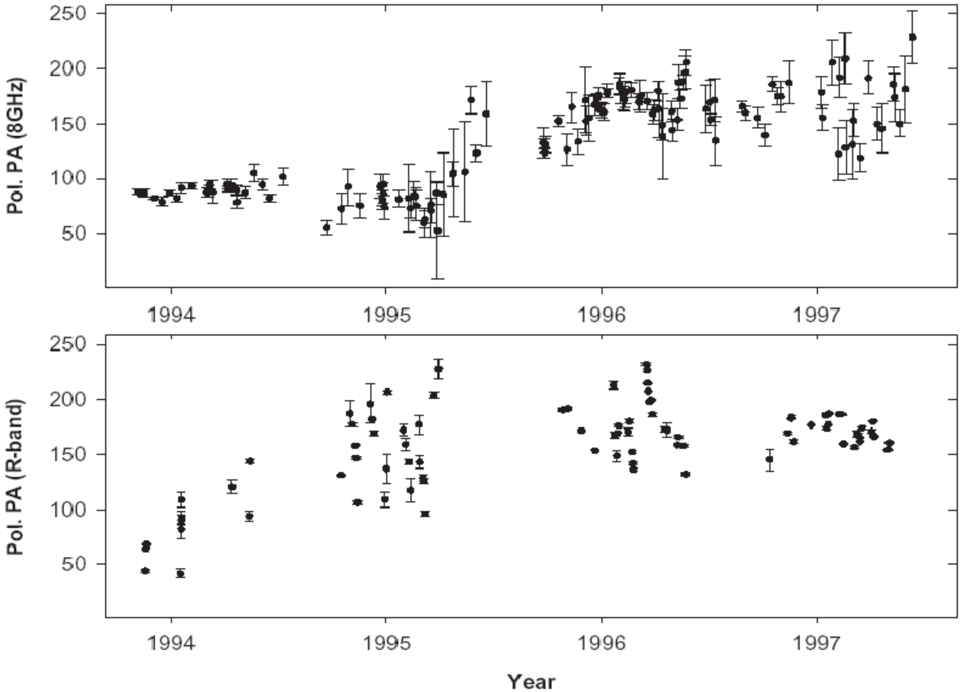

Pursimo et al. (2000)

3mm polarimetric monitoring of OJ287

Collaborators:

T. Krichbaum, C. Thum, H. Ungerechts, H. Wiesemeyer

To help providing new data to fix or rule out the models and to help establishing the possible casual connection between the second optical flare and the radio flares

We have proposed a monitoring of OJ287 with the new IRAM 30m polarimeter (XPOL)

86 GHz measurements every 15 days during the next 6 months (have been already approved)

4-Stokes parameters => circ. pol. Densely time sampled for an AGN for the first time at 3mm

Our observations will also support the interp. of mm-VLBI monitorings

NOTE: OJ287 displayed ~6Jy at 3mm 3 days ago

Summary and conclusions

• Blazars as 0716+714 can have abrupt variability in the mm range which have to be intrinsic to the source

• They can also largely exceed the IC limit for the apparent Tb without producing IC catastrophes (relativistic beaming easily explains the lack of catastrophes)

• There is one source (0735+178) for which the brightness, the jet structure and its kinematics seem to be well related:

Low activity + weak emission + curved structure + slow motions

High activity + strong emission + linear structure + superluminal motions

• Jet curvatures in blazars seem to be produced in their innermost regions (most probably close to or in the formation region)

• An increasing number of blazars present periodic or quasi-periodic jet wobblings

• This phenomenon should be tied to the intrinsic properties of the accretion system (where the jets are formed)

Welcome talk by Kanaris Tsinganos, node leader of the Athens team, to 7th ENIGMA mtg in the Hydra Island, on why Hydra was chosen to be the site of this mtg, its relation to the Sphinx (the emblem of ENIGMA network) and also the Hydra constellation.

The 3 reasons to have the 7th ENIGMA meeting in Hydra

Further, to get you into a "Greek" mood, we invite you to think about the following:
"Why did the Greek team choose the island of Hydra for the 7th Enigma meeting?"
The first complete answer to be sent to us by email, will earn an attractive price.
(from the webpage of the 7th Enigma mtg)

1. ?
2. ?
3. ?

ENIGMA

is the acronym of our European Network for the Investigation of Galactic nuclei via Multifrequency Analysis.

An enigma is a riddle. In Boeotian Thebes of ancient Greece the winged sphinx posed a riddle taught her by the Muses .

Σφίγξ

In modern times Blazars pose many riddles to astrophysicists working in all branches of astronomy.

Sphinx is a symbol of enigmatic behaviour, as is frequently displayed by Blazars. The sphinx is thus a symbol for the riddles posed by Blazars which are tackled in our network ENIGMA, which started on November 1, 2002 and deals with investigations of the structure and radiation processes of Quasars through multifrequency studies.

Σφίγξ

Sphinx. Apulie. "Peintre de Schultess", vers 340 avant J.-C. Photo © Maicar Förlag - GML

Further, to get you into a "Greek" mood, we invite you to think about the following:
"Why did the Greek team choose the island of Hydra for the 7th Enigma meeting?"
The first complete answer to be sent to us by email, will earn an attractive price.
(from the webpage of the 7th Enigma mtg)

Σφίγξ

.. + the 7th ENIGMA mtg participants

Sphinx was one of the ill-fated offsprings of the monsters Typhoon (which breathed fire from a hundred venomous heads and was eventually pinned by Zeus under Aetna) and Echidna (which had a beautiful numph's head and the body of a giant serpent). Other offsprings of Echidna were :

The Nemean Lion, Ladon, Chimera, Cerberus and… ????

Tellus. Romersk, 9 f. Kr. Marmor, Ara Pacis. Photo ©Maicar Förlag-GML

Echidna: was the black-eyed daughter of Tartarus and Gaea. She was half-woman, half-serpent, and mated with her brother, the monster Typhoon.
Echidna lived wih Typhon in Asia. She once stole the horses of Heracles, and would not return them until he slept with her. From this the triplets Agathyrsus, Gelanus and Scythes - the king of the Scythians - were born.

Typhoon : was born by Gaea as a last effort, to prevent Olympians from gaining power over her children the Titans. He was a fire breathing dragon with a hundred heads that never rested, but lost a fierce battle with Zeus. It came close to succeeding, setting most of the gods to flight and capturing Zeus but Hermes was able to free Zeus. Zeus was then able to dispatch Typhoon with his lightning bolts - Typhoon was buried under Mount Etna in Sicily.

Cerberus is another offspring of Typhoon and Echidna. It was a three headed dog with a snake tail and snake heads proturding from his back. He guarded the entrance to the underworld, allowing the dead to enter but, never to leave. One of the few living mortals to get past Cerberus was Orpheus who charmed it to sleep with his song during his attempt to rescue Eurydice from death. Fetching Cerberus from the underworld and displaying him to King Eurystheus was the last labor of Heracles.

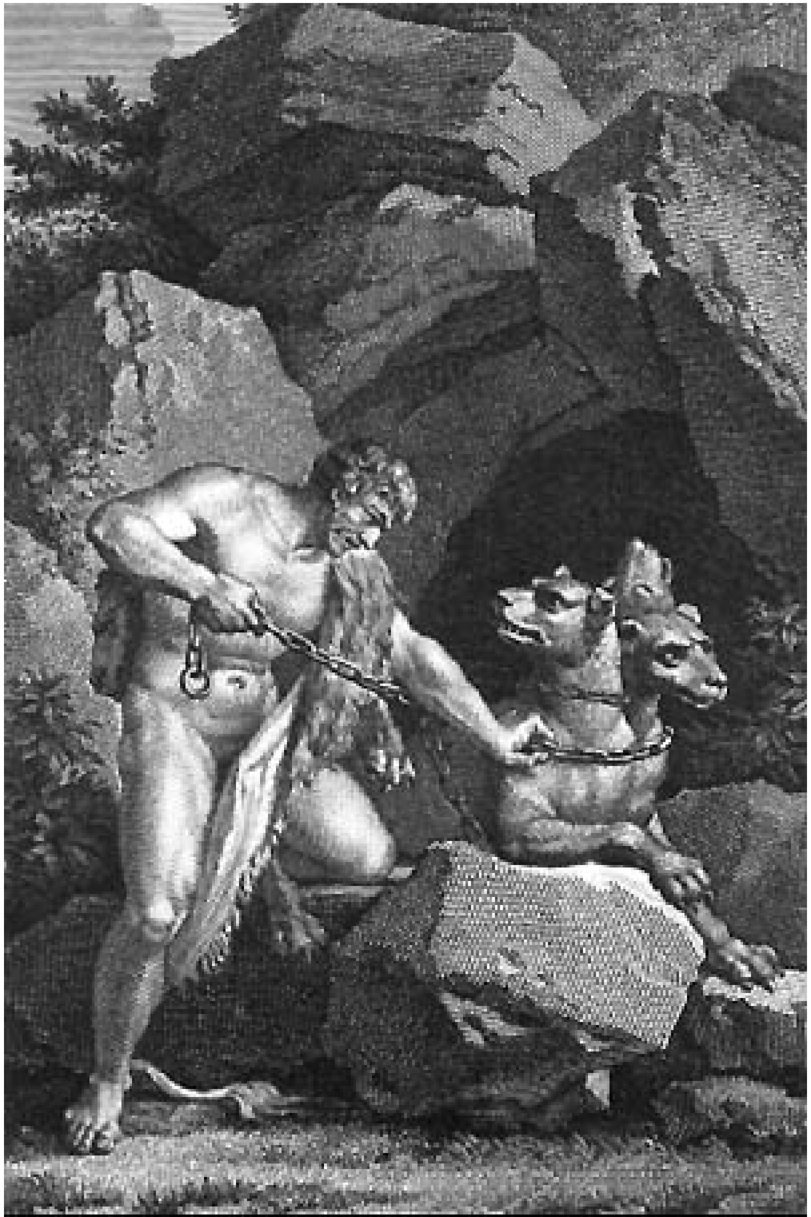

J.-J.-F. Le Barbier the Elder 1738-1826: Heracles & Cerberus.
Photo © Maicar Förlag - GML.

Ladon: was a many-headed dragon who watched over the garden of the Hesperides. When Heracles as one of his Labors sought the golden apples in the keeping of these Daughters of the Evening, he had to enlist the aid of the Titan Atlas. Atlas was willing to steal the apples if Heracles relieved him of his burden of holding up the heavens, but only if the hero first did something about Ladon. Heracles killed the dragon with an arrow over the garden wall.

Ἑσπερίδες

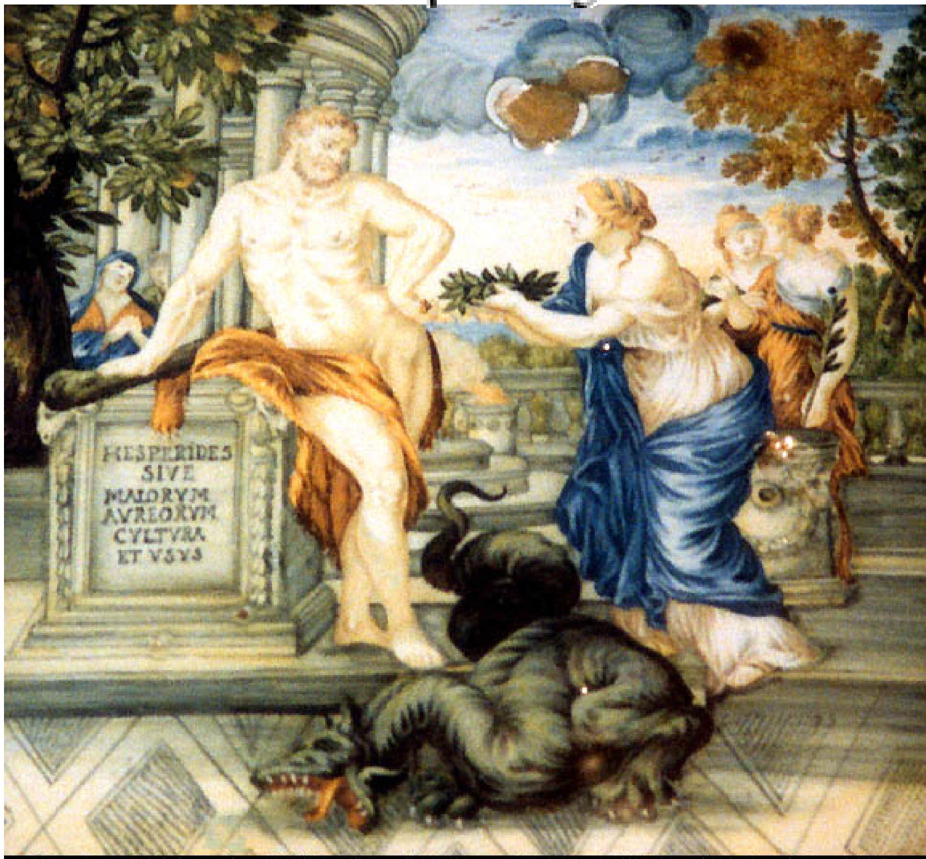

Heracles and the Hesperides. Maioliche di Castelli d'Abruzzo del XVII e XVIII. Photo © Maicar Förlag - GML

The **Nemean Lion** was also one of the many offspring of half-woman and half-serpent Echidna and her husband, the 100-headed Typhoon. It lived in Argolis terrifying people. The skin of the lion was impenetrable, so when Hercules tried to shoot it from a distance, he failed to kill it. It wasn't until Hercules used his olive-wood club to stun the beast, that he was then able to strangle it to death. Hercules decided to wear the Nemean Lion skin as protection, but couldn't skin the animal until he took one of the Nemean Lion's own claws to rip up the skin.

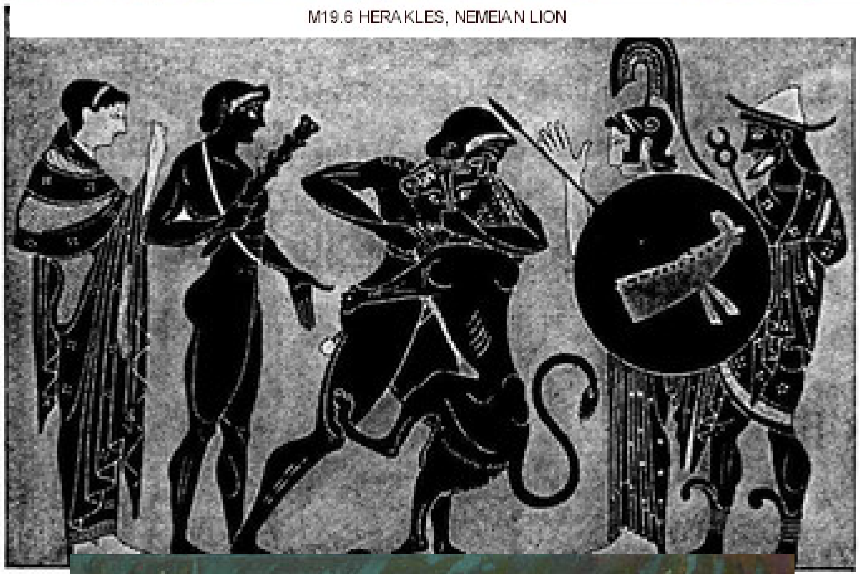

Chimaera:

Spawned by Typhoons and Echidna, the Chimaera had three heads - lion, goat, and snake. Its body was also mixed having the front part of a lion, middle of a goat, and snake for a tail. It breathed fire. It ravaged Lycia, killing cattle and setting fires until it was killed by Bellerophon.

Johan Nepomuk Schaller 1777-1842: Bellerophon in kampf mit Chimaira.
Photo © Maicar Förlag - GML

Terracotta relief. Bellerophon and the Chimaera. Melos about 450 BC. Photo © Maicar Förlag - GML

When King Laius 1 of Thebes was murdered, along with his herald, by an unknown in a Phocian road, the king's brother-in-law Creon 2 came to power. It is during this first regency of Creon 2 that the Sphinx came to Boeotia and Thebes, some say sent by Hera, others by Hades, and systematically started ravaging the fields and gobbling up people.
The Sphinx had the face of a woman, the breast, feet and tail of a lion, and the wings of a bird. She had learned a riddle from the Muses, which she chanted in inharmonious songs, and sitting on a nearby mountain, propounded it to any Theban willing to take the risk of solving it. As she declared that she would not depart unless anyone interpreted her riddle, Creon 2, in accordance with an oracle, issued a proclamation promising that he would give the kingdom of Thebes and his sister Iocaste in marriage to the person solving the riddle of the Sphinx.

"What is that beeing which has one voice and yet becomes four-footed (in the morning), two-footed (at noon) and three-footed (in the afternoon) ?" [Apollodorus]

When many had already perished, Oedipus, having heard the proclamation, came to Thebes, and meeting the Sphinx, gave the right answer, declaring that the riddle referred to man; for as a little child he is four-footed, as an adult two-footed, and as an old man he uses a staff as a third limb.
The Sphinx kept her promise, for on hearing the solution to her riddle, she threw herself from the citadel and died. In this way Oedipus became king of Thebes, and by marrying his own mother Queen Iocasti, he unwittingly fulfilled the oracles that had declared that he would kill his father and lie with his mother.

Rudolph Tegner, 1873-1950: Oedipus and Antigone. Photo ©Maicar Förlag-GML

Further, to get you into a "Greek" mood, we invite you to think about the following:
"Why did the Greek team choose the island of Hydra for the 7th Enigma meeting?"
The first complete answer to be sent to us by email, will earn an attractive price.

Σφίγξ

.. + the 7th ENIGMA mtg participants

Sphinx was one of the ill-fated offsprings of the monsters Typhoon (which breathed fire from a hundred venomous heads and was eventually pinned by Zeus under Aetna) and Echidna (which had a beautiful numph’s head and the body of a giant serpent). Other offsprings of Echidna were :

The Nemean Lion, Ladon, Chimera, Cerberus and… Hydra !

The 3 reasons to have the 7th ENIGMA meeting in Hydra

1. Herculean efforts are needed to solve the pbs posed by the Monstrous AGNs

2. Hydra (island) is one of the smallest islands on EARTH but in the heavens is the largest constellation

3. Hydra was the sister of Sphinx, the emblem of ENIGMA

Hydra: in Greek mythology was a many-headed water serpent also an offspring of Typhon and Echidna. When one of its heads was cut off, two new heads appeared. The second labor of Hercules was to kill the monster. He did so by burning the neck after cutting off each head assisted by Iolaos. The Hydra which lived in the swamps near to the ancient city of Lerna in Argolis.

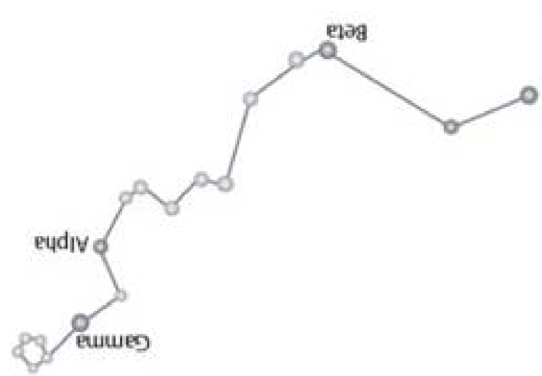

The Hydra is the largest constellation in the heavens !

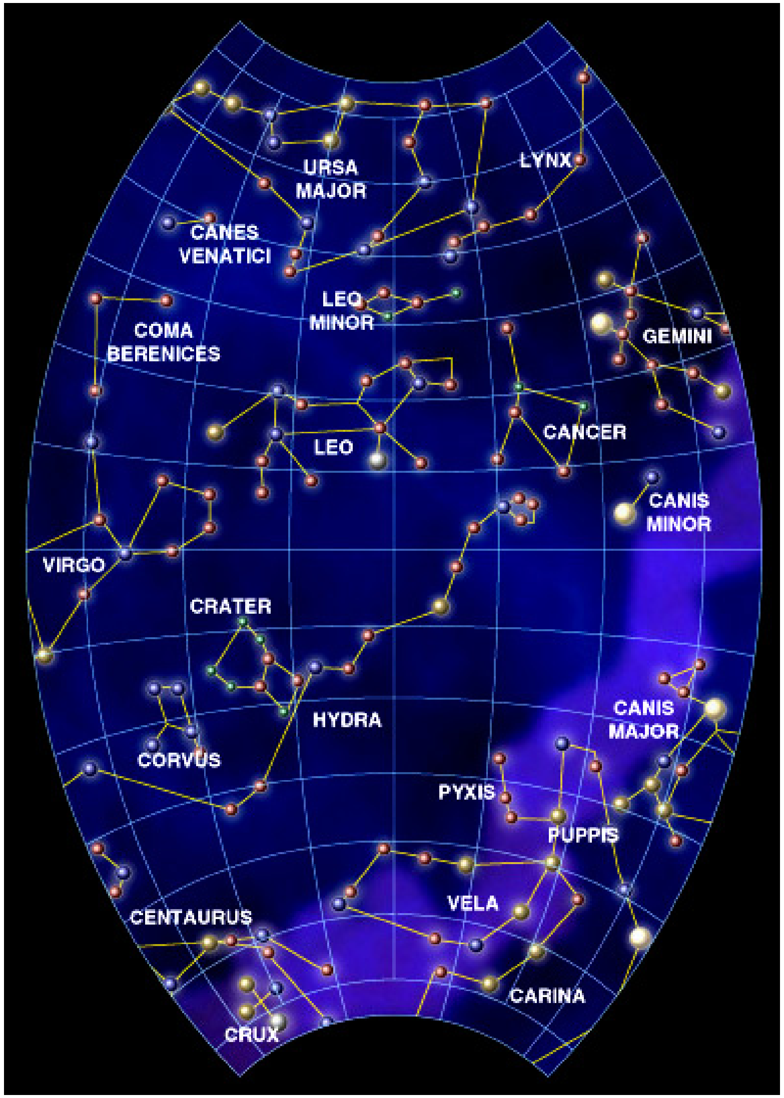

Hydra and Leo constellations

The Hydra Cluster of Galaxies (Abell 1060) contains well over 100 bright galaxies (.. but perhaps fewer galaxies than might be expected from its mass) and spans about ten million light years and is part of the Hydra-Centaurus supercluster.

Some prominent members of the large Hydra constellation:

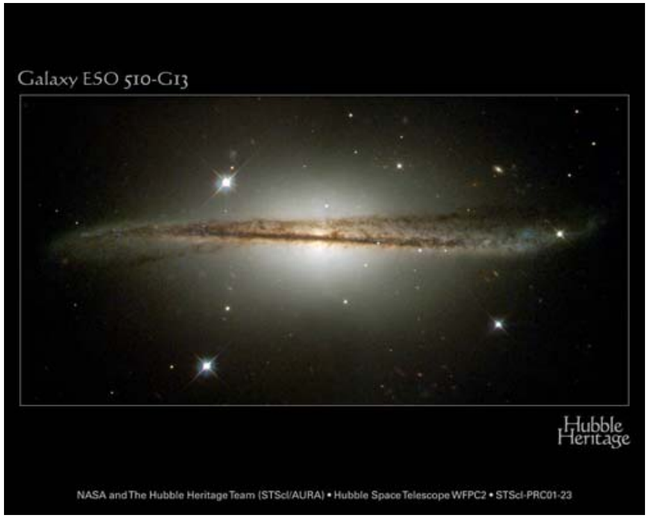

ESO510-G13

M83

NGC 3314

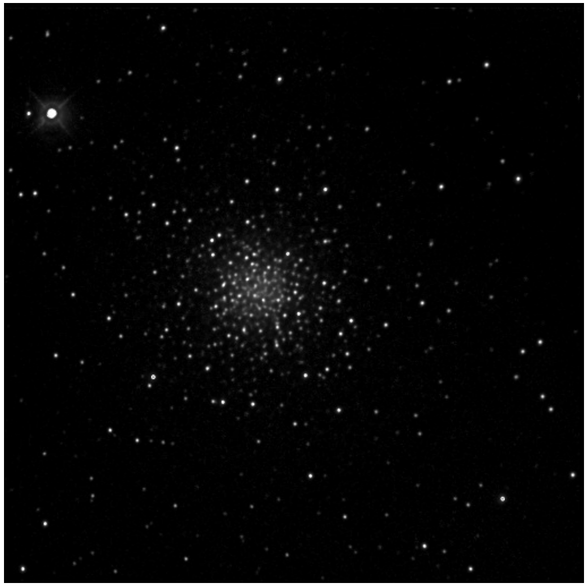

Globular Star Cluster M-68 (NGC 4590)

Open Cluster M48 *in Hydra*

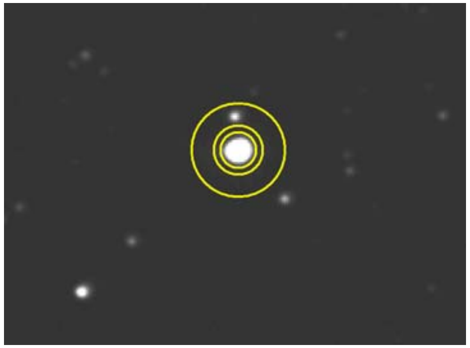

HD74156 Planetary System

Chandra and Hydra – multiwavelength observations:

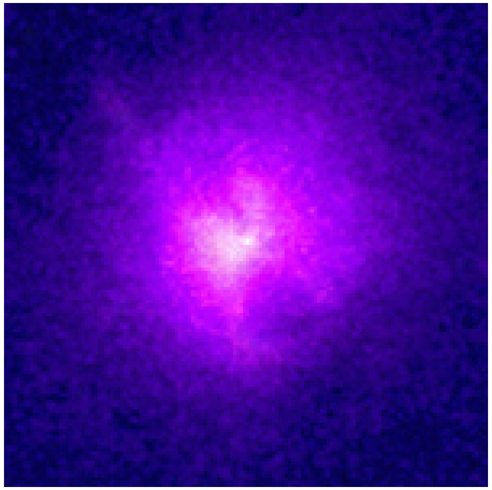

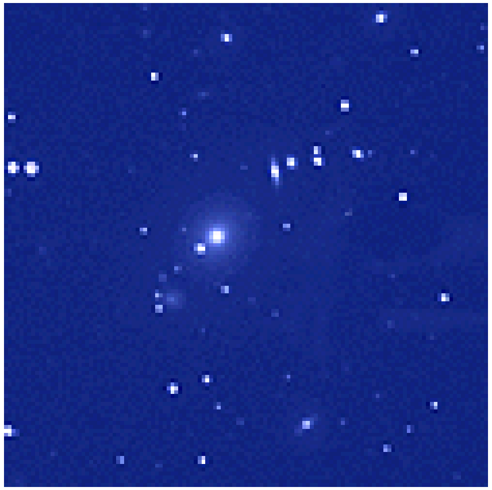

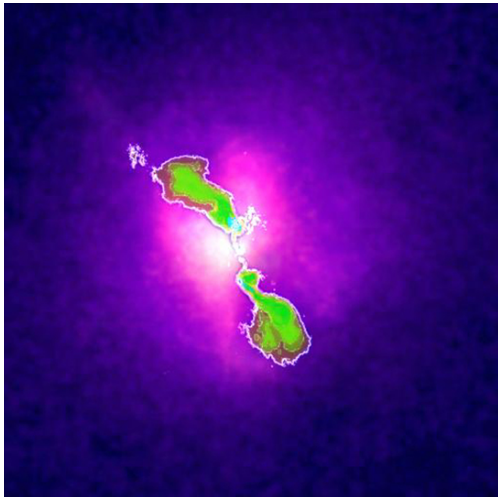

Hydra A is a galaxy cluster that is 840 million light years from Earth at redshift = 0.054. The cluster gets its name from the strong radio source, Hydra A, that originates in a galaxy near the center of the cluster. Optical observations show a few hundred galaxies in the cluster. Chandra X-ray observations reveal a large cloud of hot gas that extends throughout the cluster. The gas cloud is several million light years across and has a temperature of about 40 million degrees in the outer parts decreasing to about 35 million degrees in the inner region. The X-ray image also reveals a bright wedge (shown in white) of hot multimillion degree gas pushing into the heart of the cluster. Like the legendary Hercules who had to contend with the multiple heads of the monstrous Hydra, astrophysicists now know they must deal with the effects of magnetic fields, star formation, rotation, and black holes if they are to understand what is happening in the inner regions of the galaxy cluster.

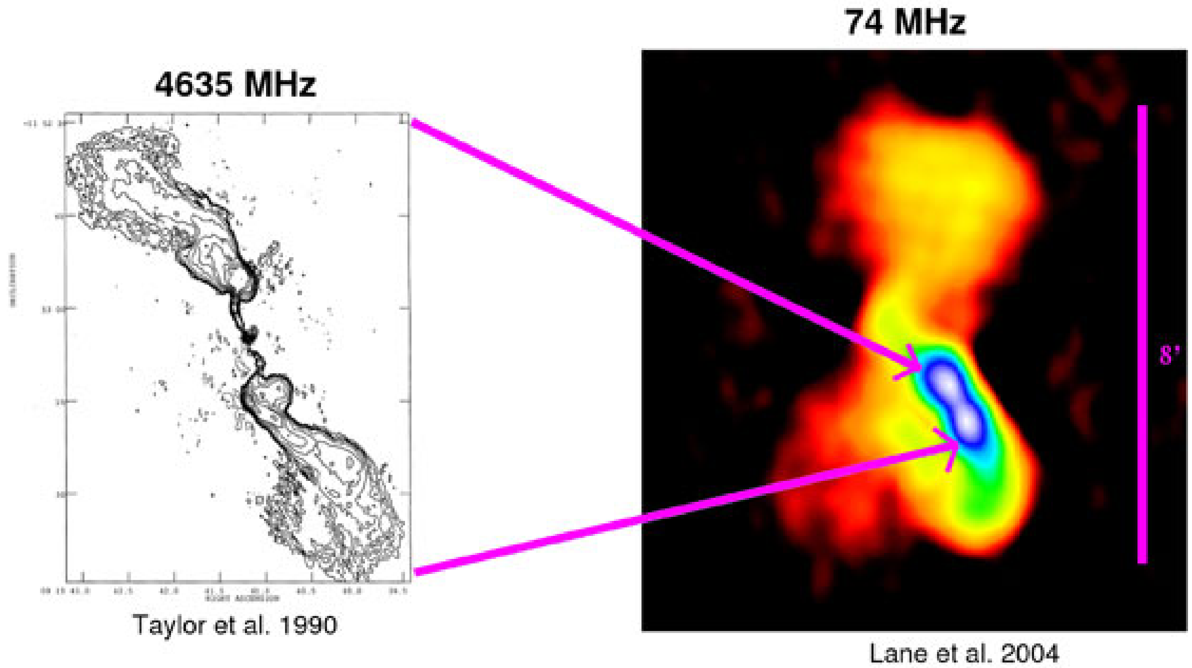

Images of Hydra A (3C 218), a giant radio galaxy near the middle of a large cluster of galaxies. At short radio wavelengths (6 centimeters or 4635 MHz; left) the radio galaxy appears fairly small, with an extent of about 1.5 arcminutes (or about 1/20 the diameter of the full Moon). At long radio wavelengths (4 meters or 74 MHz; right), the size of the radio galaxy is substantially larger, about 8 arcminutes or nearly 5 times larger, with extensive outer radio lobes are revealed. The radio emission results from highly relativistic electrons, moving at nearly the speed of light, which are ejected from the central part of the radio galaxy, presumably in the local environment of a supermassive black hole. The long wavelength radio observations clearly provide a more accurate measure of the amount of material ejected from central regions of the galaxy. In turn, this provides a means of measuring the influence of the supermassive black hole upon its environment and the interaction of the radio galaxy with the cluster of galaxies in which it is located.

But, the cosmical Sphinx + Muses ask us to go back to work in order to try to solve more astrophysical enigmas here in the Island of Hydra …

We wish you an enjoyable and productive stay in Hydra !

Stavros Dimitrakoudis, University of Athens

The Sphinx as a Riddle

What animal crouches in the south, walks on five legs in the east and perches in the north?

Genealogy of the Greek Sphinx

Typhaon and Echidna

The parents (or grandparents)

Their
Offspring:

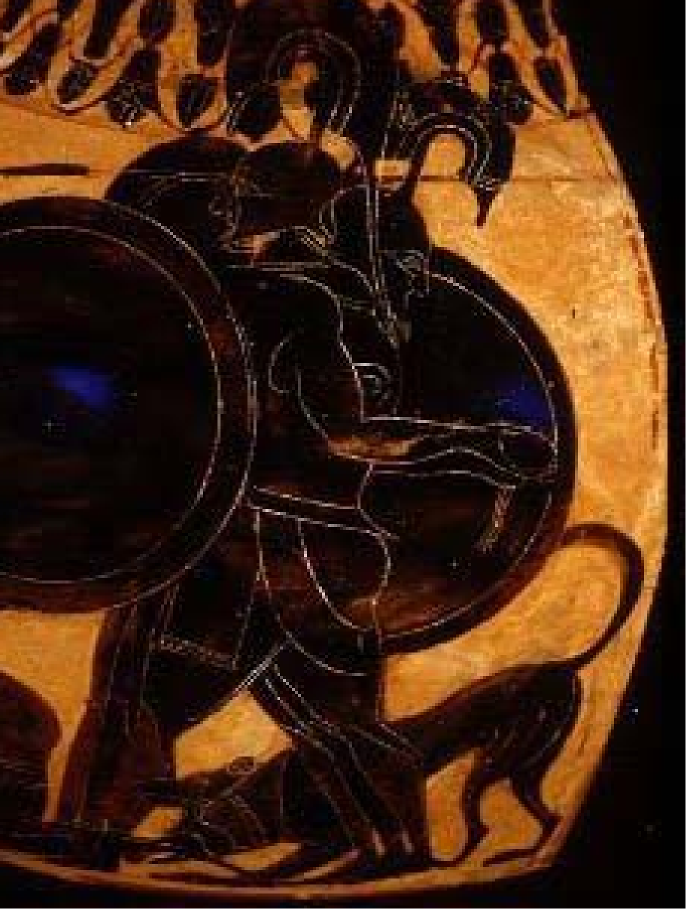

1) Orthos

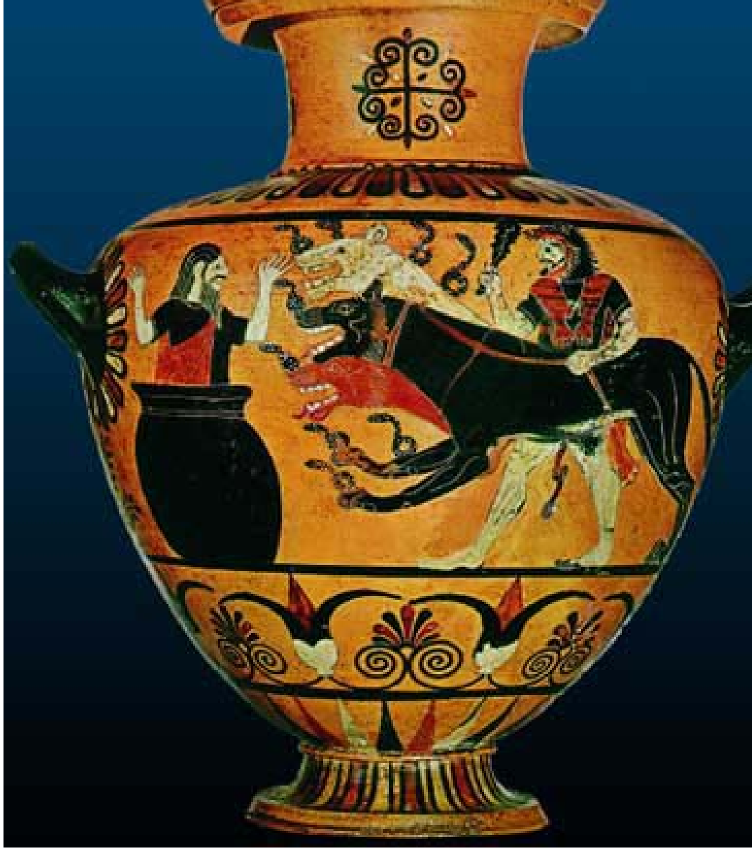

2) Cerberus

3) Hydra

4) Chimera


Orthos + Chimera (or Echidna)

1) Phix (a.k.a. Sphinx)

2) Nemean Lion

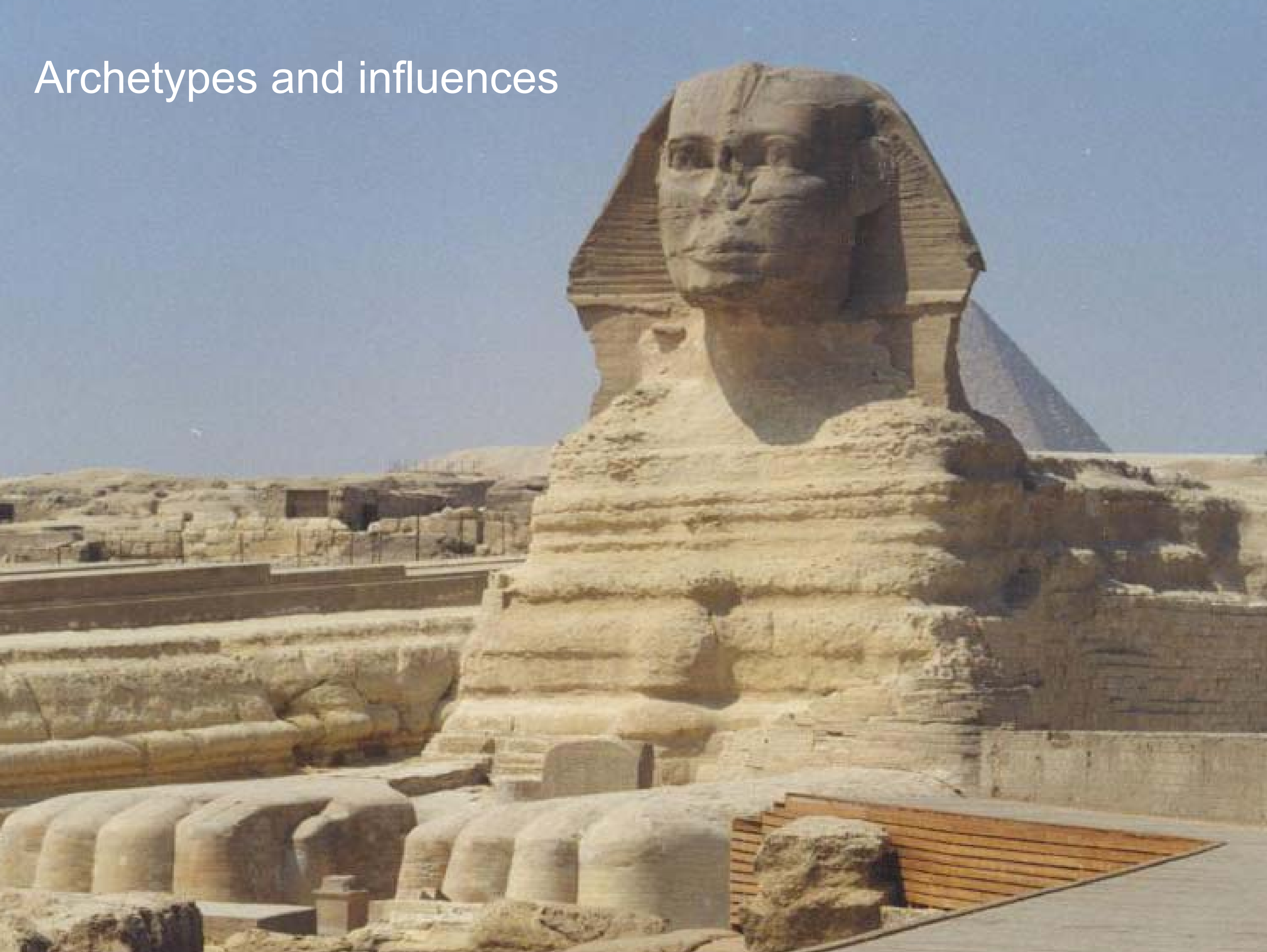
Archetypes and influences

Egyptian sphinxes

3 types of heads; No wings;
Predominantly male.

Androsphinx (man-sphinx)

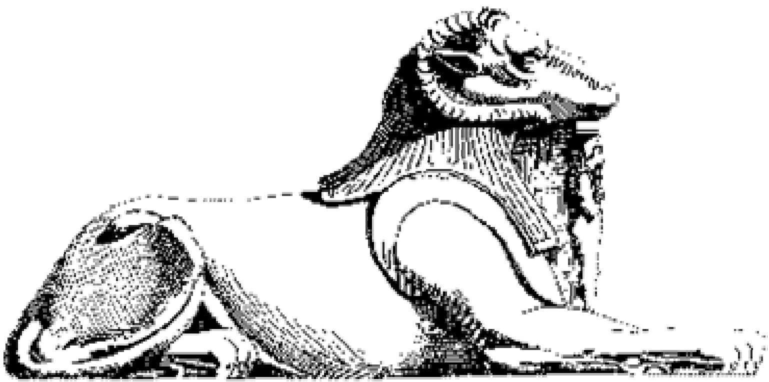

Criosphinx (ram-sphinx)

Hieracosphinx (hawk-sphinx)

With the exception of the Great Sphinx at Giza, all Egyptian sphinx statues come in pairs. They stood as guardians at entrances or along avenues.

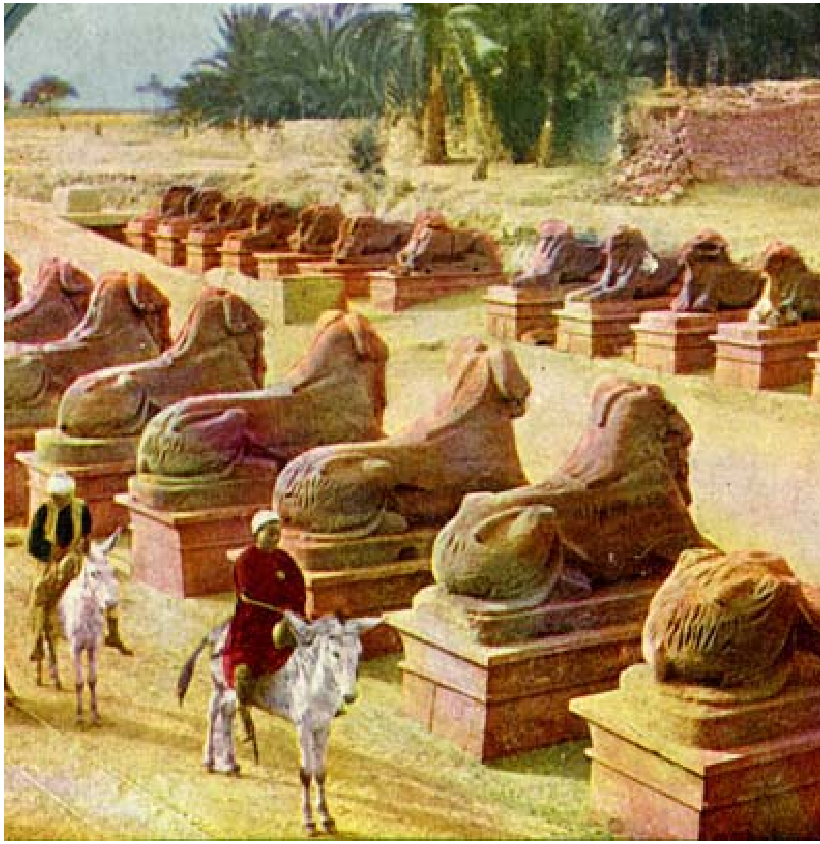

Lions or lion-bodied beings as guardians of thresholds were a common motif throughout the eastern Mediterranean and Mesopotamia since at least the Bronze Age.

Lions Gate, Hattusa (capital of the Hittite Empire)

Lions Gate, Mycenae (prominent city of the Achaeans)

Sphinxes appear in the Aegean region (Minoan and Mycenean civilizations) at around 1600 BC. They appear in Mesopotamia at around 1500 BC. In both regions they were depicted with wings, which is considered an Asian influence.

Wingless Minoan Sphinx from Mallia. Molded clay. 2000-1550 BC.

Gold ornaments from Mycenae, 2nd half of 16th c.BC. The upper left one shows a sphinx

Earlier composite creatures in ancient Mesopotamian art

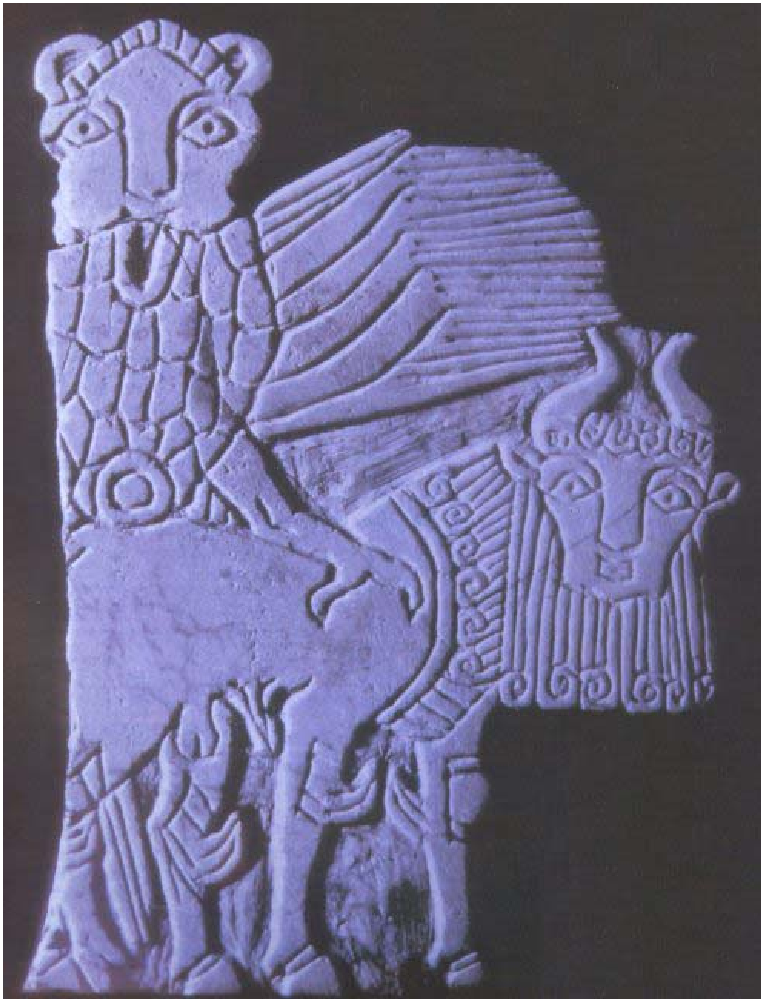

Ebla, around 2400 BC

Ebla, around 2300 BC

Lamassu and Shedu (Neo-Assyrian Mesopotamia)

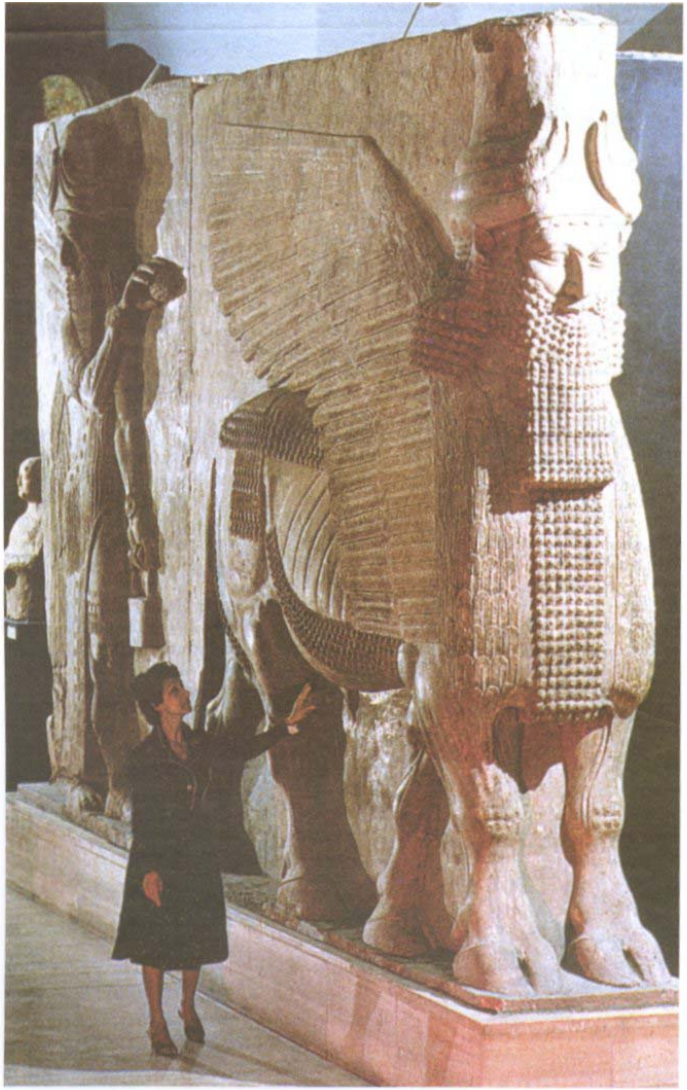

Bull-bodied shedu from Khorsabad

Lion-bodied lamassu (sphinx)

Cross-cultural designs in the Neo-Assyrian Middle East

Horse blinker with sphinx, 8th–7th century B.C.; Neo-Assyrian
Mesopotamia, Nimrud (ancient Kalhu)
Ivory; H. 4.13 in. (10.49 cm)

Plaque with sphinxes, 9th–8th century B.C.; Neo-Assyrian period; Syrian style
Arslan Tash(?), Syria
Ivory with traces of gold foil; L. 4 1/4 in. (10.8 cm)

The sphinx reappears in Greek art at around 750 BC

690 BC

Rhodian sphinx plate, about 600BC

The sphinx in the myth of Oedipus

Homer refers briefly to the story of Oedipus (11.271-280), but makes no mention of the sphinx.

Hesiod introduces her as ‘Phix’ (presumably ‘Sphix’ in the Boeotean dialect) in ‘Theogony’ (326). He gives no description of her form, but mentions that she was disastrous to the ‘Cadmeans’ (Thebans).

The ‘Oedipodeia’ of Cinaethon (Epic Cycle) expands on the myth.

Aeschylus, Euripides and Sophocles wrote tragedies on the House of Laius, that feature the sphinx.

Apollodorus (1^{st} or 2^{nd} c. AD) wrote his mythological “Library” based on the works of ancient mythographers (especially Pherecydes of Leros (5th century BC)). He is one of the main sources on the myth of Oedipus and the Sphinx.

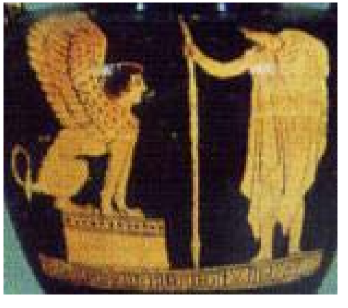

The sphinx is sent by Hera to punish the Thebans (for vague reasons). She perches atop mount Phicion (lit. the mountain of the sphinx) and asks the Thebans a riddle given to her by the muses:

"What animal has one voice, but goes on four legs in the morning,
two legs at noon, and upon three legs in the evening?"

The monster kills anyone who fails to answer the riddle correctly. After she kills Aemon, son of Creon, he proclaims that whoever get rid of the sphinx will receive the hand of Iocaste (widow of king Laius) in marriage and rule Thebes. Oedipus, who recently killed Laius, his own father, unknowingly, answers the riddle, marries his mother, and more tragic stuff happens.

"Why didn't the Thebans simply shoot the sphinx with arrows rather than stand by and see their fellow citizens devoured? Ridiculous!"

Palaephatus, 4th century BC skeptic, “περι απιστων” ("Concerning Incredible Tales“)

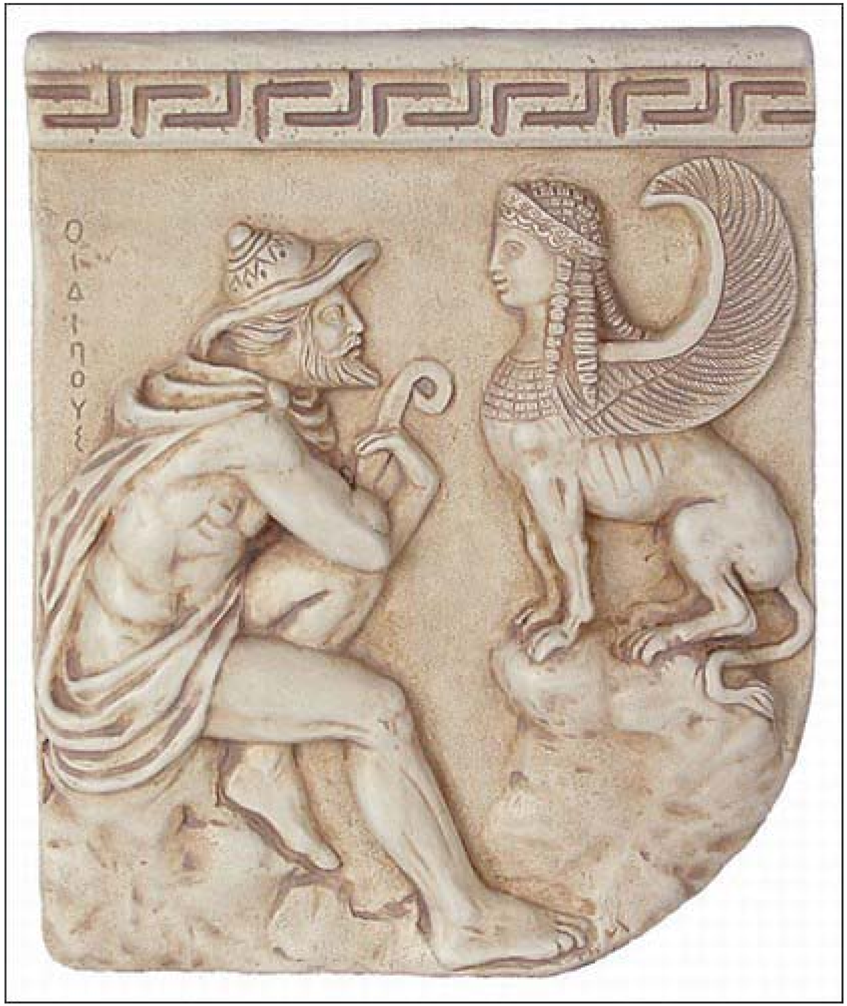

In earlier versions of the myth, emphasis is placed upon Oedipus' unspeakable crimes and their consequences, down to the death of his accursed sons, and the subjugation of Thebes in the War of the Epigones.

In Thebes Oedipus was probably a local hero before he became infamous throughout the Hellenic world. He fought wars, killed local monsters (Teumesian Fox), ruled Thebes.

The Sphinx incident makes him look smart (he uses his intellect to defeat the monster).

Pausanias’ version (more down to earth).

[2] Farther on we come to the mountain from which they say the Sphinx, chanting a riddle, sallied to bring death upon those she caught. Others say that roving with a force of ships on a piratical expedition she put in at Anthedon, seized the mountain I mentioned, and used it for plundering raids until Oedipus overwhelmed her by the superior numbers of the army he had with him on his arrival from Corinth.

[3] There is another version of the story which makes her the natural daughter of Laius, who, because he was fond of her, told her the oracle delivered to Cadmus from Delphi. No one, they say, except the kings knew the oracle. Now Laius (the story goes on to say) had sons by concubines, and the oracle delivered from Delphi applied only to Epicaste and her sons. So when any of her brothers came in order to claim the throne from the Sphinx, she resorted to trickery in dealing with them, saying that if they were sons of Laius they should know the oracle that came to Cadmus.

[4] When they could not answer she would punish them with death, on the ground that they had no valid claim to the kingdom or to relationship. But Oedipus came because it appears he had been told the oracle in a dream.

Why a sphinx?

a) It was mythologically available

b) No other hero had killed it yet

c) It provides a heroic excuse for Oedipus to reclaim his throne

d) Its allusions to Egypt and the Orient gave it an aura of wisdom

The Riddle

The riddle of the Sphinx is, in essence, the question of who we are.

It is asked by a composite being, and it is a composite question. Only when the parts are connected does the underlying model beneath the disparate observations emerge, and we reach a simplicity that is thereafter considered self-evident. The complexity symbolized by the polymorphous monster crumbles (literarily, in the ancient myth) and the solver of the riddle can move on unimpeded to new challenges (in Oedipus' case, ruling Thebes).

And on to new riddles...

What animal is narrow on the waist, broad on the neck and blazing on top of its head?

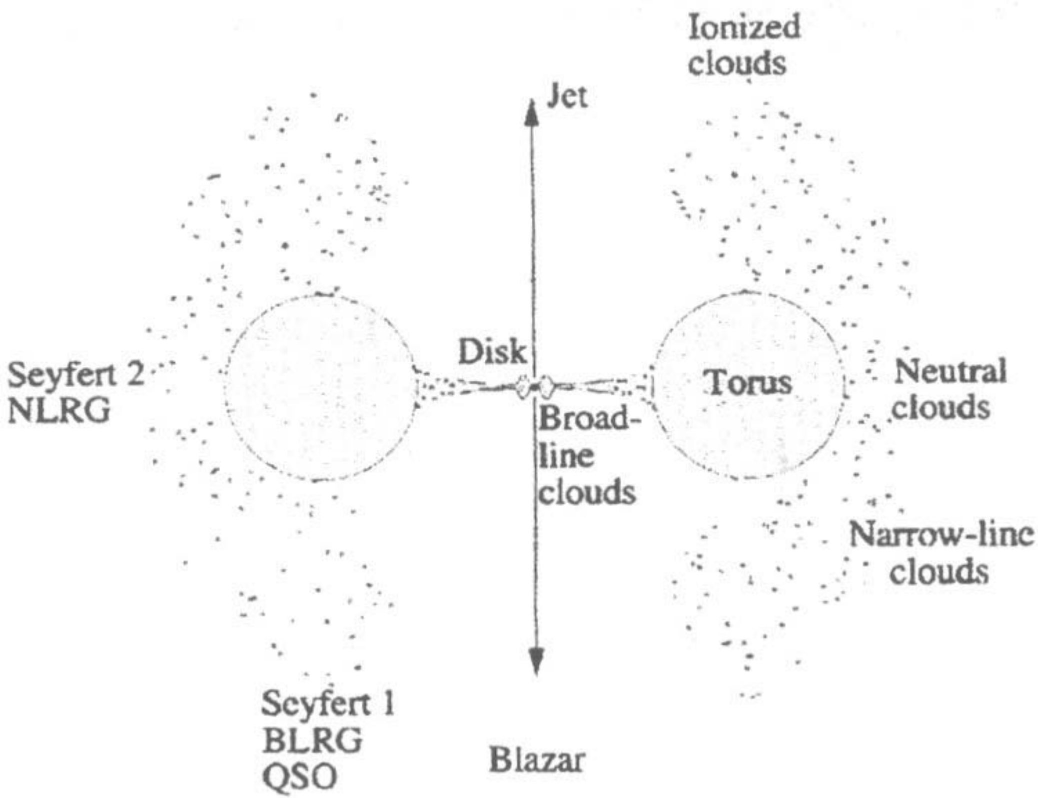

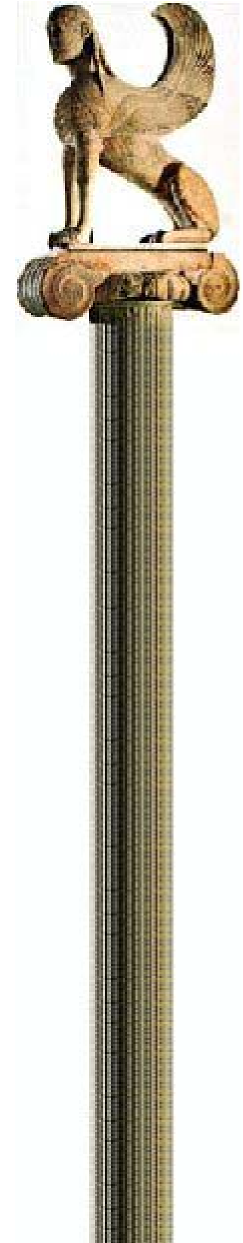

Stefano Ciprini

1.Tuorla Observatory (Turku Univ.), Finland
2.Perugia Phys. Dept. (INAF Torino Obs. subnode), Italy
(EC Young Researcher Training Network ENIGMA)

OJ 287: update on the XMM-Newton campaign

7th ENIGMA Meeting
May 08-10, 2006 – Hydra Island, GREECE

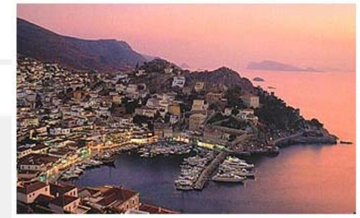

Summary

- OJ 287: update on the XMM-Newton observations and the coordinated multifrequency campaign.

- Appendix: a new ESO-VLT blazar spectroscopy program.

News about OJ 287 campaigns

OJ 287: 2005-2008 long-term project (ENIGMA Campaign):

www.astro.utu.fi/OJ287MMVI/ *

Latest NEWS:

- Optical photometry and polarimetry monitoring program on OJ 287 is ongoing (see Jochen's talk).

- 2 XMM-Newton observations of OJ 287 (Cycle AO-4) and coordinated core (short) campaign by the WEBT consortium have been performed (April & November 2005).

- A 3rd XMM-Newton observation of OJ 287 granted (Cycle AO-5) and scheduled on next November 2006.

- MAGIC ToO observations of OJ 287 performed in Nov.1-4 and Nov..10-13, 2005.

- Effelsberg IDV "minicampaign" on OJ 287 has been performed (Apr.12 and Nov. 8-9-10, 2005, see Lars' talk).

* MMVI = 2006

OJ 287: XMM proposals

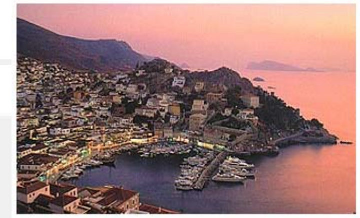

- XMM-Newton observations (Cycle AO-4, PI:S. Ciprini, COIs: C.M. Raiteri, L.O. Takalo, A. Sillänpää, M. Villata, L. Ostorero, M. Fiorucci), and coordinated short WEBT campaign (CM: S. Ciprini). Satellite pointing dates: April 12, and Nov. 3-4, 2005.

- 3rd XMM-Newton observation granted (Cycle AO-5, PI: S. Ciprini, COIs: C.M. Raiteri, G.Tosti, L.O. Takalo) to be scheduled in a day between Nov.15-Nov.21, 2006 (43ksec).

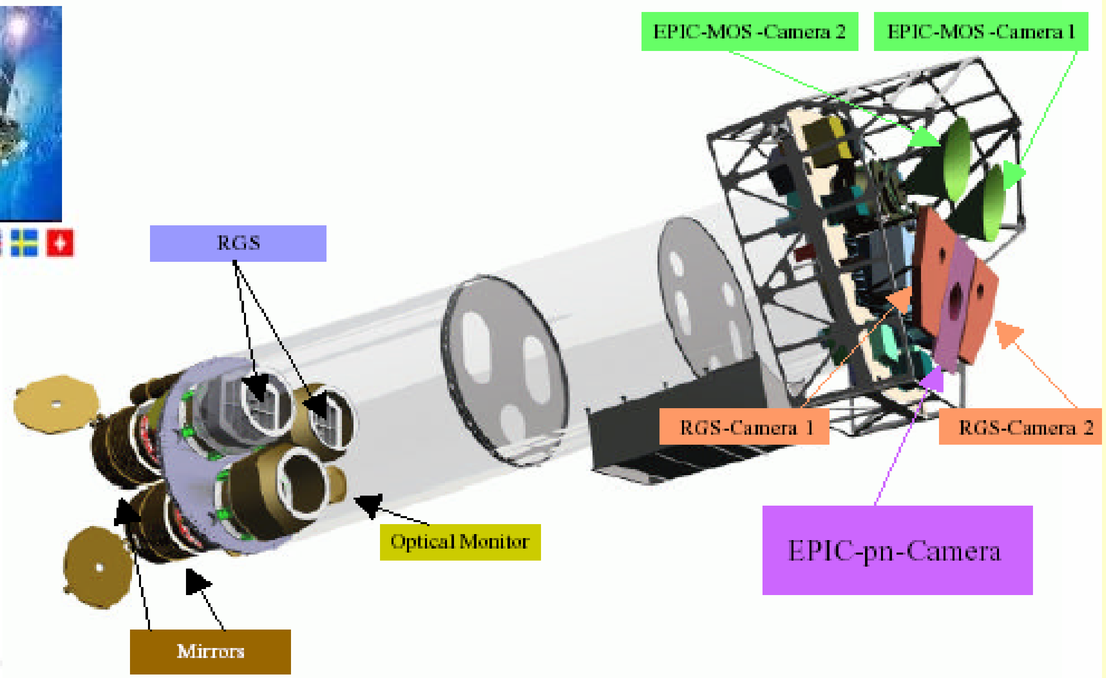

OJ 287 XMM-Newton: EPIC image April 12, 2005

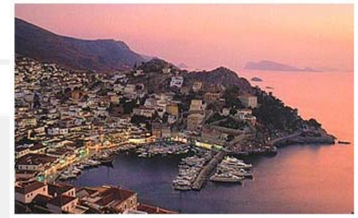

EPIC: large frame + medium filter used.
Data processed with XMM-SAS v. 6.5.
Intervals of high background filtered.
Spectral analysis of PN + MOS1+MOS2 data with XSPEC

0300480201 Observation Data Summary

Revolution	Target	Scheduled Length
0978	OJ 287	38913

Guest Observer Information

```
Dr    Stefano            Ciprini
Tuorla Observatory, Turku Univ
Vaisalantie 20
Piikkio
FINLAND
21500
```

Proposal Target Information

```
Target          : OJ 287
RA              : 8.9135750
Dec             : 20.1085000
Prop Duration   : 32200
Alt Names       : PKS 0851+202 ;  RX J0854.8+2006
Boresight RA    : 8.9135750
Boresight Dec   : 20.1085000
Lower Pos Ang   : 0
Upper Pos Ang   : 360
SC Pos Ang      : N
AO Number       : 4
SCIENCE_TYPE+   : F
```

Observation Record

```
Observation ID : 0300480201
Revolution     : 0978
Start time     : 2005-04-12T13:13:21.000
Stop time      : 2005-04-13T00:01:54.000
```

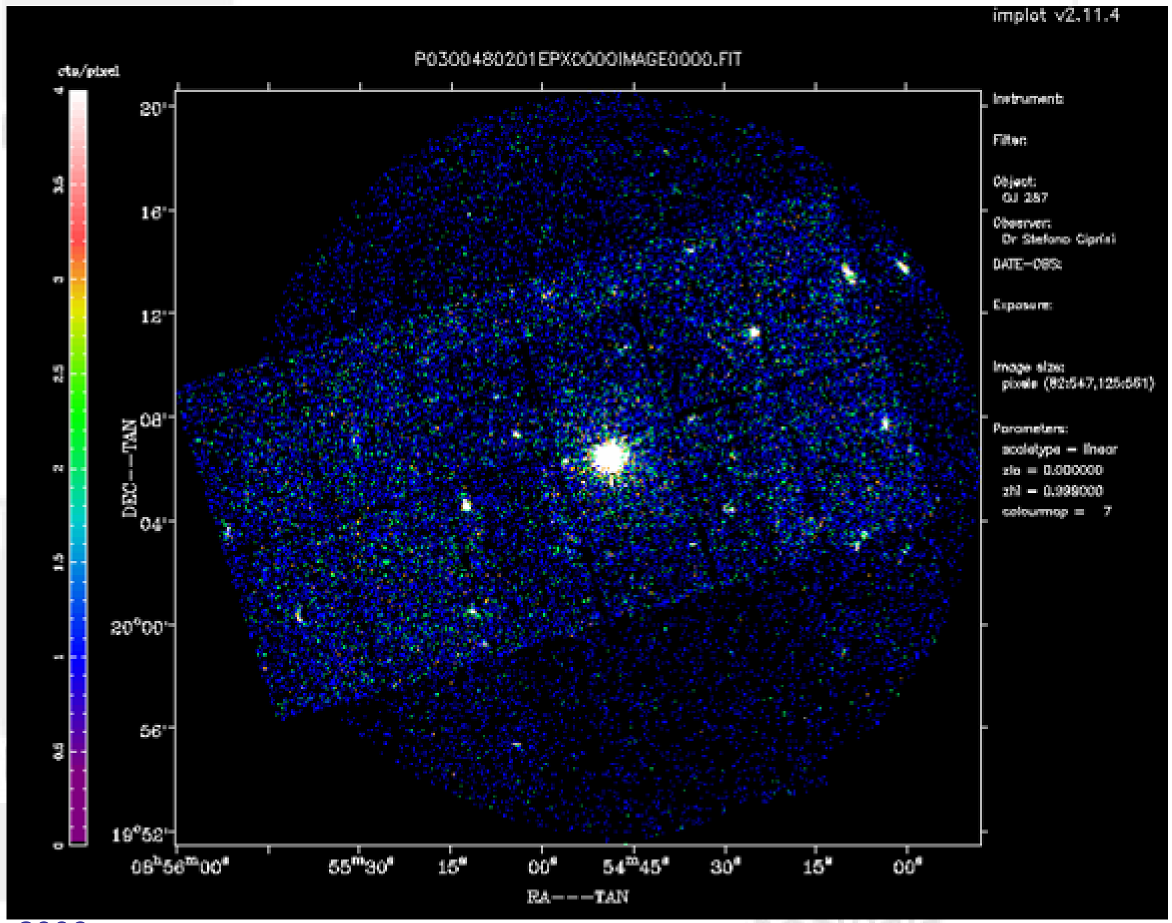

OJ 287 XMM-Newton: EPIC image Nov. 3-4, 2005

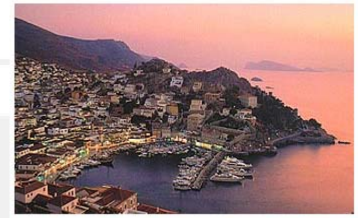

EPIC: large frame + medium filter used.
Data processed with XMM-SAS v. 6.5.
Intervals of high background filtered.
Spectral analysis of PN + MOS1+MOS2 data with XSPEC.

0300480301 Observation Data Summary

Revolution	Target	Scheduled Length
1081	OJ 287	48059

Guest Observer Information

```
Dr    Stefano               Ciprini
Tuorla Observatory, Turku Univ
Vaisalantie 20
Piikkio
FINLAND
21500
```

Proposal Target Information

```
Target         : OJ 287
RA             : 8.9135750
Dec            : 20.1085000
Prop Duration  : 50800
Alt Names      : PKS 0851+202 ;  RX J0854.8+2006
Boresight RA   : 8.9135750
Boresight Dec  : 20.1085000
Lower Pos Ang  : 0
Upper Pos Ang  : 360
SC Pos Ang     : N
AO Number      : 4
SCIENCE_TYPE+  : F
```

Observation Record

```
Observation ID : 0300480301
Revolution     : 1081
Start time     : 2005-11-03T21:16:31.000
Stop time      : 2005-11-04T10:37:30.000
```

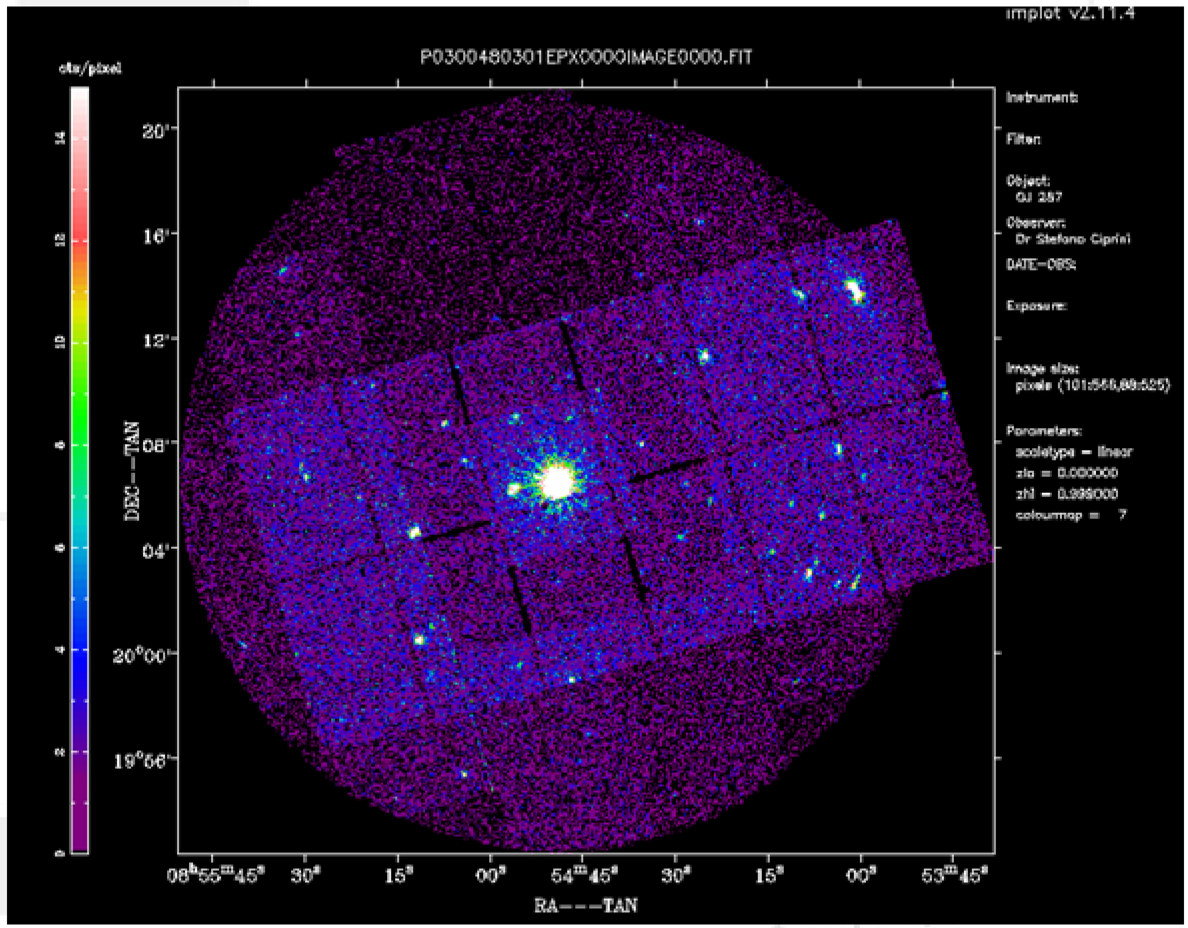

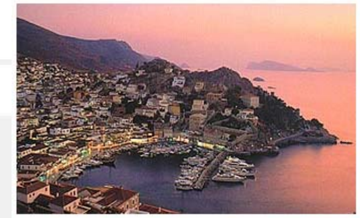

OJ 287 XMM-Newton: EPIC spectrum April 12, 2005

Date: April 12, 2005 - OJ 287, z=0.306.

XMM-Newton *EPIC: PN* + *MOS1* + *MOS2* spectra

Model: single power law + galactic absorption in the 0.2-10 KeV range

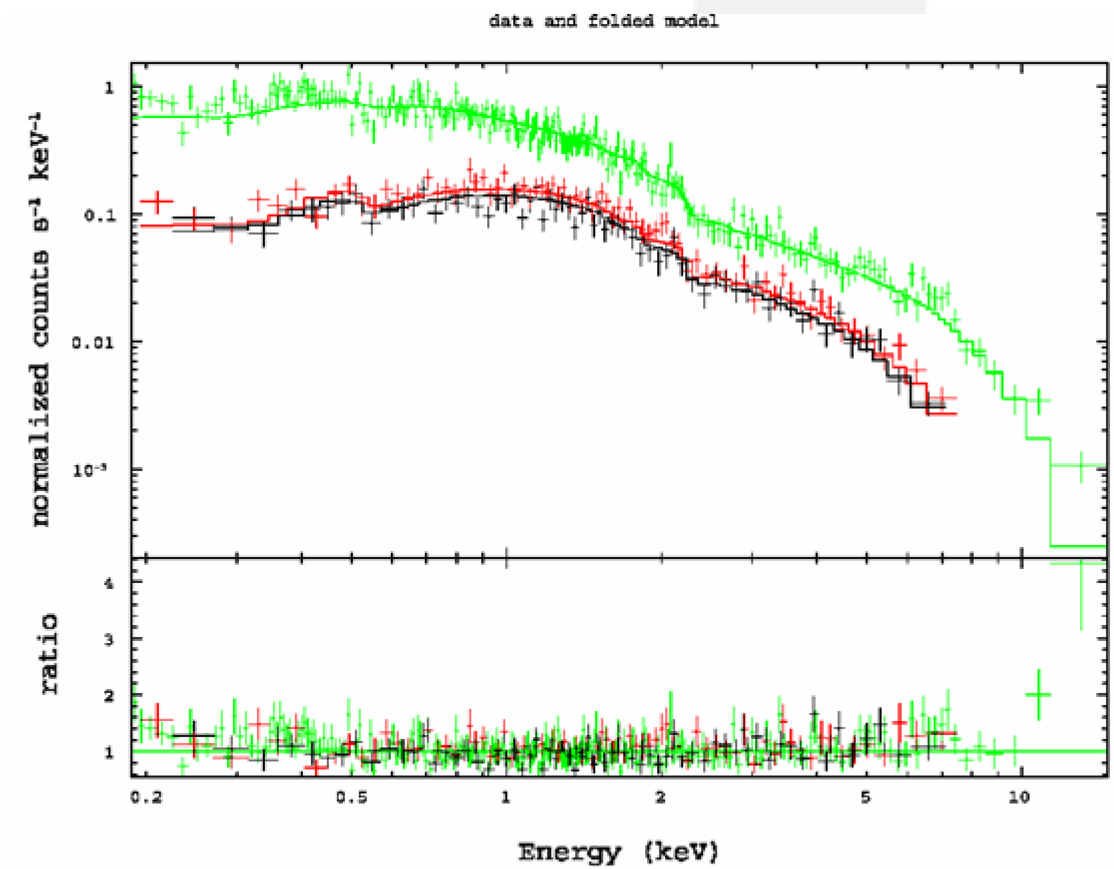

H column density:

$N_H = 3.09 \times 10^{20}$ cm^{-2}

Power-law photon index:

$\Gamma = 1.628 \pm 0.023$

Reduced chi-squared:

$\chi_r^2 = 1.035$, d.o.f.=367

Flux density (2-10 KeV):

$F_{2-10keV} = (2.47 \pm 0.8) \times 10^{-12}$ erg s^{-1} cm^{-2}

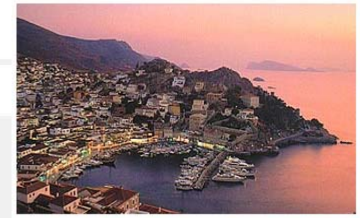

OJ 287 XMM-Newton: EPIC spectrum Nov. 3-4, 2005

Date: November 3-4, 2005 - OJ 287, z=0.306.

XMM-Newton *EPIC: PN* + *MOS1* + *MOS2* spectra

Model: broken power law + galactic absorption in the 0.2-10 KeV range

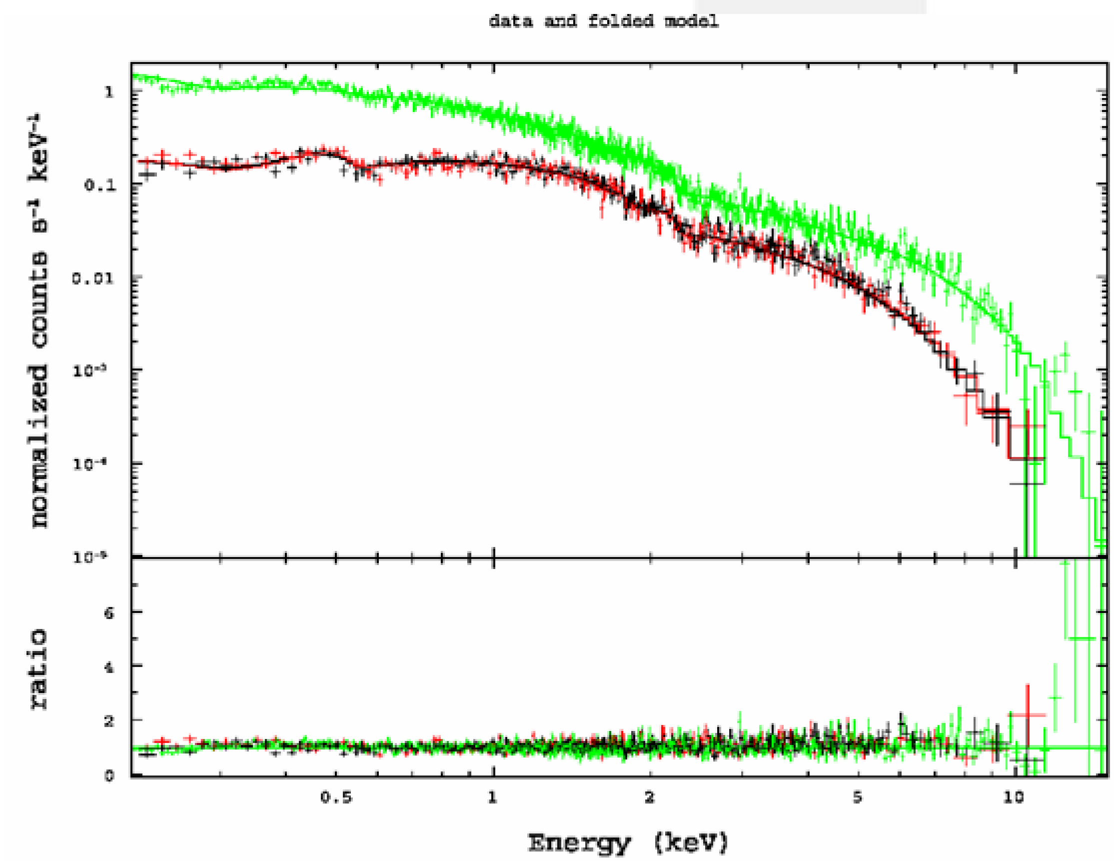

H column density:

$N_H = 3.09 \times 10^{20}\ cm^{-2}$

Broken power-law photon indexes:

$\Gamma_1 = 2.65\,(-0.07/+0.12)$

$\Gamma_2 = 1.79 \pm 0.02$

break energy: 0.69 KeV

Reduced chi-squared:

$\chi_r^2 = 1.030$, d.o.f.=927

Flux density (2-10 KeV):

$F_{2-10keV} = (1.82 \pm 0.07) \times 10^{-12}$ erg s^{-1} cm^{-2}

Preliminary summary on the X-ray observations

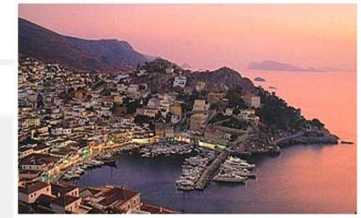

- Apr.12 (XMM 1st obs.): Best fit: simple single power law component (IC?).

- Nov.3-4 (XMM 2nd obs.): Best fit: broken power law component (break ~0.7 keV), (Synch.tail+IC ? Break signature between the synchrotron and IC components ?)

- X-ray observations provided information on the high-energy (inverse Compton) spectral component.

- Different brightness states, flux variations:
$F_{2-10keV}=2.47\times10^{-12}$(1st), and $F_{2-10keV}=1.82\times10^{-12}$(2nd), $erg\ s^{-1}\ cm^{-2}$ (previous obs.: fluxes in the range $1.35-5.0\times10^{-12}\ erg\ s^{-1}\ cm^{-2}$).

- Spectral variability: single/broken power law, slope variation.

OJ 287 XMM-Newton: OM opt-UV observations

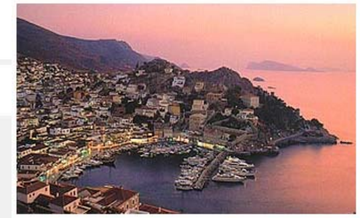

❑ Optical Monitoring instrument (OM). Summary of the observations obtained:

	UVW2	UVM2	UVW1	U	B	V
lambda (A)	2120	2310	2910	3440	4500	5430
Num. of images (Apr.12):	1	2	2	1	1	1
Num. of images (Nov.3-4):	0	0	8	1	1	1

Example of 2 ultraviolet (UV) images

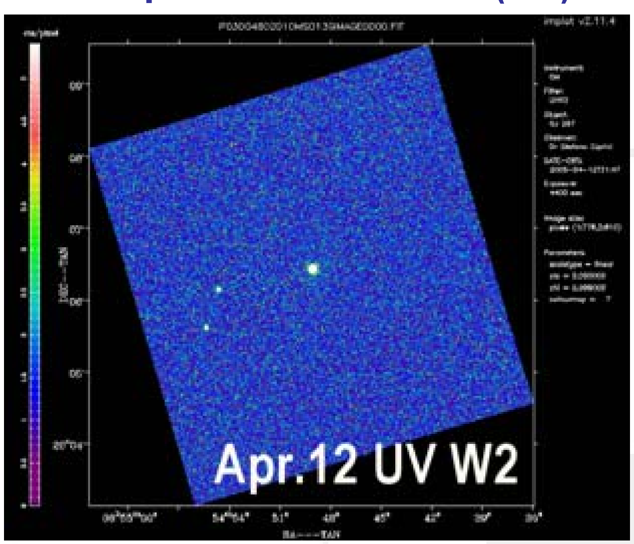

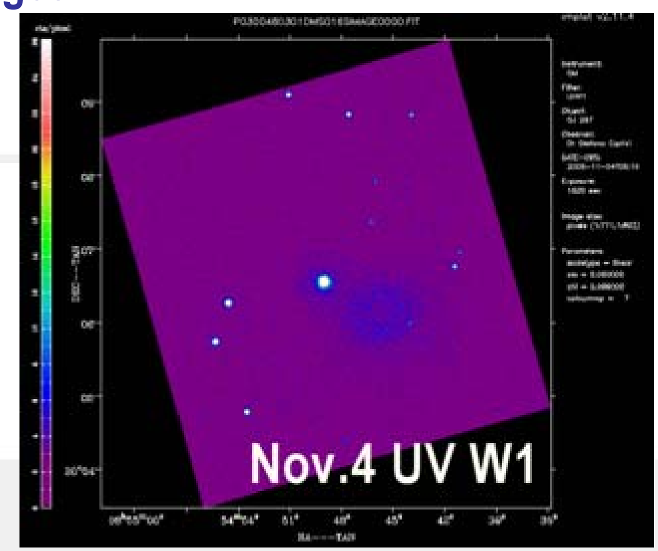

The “usual” optical finding chart

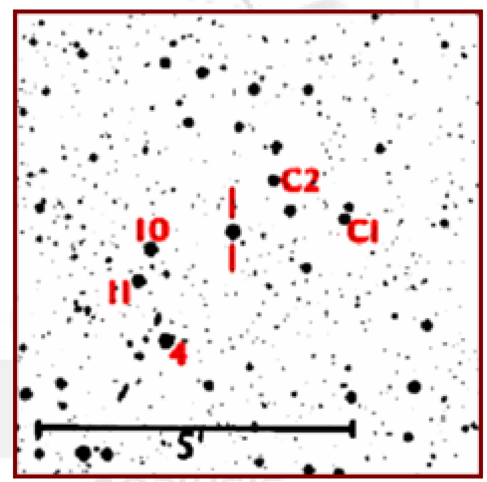

OJ 287 XMM-Newton: OM opt-UV observations

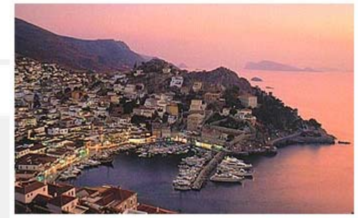

Preliminary results:

	UVW2	UVM2	UVW1	U	B	V
lambda (A)	2120	2310	2910	3440	4500	5430

❑ Agreement of the U,B,V calibrated OM mags with the reported comparison stars values. (XMM-OM "space"-mags are suitable to make a nice comp. stars calibration sequence for the OJ 287 field in opt. UBV filters).

❑ High brightness of OJ 287 in UV bands during both the pointings (synch. peak in UV, or UV therm. bump, or…?).

Apr.12, 2005: OJ 287 magnitudes

OM-band	MAG	ERR
V		0.01
B		0.01
U		0.01
UV-W1		0.01
UV-W1		0.01
UV-M2		0.01
UV-M2		0.01
UV-W2		0.01

Preliminary values

Nov.3-4, 2005: OJ 287 magnitudes

OM-band	MAG	ERR
V		0.01
B		0.01
U		0.01
UV-W1		0.01
UV-W1		0.01
UV-W1		0.01
UV-W1		0.01
UV-W1		0.01
UV-W1		0.01
UV-W1		0.01
UV-W1		0.01

Preliminary values

OJ 287: previous broadband SEDs

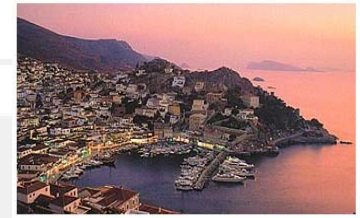

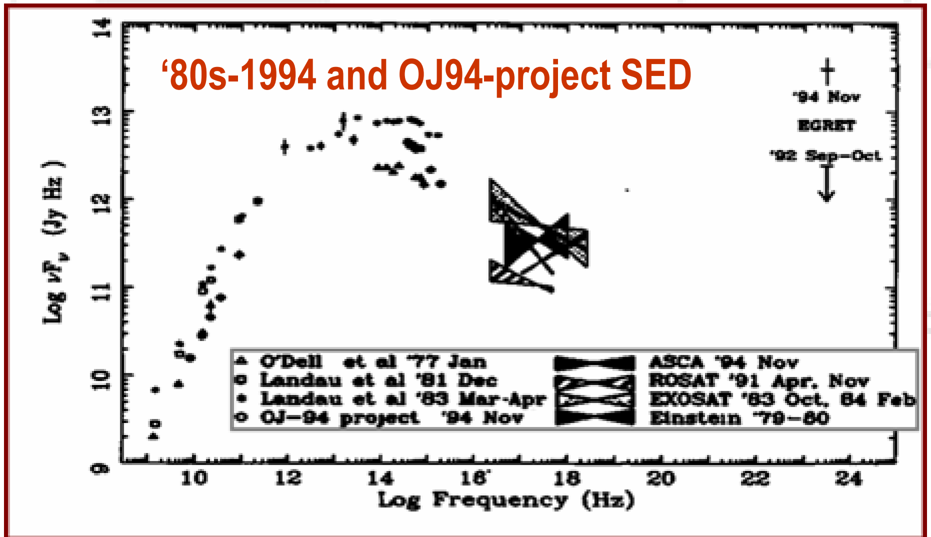

Idesawa et al. (1997)

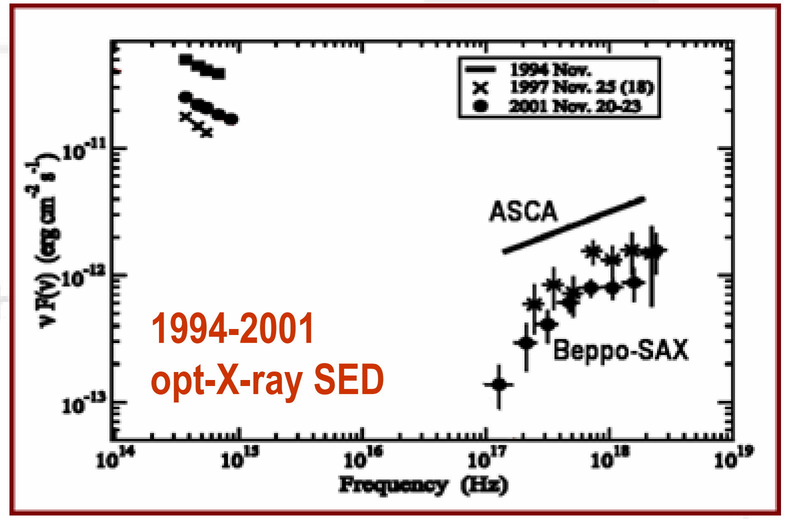

Massaro et al. (2003)

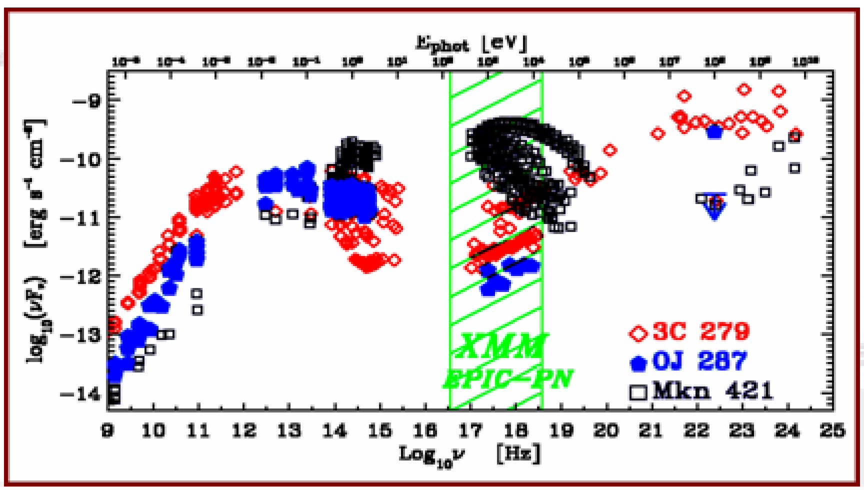

Comparison among the SED of OJ 287 SED, with the SED of a HBL (TeV) blazar and a FSRQ prototype (Mkn 421 and 3C 279).

Coord. campaign: season 2004-05 optical light-curve

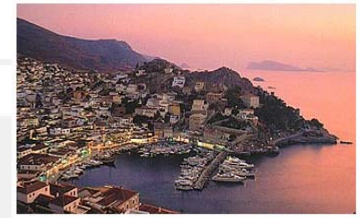

Date: Oct. 2004 - May 2005 (last observing season)

ENIGMA monitoring observations + intensive WEBT campaign (part 1):

- ❑ Intermediate/high brightness level. Brightness increased of 2 mag in about 2.5 months.
- ❑ Optical flare during the 1st XMM-Newton pointing (April 12): increase of ~ 0.8 mag in 8 days, large drop of ~ 1.4 mag in 13 days.

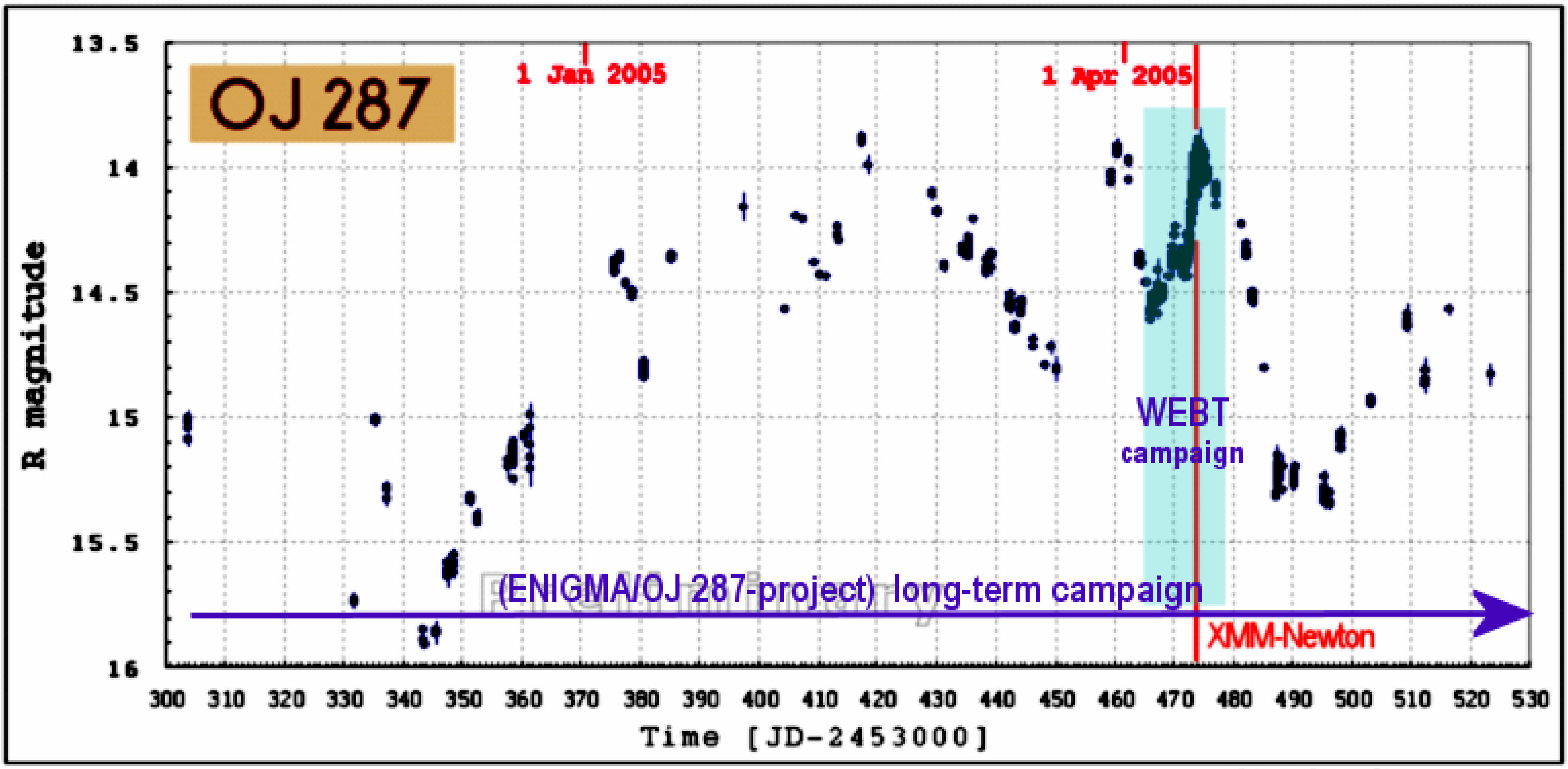

Coord. Campaign: WEBT
5-days light-curve

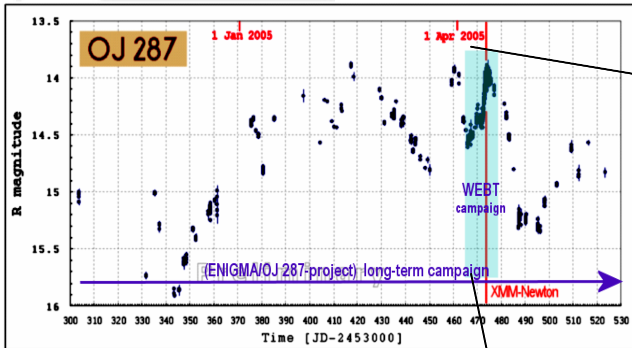

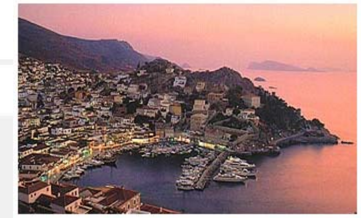

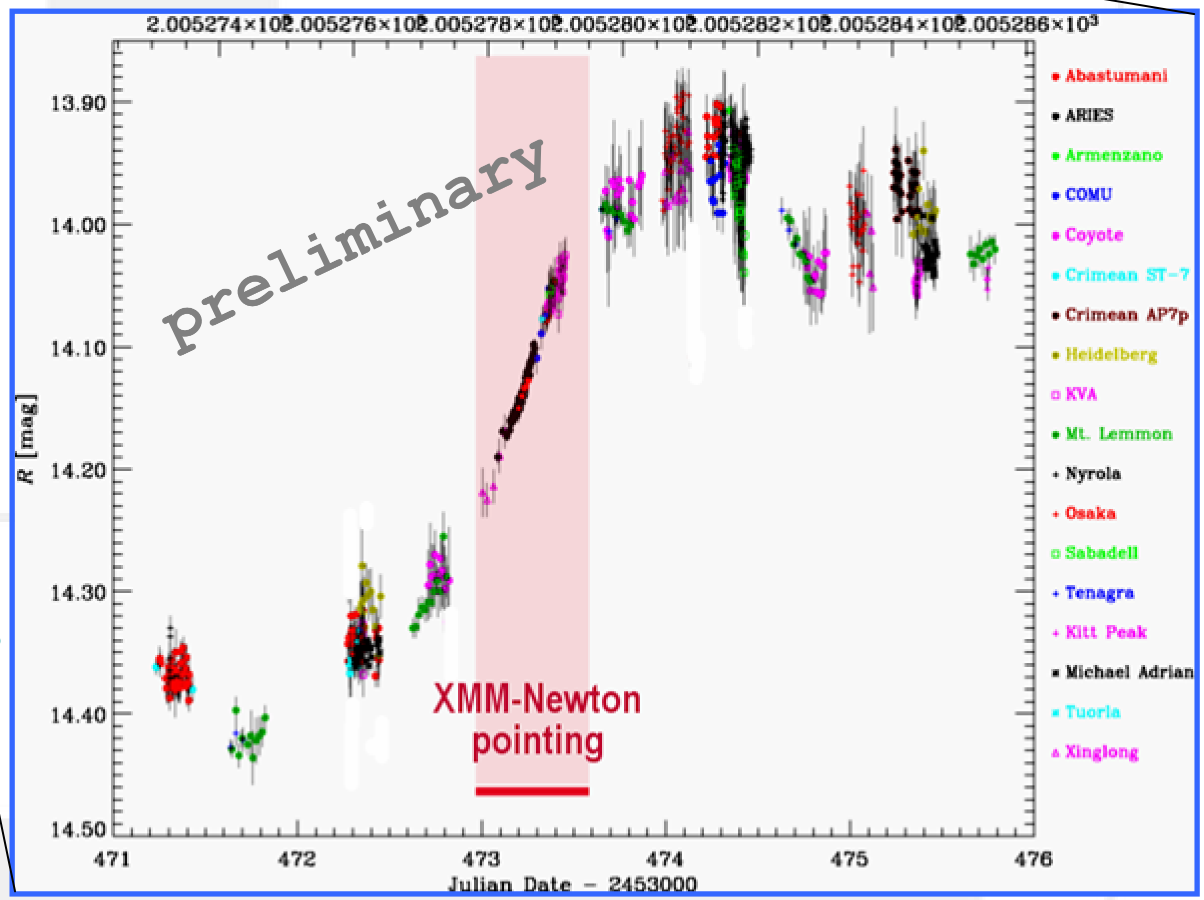

Date: April 10-14
(XMM-Newton 1st pointing: April 12)

❑ Almost 0.3 mag brightness increase in less than 9 hours!

Season 2004-05 and Nov.-Dec.2005 part comparison

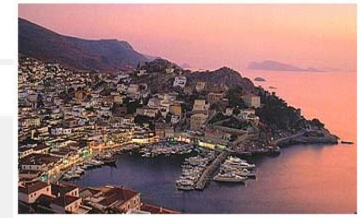

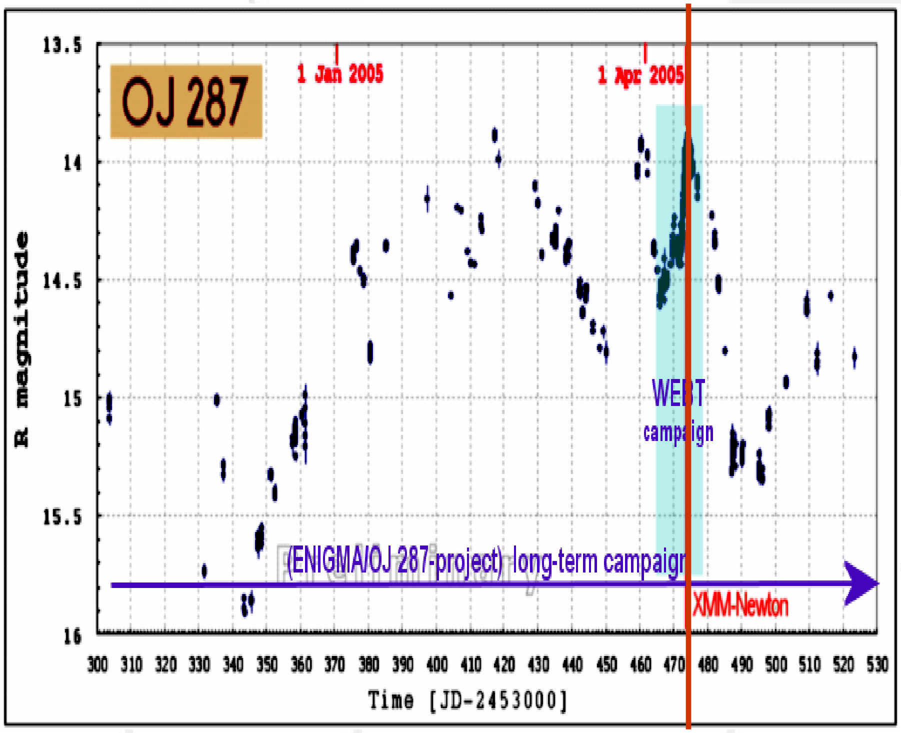

sun

conjunction

interruption

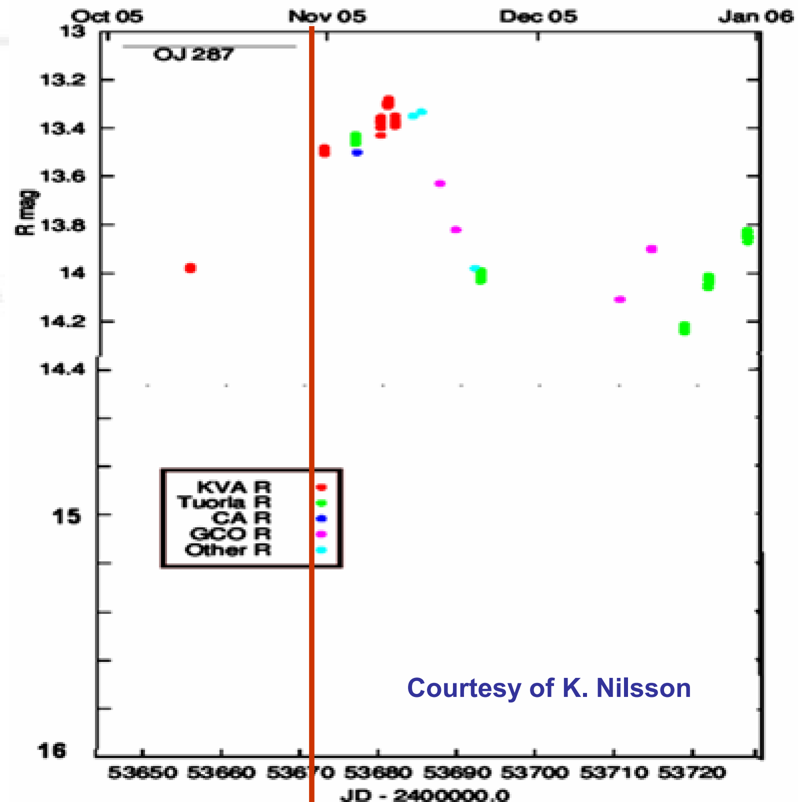

XMM-Newton,

1st pointing

XMM-Newton,

2nd pointing

Coord. campaign participants: season 2005-06

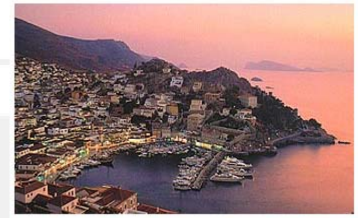

XMM-campaign part 2 (Oct. ~ Dec.05/Jan.06): Participating Obs.

Institutes/Observatories and contact-person(s) - list updated by April 13, 2006:

- Osaka University - Osaka, Japan (K. Torii)
- Sobaeksan KASI Optical Astronomy Observatory - Sobaeksan, Korea (C.-U. Lee)
- Lulin Observatory - Lulin, Taiwan (W.-P. Chen)
- Tsinghua University - Beijing, China (J. Li)
- Xinglong Station of NAOC - Yanshan Mountains, China, (J.-H. Wu)
- ARIES Sampurnanand Telescope - Naini Tal, Uttaranchal, India (R. Sagar, G. Krishna)
- Mount Maidanak Observatory, Ulugh Beg Astronomical Institute - Mount Maidanak, Uzbekistan (M. A. Ibrahimov)
- Abastumani Astrophysical Observatory - Mt. Kanobil, Georgia, (O. Kurtanidze)
- Crimean Astrophysical Observatory - Nauchny, Crimea, Ukraine (Y. Efimov, V. Larionov)
- Çanakkale Onsekiz Mart University Observatory - Çanakkale, Turkey (A. Erdem)
- Saint Petersburg State University Observatory - St. Petersburg, Russia (V. M. Larionov)
- Bulgaria National Astronomical Observatory - Rozhen, Bulgaria (E. Ovcharov, A. Kostov)
- Jakokoski Observatory - Jakokoski, Finland (P. Pääkkönen)
- Tuorla Observatory - Piikkio, Finland (L. Takalo, A. Sillanpää)
- MonteBoo Observatory, Masaryk University - Brno, Czech Republic (F. Hroch)
- Catania Observatory - Catania, Italy (A. Frasca)
- Campo Imperatore Observatory - Assergi, L'Aquila, Italy (A. Arkharov)
- Armenzano Observatory - Armenzano, Assisi, Italy (D. Carosati)
- Porziano Observatory - Porziano, Assisi, Italy (D. Capezzali)

…. cont.

Coord. campaign participants: season 2005-06

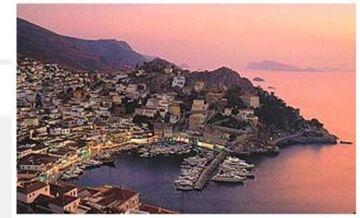

- Perugia Observatory - Perugia, Italy (G. Tosti, S. Ciprini)
- Torino Observatory - Torino, Italy (C. Raiteri, M. Villata)
- Heidelberg Observatory - Heidelberg, Germany (L. Ostorero, D. Emmanoulopoulos)
- Michael Adrian Observatory- Trebur, Germany (J . Ohlert)
- KVA Telescope - La Palma, Canary Islands, Spain (L. Takalo, A. Sillanpää)
- Nordic Optical Telescope - La Palma, Canary Islands, Spain (T. Pursimo)
- INAOE Tonantzintla Observatory - Tonantzintla, Puebla, Mexico (O. Lopez-Cruz)
- Mt. Lemmon KASI Observatory - Mount Lemmon, Arizona, USA (C.-U. Lee)
- Ohio University MDM Observatory - Kitt Peak , Arizona, USA (M. Boettcher)
- Kitt Peak SARA Observatory - Kitt Peak, Arizona, USA (J. Webb)
- Tenagra Observatories - Sonoran desert, Arizona, USA (A. Sadun)
- National Astronomical Observatory of San Pedro Mártir - Baja California Peninsula, Mexico (E. Benitez, D. Dultzin-Hacyan.)
- Coyote Hill Observatory - Wilton, Sacramento, California, USA (C. Pullen)

- RATAN-600 (Special Astrophysical Observatory) (576 m) - Zelenchukskaya, Russia (Y. Kovalev)
- RT-22 Crimean Astrophysical Observatory (22m) - Simeiz, Crimea, Ukraine (A. Volvach)
- Metsähovi Radio Telescope (14 m) - Metsähovi, Finland (M. Tornikoski, A. Lahteenmaki)
- Noto Radio Observatory (32m) - Noto, Siracusa, Italy (P. Leto, C. Raiteri)
- Effelsberg Radio Telescope (100 m) - Effelsberg, Germany (T. Krichbaum, L. Fuhrmann)
- IRAM Millimeter Telescope (30 m) - Pico Veleta, Spain (T. Krichbaum, H. Ungerechts)
- University of Michigan Radio Astronomy Observatory (UMRAO) (26 m) - Dexter, Michigan, USA (M. Aller)

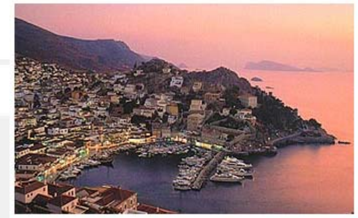

European Network for the Investigation of Galactic nuclei through Multifrequency Analysis

Appendix:

ESO-VLT blazar spectroscopy

ESO VLT high S/N spectroscopy of blazars with unknown redshift

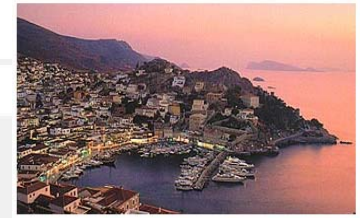

❑ Redshift z (i.e. distance) of blazars is a fundamental parameter to understand and constraint the physics of relativistic jets, multiwavelength (MW) emission models and the bolometric power emitted in gamma-rays.

❑ Spectral cutoffs due to gamma-ray absorption produced by the IR-opt-UV extragalactic background light (EBL), can be well studied using blazar-probes at different redshifts.

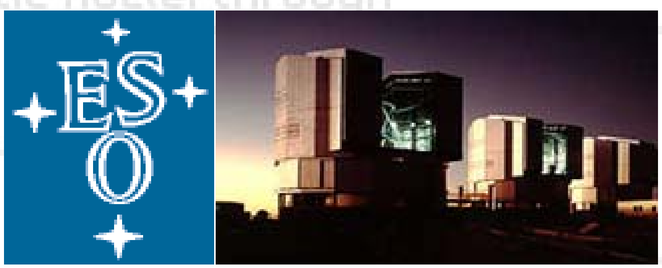

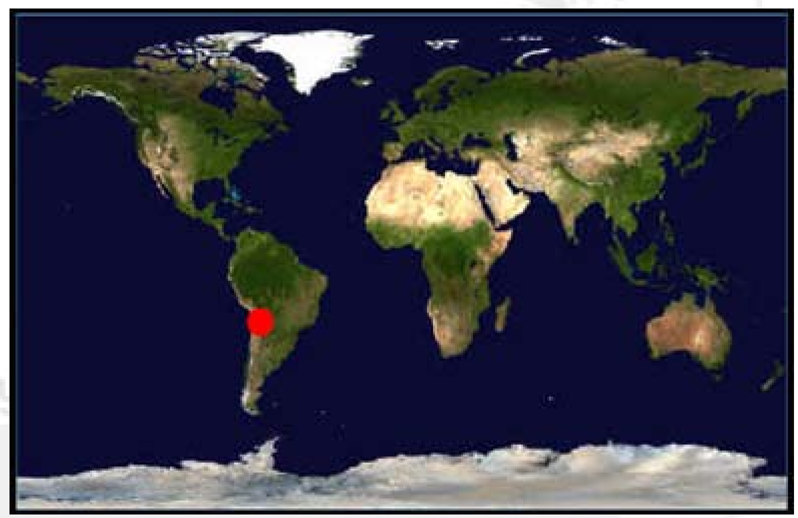

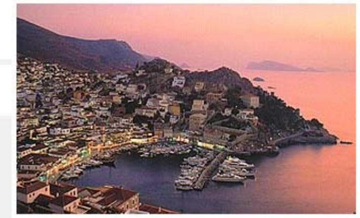

ESO VLT high S/N spectroscopy of blazars with unknown redshift

- ❑ A first observing program was accepted at the Very Large Telescope (VLT) of the European Southern Observatory (ESO, Cerro Paranal, Chile):
  High S/N spectroscopy of 16 southern blazars, (Period 77A, PI: S. Ciprini, COIs: J. Kotilainen & B. Sbarufatti).
- ❑ Times: observations (service mode) to be performed in the next southern winter 2006. Expected (prudent) success rate in new redshift determinations: 50%

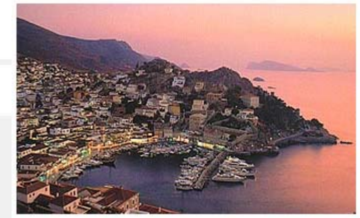

ESO VLT high S/N spectroscopy of blazars with unknown redshift

Why the VLT 8-meter (315 inch) "monster" telescopes ?

- **Especially in pure BL Lacs, the quasi-featureless optical spectra hinders the determination of z, while new catalogues of fainter blazars are being assembled. Moreover currently a squad of well known and monitored blazars have still unknown redshift.**

- **The 4m-telescope class has achieved its limit regarding to such "hard-to-show-features" blazars, and to the new (and fainter) blazar candidates.**

- **High S/N needed in reasonable integration observing times.**

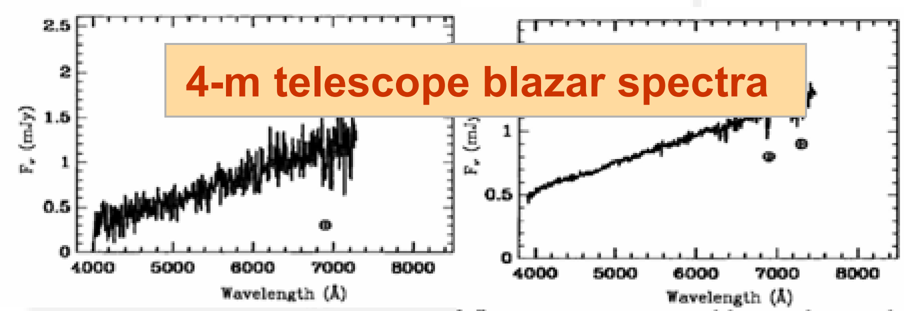

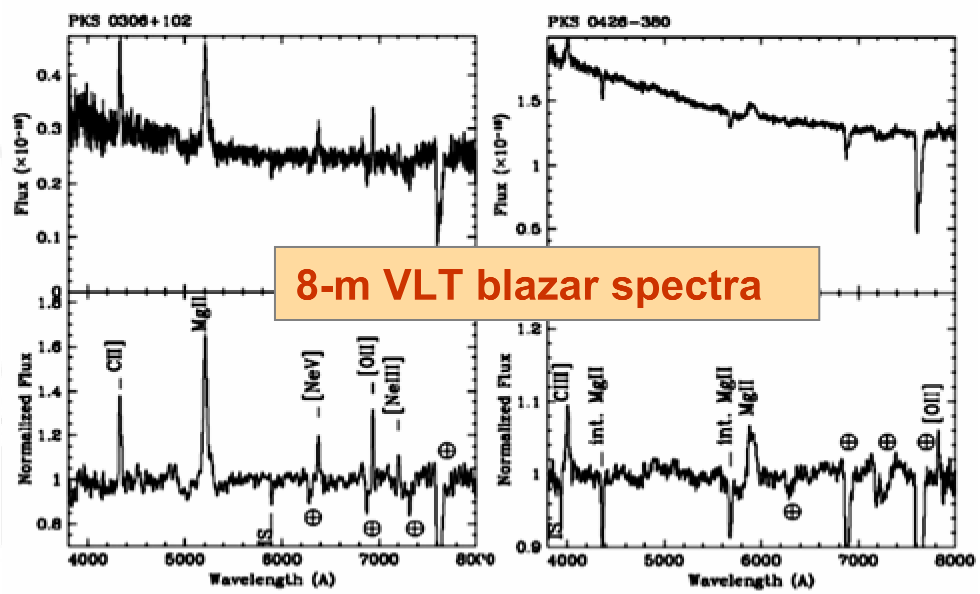

ESO VLT high S/N spectroscopy of blazars with unknown redshift

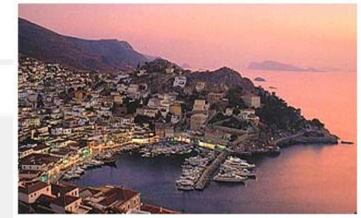

- Critical parameters for detection of spectral features are: (a) luminosity ratio between the nuclear and galaxy components; (b) the S/N of the observed spectrum; (c) redshift value and and the observed wavelength range.

- Criteria adopted in the sample selection: (a) sources classified as blazars (especially BL Lacs) with unknown redshift in the main surveys/catalogs/databases; (b) sources with DEC < +20°, mag(V) < 21; (c) sources with featureless spectra observed in 4-m telescopes; (d) new gamma-ray blazar candidates.

- Previous VLT program results (P71-P73, PI: A. Treves): high S/N level reached (up to 500) and features detected down to line EW = 1 Å. A total of 42 targets observed: new z determinations for 18 BL Lac objects (12 through emission lines, 5 through host galaxy absorption features, 1 trough both), lower limit to z for 2 objects (through MgII intervening systems), 6 misclassifications, and 18 blazars were found still featureless. Results published in Sbarufatti et al. (2005,2006).

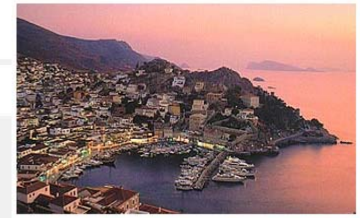

Epilogue

Two main astrophysical facilities of the:

European Space Agency (ESA)

and the:

European Southern Observatory (ESO)

have been successfully used.

Thank you for the attention.

7th ENIGMA Meeting

May 08-10, 2006 – Hydra Island, GREECE

The OJ 287 polarization monitoring programme at Calar Alto

Jochen Heidt (LSW), Kari Nilsson (Turku)
& the ENIGMA-team

in support of
the OJ2005-2008 campaign

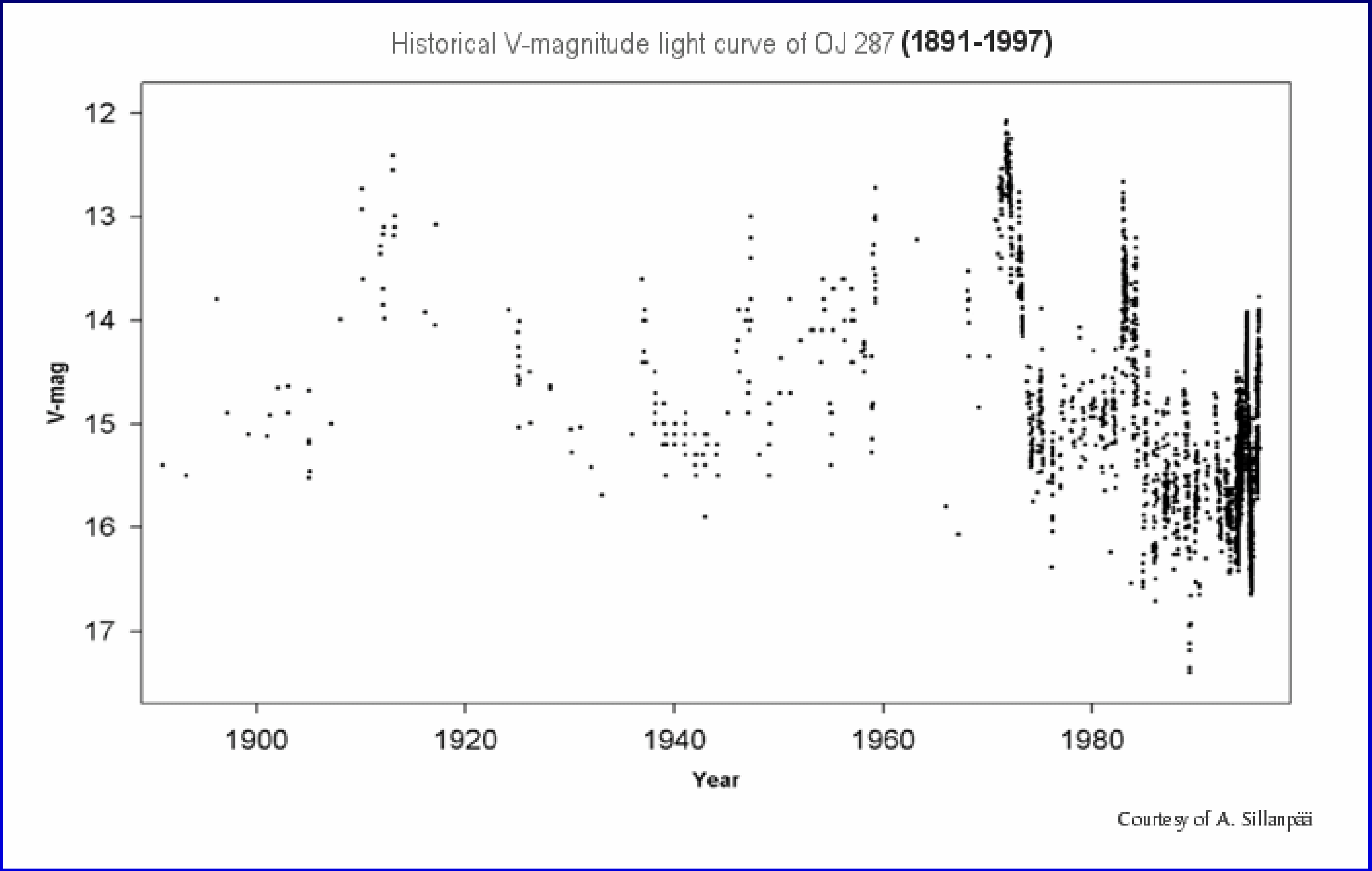

Periodic outbursts on timescales of about 12 years:

Binary BH in center of OJ 287, flares are caused by secondary hitting the accretion disk of the primary (Sillanpää et al. 1988)

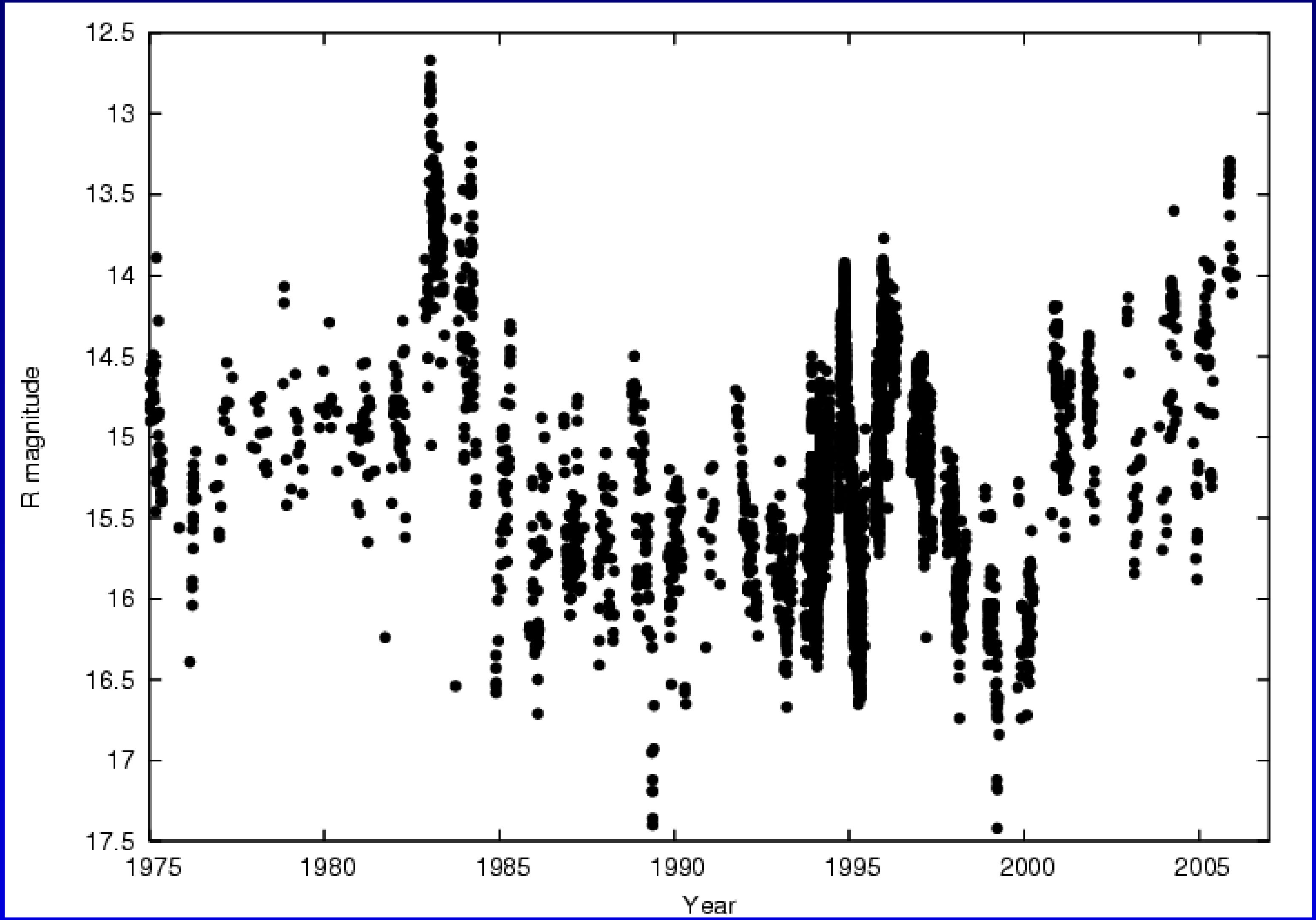

OJ-94 project: monitor the expected outburst in 1994

➔Somewhat unexpected: double-peaked outburst (as in 1982/1983)

➔New (refined) models!!!

Models to be tested

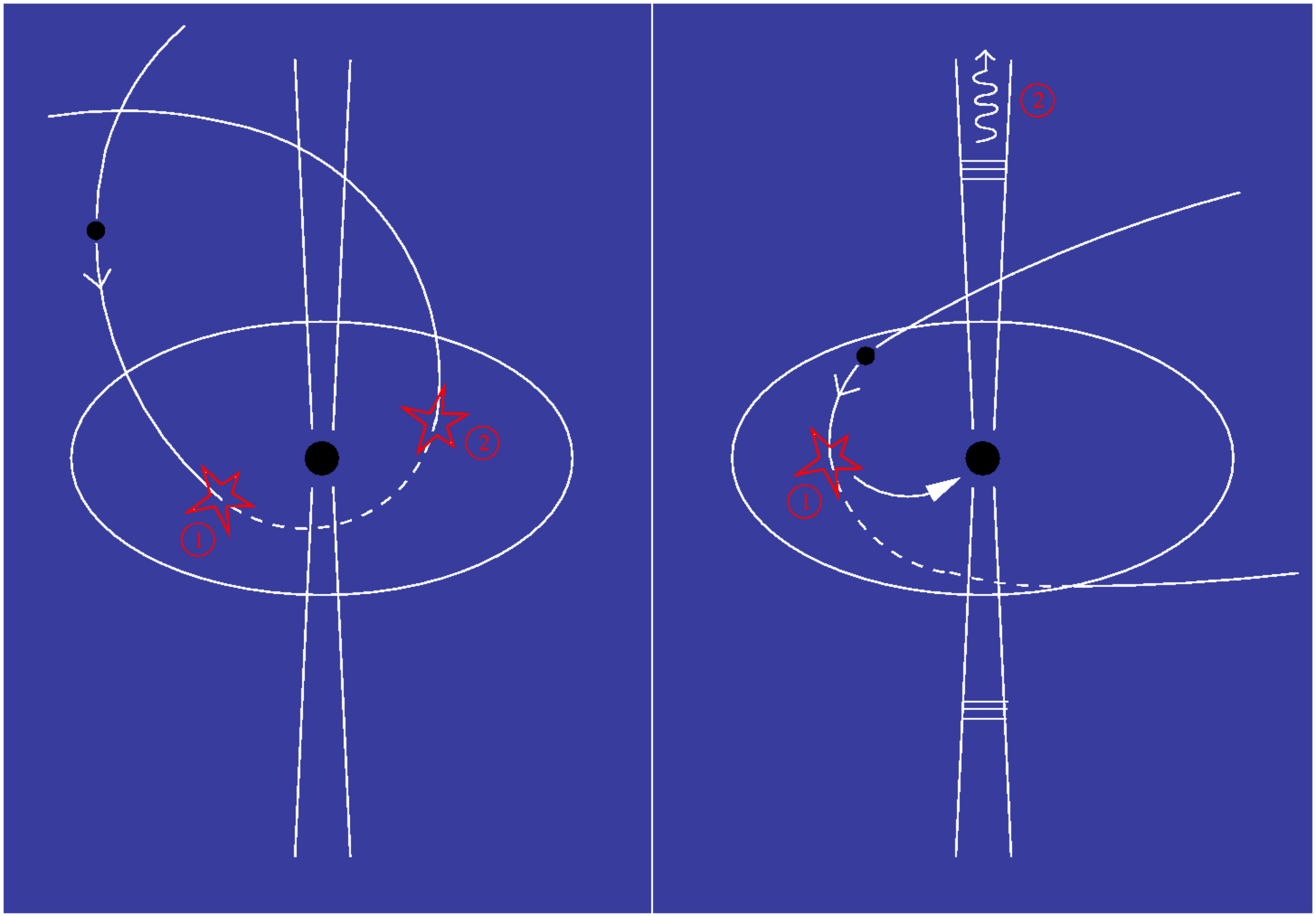

LV (Lehto & Valtonen 1998) SV (Sillanpää, Valtaoja 1988, 2000)

LV model

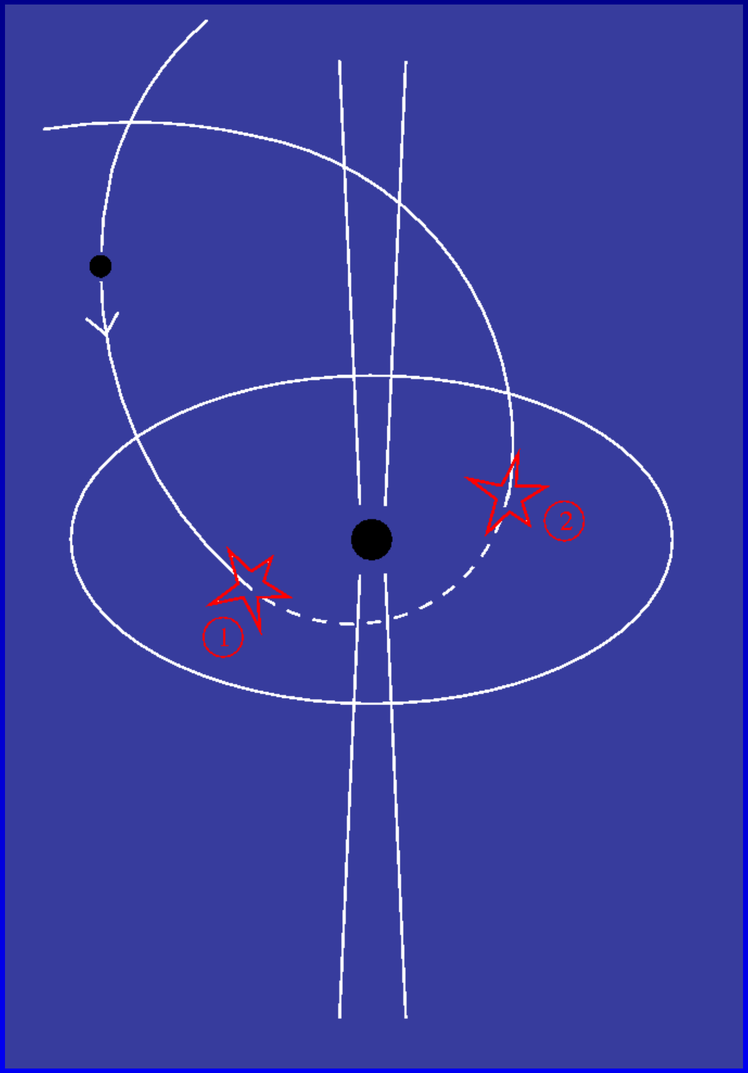

High primary mass ($1.7 \bullet 10^{10} M_{\odot}$)

$P_{orb} = 12.07$ y

Strong precession of the orbit

SV model

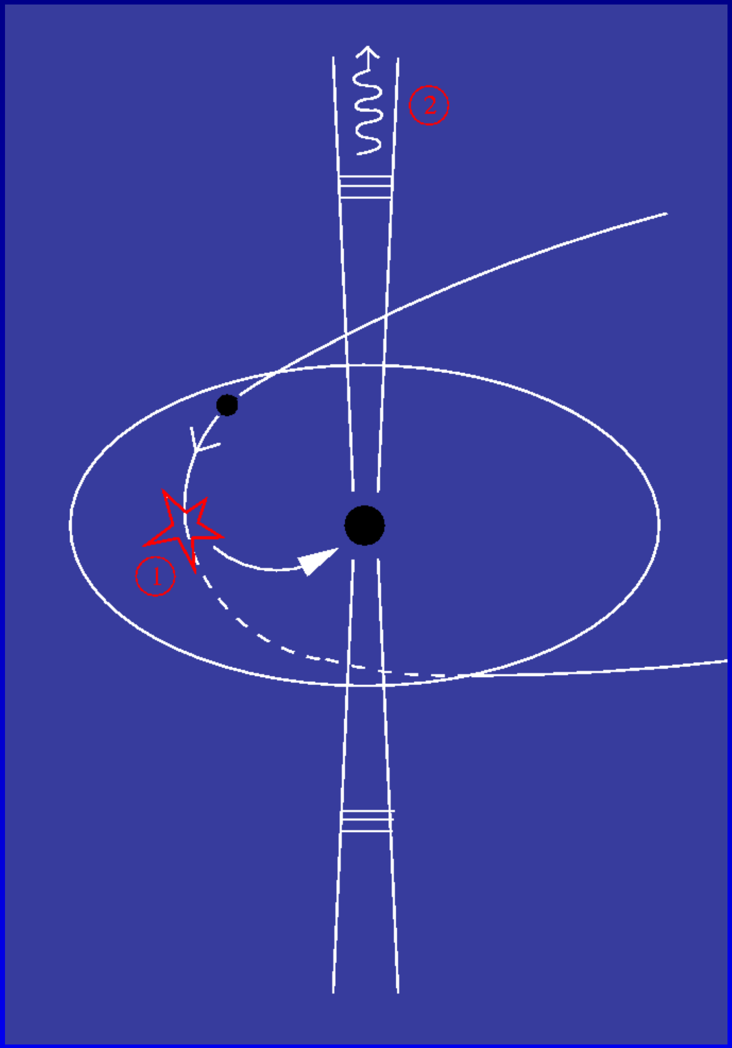

No constraint on BH masses

P_{orb}= 11.86 y

No precession

Different predictions

	LV-model	SV-model
Outburst 1:	March 2006	September 2006
	not polarized	not polarized
	P decreases, PA no change (both models)	
Outburst2:	April 2007	October 2007
	not polarized	polarized
	P decreases, PA no change	P changes, PA changes

➔➔ Polarization measurements may help to distinguish between models!!!

The long-term polarization monitoring programme at Calar Alto

Calar Alto, 2.2m telescope + CAFOS equipped with Savart plate

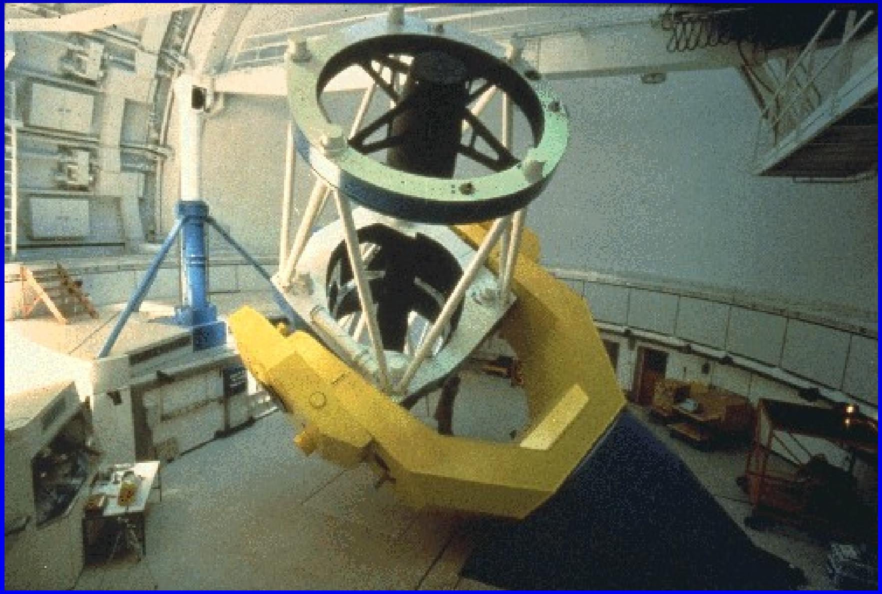

Observing strategy

Running time: Jan 2006 – May 2008

1 measurement every 3rd night in R-filter , whenever CAFOS is mounted and Fabry-Perot not in use
(AM < 2, from mid-September until end of May)

~30min per measurement, 4 angles (0, 22.5, 45, 67.5) to derive polarization degree and polarization angle ➔ 15n in total

➔Test observations on Nov, 4th ➔ only 15-20min tel.time required

Logistics (expo-times depending on brightness, archiving etc.) via JH, “online“ data reduction, feeding the WEB by KN

Provide “backbone“ of polarization monitoring in combination with KVA (Swedish robotic 60cm telescope on La Palma)

Current status:

~18 observations since Jan, 4th 2006 (only 5 in Jan/Feb due to bad weather)

➔➔ Interaction with and SM done at CA works perfectly

➔ Prompt E-mail notification once data taken

➔ Easy retrieval from archive (ftp)

➔ Data are reduced and analyzed the next morning

➔ Results are immediately displayed afterwards at

http://users.utu.fi/~kani

And the results so far?

➔➔ Some surprises!!!

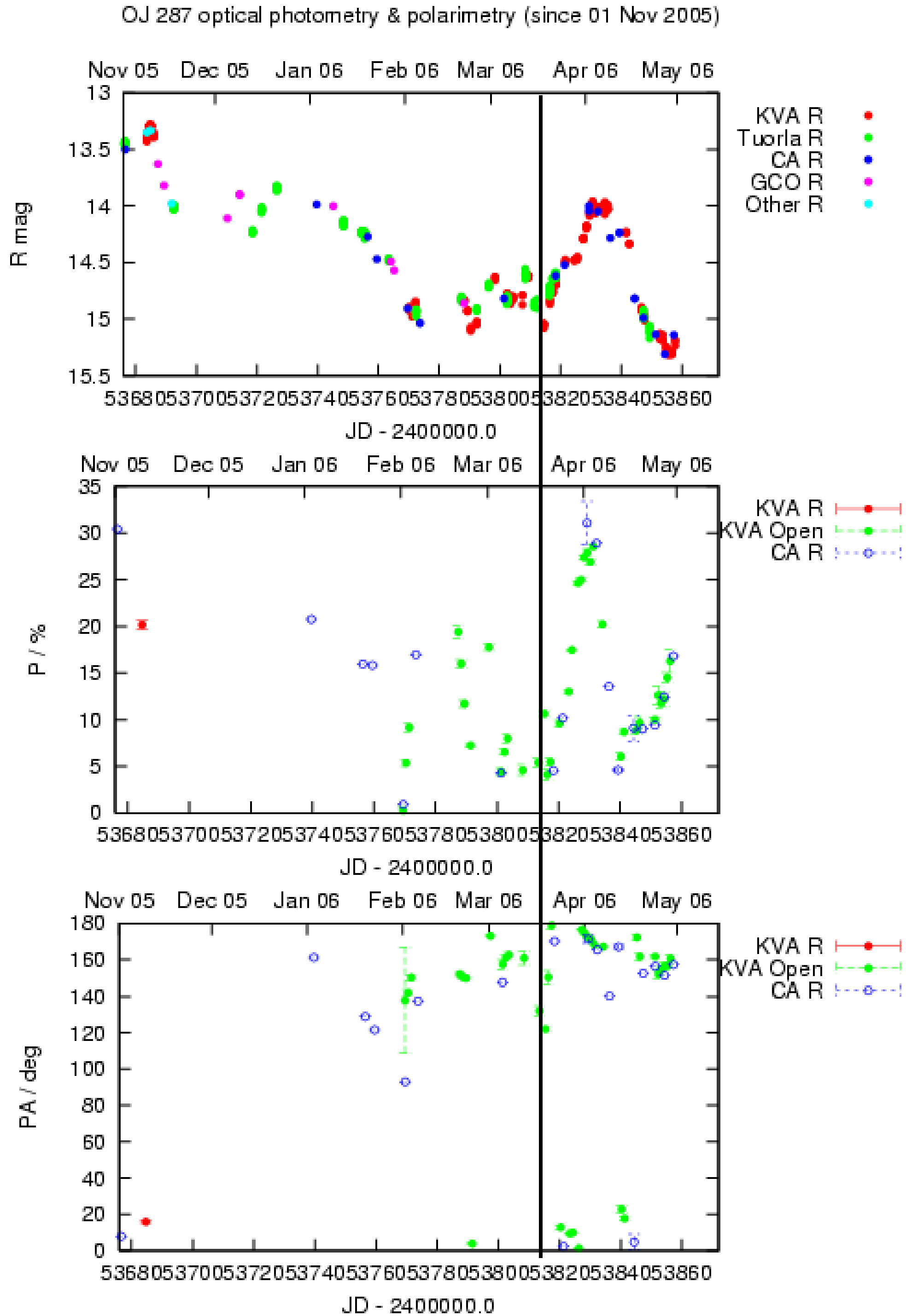

- Last update: May, 2!
- No outburst as expected for the LV-model (black-line)
- 1 mag outburst + increase of polarization by 30º a few weeks later; ➔ synchrotron ,NOT LV
- Strong variation of flux, polarization and polarization angle, but not always 1:1 correspondence!
- Average PA seem to have changed by ~40º
- CA + KVA-data nicely agree + cancel out bad weather at least in part

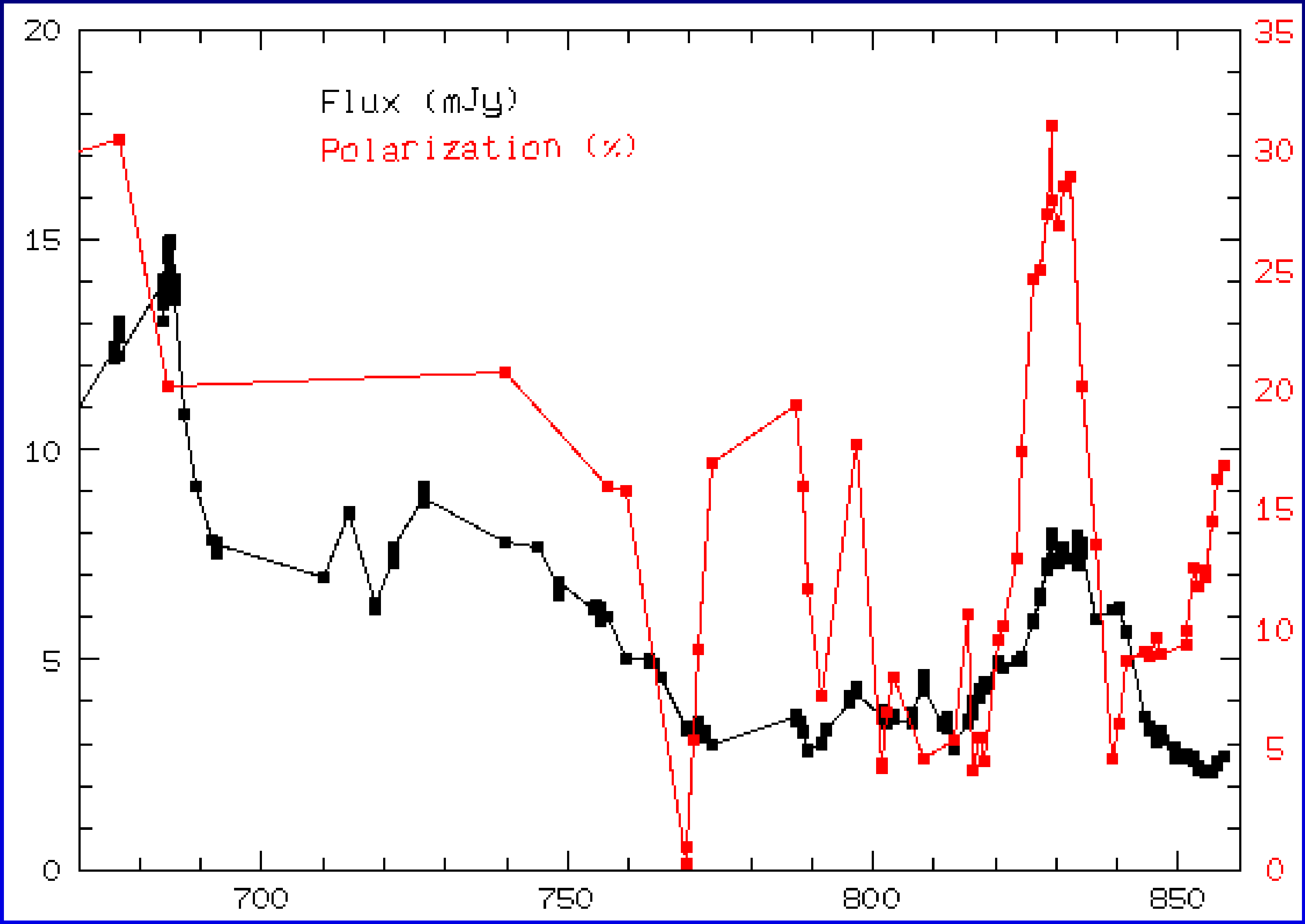

Photometric and polarimetric behaviour of OJ 827 since Nov 2005

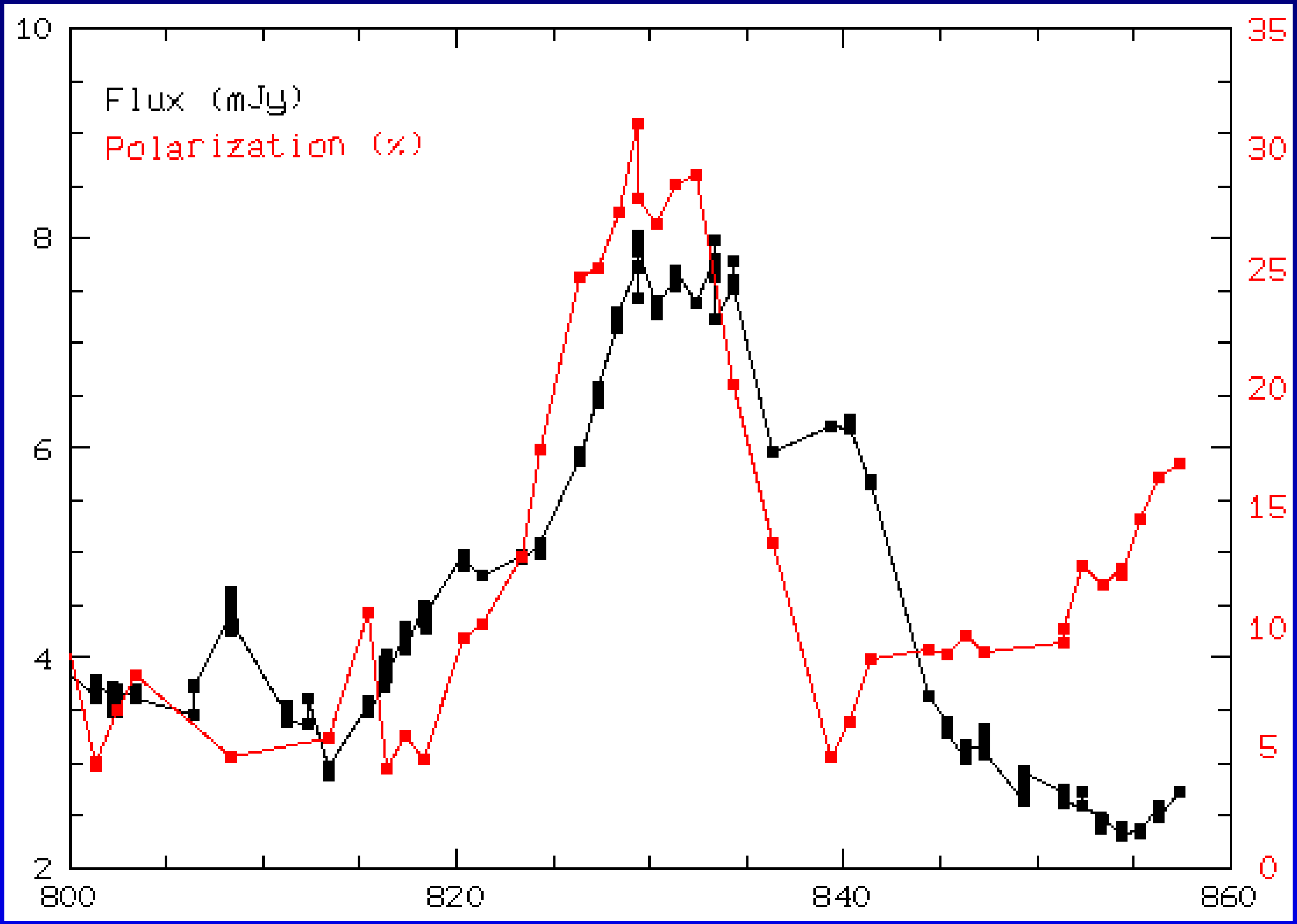

Photometric and polarimetric behaviour of OJ 827 during flare in April 2006

Lessons for the future???

It will be very hard to determine a typical photometric/polarimetric behaviour of OJ 287 and to separate it from the “hunted“ outbursts,

BUT:

- The SV-model MUST be correct (otherwise we are in trouble)
- Next (first) outburst MUST happen in September
- Increase the sampling 1 per night during the expected outburst period (from the observability of OJ 287 until end of October), 1 per 3 night for the rest of the observing season (meanwhile approved for autumn 2006 by CA-TAC, top-ranked proposal!!!)
- Do possibly the same for the expected 2nd outburst in 2008 then (if the 1st occurs)
- Apart from that: First long-term polarimetric program of any BL Lac/QSO ➔ photometric/polarimetric flare unique ➔ publication?

The broad band campaign of OJ 287 – First results in terms of short-term variability

Lars Fuhrmann

Torino/Perugia team

S. Ciprini, N. Marchili, C. Raiteri, M. Villata, E. Angelakis, G. Tosti,
T. P. Krichbaum, A. Witzel
&
the WEBT

7th ENIGMA meeting, May 2006

Overview

- Introduction
- Radio observations at 5 and 10 GHz with Effelsberg
- First results
- Optical R band data
- Conclusions

Introduction

- core campaign in April and November 05:
  simultaneous radio observations with Effelsberg
  at 6 and 2.8 cm

- 1) 12/13. April 2004: ~10 hrs (Epoch 1)
  2) 7 – 10. November 2004: 3 x ~10 hrs (Epoch 2)

- **Motivation:**
  - simult. data in the radio/optical/X-ray on short (hours/days) time scales:

→ study of short-term variability behaviour before and during outburst

→ search for broad band correlations and possible time lags

→ radio: IDV behaviour still poorly known
  Epstein et al. (1972): short-term variability in OJ 287

Introduction

is OJ 287 really an IDV source also in the radio ?

correlated radio/optical IDV ?

intrinsic/extrinsic (interstellar scintillation) ?

Radio observations

- Effelsberg at 2.8 and 6 cm
- Epoch 1: 1 session of about 10 hrs simult. to XMM pointing
- Epoch 2: 3 runs with delay w.r.t. XMM pointing
  11 cm observations failed
- fast duty cycle: 1 scan per frequency every ~ 20 min
- same duty cycle for sec. calibrators: 0827+24, 0836+71,
- tau-, gain-correction, time-dependent correction
- primary calibrators: 3C286, NGC7027, 3C295
- weather not perfect
- measurement errors: ≤ 1%
- standard IDV analysis

Epoch 1

First results

6cm m_0=0.28

$<S>$[Jy]	m[%]	Y[%]	χ^2_{red}	$\chi^2_{99.9\%}$
1.598	0.65	1.74	3.87	2.19

2.8cm m_0=0.35

$<S>$[Jy]	m[%]	Y[%]	χ^2_{red}	$\chi^2_{99.9\%}$
2.072	0.76	2.01	4.41	1.90

$$m\,[\%] = 100\,\sigma/<S>$$

$$Y\,[\%] = 3\,(m^2 - m_0^2)^{0.5}$$

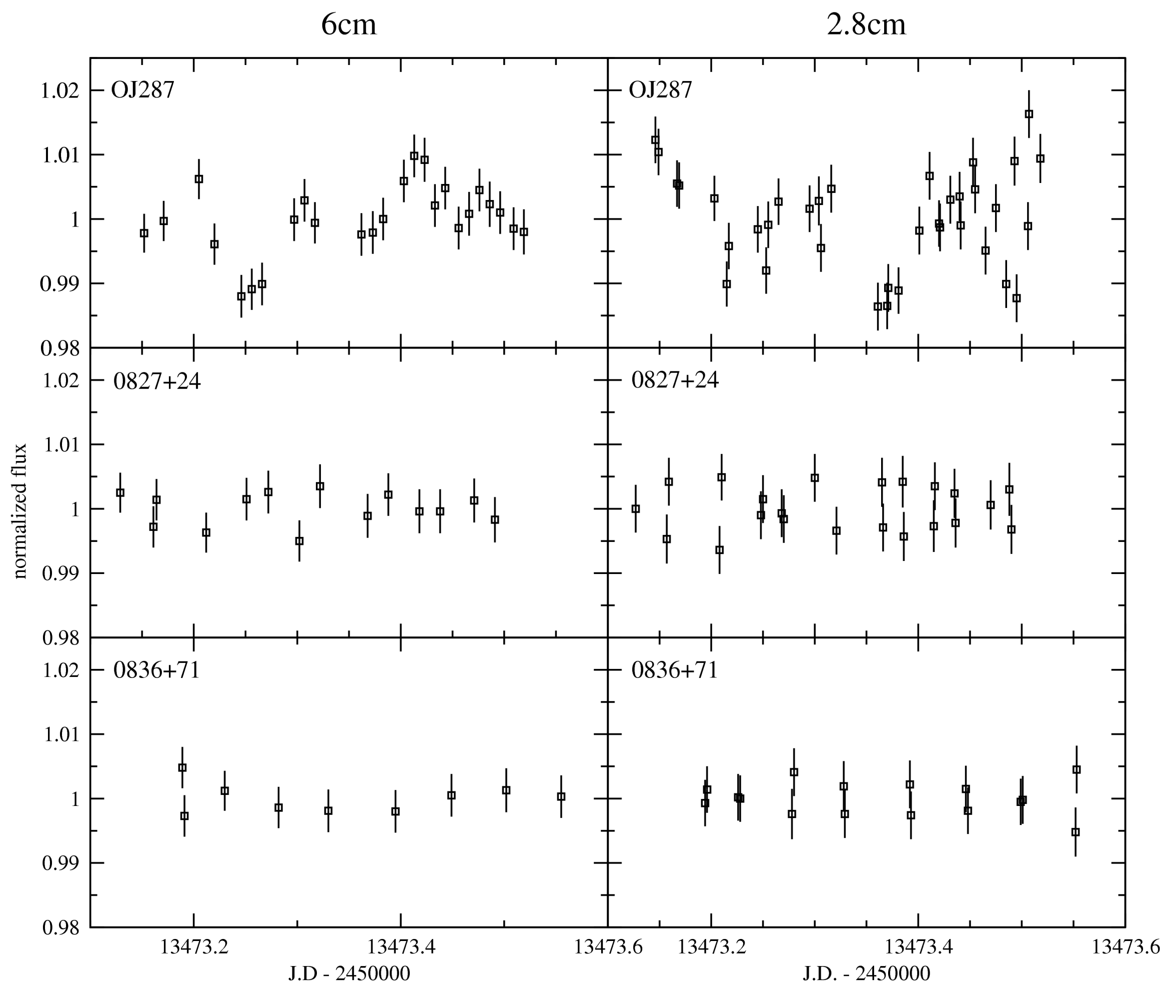

Epoch 2

First results

2.8 cm

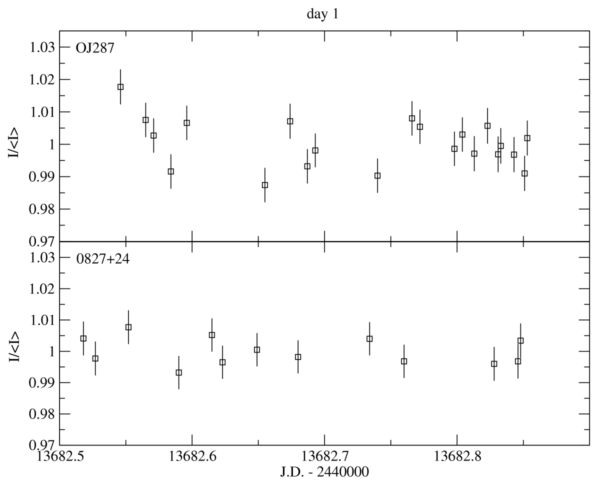

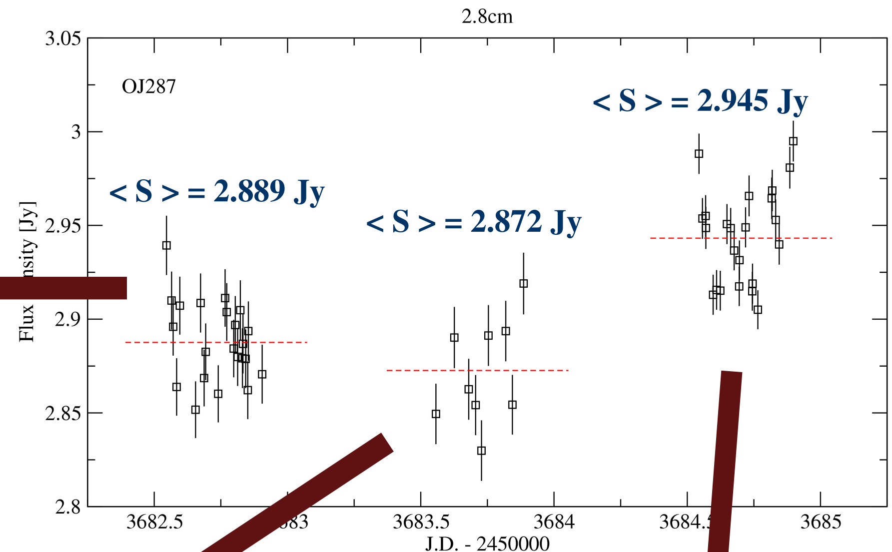

ΔS = 73 mJy
5% p2p

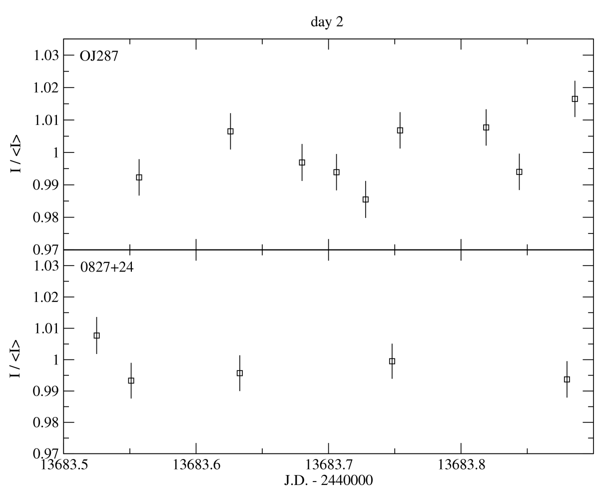

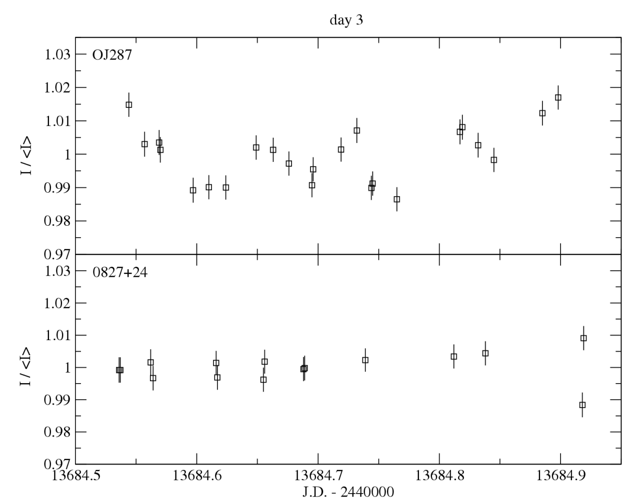

Epoch 2

First results

6 cm

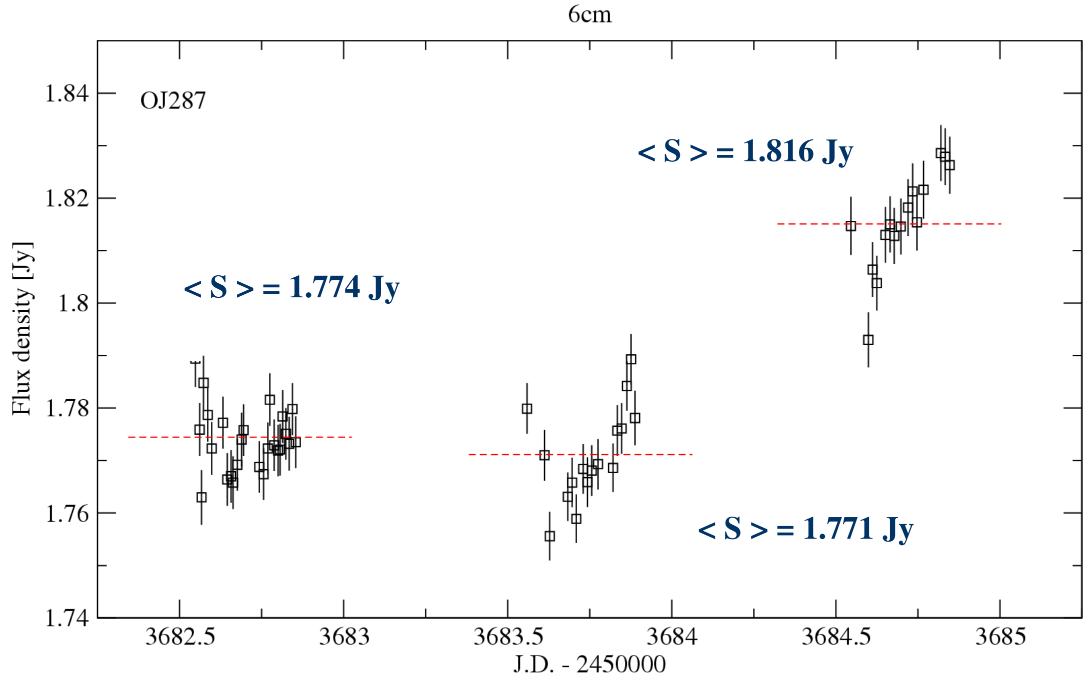

ΔS = 45 mJy
4% p2p

Epoch 1

Optical R band data

- **so far IDV data only for Epoch 1 using a sub-set of optical telescopes**

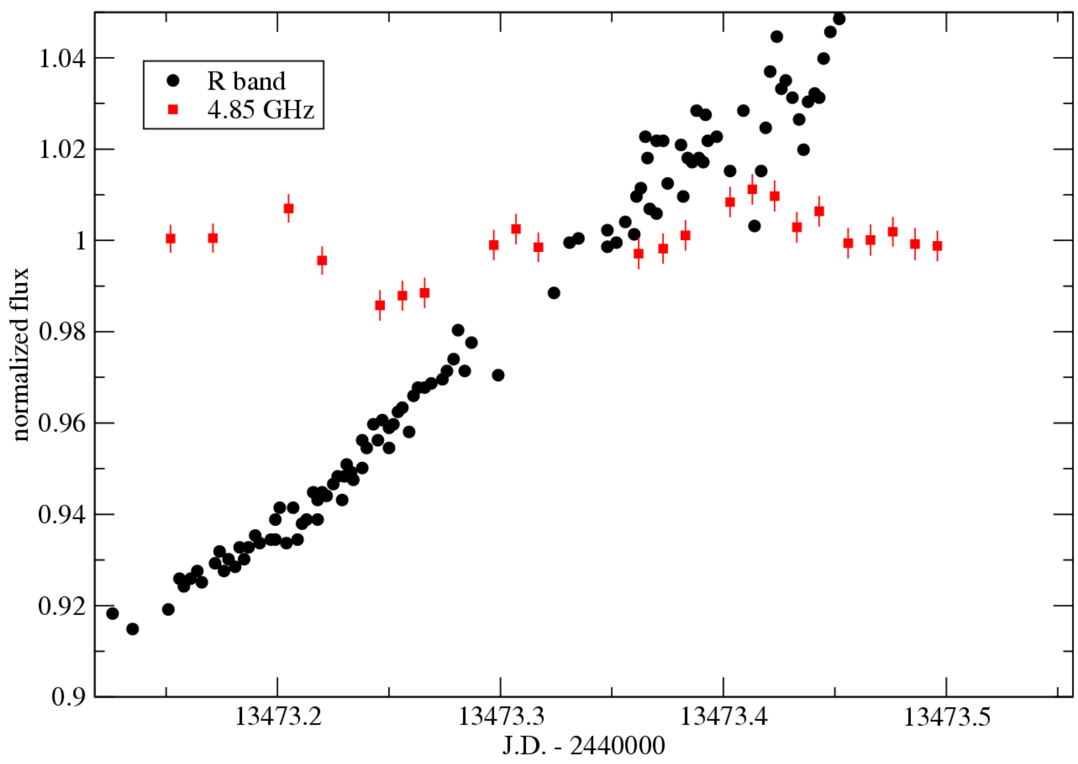

Summary

- radio: OJ 287 seems to be an IDV source
- but: only low-amplitude (2-3%) but fast variations on time scales of hours, significant only during Epoch 1
- Epoch 2: inter-day (> 1.2 days) variations significant (~ 4-5%), appear correlated
- if intrinsic: $T_B \sim 10^{15}$ K, D ~ 15
- m stronger at higher frequencies,
- optical: Epoch 1 shows IDV with $\Delta R \sim 0.3$
- no radio/optical correlation during Epoch 1

Outlook

- collect optical data of Epoch 2 and hope!!!
- compare with XMM - LCs
- propose new radio observations during Epoch 3 but more extended in time !
- add more radio frequencies → interstellar scintillation ?

Multiwavelength H.E.S.S. campaign of PKS 2155-304 during 2004

D.Emmanoulopoulos, S.Wagner

7th ENIGMA meeting, Hydra 8-10 May GREECE

Landessternwarte Heidelberg

ENIGMA

Overview

The 4th most distant TeV blazar at z=0.117.

Overview

The 4th most distant TeV blazar at z=0.117.

Previous Campaigns:

- July-October 2002, June-September 2003:
  Only H.E.S.S. 7 nights (1-2 N_{tel})
- October-November 2003:
  H.E.S.S., RXTE, ROTSE, Nançay 16 nights
  (2-3 N_{tel})

Overview

The 4th most distant TeV blazar at z=0.117.

<u>This Campaign:</u>

- August-September 2004:
  H.E.S.S., RXTE, ROTSE, La Palma (KVA), Nançay, Boyden, REM, CTIO, Siding Springs.
  21 nights ($\sim$ 30 after weather corrections)
  (4 $N_{\rm tel}$)

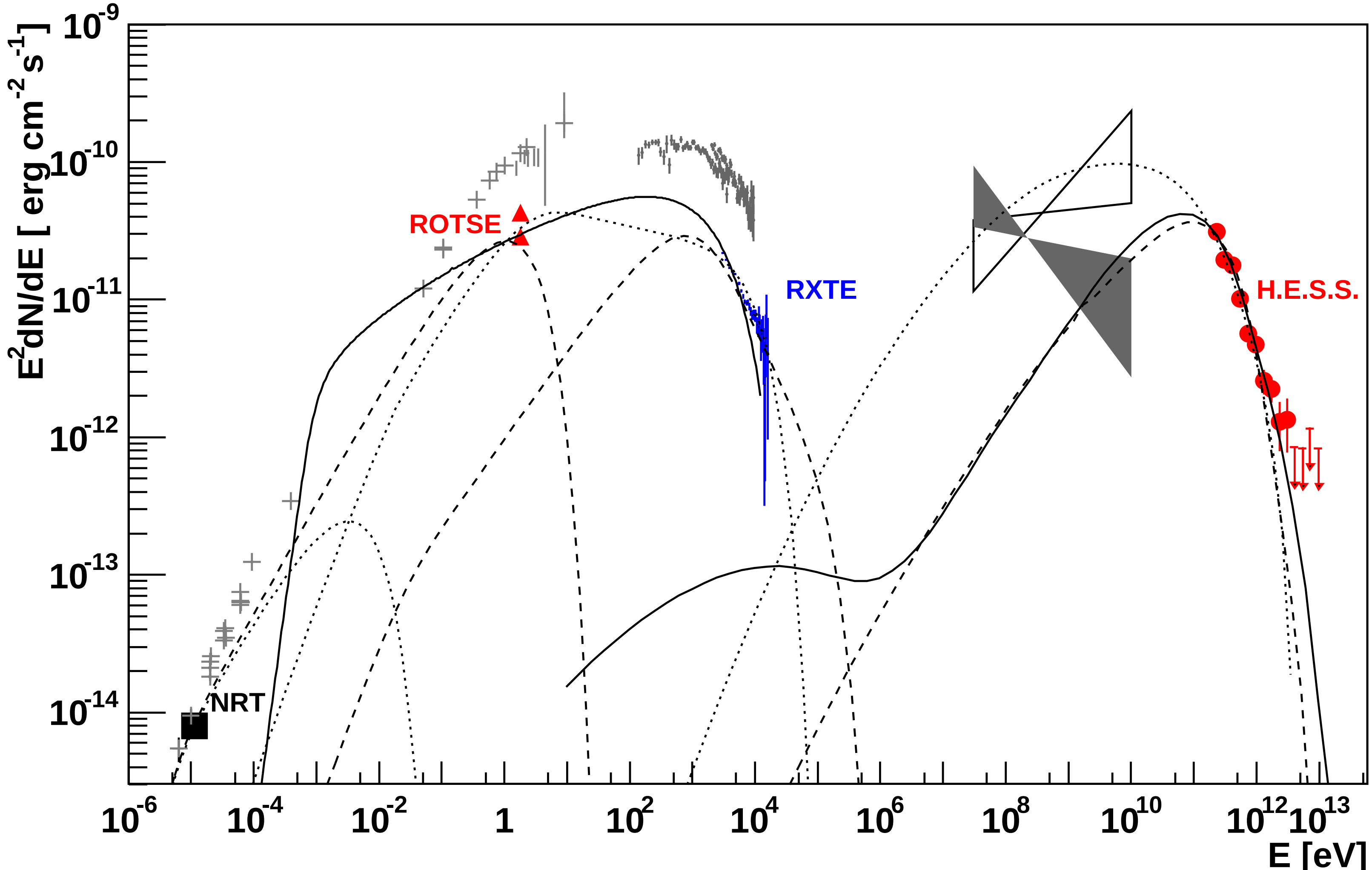

Aharonian et al. 2005

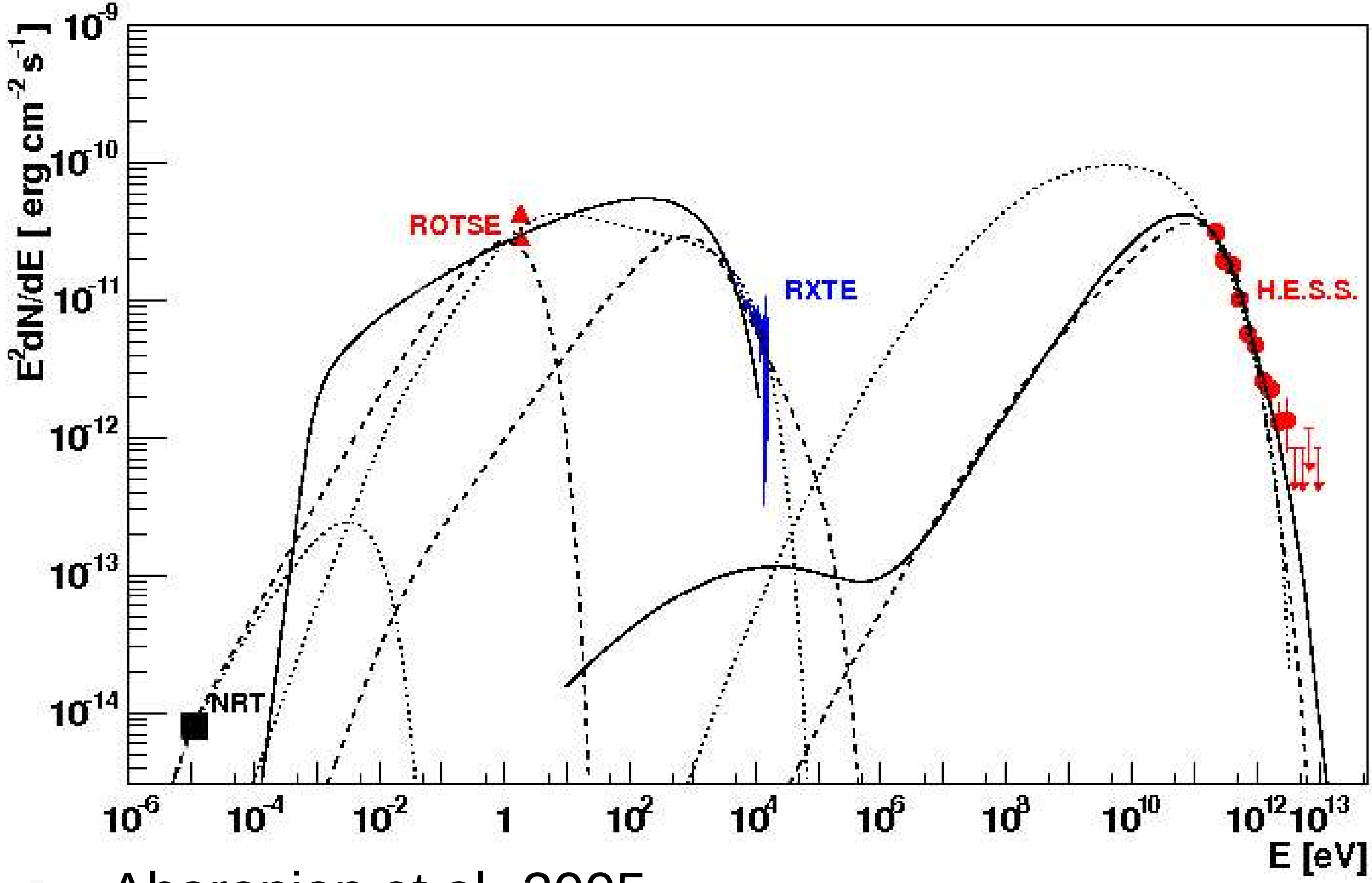

Aharonian et al. 2005

What is H.E.S.S.?

What is H.E.S.S.?

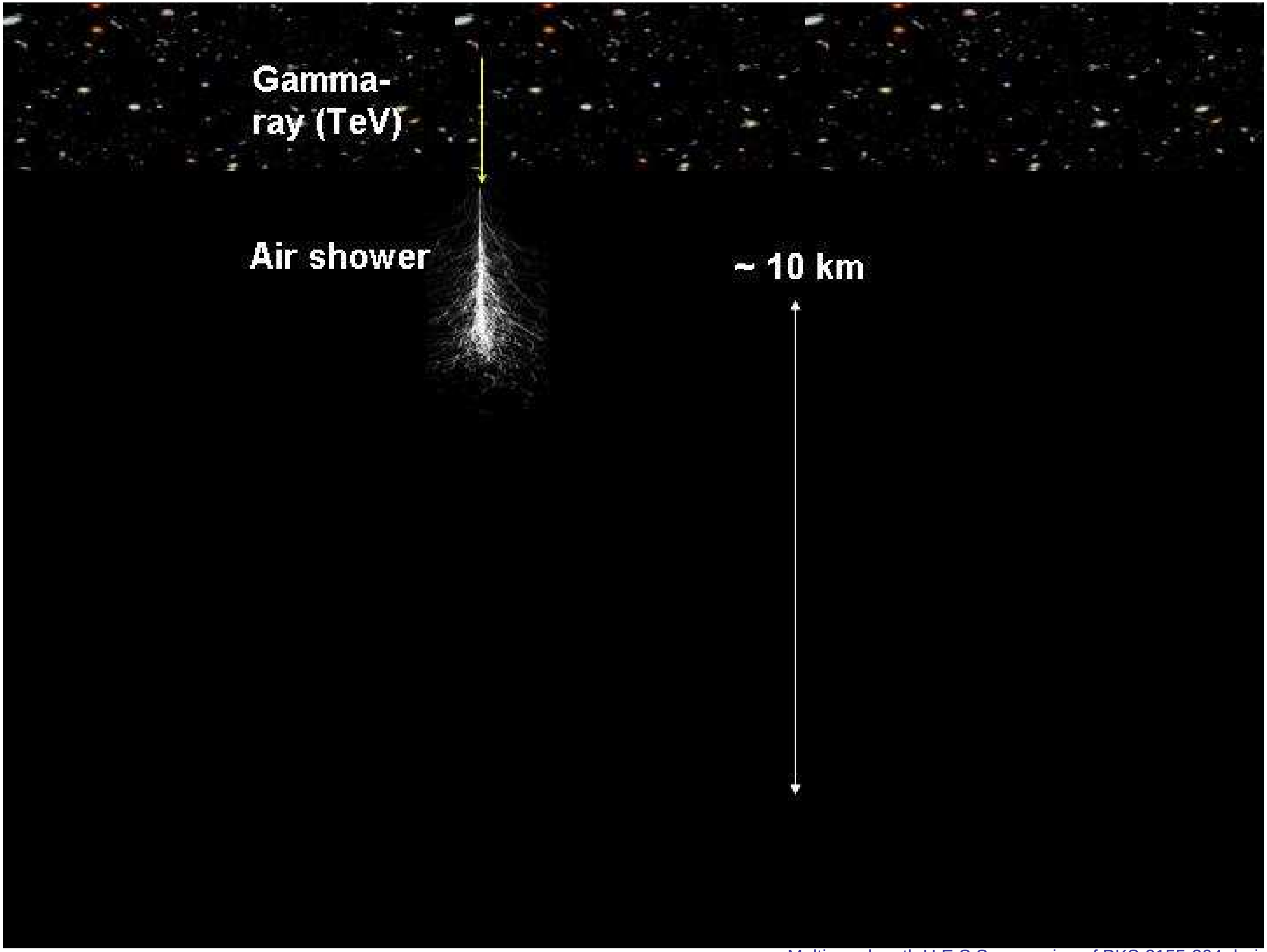

What is H.E.S.S.?

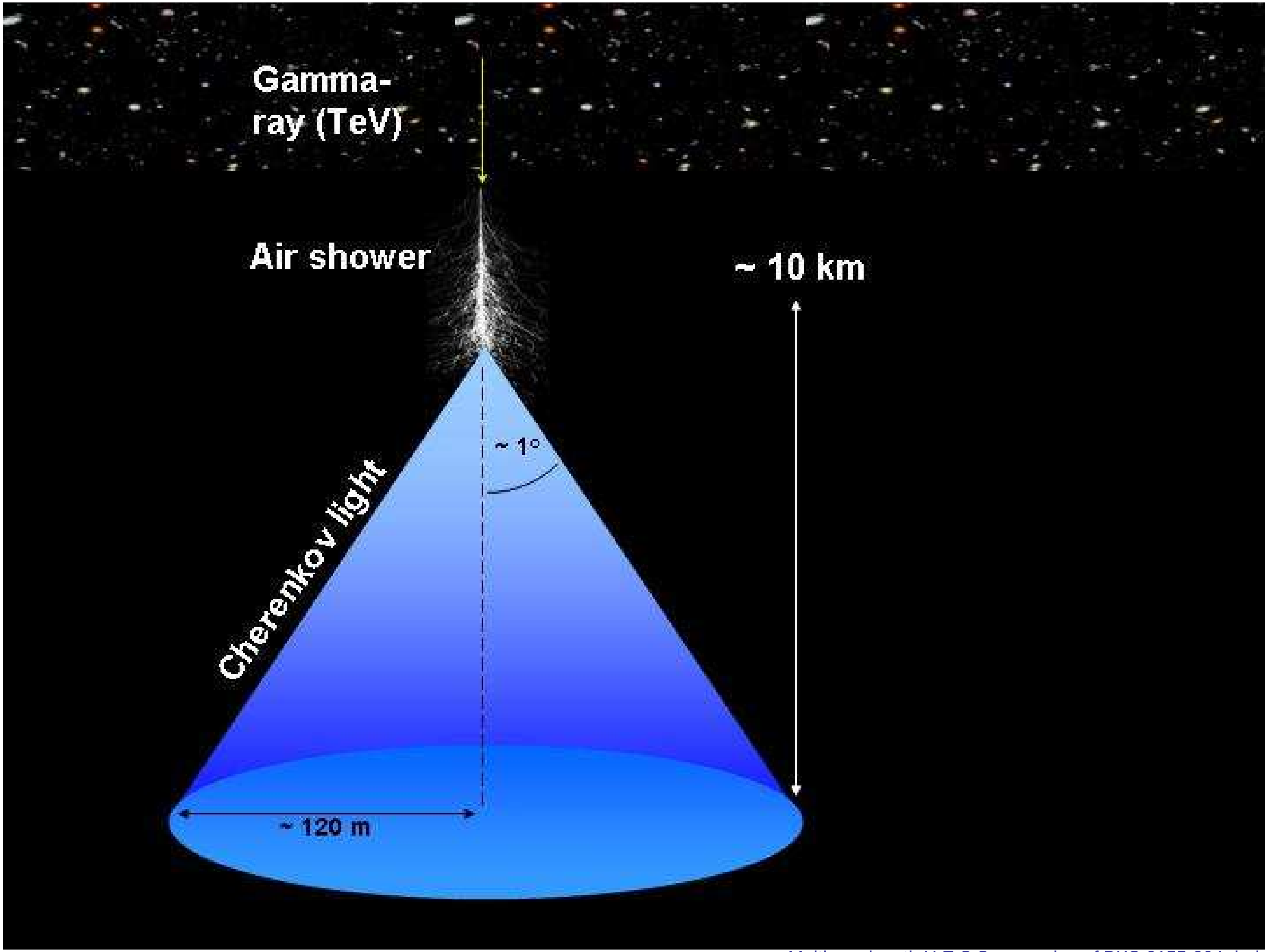

What is H.E.S.S.?

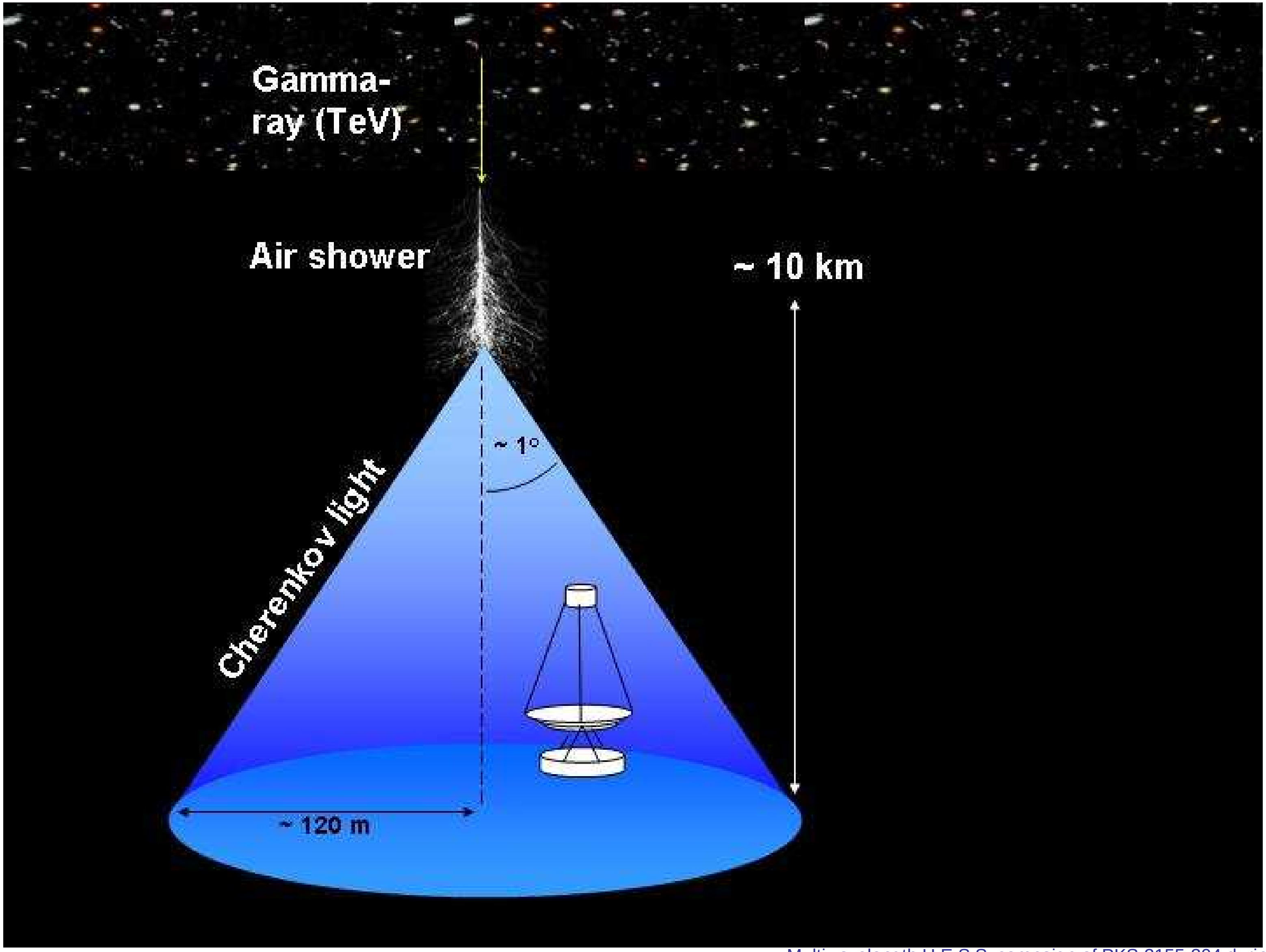

What is H.E.S.S.?

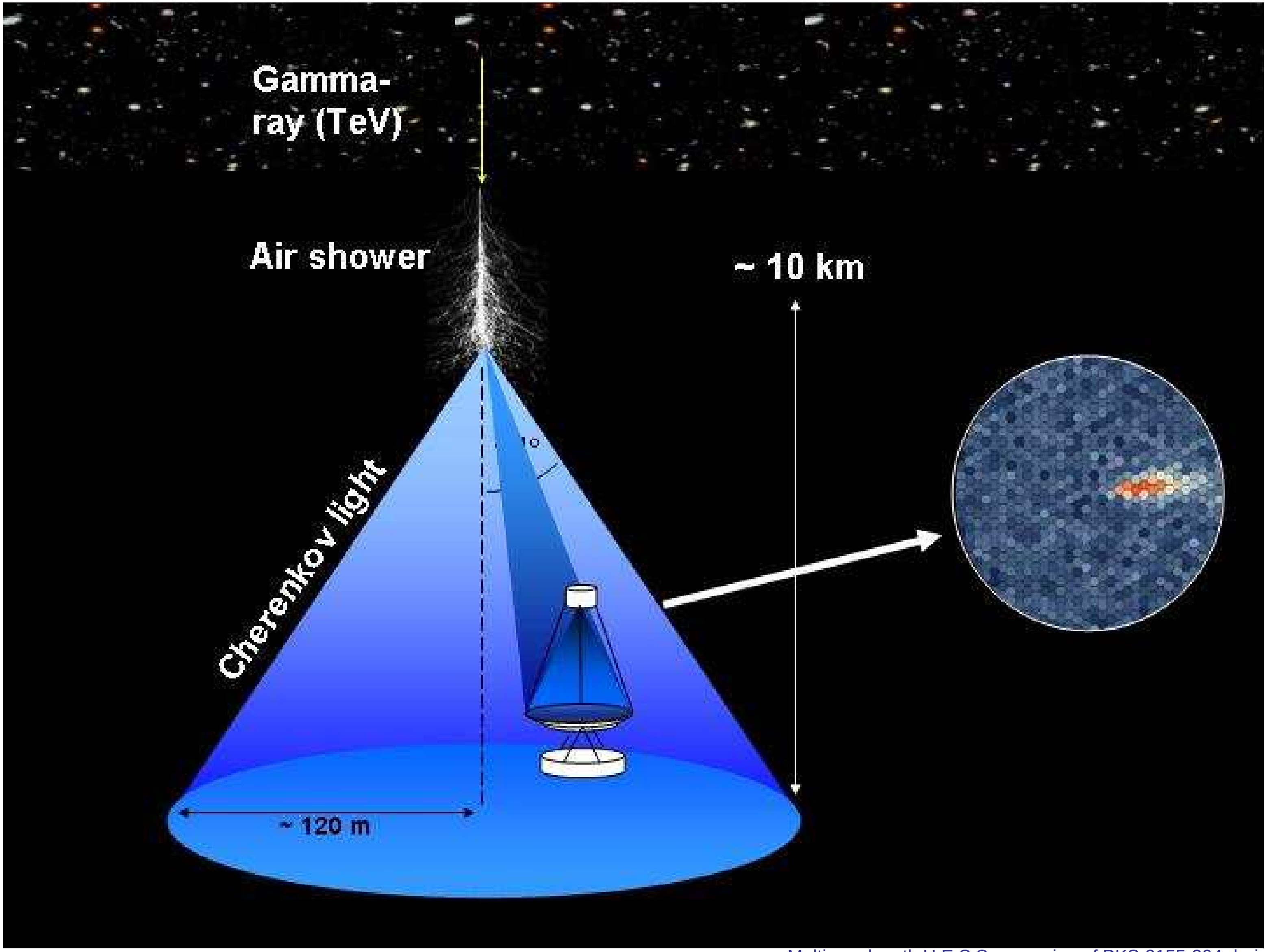

What is H.E.S.S.?

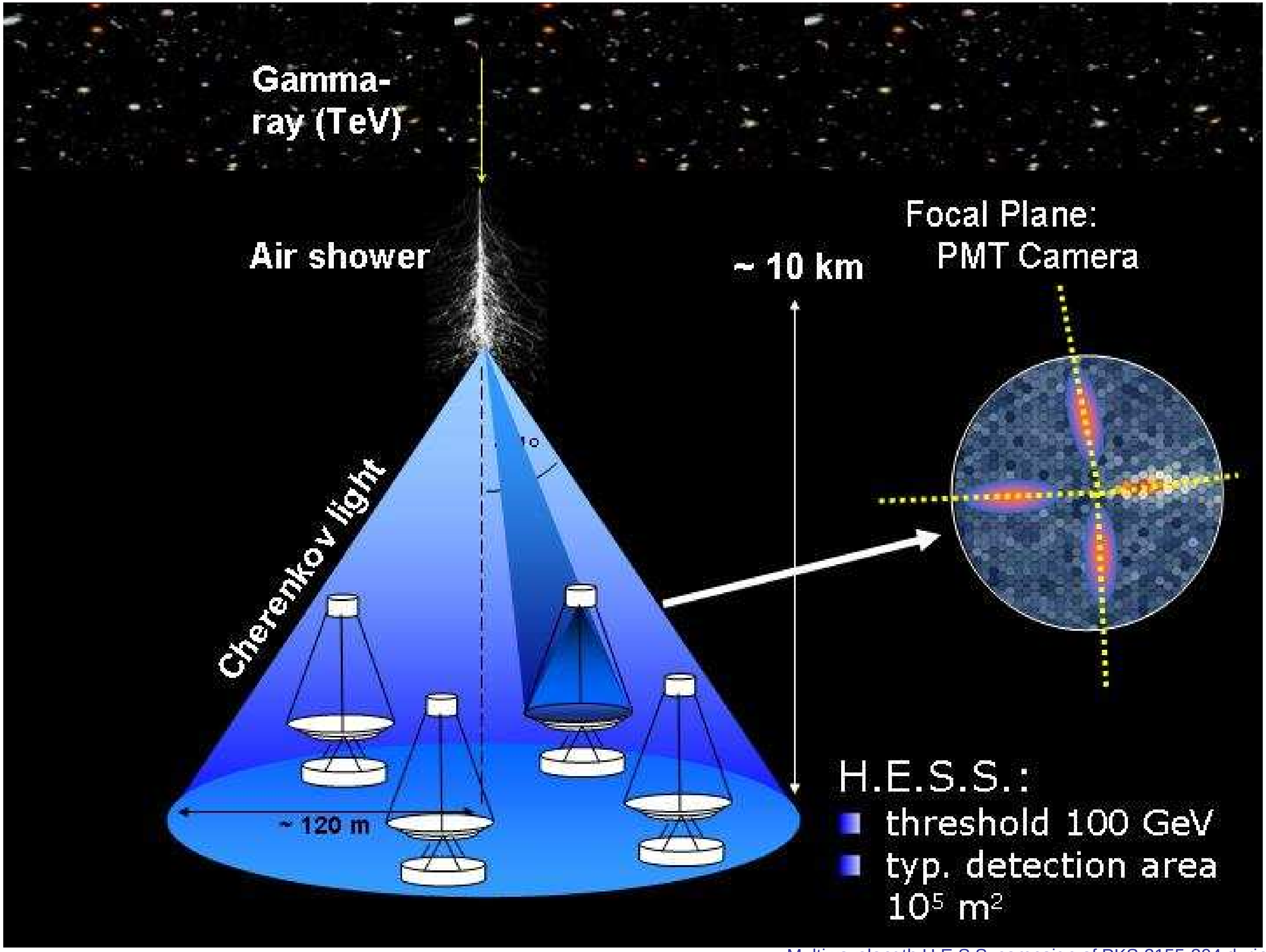
Gamma-
ray (TeV)
Air shower
~ 10 km
Focal Plane:
PMT Camera
Cherenkov light
1°
~ 120 m
H.E.S.S.:
threshold 100 GeV
typ. detection area
10⁵ m²

The Light Curves

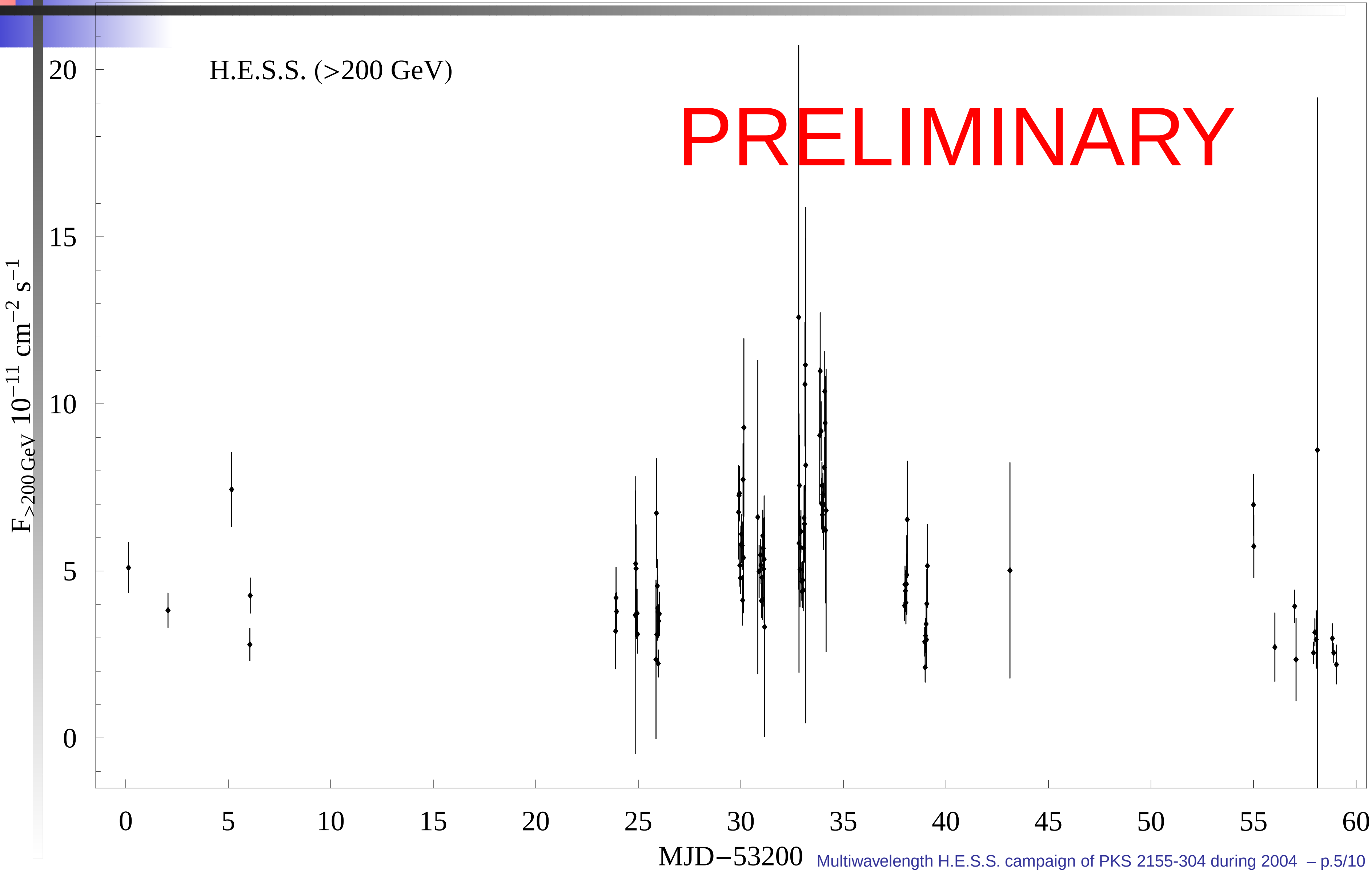

The Light Curves

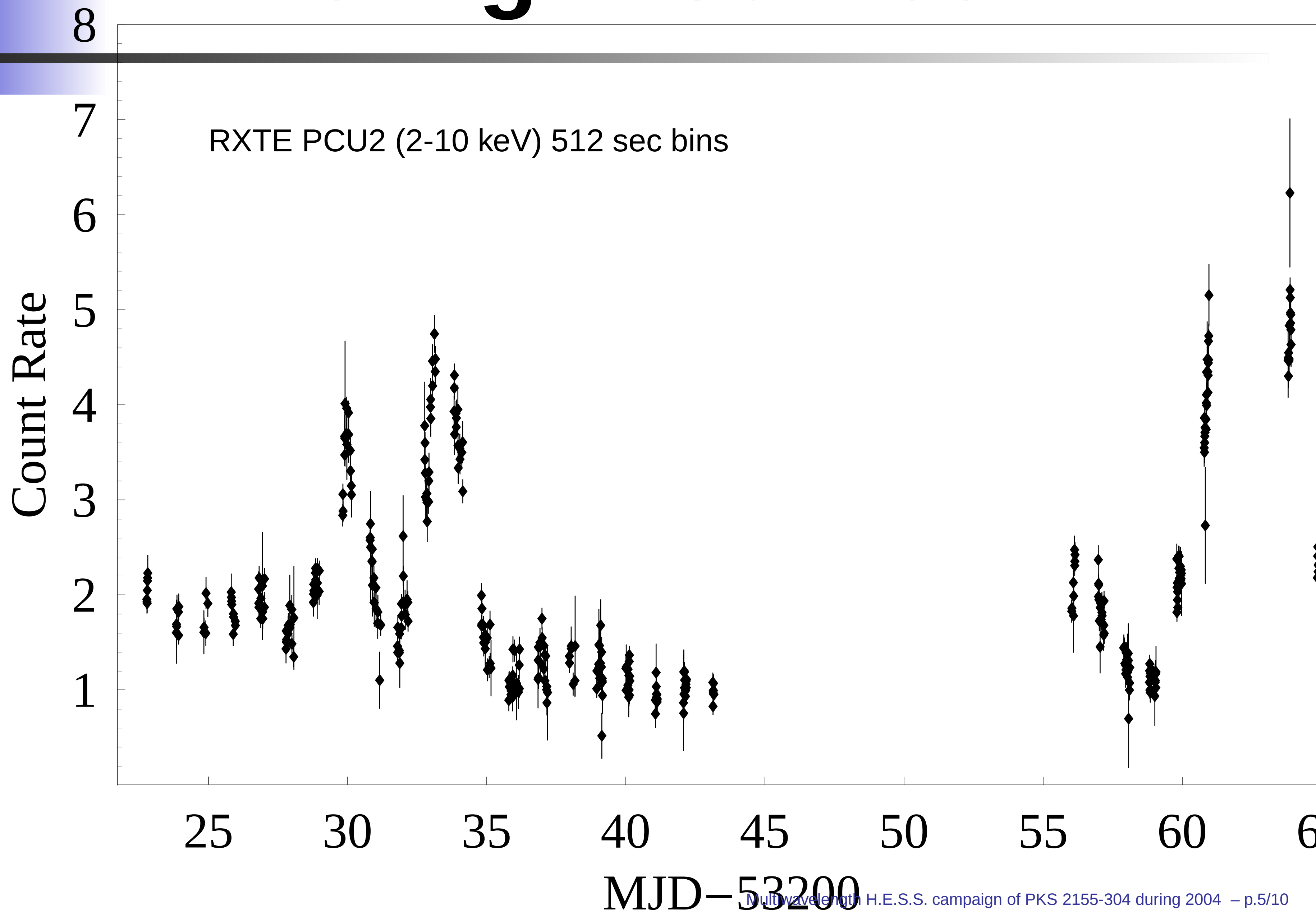

The Light Curves

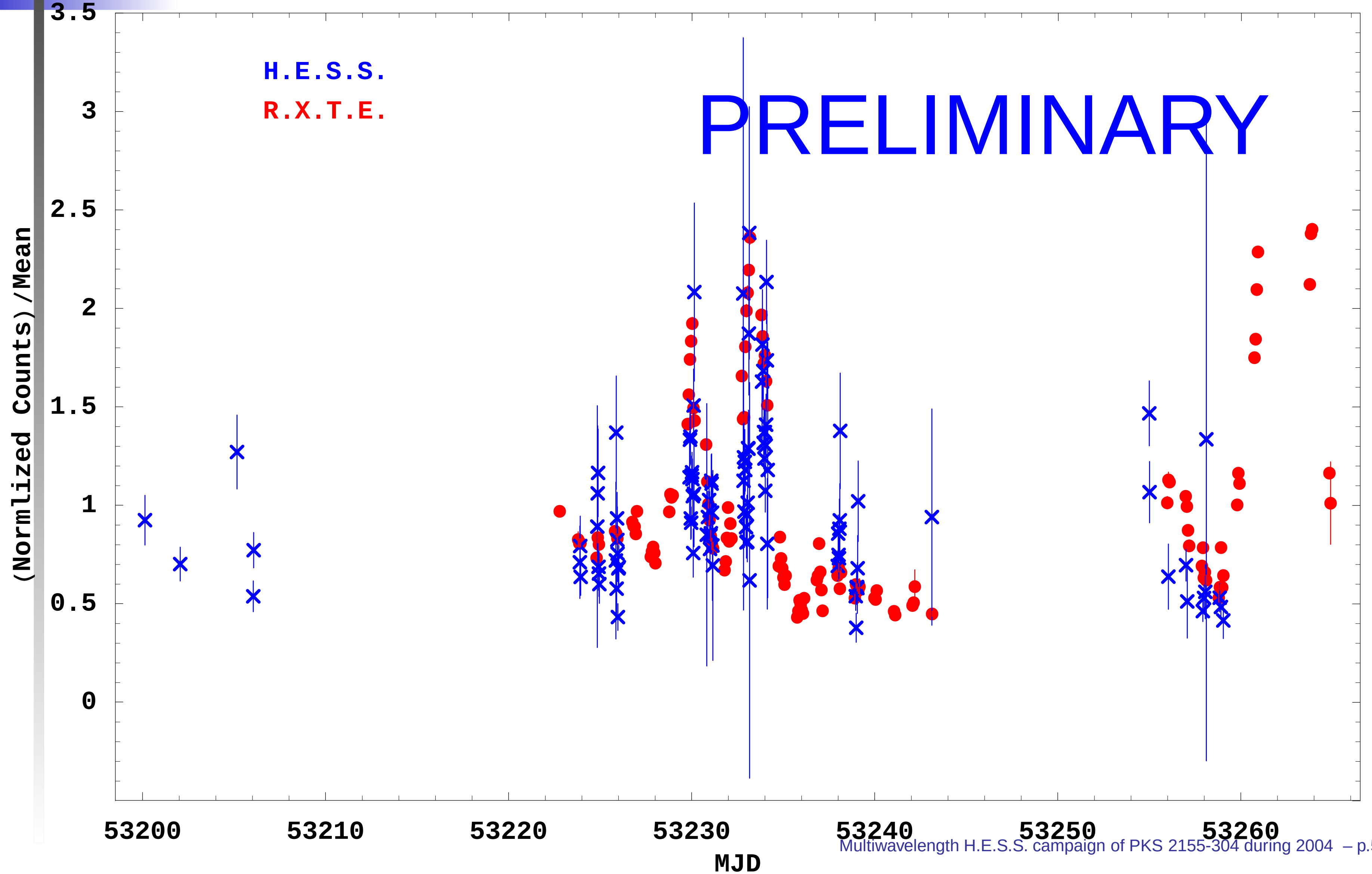

The Light Curves

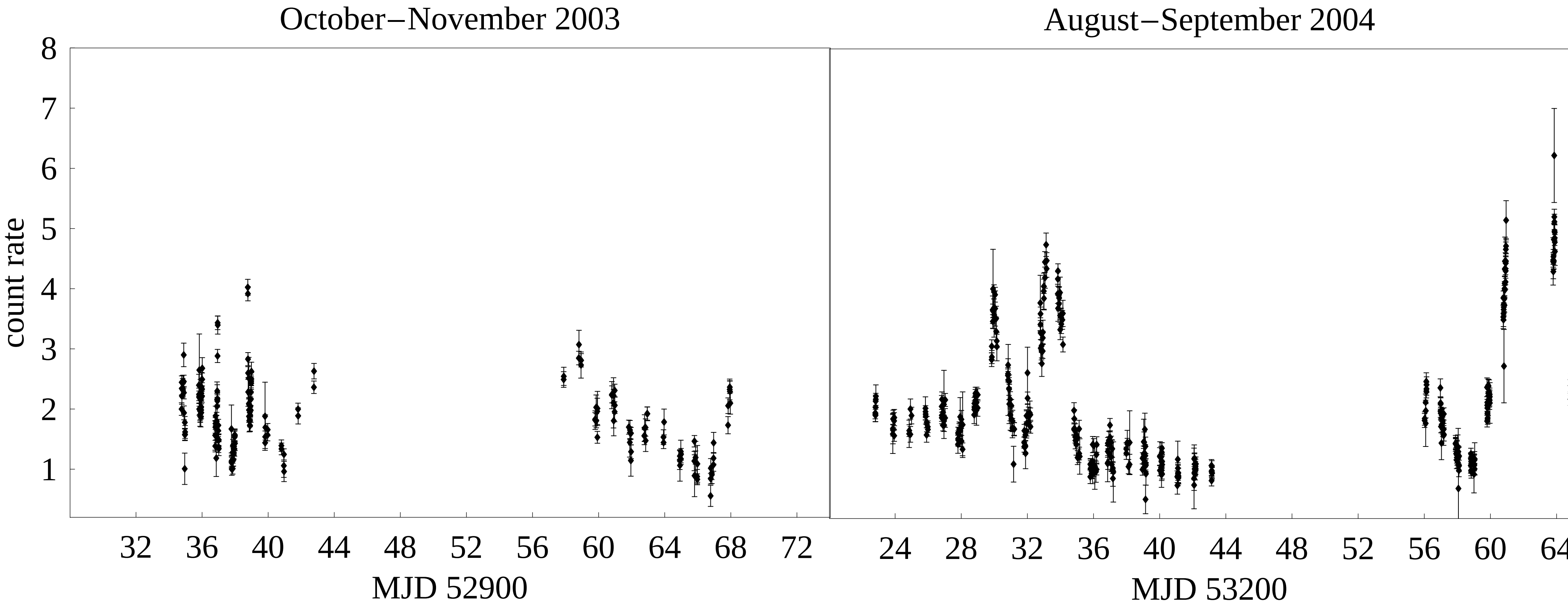

X-ray Data Analysis

a Analysis

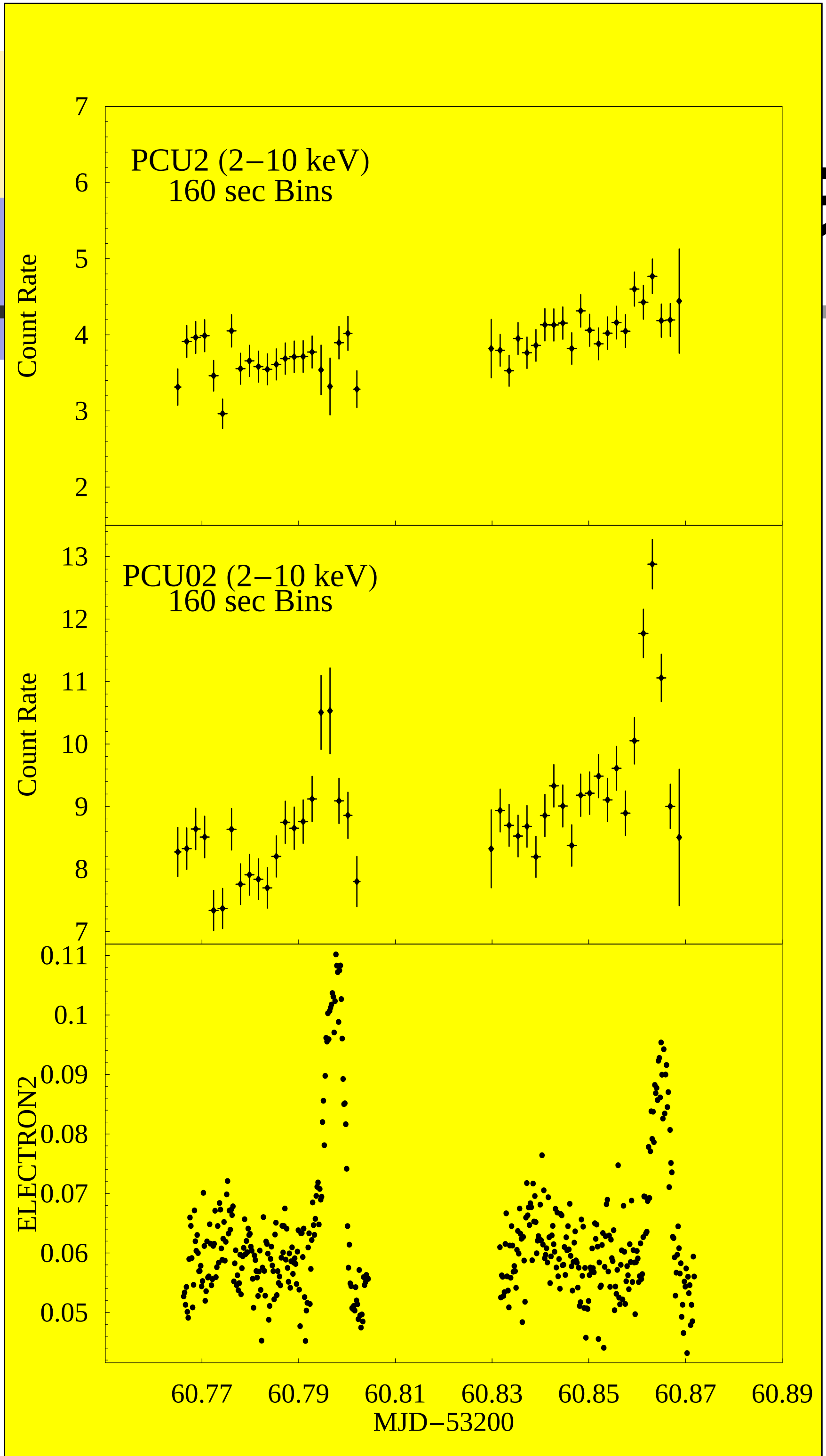

PCU0 is sensitive to un
modelled "Backgroun
events"

X-ray Spectral Studies

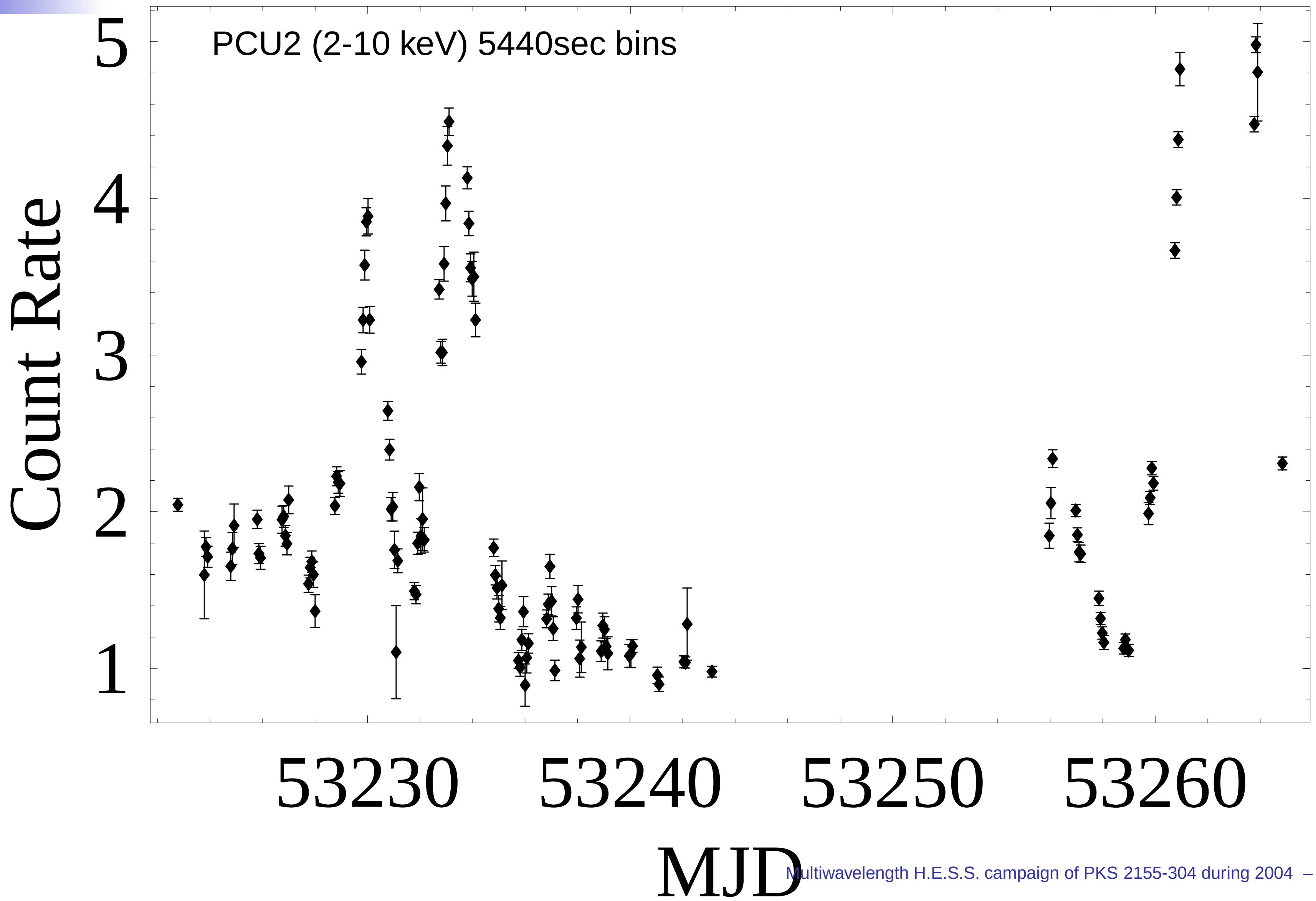

X-ray Spectral Studies

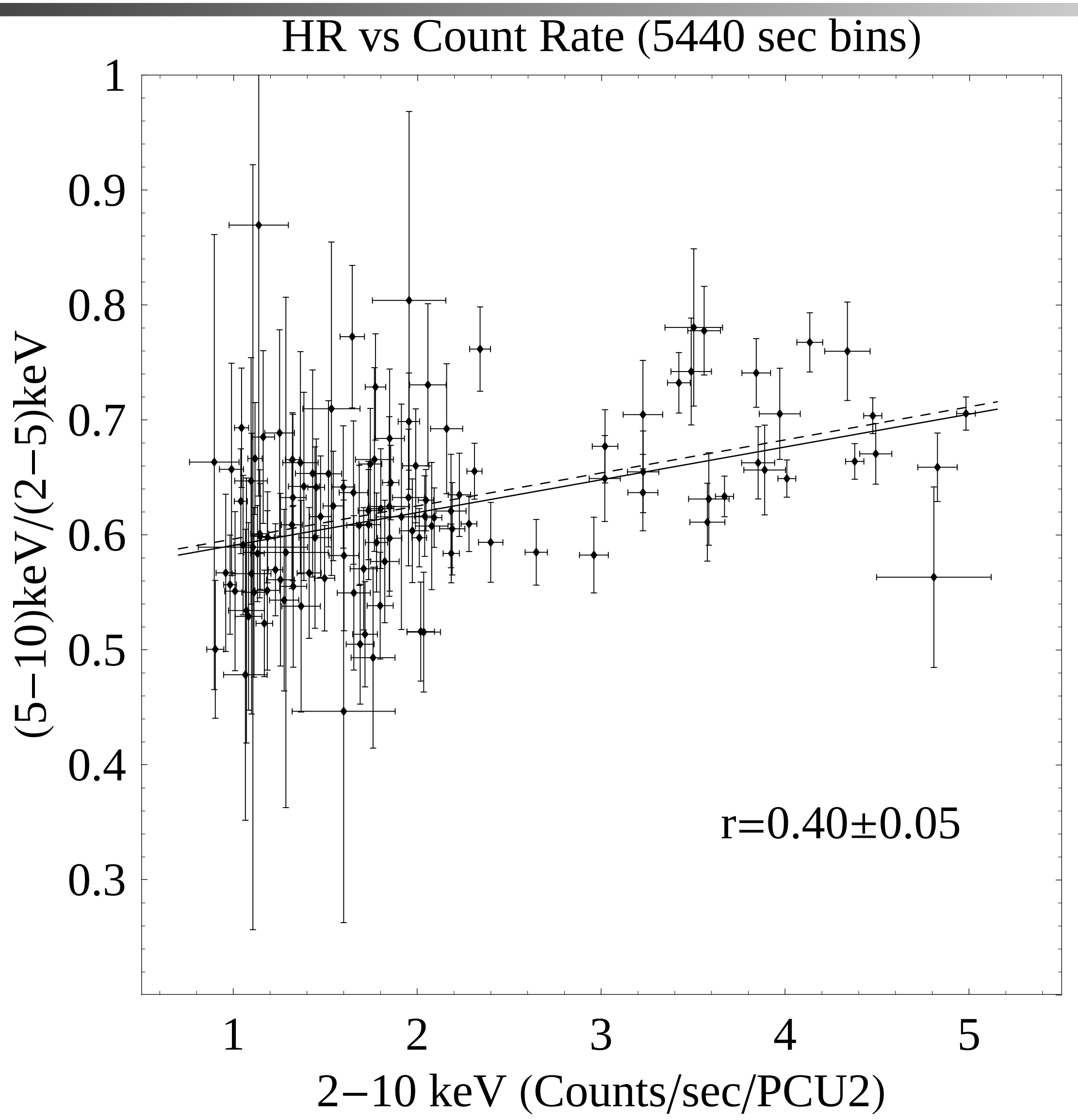

X-ray Spectral Studies

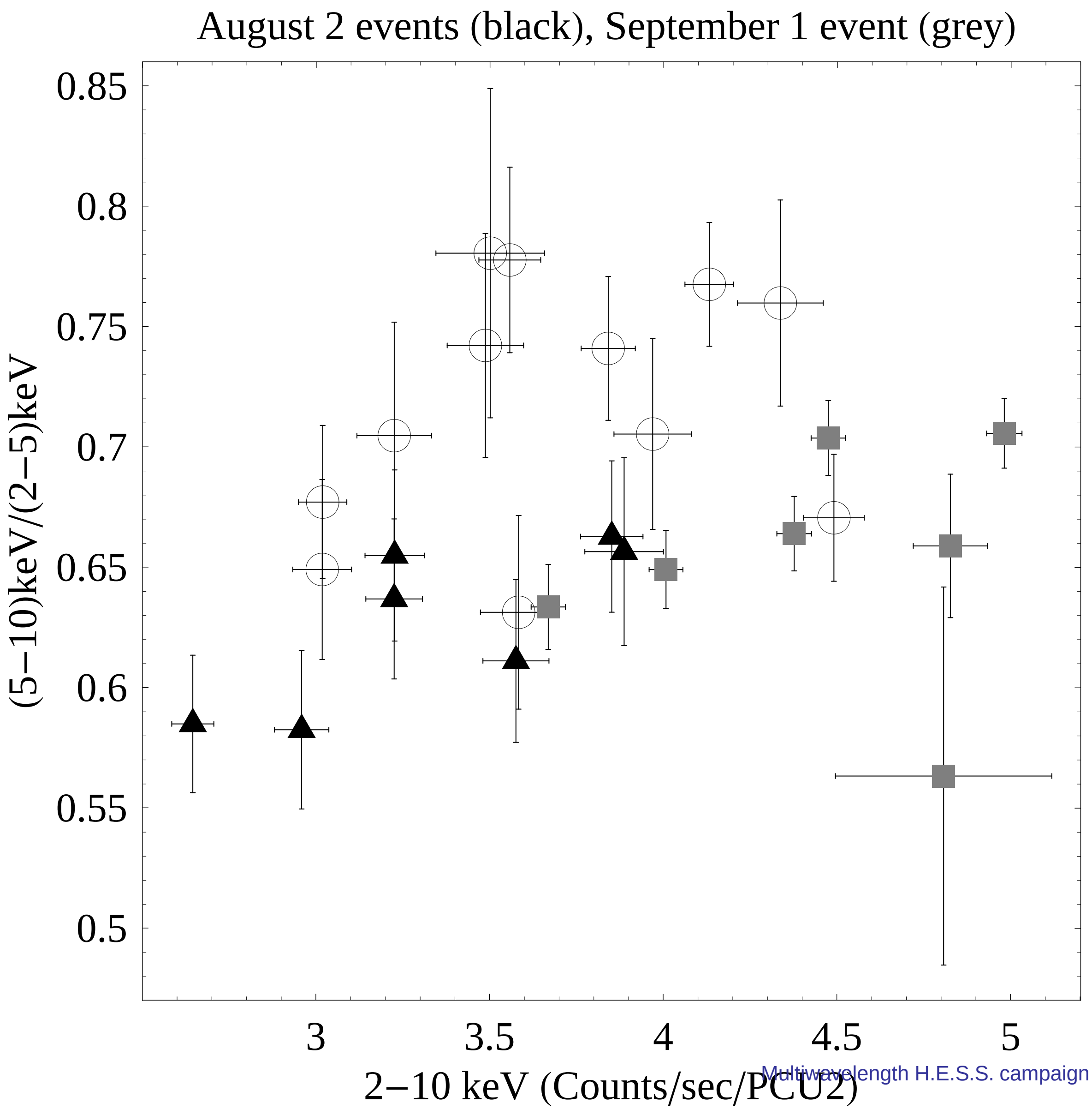

X-ray Spectral Studies

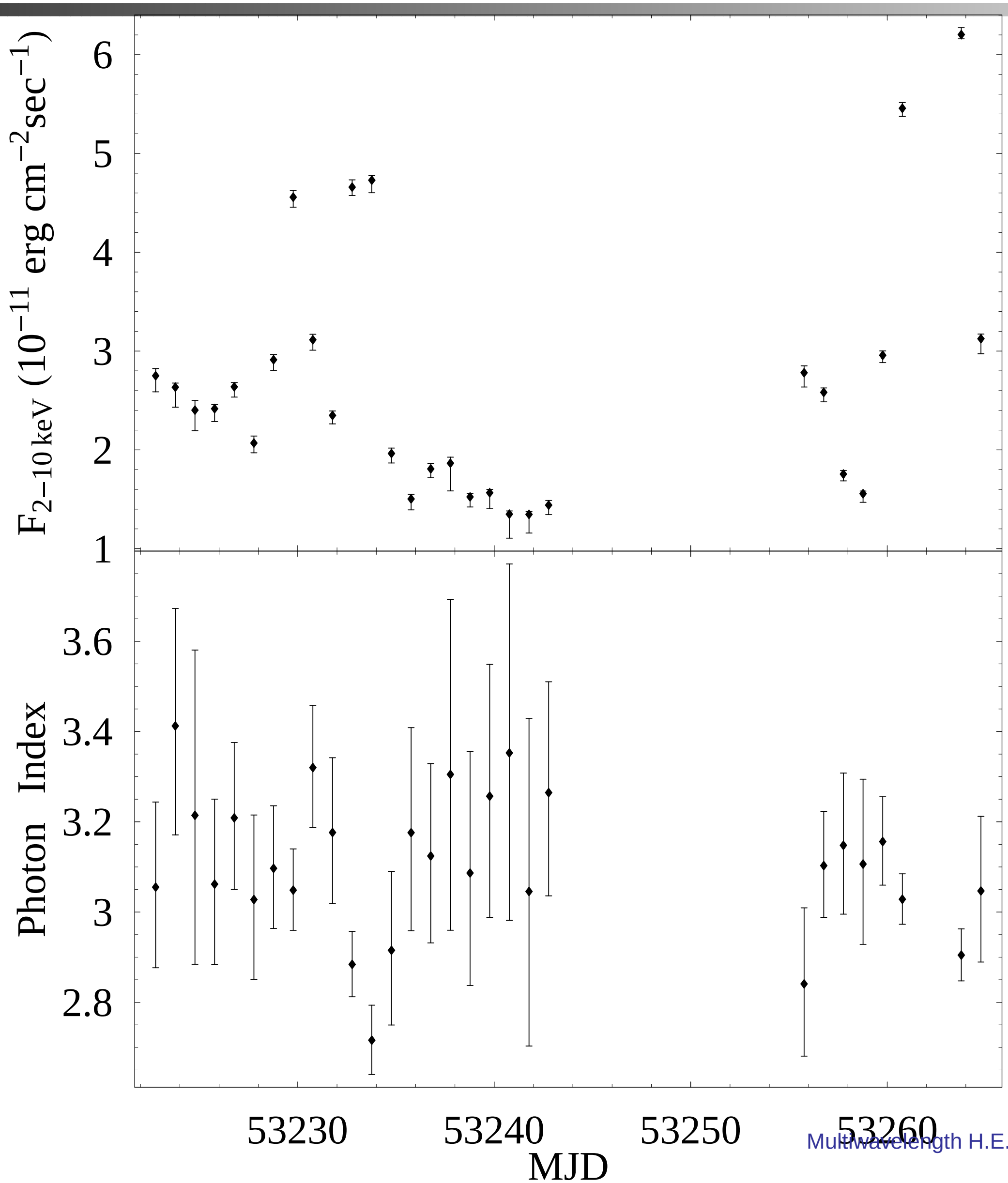

X-ray Spectral Studies

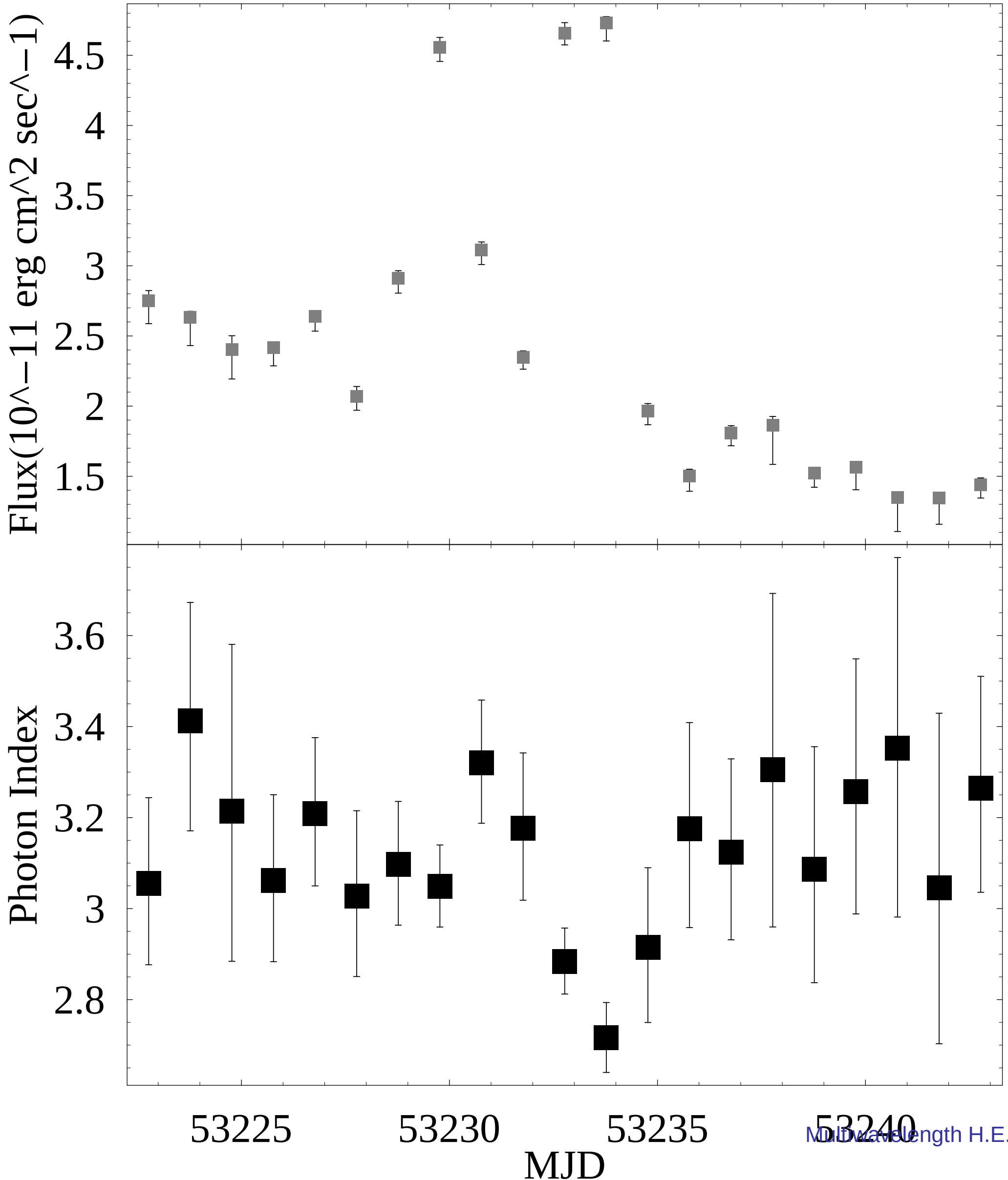

X-ray Spectral Studies

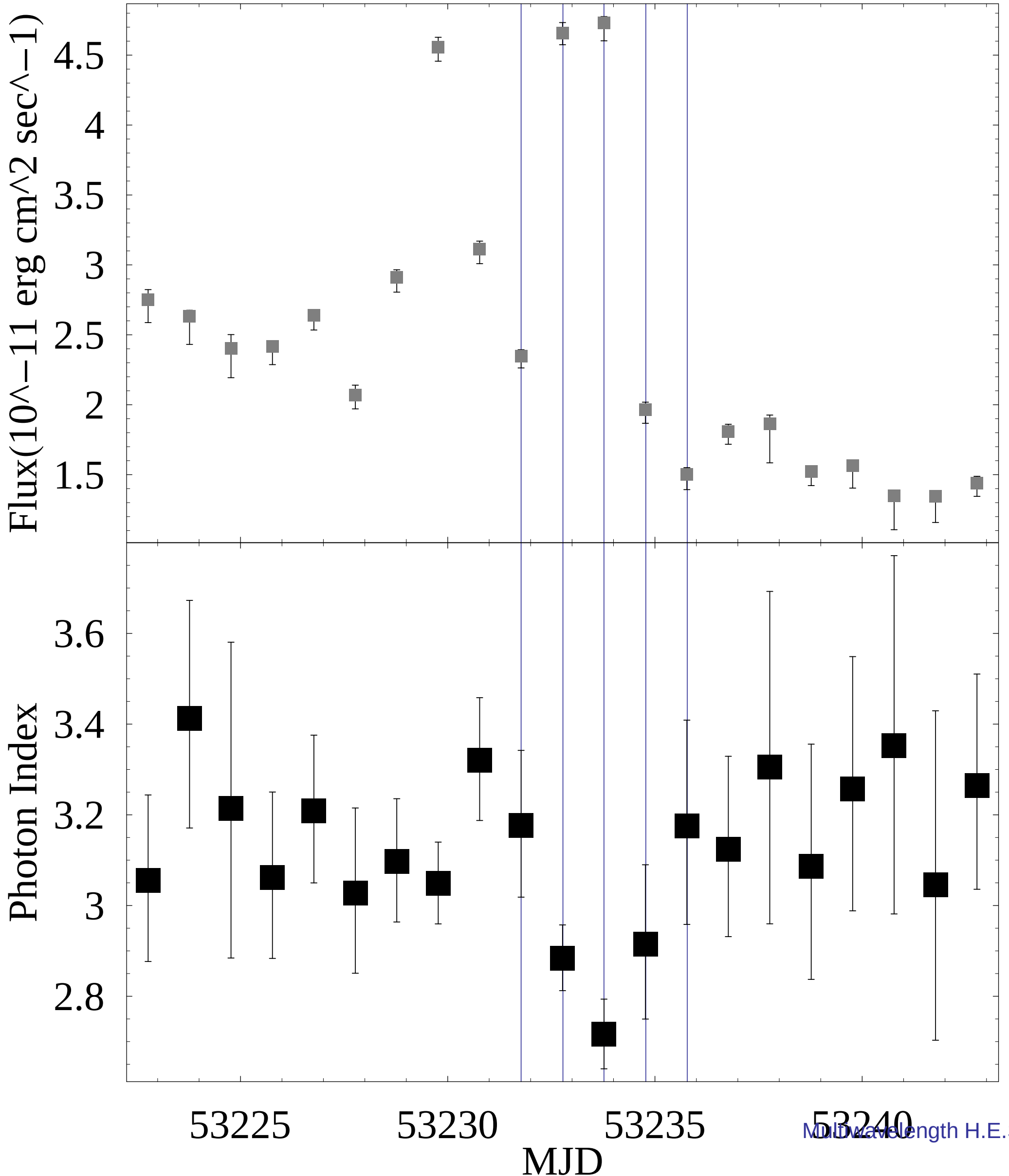

X-ray Spectral Studies

1st flare: No spectral changes $\Rightarrow$ Not enough time for particles to accelerate/cool efficient

2nd flare: Spectral changes $\Rightarrow$ The spectrum becomes gradually harder and then softer.

X-ray Spectral Studies

1st flare: No spectral changes $\Rightarrow$ Not enough time for particles to accelerate/cool efficient

2nd flare: Spectral changes $\Rightarrow$ The spectrum becomes gradually harder and then softer.

Table 1: Power law with N_H=1.69$\times 10^{20}\mathrm{cm}^{-2}$

Month	Phot.Ind	$F_{2-10\mathrm{keV}} \times 10^{-11} \frac{\mathrm{erg}}{\mathrm{cm}^2\mathrm{s}}$
August	3.06$\pm$0.04	2.52± 0.02
September	3.03$\pm$0.04	3.21± 0.02

Optical Data

KVA data:
S.Ciprini, E.Lindfors, K.Nilsson, L.Ostorero
(astro-ph/0509023)

Optical Data

KVA data:

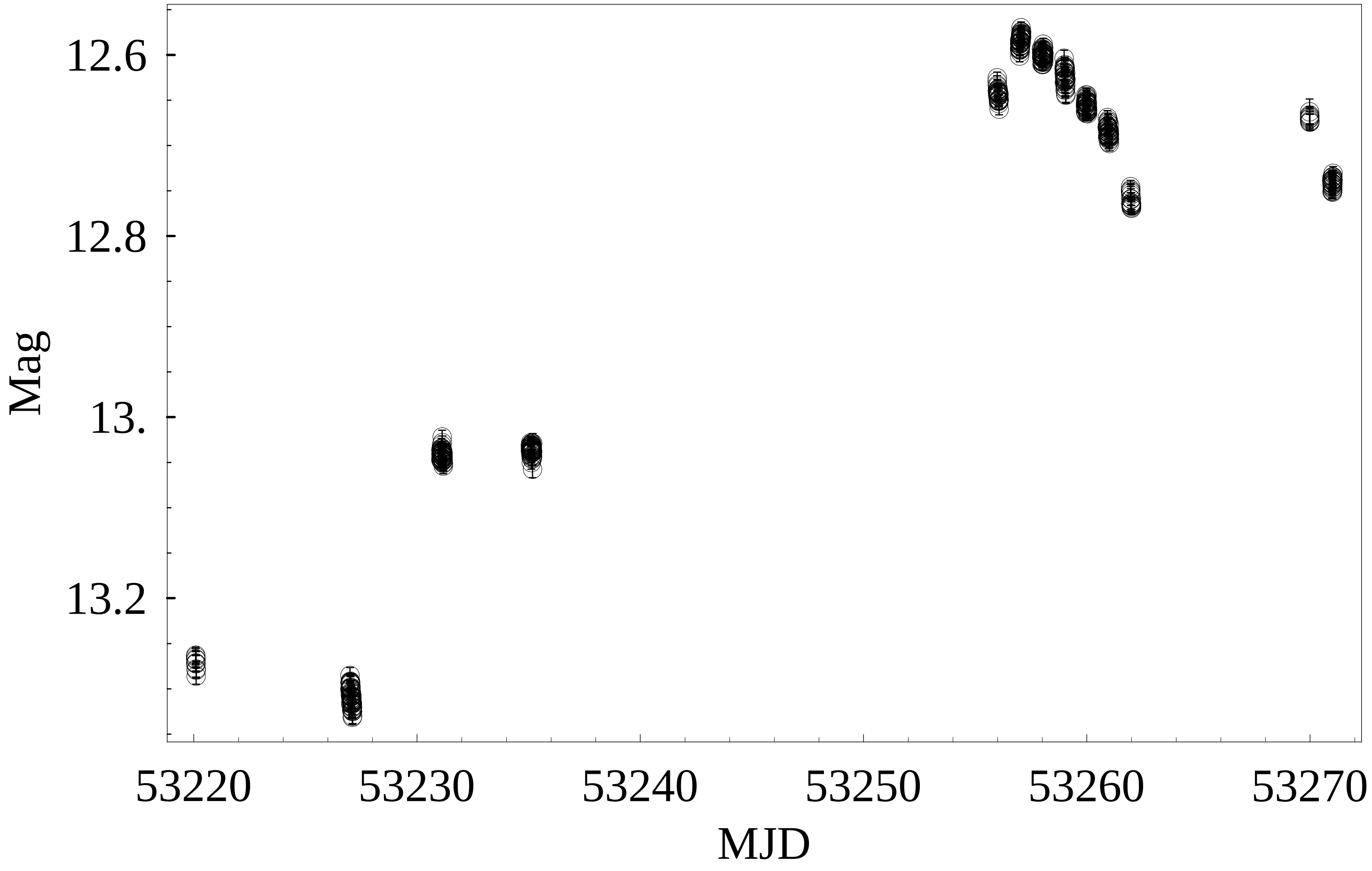

Optical Data

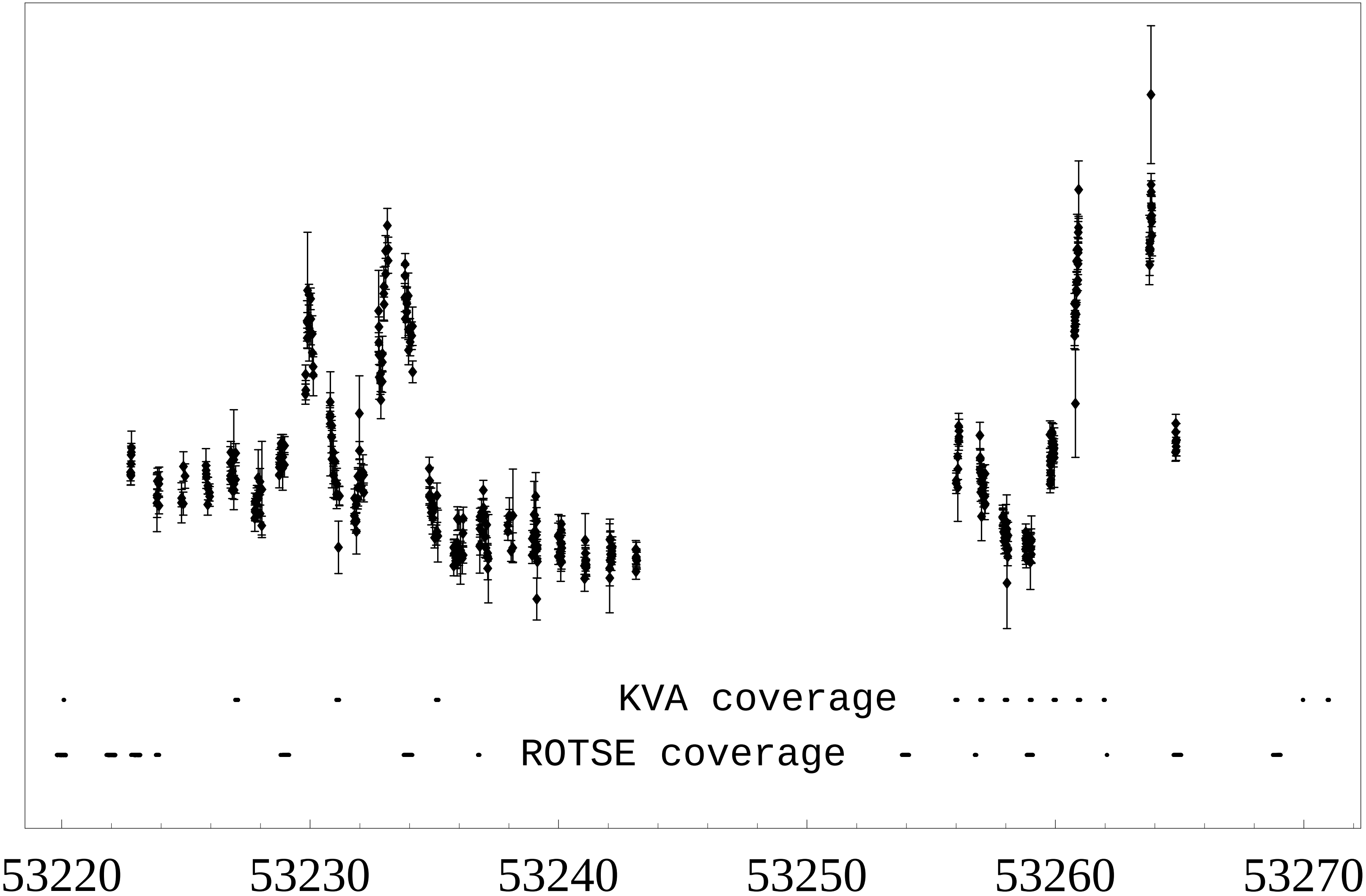

Correlations

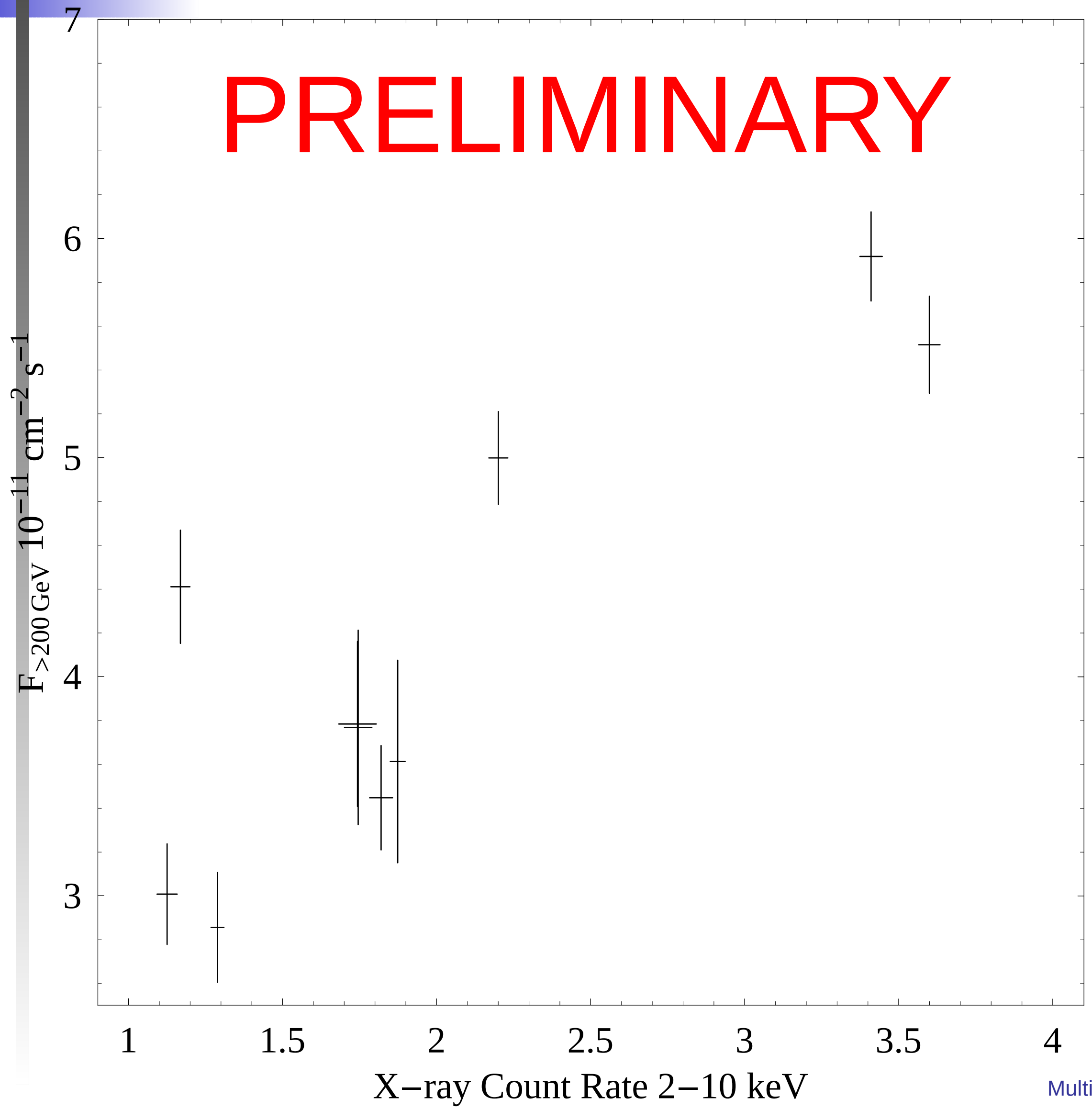

Daily Correaltions

r=0.89±0.02

$P(0.89, 11) = 5 \times 10^{-}$

Was-Will be DONE

1st campaign (2002-2003)

- Robust detection of $\sim 45\sigma$
- VHE variations lasting $\sim$ 1h.
- No continuous coverage (07/10/11-2002, 06/07/08/09/09-2003)
- No Spectral variability w.r.t. time

Was-Will be DONE

2nd campaign (October-November 2003)

- Transient X-ray event of 1.5ksec
- VHE spectrum up to 3 TeV (up to 10 TeV (upper Limits))
- No correlations beetween any bands
- No indication of VHE variations lasting less than 1h.

Was-Will be DONE

3rd campaign (August-September 2004)

- The most continuous VHE coverage of the source (quiscent and flaring state)
- Time resolution of VHE light curve can go down to 1 min
- Spectral studies can be conducted on 30 min time scales
- Correlation Studies (20 min time scales)
- No good weather conditions (for $\sim$10 days)

Multi-frequency monitoring of γ-ray blazars

Uwe Bach
INAF-Osservatorio Astronomico di Torino

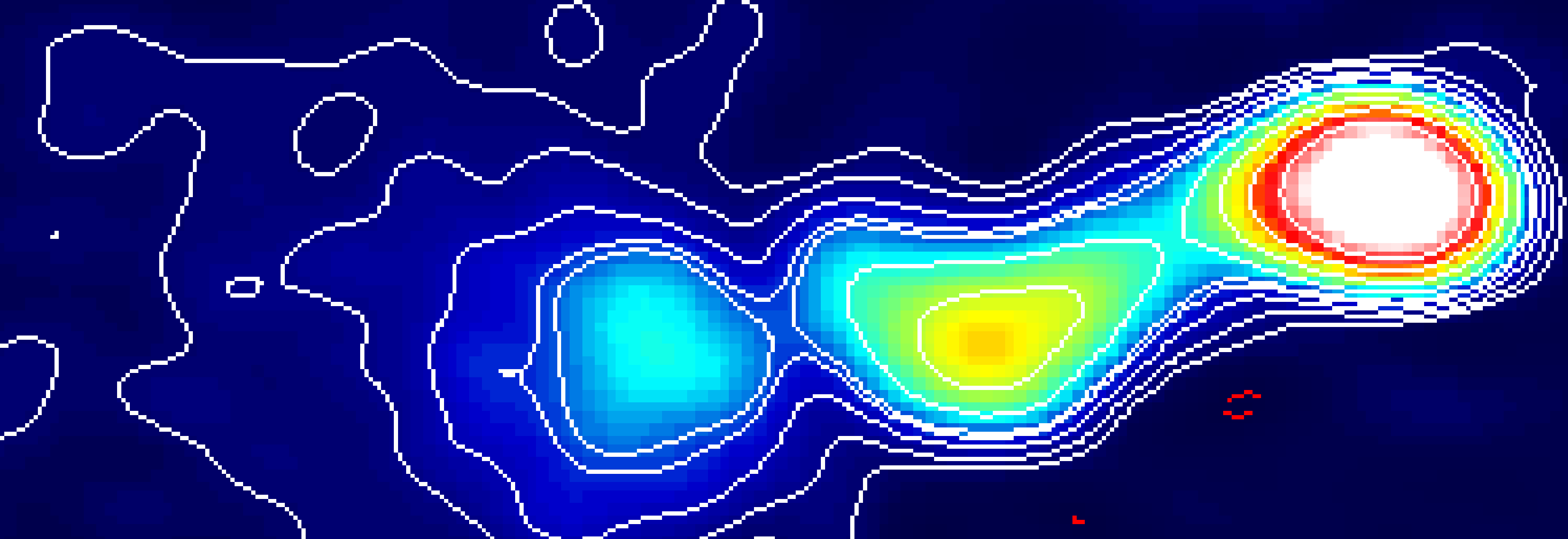

in collaboration with: C.M. Raiteri, M. Villata, L. Lanteri (INAF-OATo), L. Fuhrmann, G. Tosti (Perugia University), C. Buemi, P. Leto, C. Trigilio, G. Umana (IRA, Noto), G. Maccaferri, A. Orlati (IRA, Medicina), V.M. Larionov (St.-Petersburg State University), M. Dolci (INAF-OATR), A. Di Paola (INAF-OAR), and et al.

Contents

- Introduction
  - Motivation
  - The Sample
  - Observations
- Radio light curves
- SEDs
- Future Plans

Introduction

- Motivation:
  - Elucidate the physics of extragalactic jets
  - How is the energy extracted from the central black hole in radio-loud AGN
- Method:
  - Crucial information is provided by blazars SED
  - In Dec 2004 a monthly radio, near-IR, and optical monitoring of now 35 blazars was started
  - Some of the targets will be or were observed by high energy satellites
- Current results:
  - About 4000 data points in the radio bands (800 h) and ~5500 near-IR and optical measurements

Participants

- Radio antennas:
  Medicina and Noto (IRA)
- Near-IR:
  Campo Imperatore Observatory (OAR)
- Optical Observatories:
  Torino, Perugia, Crimea, Abastumani, and Maidanak

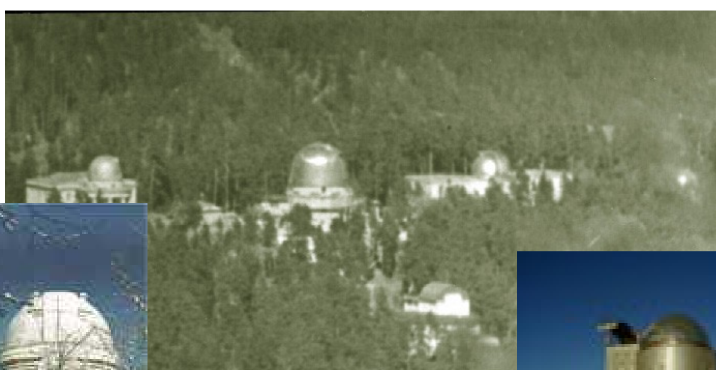

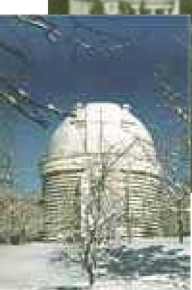

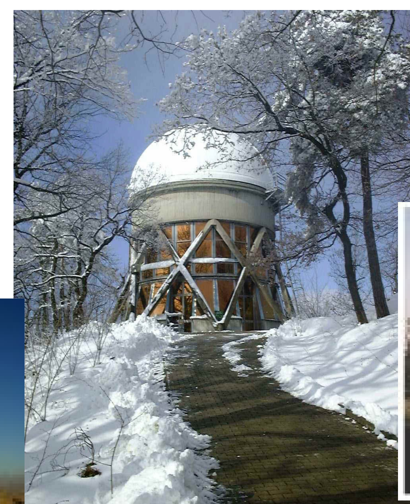

The Sample

IAU Name	Other Name	IAU Name	Other Name
0219+428	3C 66A	**1253–055**	3C 279
0235+164	AO 0235+16	1334–127	PKS 1335–127
0336–019	CTA 026	1354+195	4C +19.44
0420–014	PKS 0420–01	**1510–089**	PKS 1510–08
0440–003	NRAO 190	1606+105	4C +10.45
0528+134	PKS 0528+134	**1611+343**	
0716+714	S5 0716+71	**1633+382**	S4 1633+38
0735+178	PKS 0735+17	**1641+399**	3C 345
0736+017	PKS 0736+01	**1730–130**	NRAO 530
0827+243	OJ 248	**1741–038**	PKS 1741–03
0829+046	PKS 0829+046	1807+698	3C 371
0836+710	S5 0836+71	**2200+420**	BL Lac
0851+202	OJ 287	2223–052	3C 446
0954+658	S4 0954+65	**2230+114**	CTA 102
1156+295	4C +29.45	**2251+158**	3C 454.3
1219+285	W Com	2344+092	4C 09.74
1226+023	3C 273		

Radio Observations

- Frequencies: 5, 8, 22, and 43 GHz*
- ONOFF measurements at Medicina:
  - 2-3 measurements of 12 to 18 min. duration
  - Flux limit ~ 0.3 Jy (0.5 Jy at 22 GHz)
  - Accuracy ~ 5-10% (10-15% at 22 GHz)
- Cross-scan measurements at Noto (22 GHz):
  - Flux limit ~ 0.2 Jy
  - Accuracy 5-10%

---

* since March 2006

Light Curves

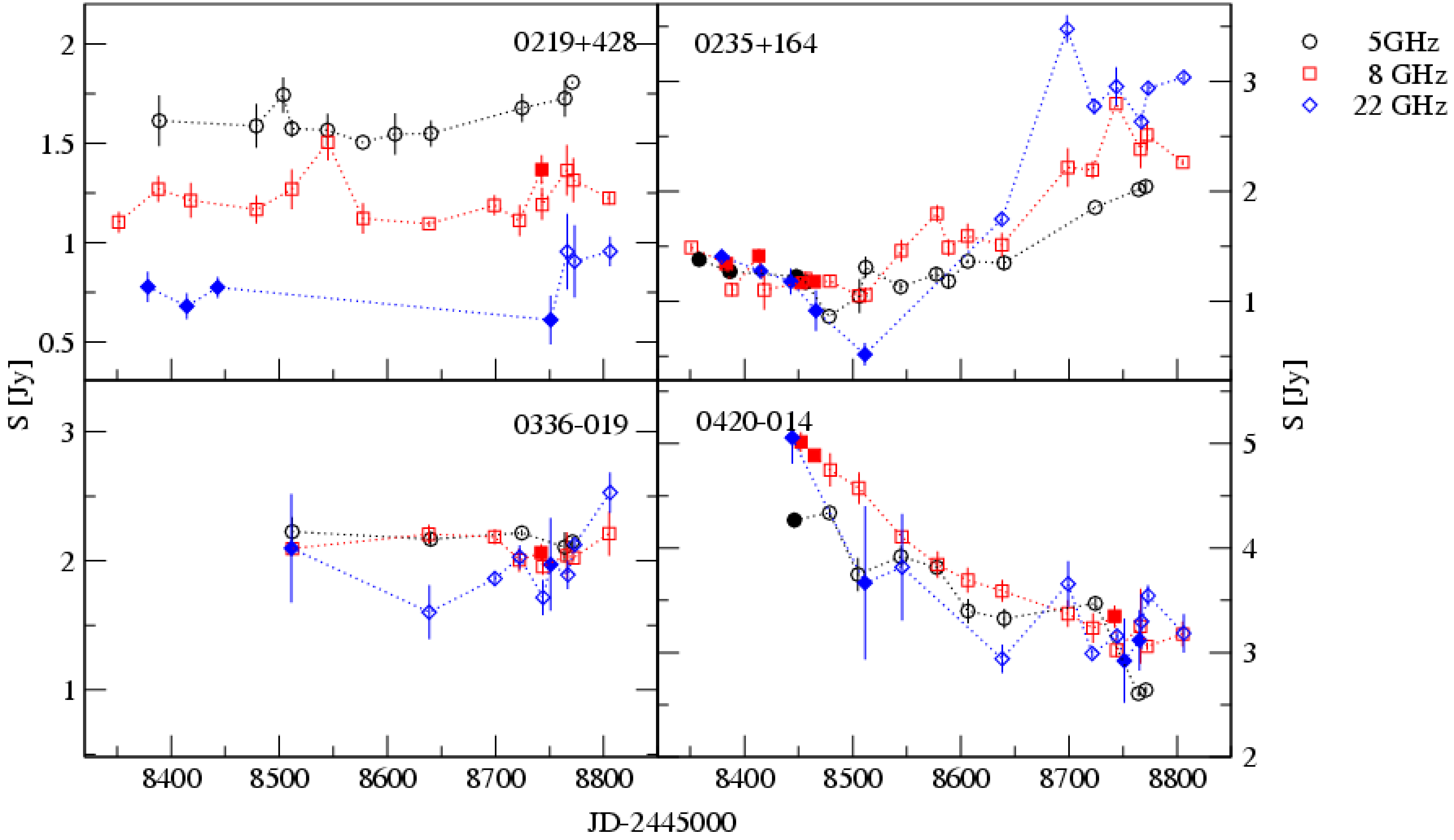

Light Curves

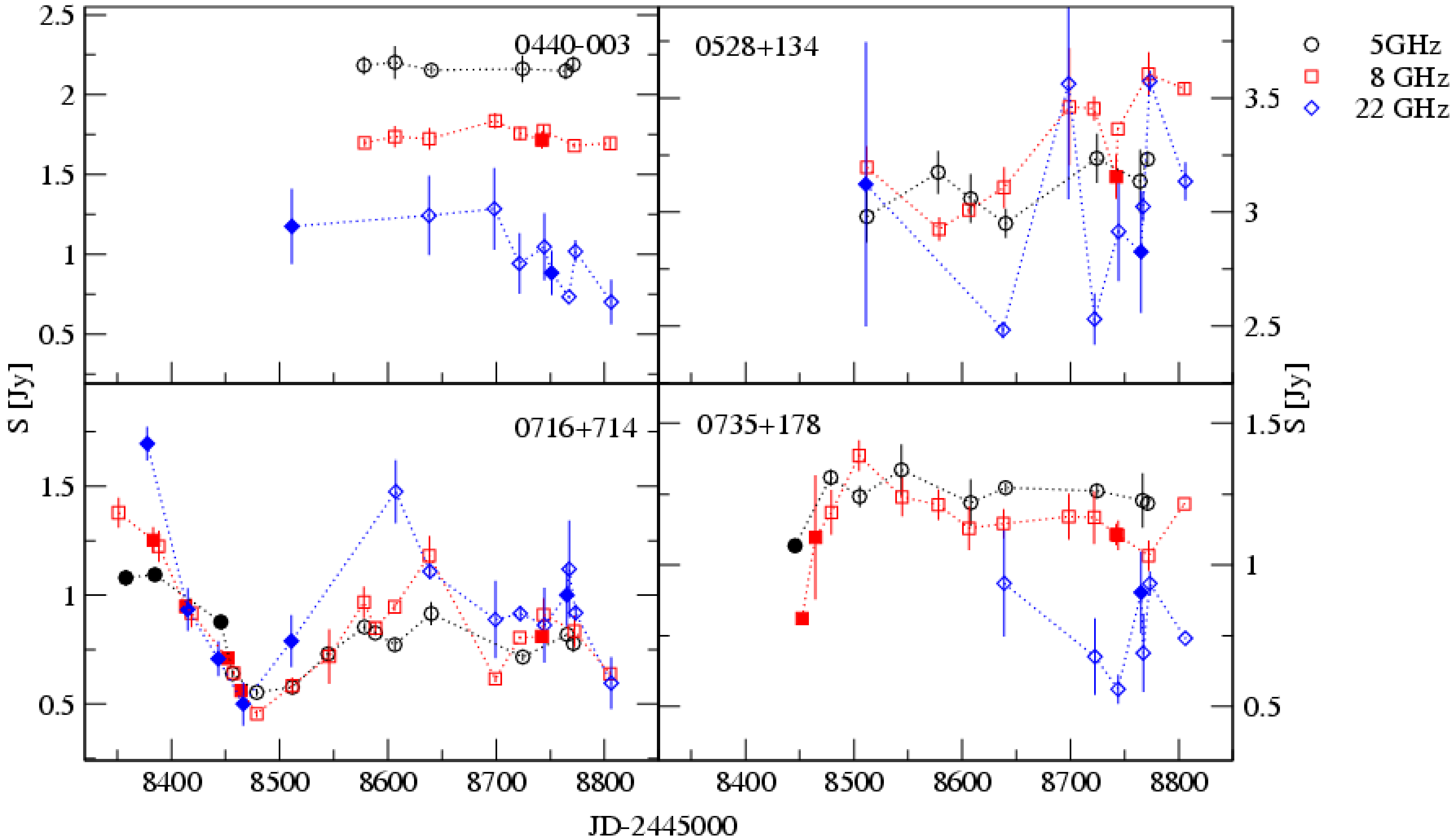

Light Curves

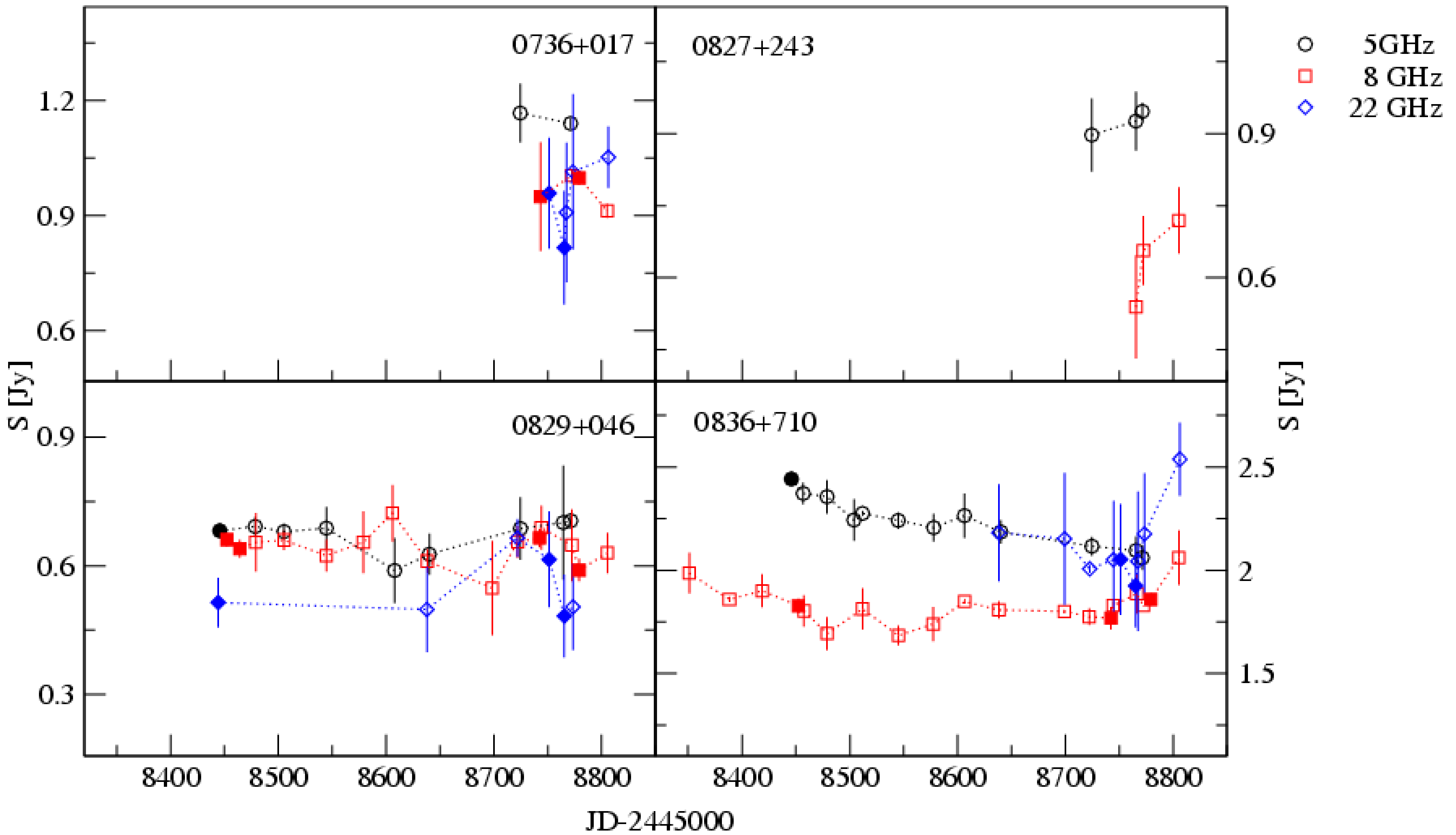

Light Curves

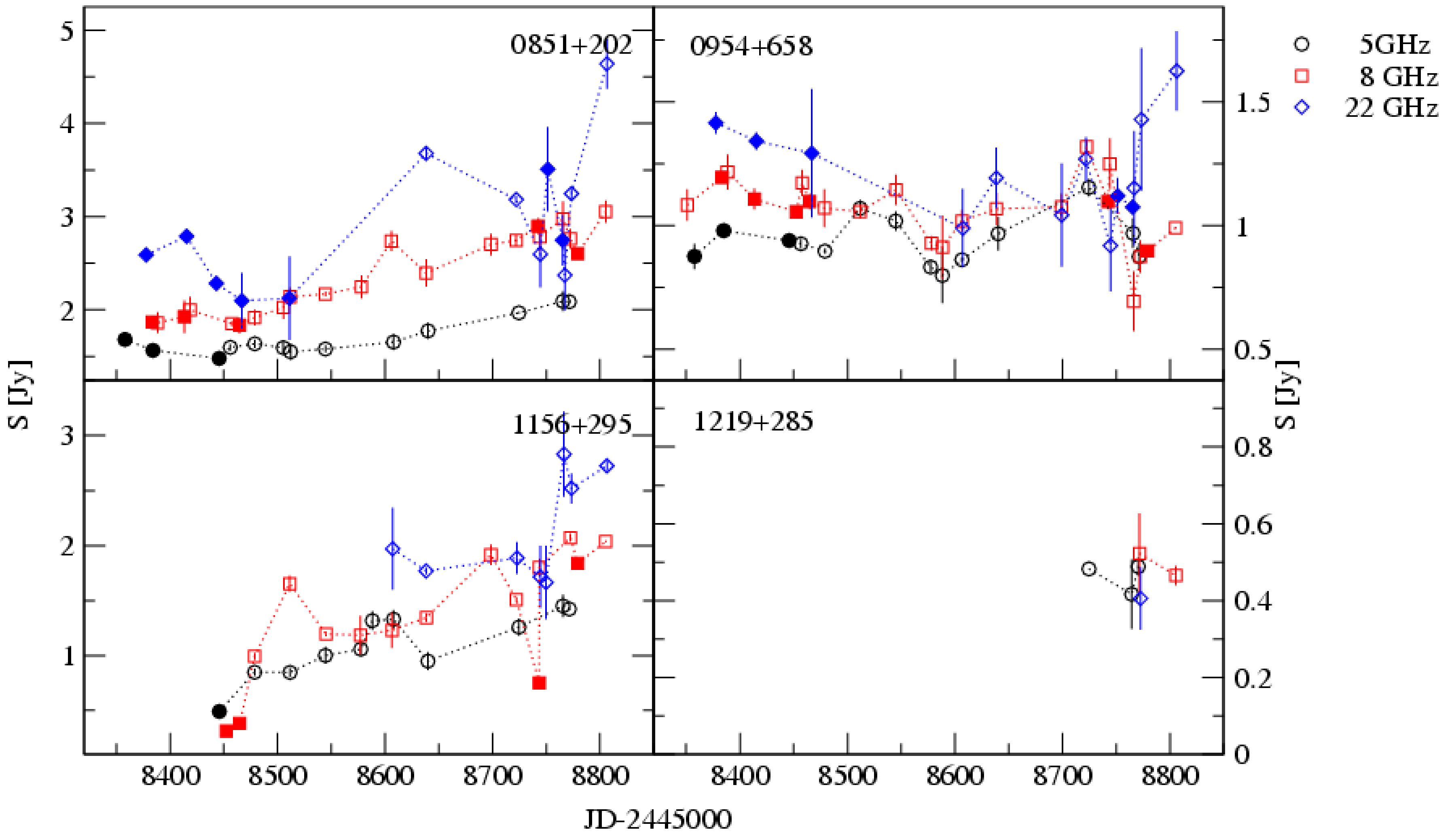

Light Curves

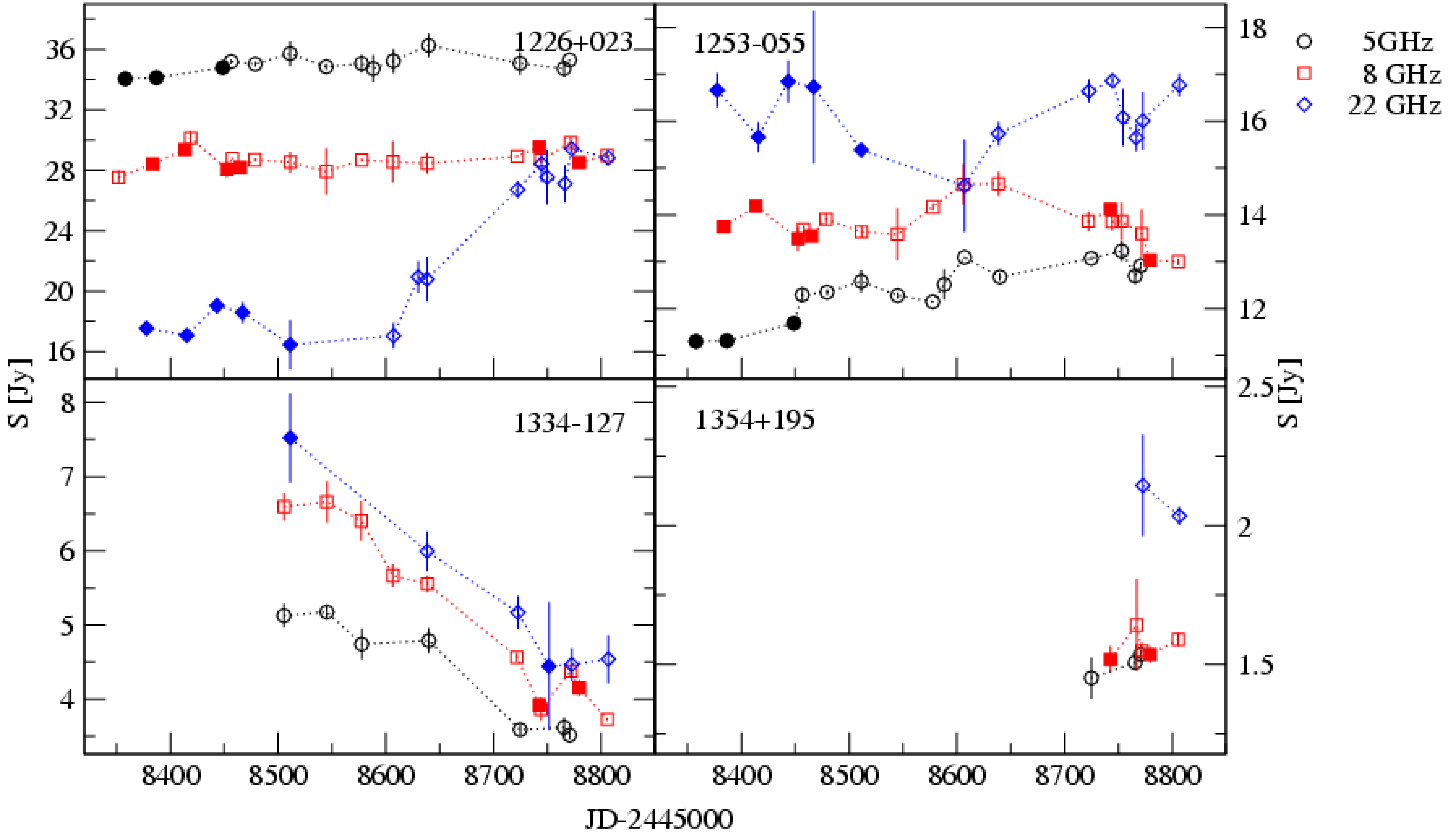

Light Curves

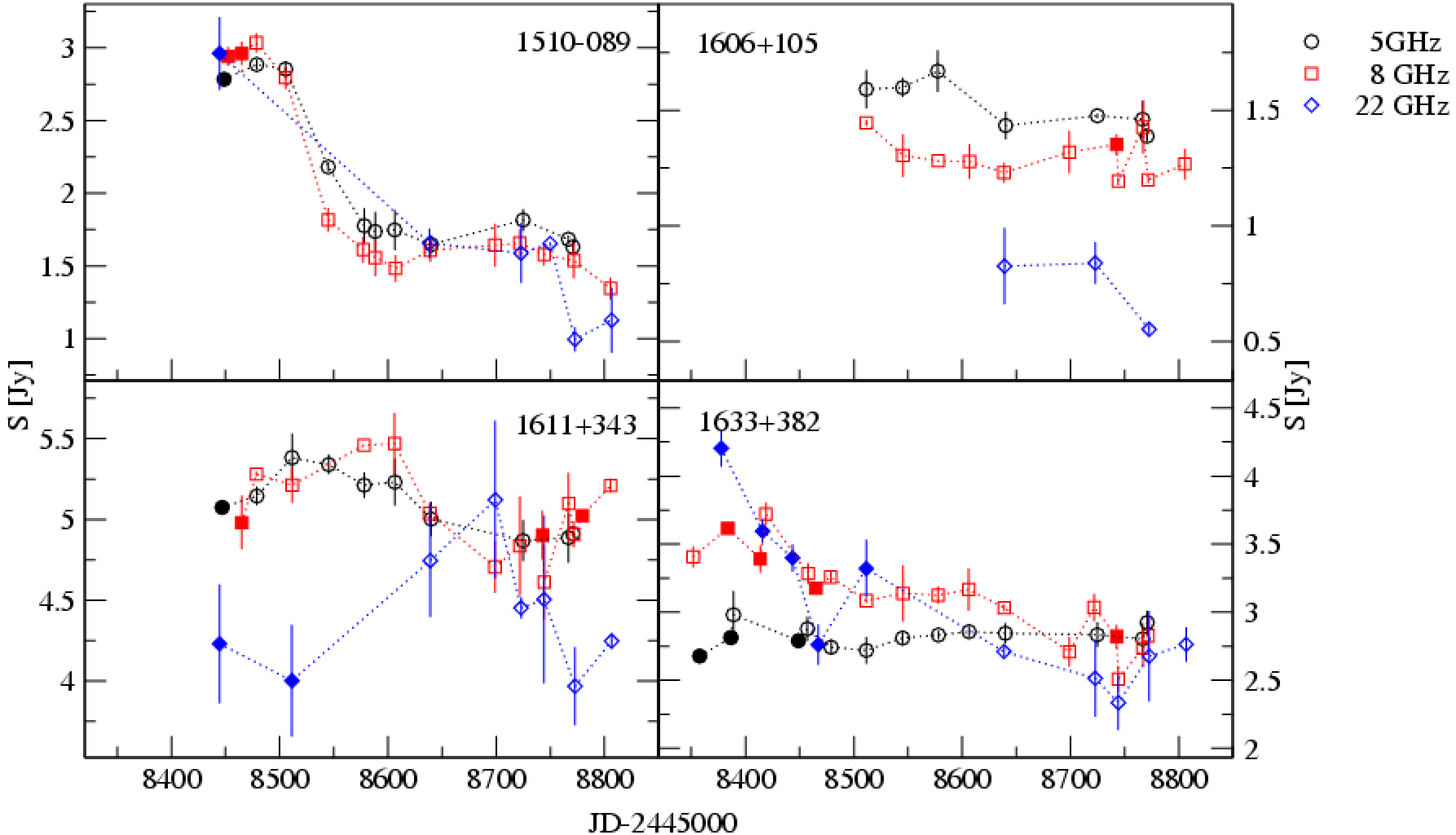

Light Curves

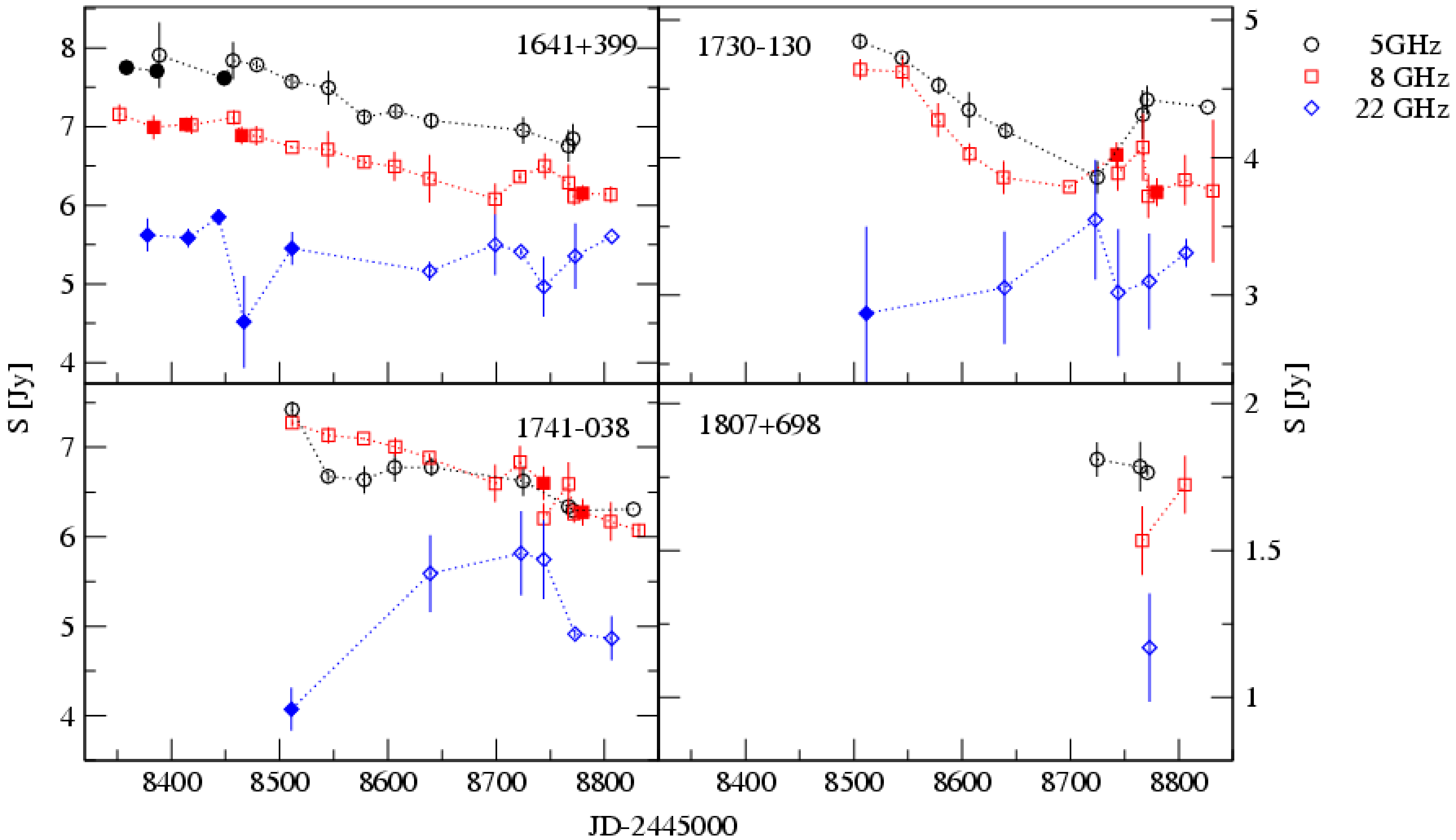

Light Curves

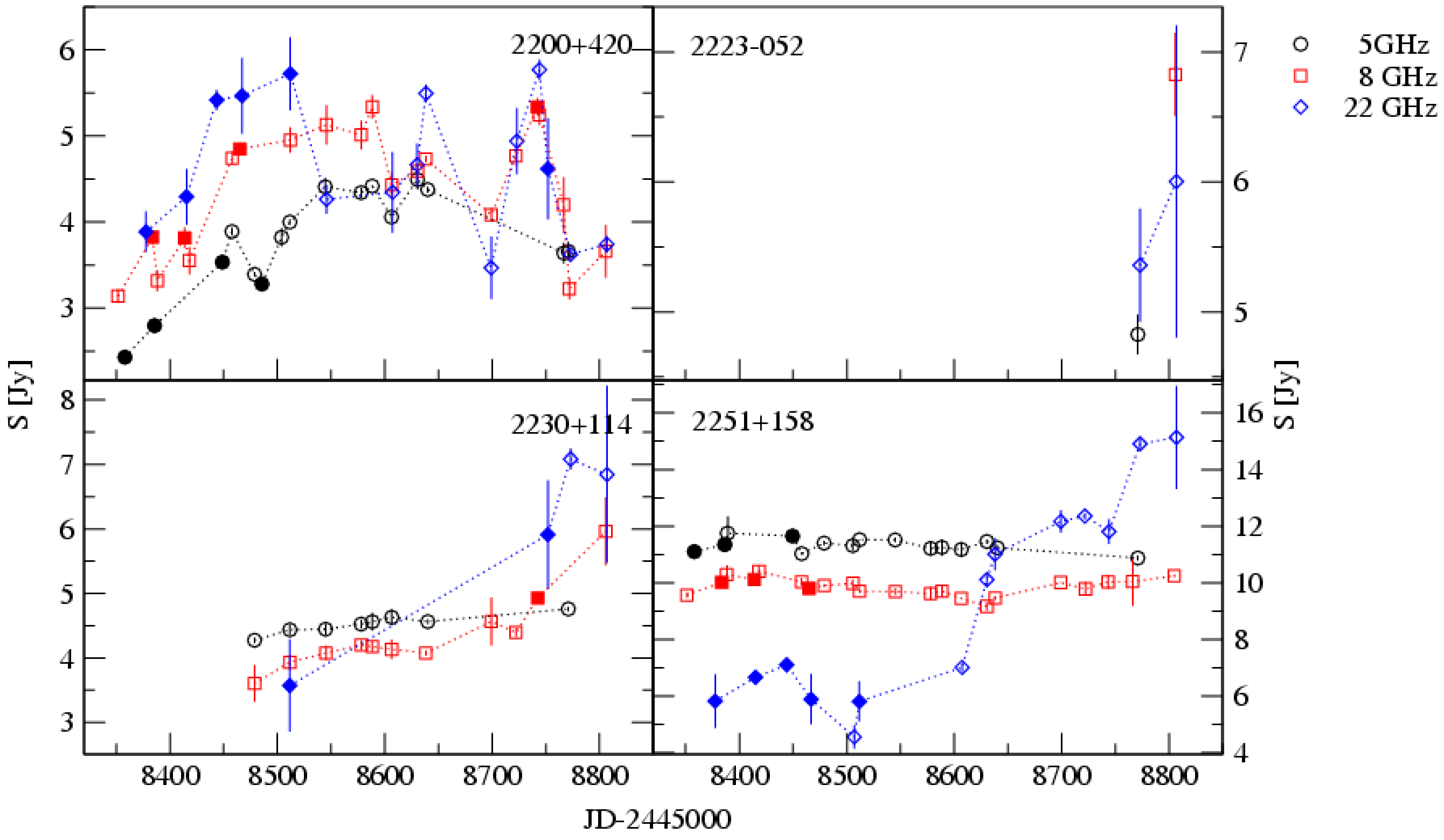

Spectral Energy Distributions

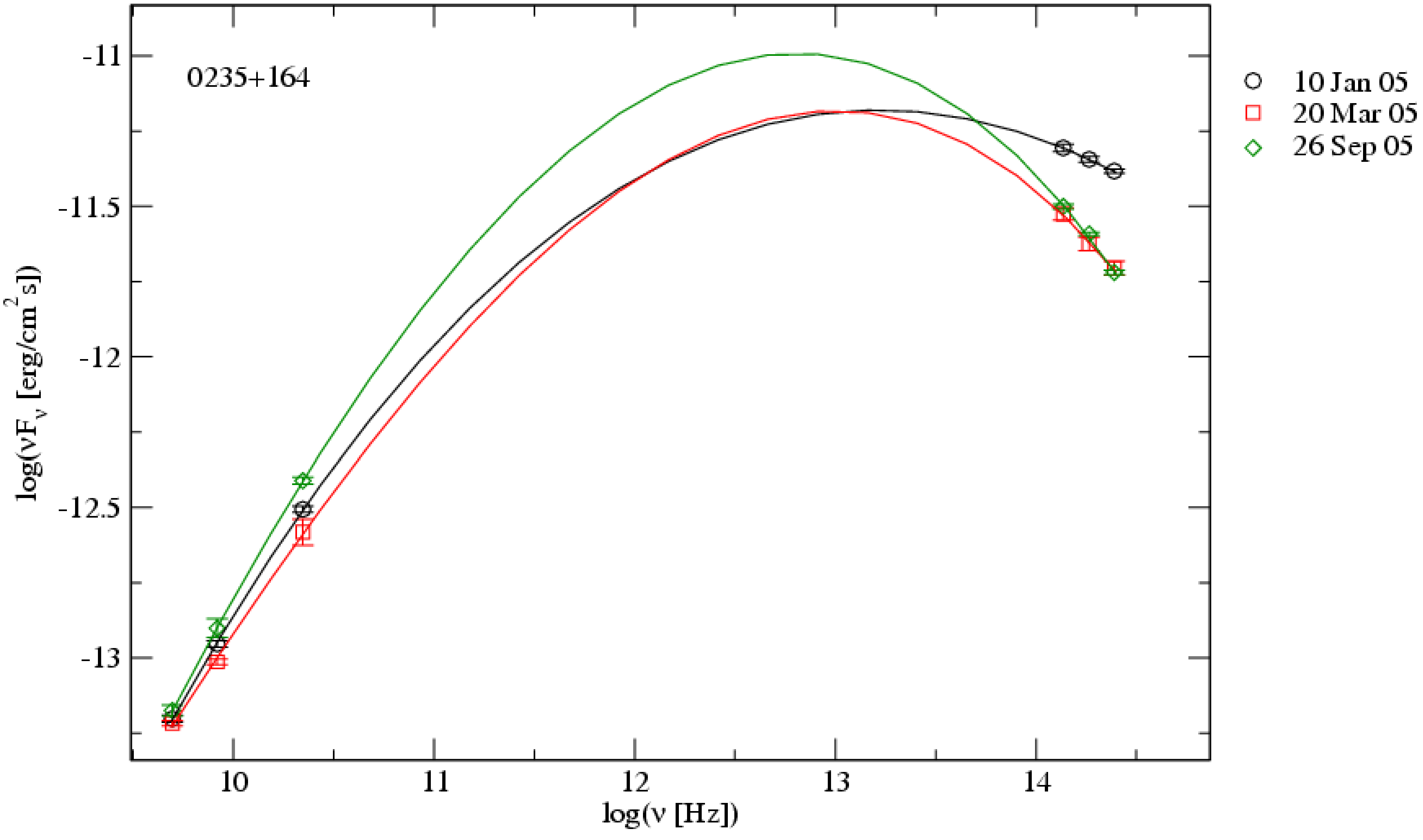

SEDs

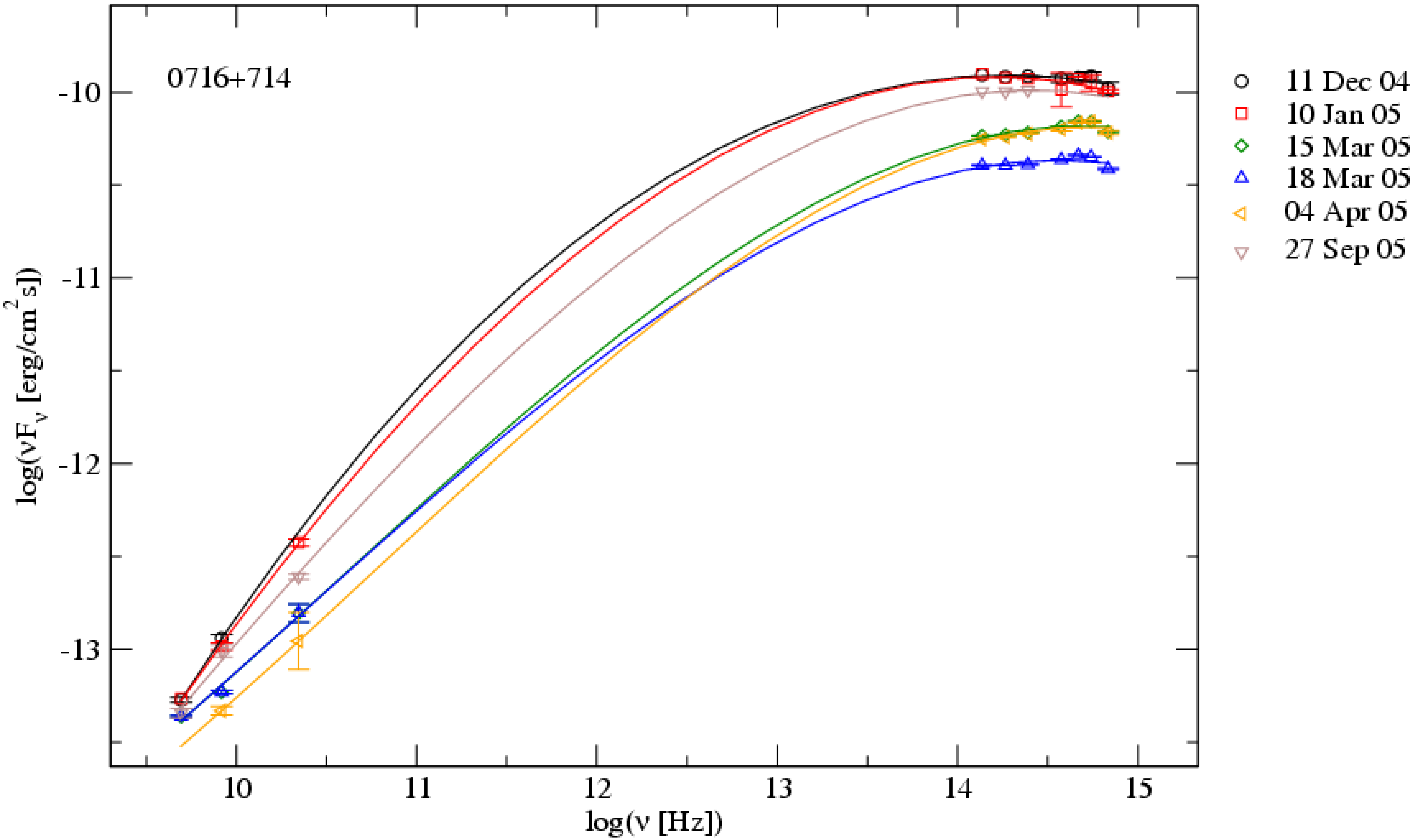
0716+714
-10
-11
-12
-13
10
11
12
13
14
15
log(ν [Hz])
log(νF$_\nu$ [erg/cm^{2}s])
11 Dec 04
10 Jan 05
15 Mar 05
18 Mar 05
04 Apr 05
27 Sep 05

SEDs

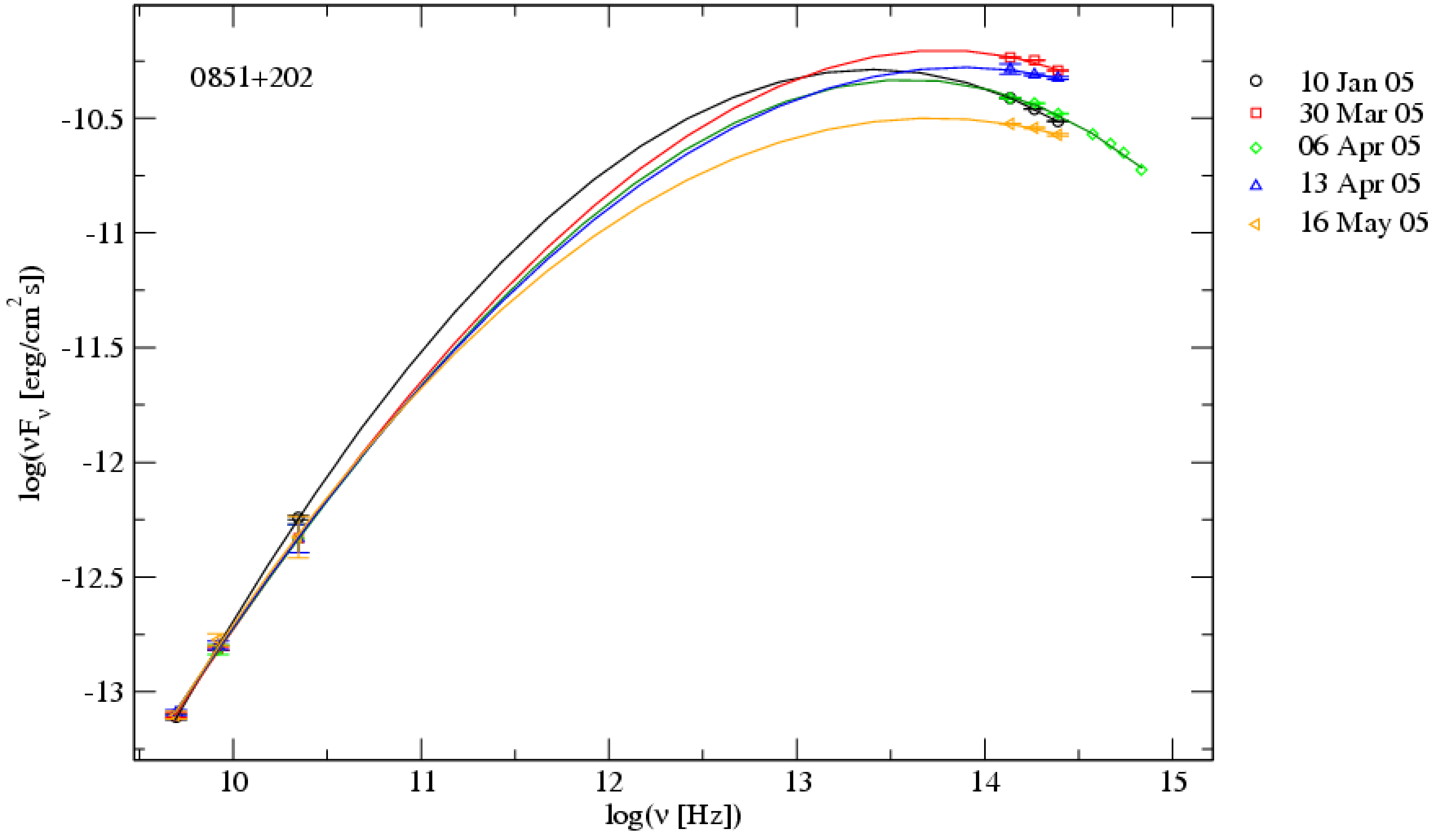
0851+202
10 Jan 05
30 Mar 05
06 Apr 05
13 Apr 05
16 May 05
-10.5
-11
-11.5
-12
-12.5
-13
10
11
12
13
14
15
log(ν [Hz])
log(νF$_ν$, [erg/cm^{2}s])

SEDs

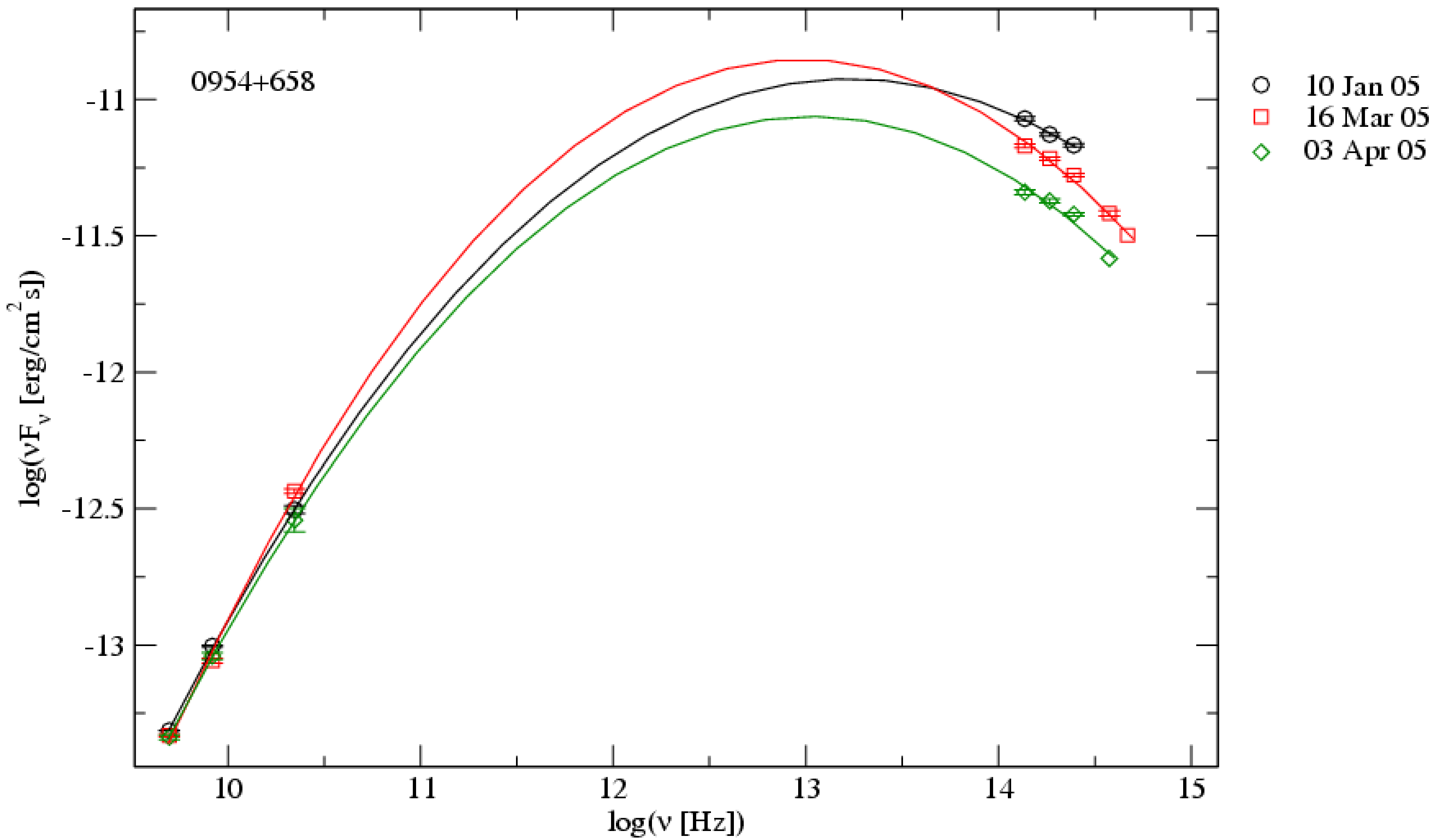
0954+658
10 Jan 05
16 Mar 05
03 Apr 05
log(νF$_\nu$ [erg/cm^{2}s])
log(ν [Hz])
-11
-11.5
-12
-12.5
-13
10
11
12
13
14
15

SEDs

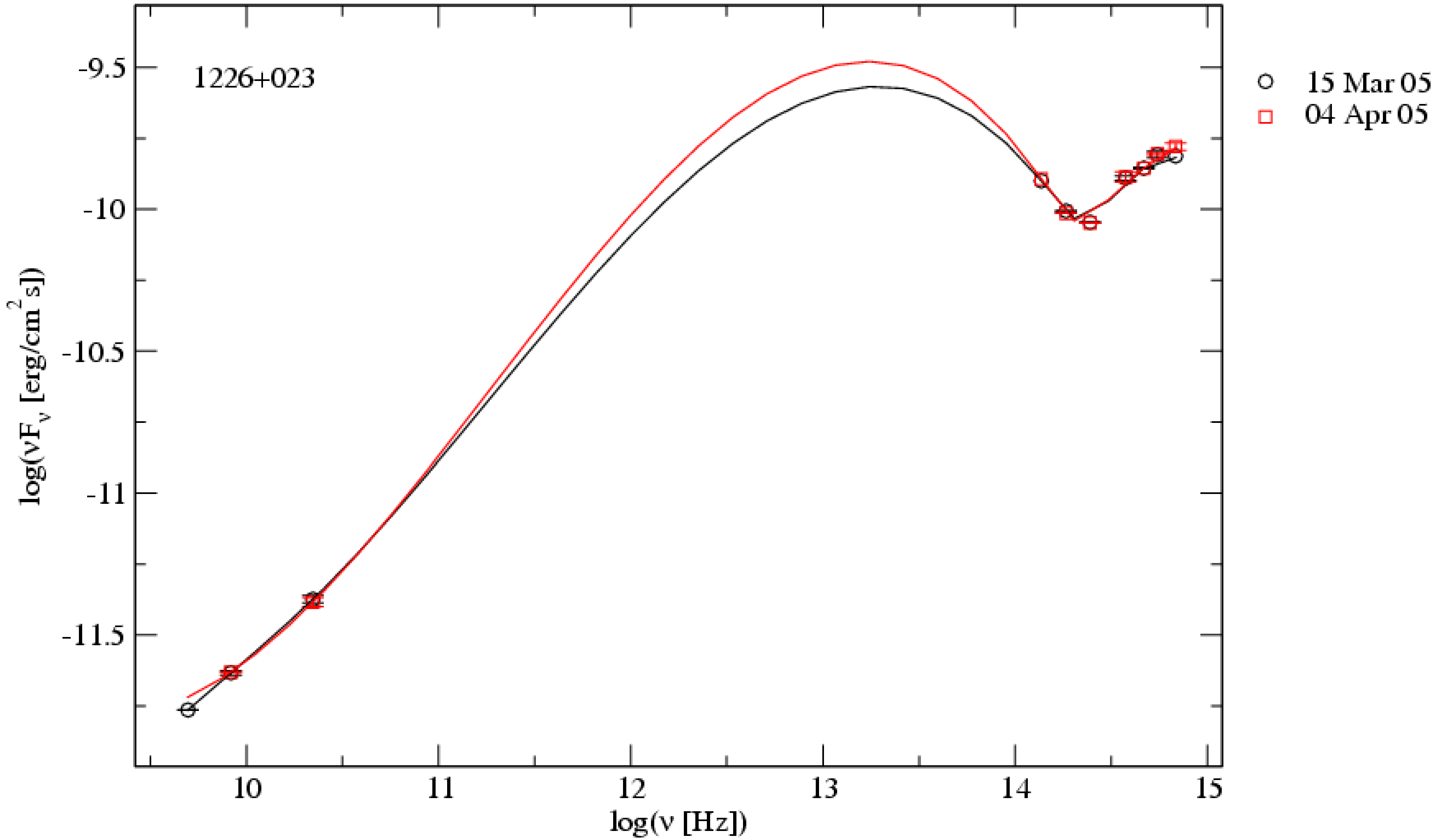
1226+023
15 Mar 05
04 Apr 05
-9.5
-10
-10.5
-11
-11.5
10
11
12
13
14
15
$\log(\nu F_\nu\ [\mathrm{erg/cm^2 s}])$
$\log(\nu\ [\mathrm{Hz}])$

SEDs

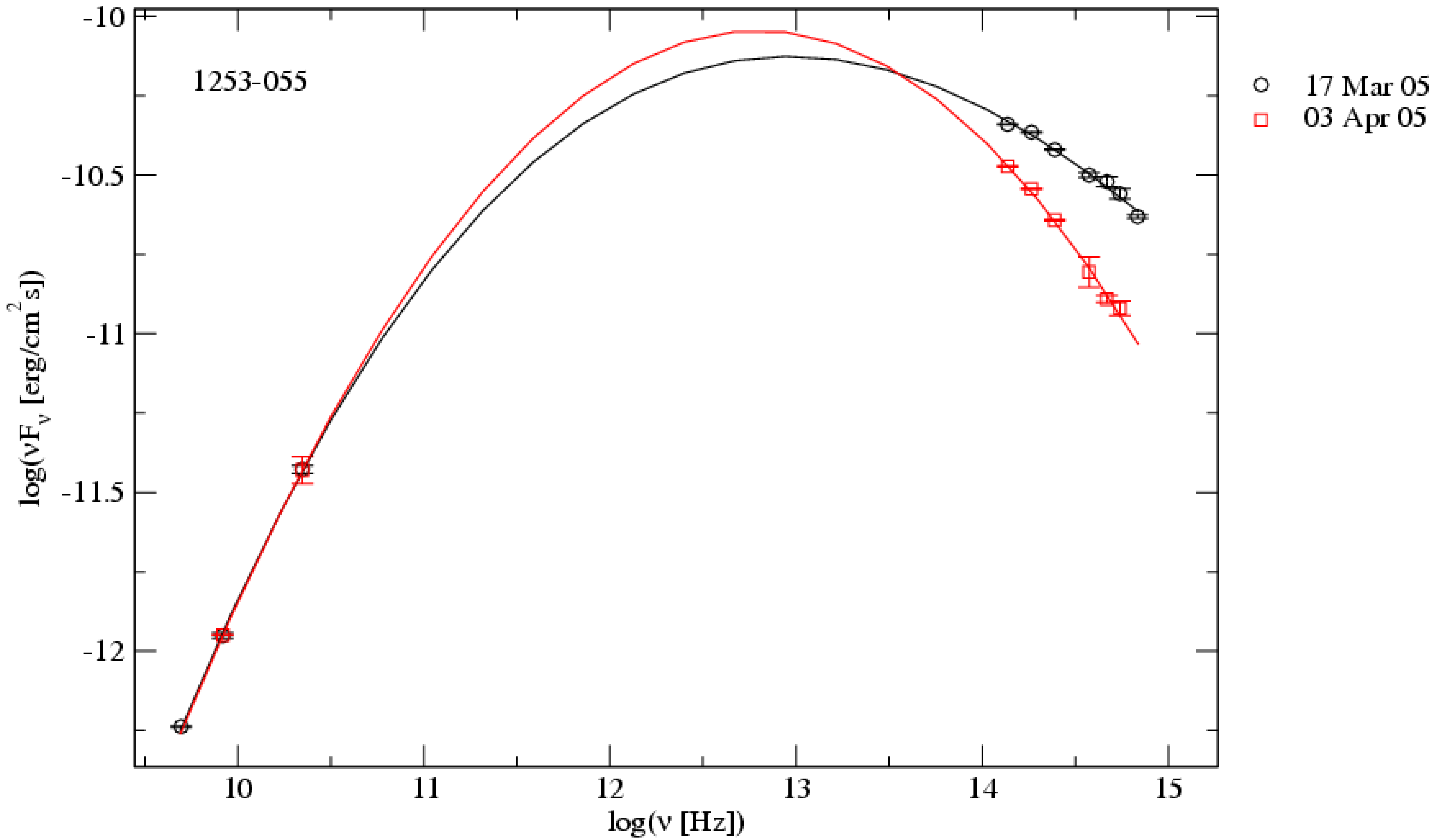
1253-055
17 Mar 05
03 Apr 05
-10
-10.5
-11
-11.5
-12
10
11
12
13
14
15
log(ν [Hz])
log(νF_ν [erg/cm^2 s])

SEDs

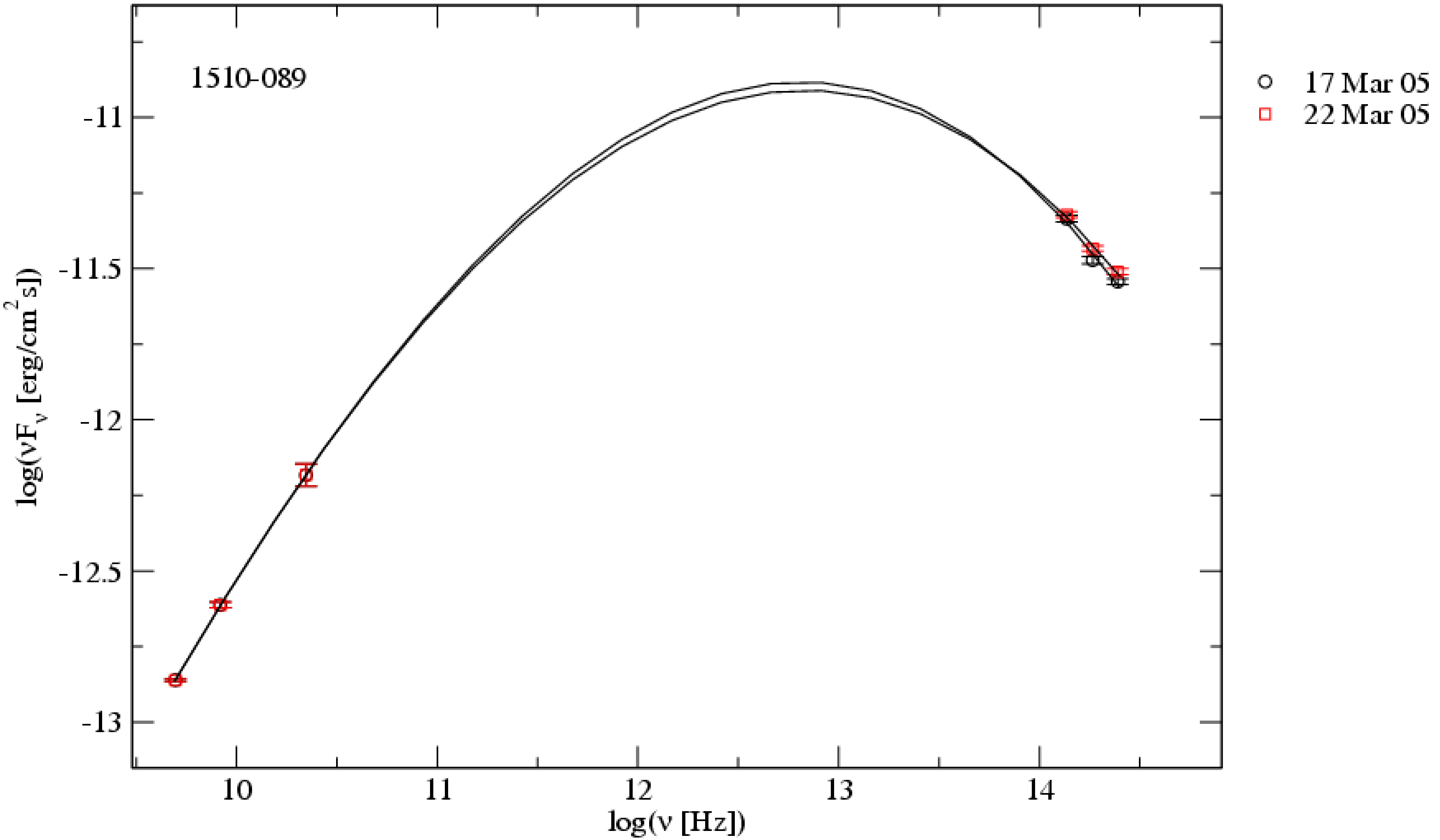

1510-089
17 Mar 05
22 Mar 05
log(νF_ν [erg/cm^2 s])
-11
-11.5
-12
-12.5
-13
10
11
12
13
14
log(ν [Hz])

SEDs

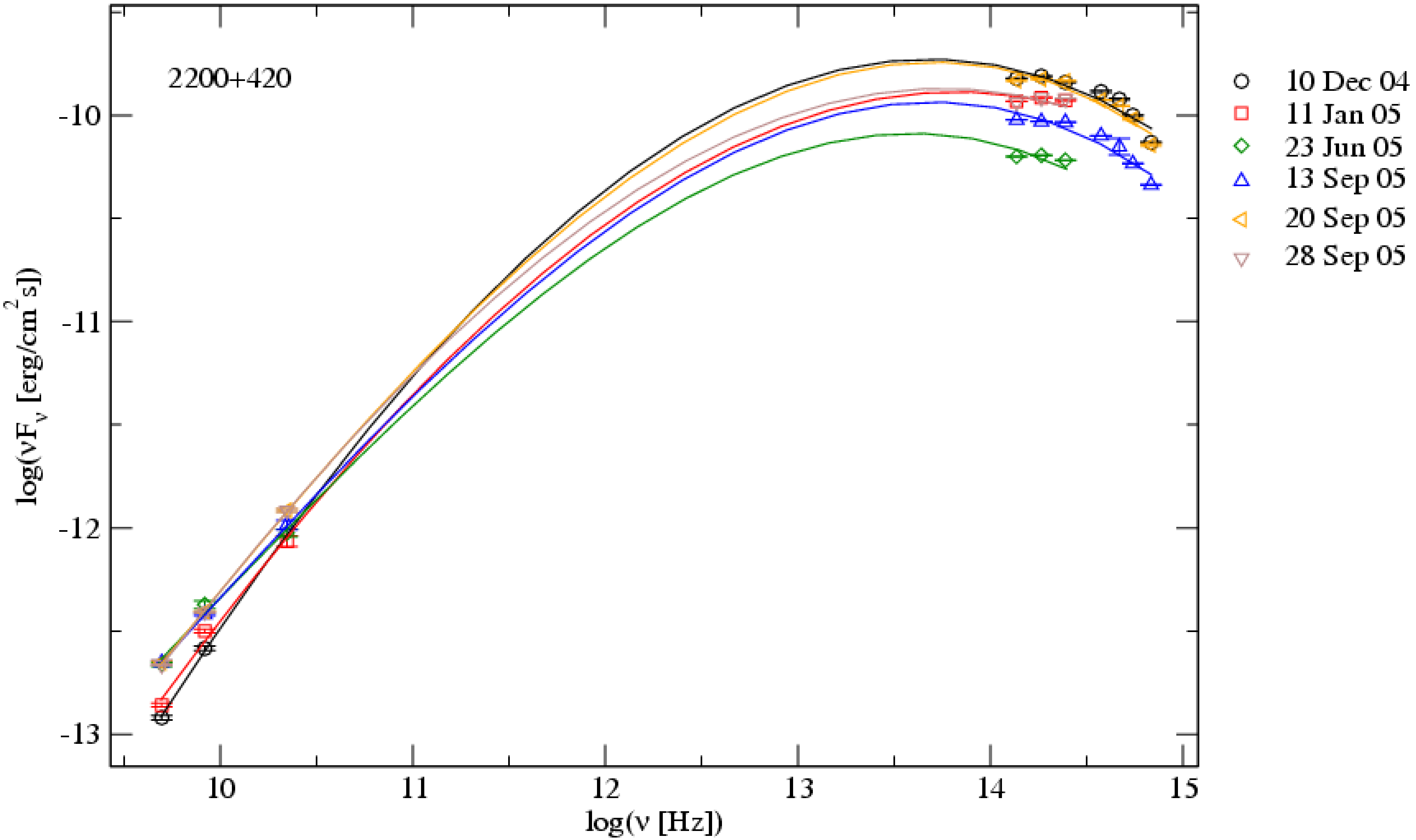
2200+420
log(νF_ν [erg/cm^2 s])
log(ν [Hz])
-10
-11
-12
-13
10
11
12
13
14
15
10 Dec 04
11 Jan 05
23 Jun 05
13 Sep 05
20 Sep 05
28 Sep 05

SEDs

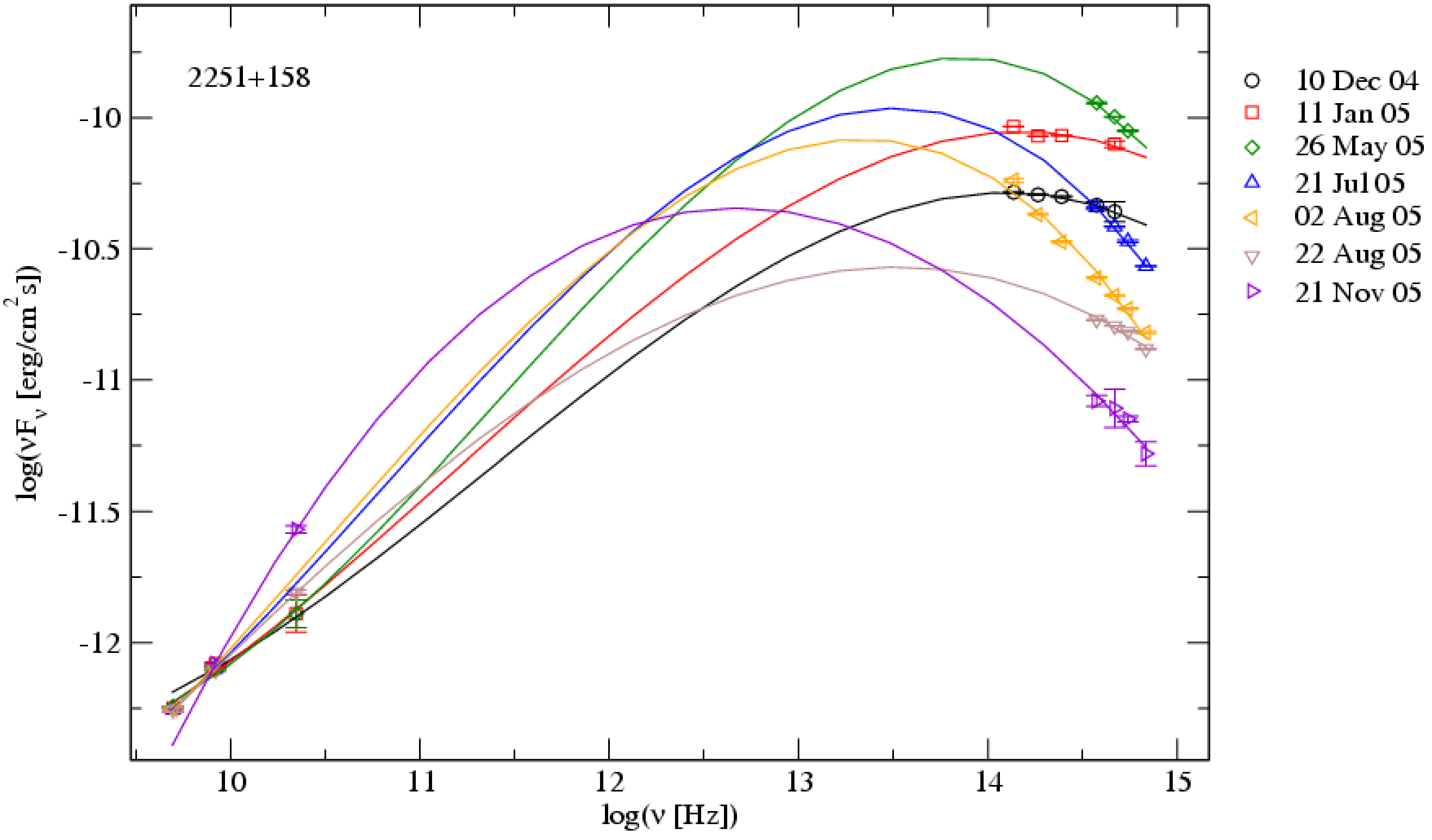
2251+158
10 Dec 04
11 Jan 05
26 May 05
21 Jul 05
02 Aug 05
22 Aug 05
21 Nov 05
log(νFν [erg/cm2 s])
log(ν [Hz])
-10
-10.5
-11
-11.5
-12
10
11
12
13
14
15

Data provided to others

Campaigns: 0235+164, OJ287, 3C 279, BL Lac, and 3C 454.3

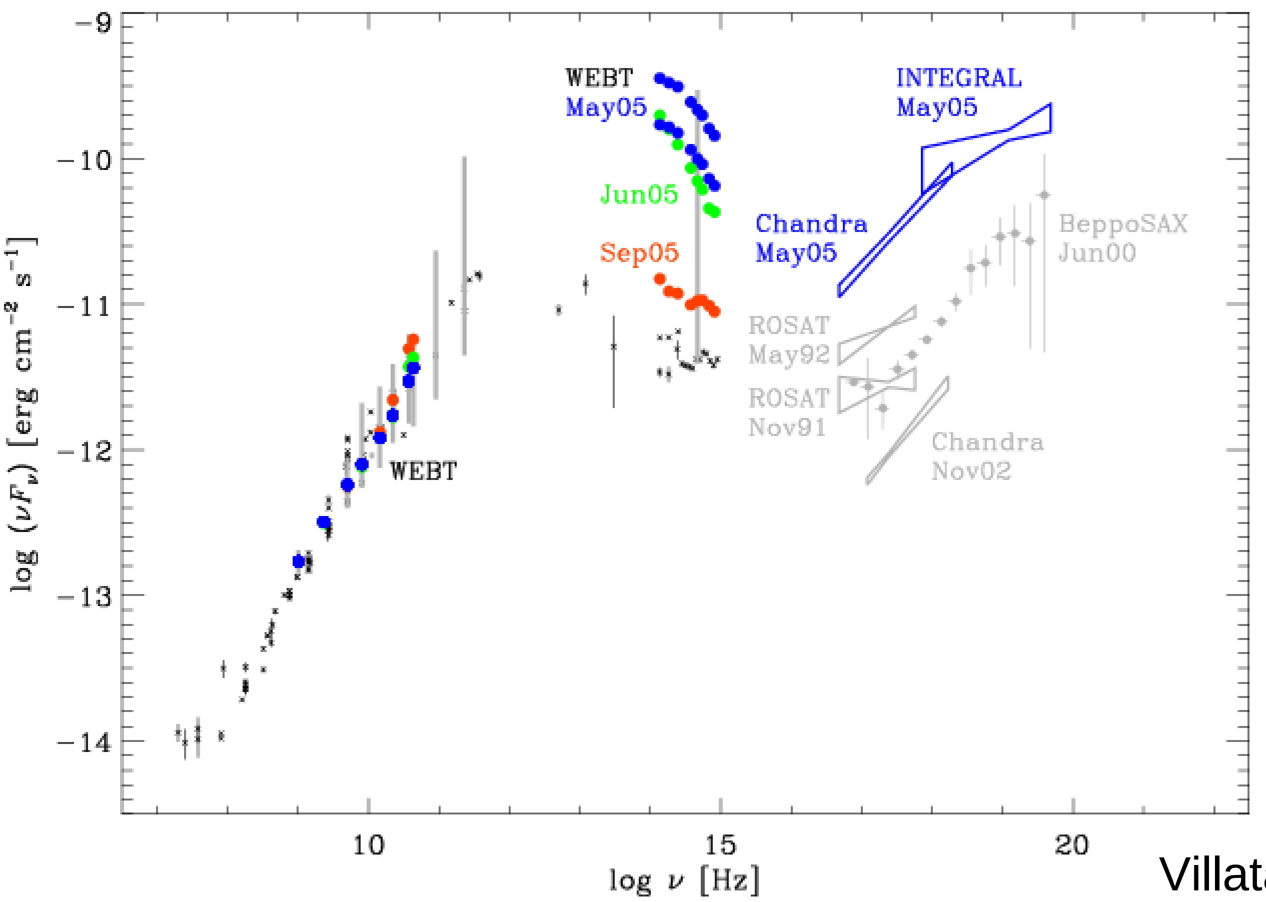

Villata et al. 2006, A&A, astro-ph/0603386

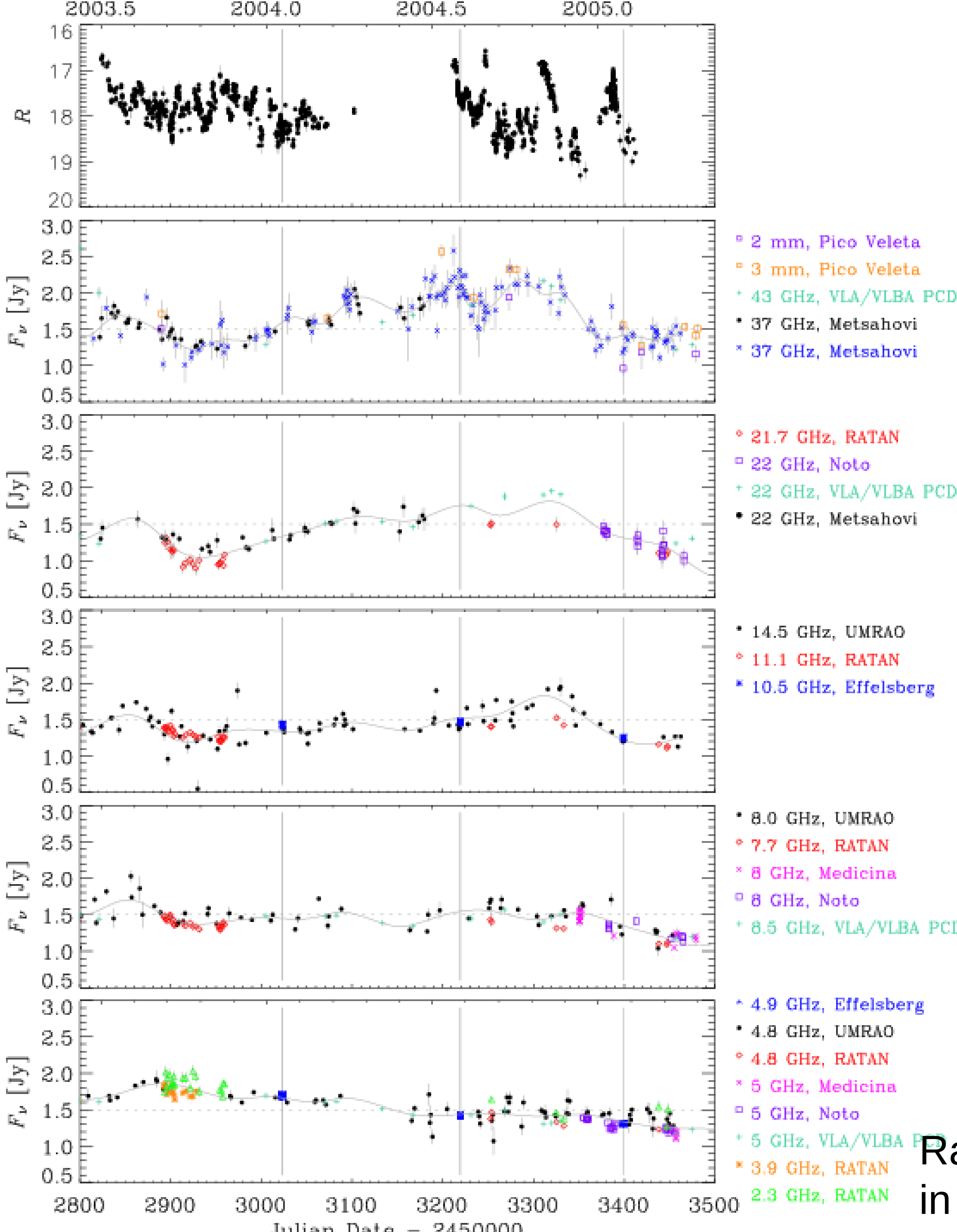

Raiteri et al. 2006, A&A, in perp.

Future Plans

- Waiting for AGILE and GLAST
- Publishing the first data with:
  - radio light curves and SEDs
  - analysis/discussion of the variability behaviour
  - fits of synchrotron models / calculation of synchrotron power?
- Add VLBI and optical polarization information
- Providing and sharing data with other multi-wavelength projects

High Energy Blazars

Science issues,
the ENIGMA context, and
future research projects

High Energy Blazars

What are (TeV)-XBL?
What do we know?
Synchrotron properties
Gamma-properties
scientific questions
what should be done
projects beyond ENIGMA

Gamma-Emission: RBL-XBL

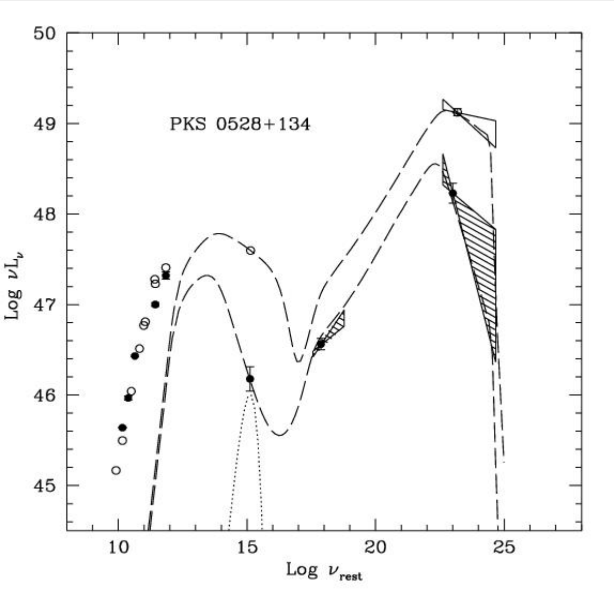

SEDs

Synchrotron
IC Component?

300 Blazars

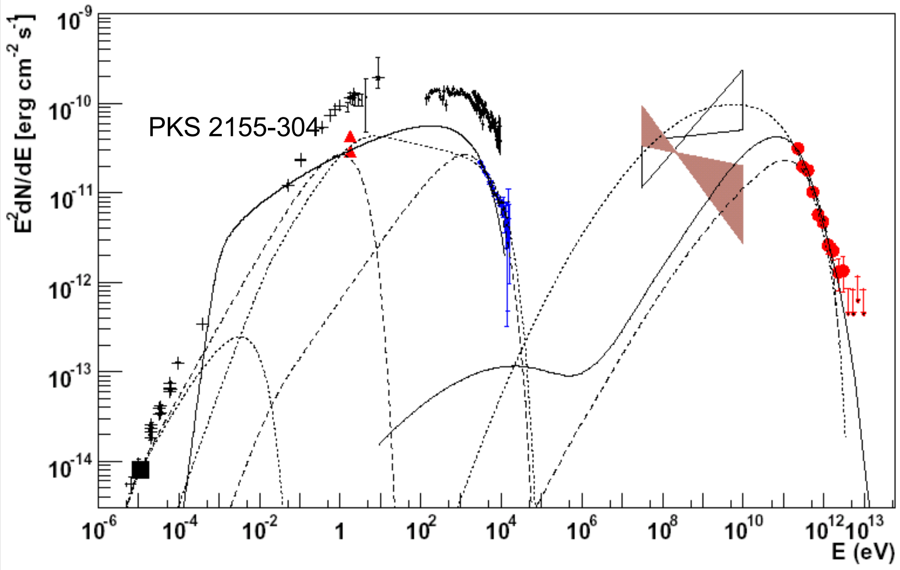

Are all Gamma-bright? What do we get from HE data?

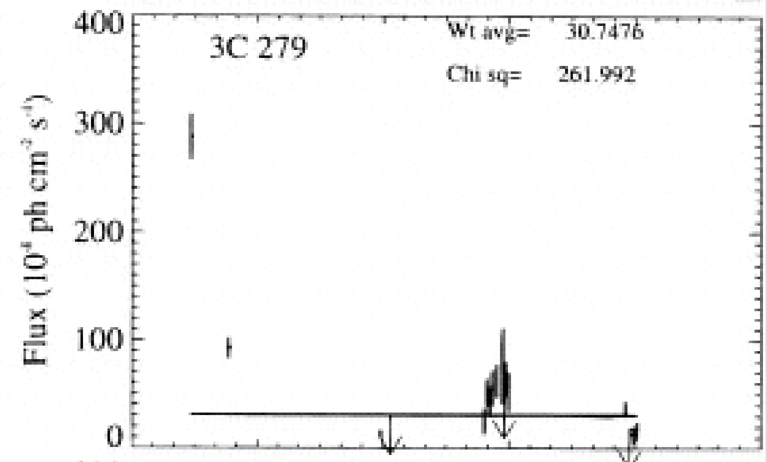

Variability:
Correlations
Parameters

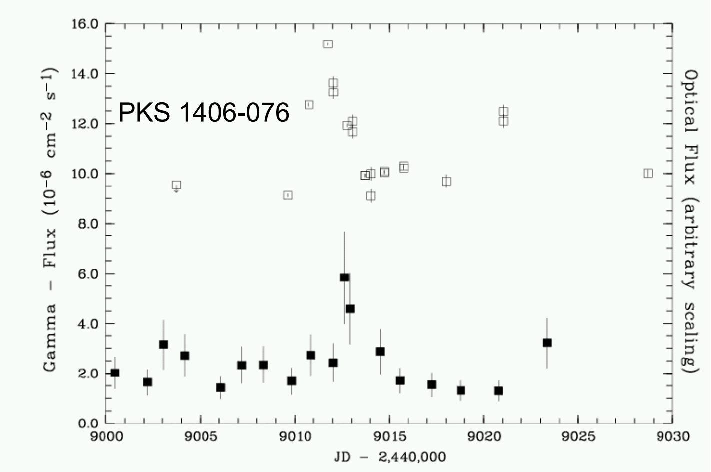

High Energy Blazars

Blazar	z	$F^{\dagger}_{min}$	$\Gamma_{1\mathrm{TeV}}$	F_{max}/F_{min}	E_{cut}/TeV
Mrk 421	0.031	<4.9	2.2	>20	var.
Mrk 501	0.034	<17	1.9	>25	>3
1ES 2344+514	0.044	<25	?	>2	?
1ES 1959+605	0.047	<19	2.8	>9	2
PKS 2005-489	0.071	<5.2	4.0	1.4	>2
PKS 2155-304	0.117	4.1	3.3	10	>4
H 1426+428	0.129	<11	2.2	>5	>3
1ES 2356-309	0.165	4.1	3.09	1.4	>1
1ES 1218+304	0.182(?)	<7	?	1?	?
1ES 1101-232	0.186	5.1	2.88	1(q)	>3
PG 1553+113	$<.25?$	4.8	4.0	1	$>.5$

$\dagger\ F_{>200\mathrm{GeV}}/10^{-12}\mathrm{cm}^{-2}\mathrm{s}^{-1}$

High Energy Blazars

RBLs: The realm of GLAST/AGILE
Science Projects: See original plan of task 6

for lack of new data: XBL
(note that most of the old data are not yet used)

Beware of uncertainties: e.g. EBL

Blazar	z	$F^{\dagger}_{min}$	$\Gamma_{1\mathrm{TeV}}$	F_{max}/F_{min}	E_{cut}/TeV
Mrk 421	0.031	<4.9	2.2	>20	var.
Mrk 501	0.034	<17	1.9	>25	>3
1ES 2344+514	0.044	<25	?	>2	?
1ES 1959+605	0.047	<19	2.8	>9	2
PKS 2005-489	0.071	<5.2	4.0	1.4	>2
PKS 2155-304	0.117	4.1	3.3	10	>4
H 1426+428	0.129	<11	2.2	>5	>3
1ES 2356-309	0.165	4.1	3.09	1.4	>1
1ES 1218+304	0.182(?)	<7	?	1?	?
1ES 1101-232	0.186	5.1	2.88	1(q)	>3
PG 1553+113	$<.25$?	4.8	4.0	1	$>.5$

† $F_{>200\mathrm{GeV}}/10^{-12}\mathrm{cm}^{-2}\mathrm{s}^{-1}$

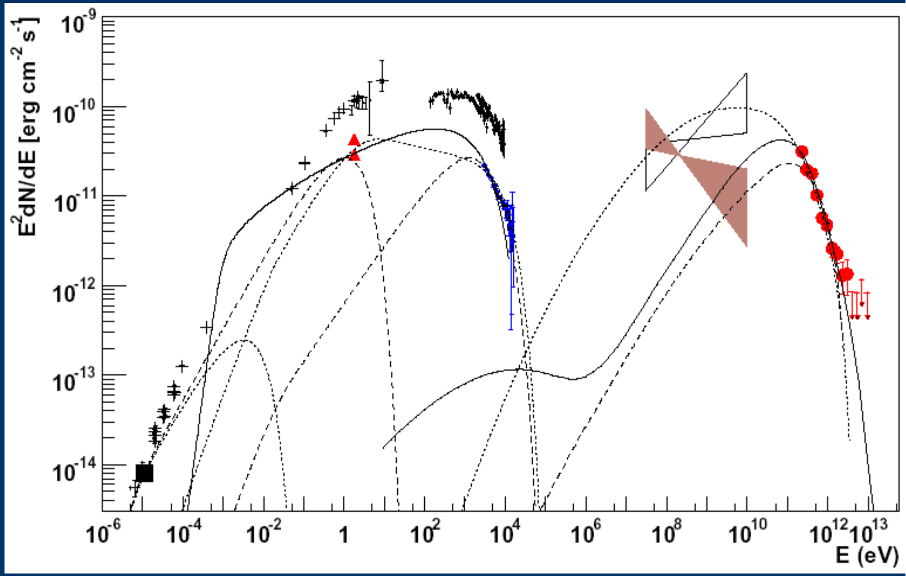

Constraints on diffuse EBL

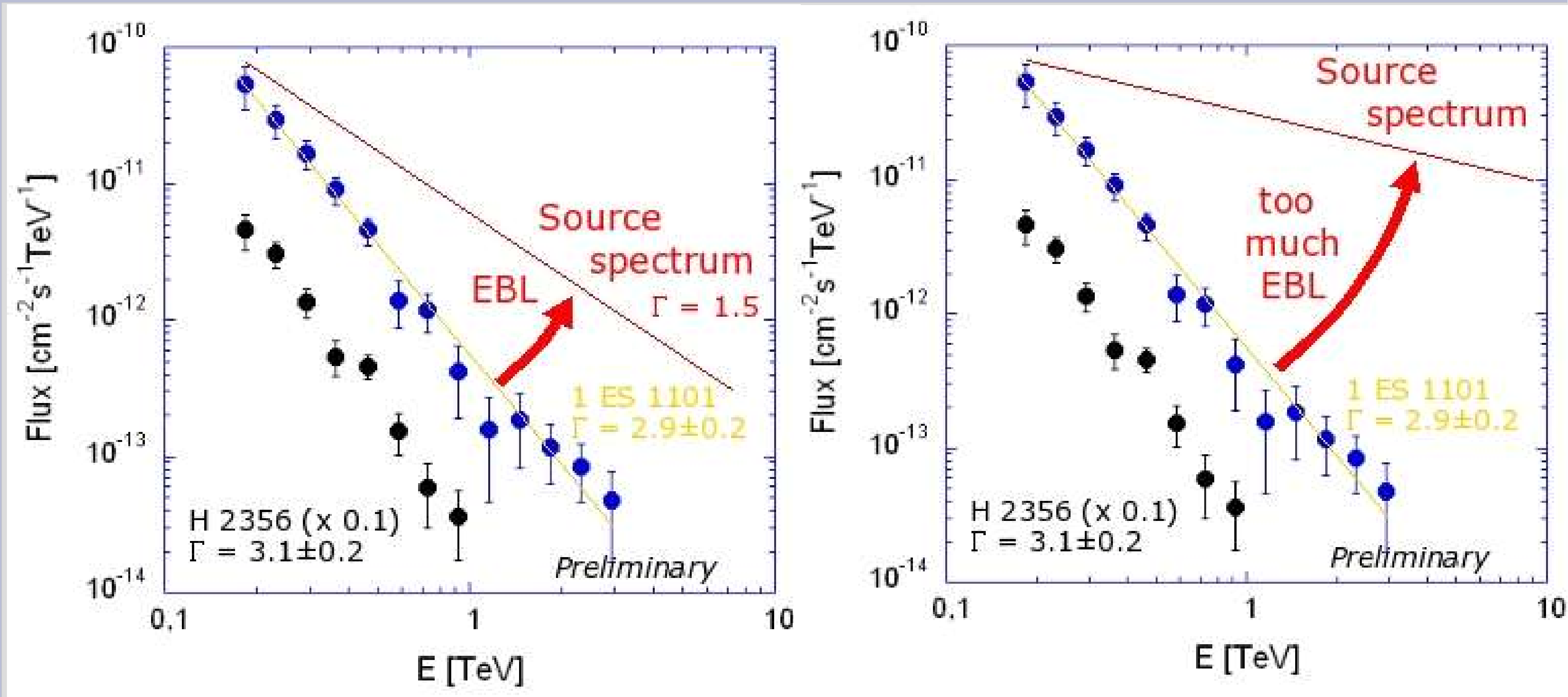

shock acceleration: s=1.5 Protons: Gamma=1.5

IC: Gamma > 1.5 unless no radiative cooling **and** IC fully in Thomson limit [Gamma = (s+1)/2 =1.25]

Constraints on diffuse EBL

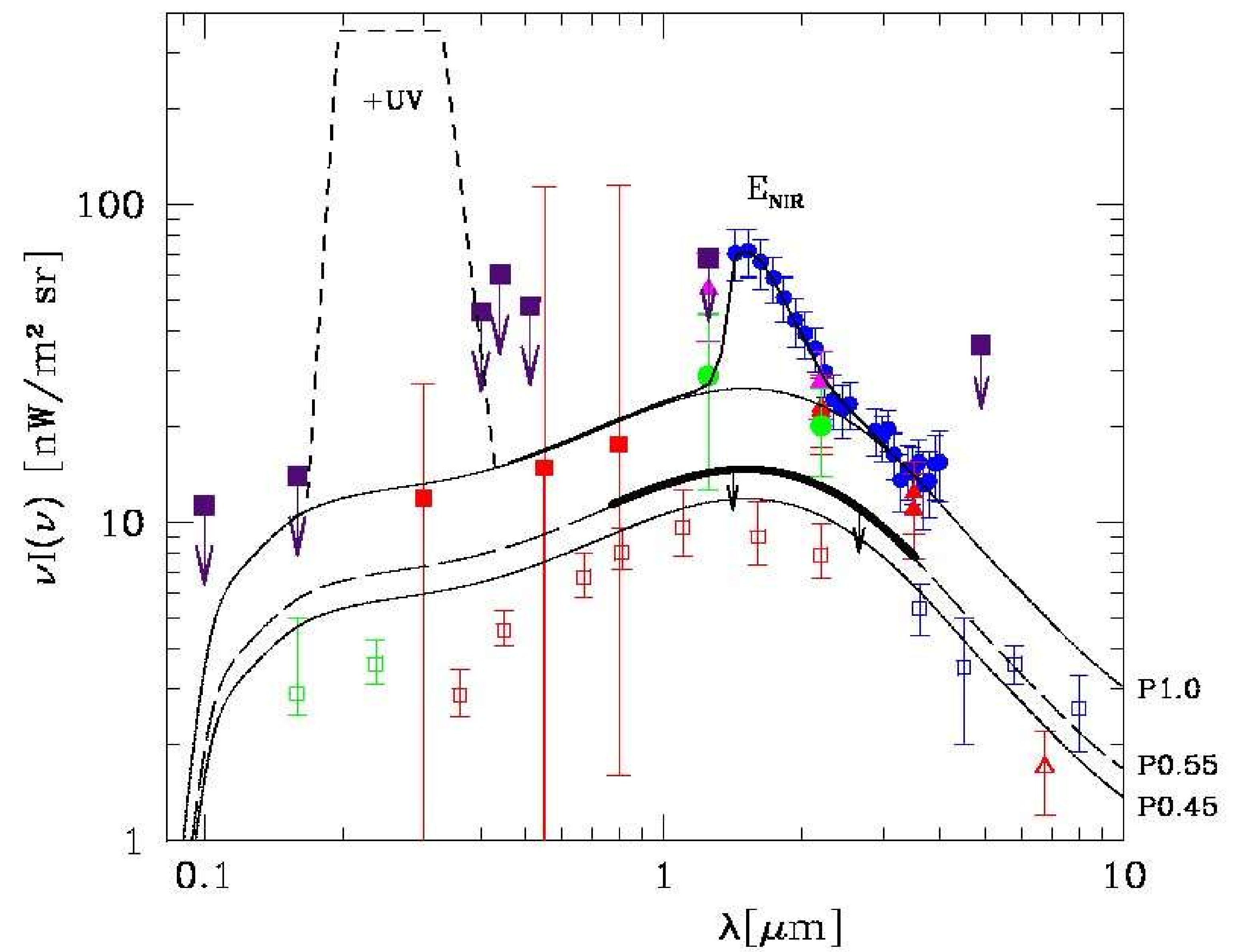

Constraints on diffuse EBL

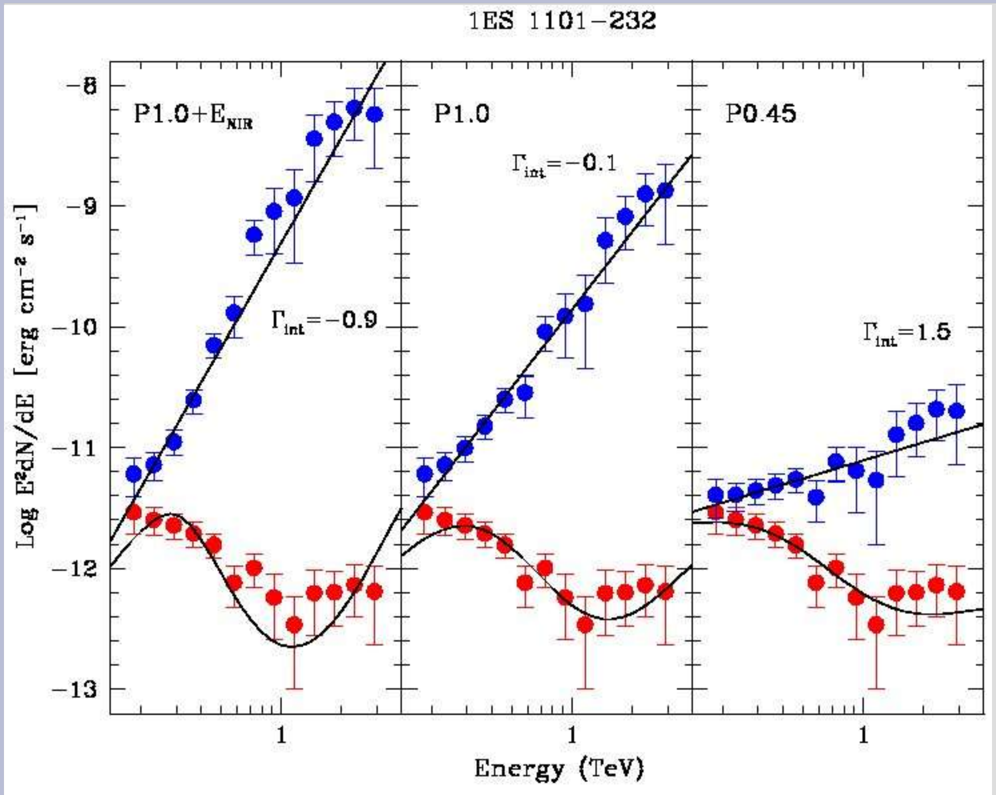

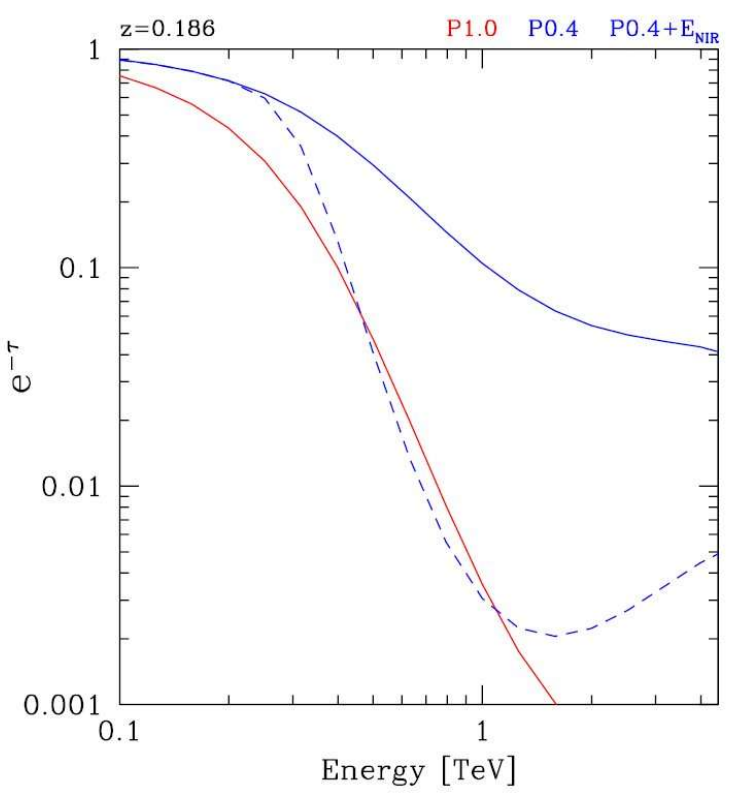

Constraints: EBL estimate Aharonian et al., 2006, Nature
Comment on pile-up spectrum (Katarzynski et al., 2006)
Difference matters for SED and physics modelling

Synchrotron Radiation:

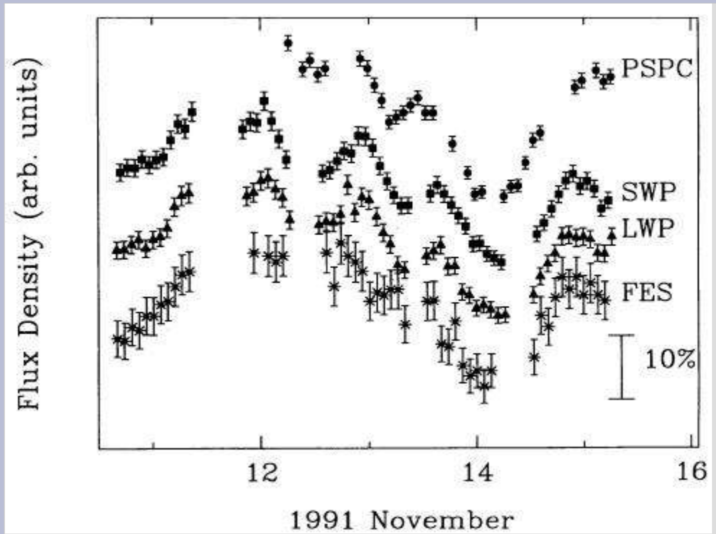

PKS 2155-304
1991 and 1994

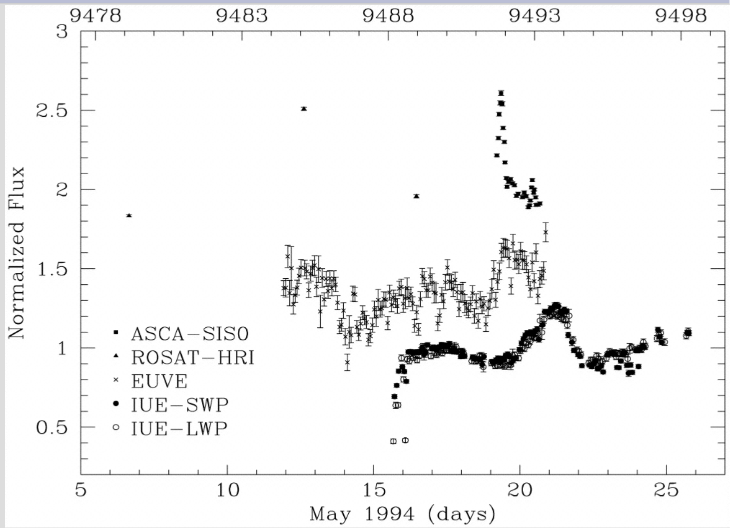

No unique spectral behavior within one source

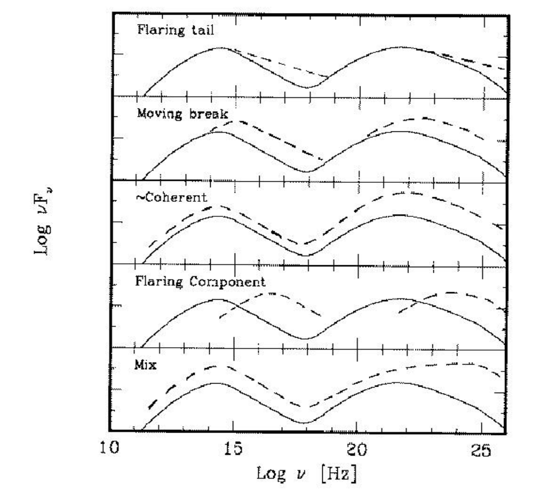

different flares act differently

(predict IC-behaviour)

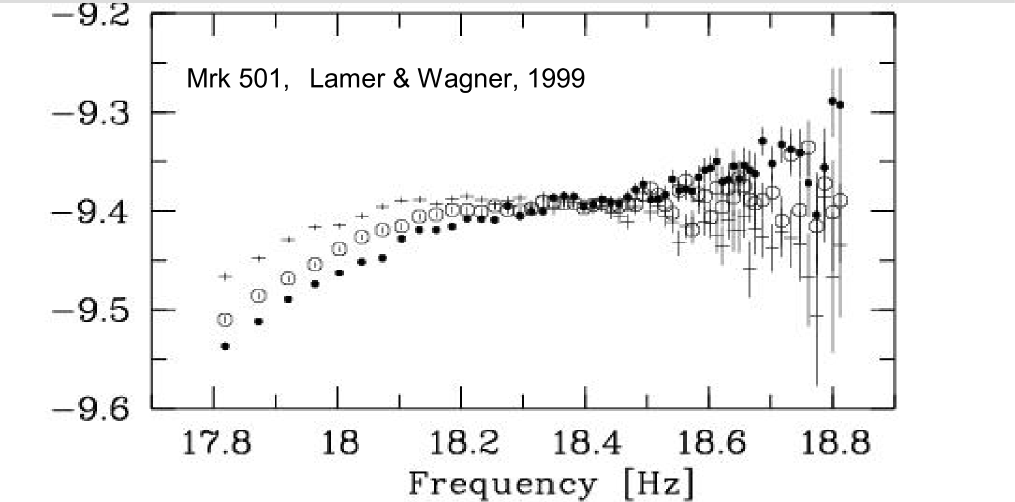

High Energy Blazars

Blazar	z	$F^{\dagger}_{min}$	$\Gamma_{1\mathrm{TeV}}$	F_{max}/F_{min}	E_{cut}/TeV
Mrk 421	0.031	<4.9	2.2	>20	var.
Mrk 501	0.034	<17	1.9	>25	>3
1ES 2344+514	0.044	<25	?	>2	?
1ES 1959+605	0.047	<19	2.8	>9	2
PKS 2005-489	0.071	<5.2	4.0	1.4	>2
PKS 2155-304	0.117	4.1	3.3	10	>4
H 1426+428	0.129	<11	2.2	>5	>3
1ES 2356-309	0.165	4.1	3.09	1.4	>1
1ES 1218+304	0.182(?)	<7	?	1?	?
1ES 1101-232	0.186	5.1	2.88	1(q)	>3
PG 1553+113	$<.25$?	4.8	4.0	1	$>.5$

$\dagger$ $F_{>200\mathrm{GeV}}/10^{-12}\mathrm{cm}^{-2}\mathrm{s}^{-1}$

PKS 2155-304

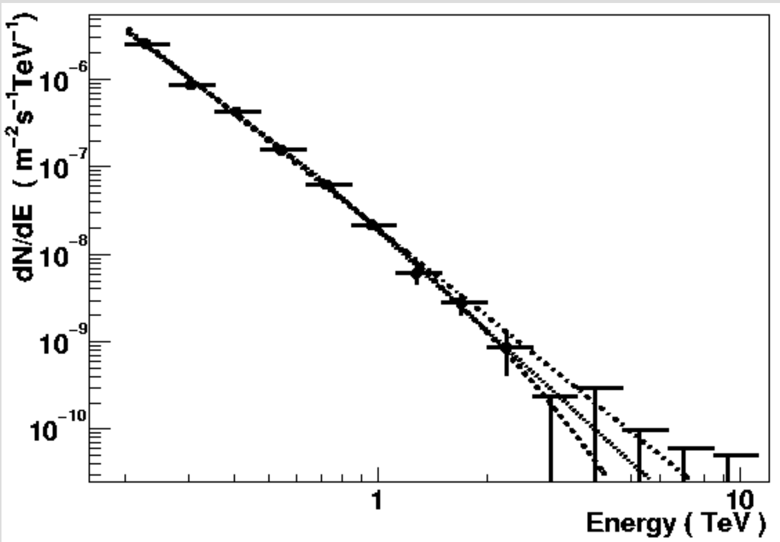

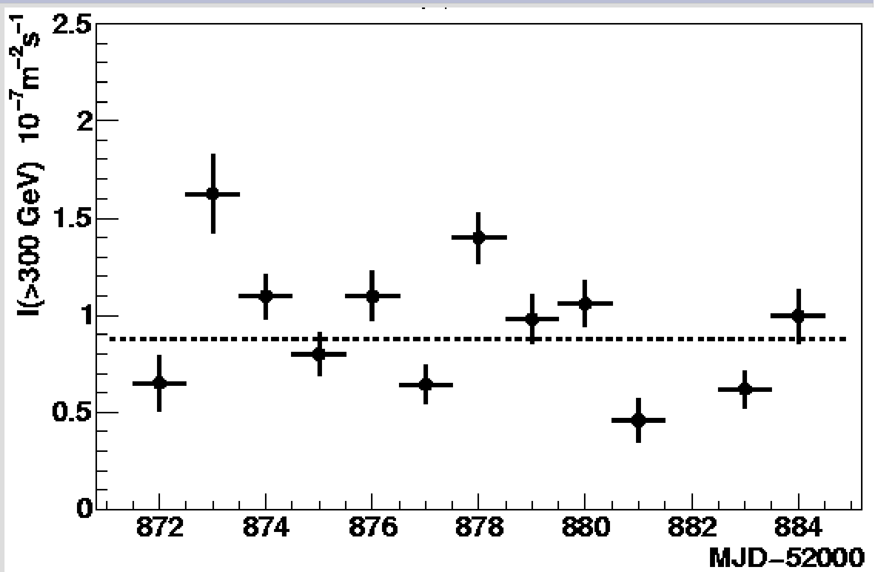

Detection in 2002, 2003 with single telescope already: astro-ph/0411582

Powerlaw spectrum, Index: -2.9
variability: years – minutes

Suggests Doppler factor $\mathcal{D}$ ~ 50

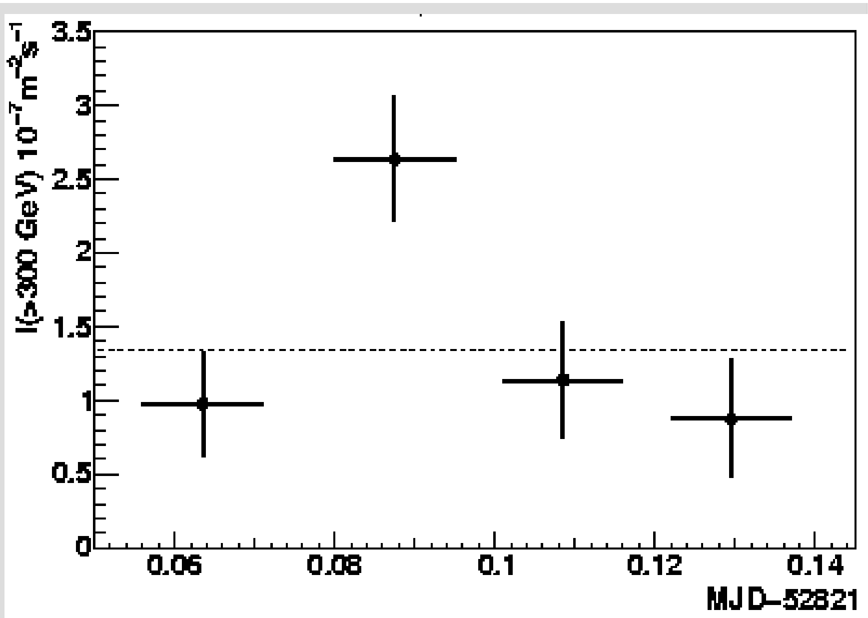

Mrk 421 I (Spectrum)

Confirmation,
improved sensitivity (spectra)

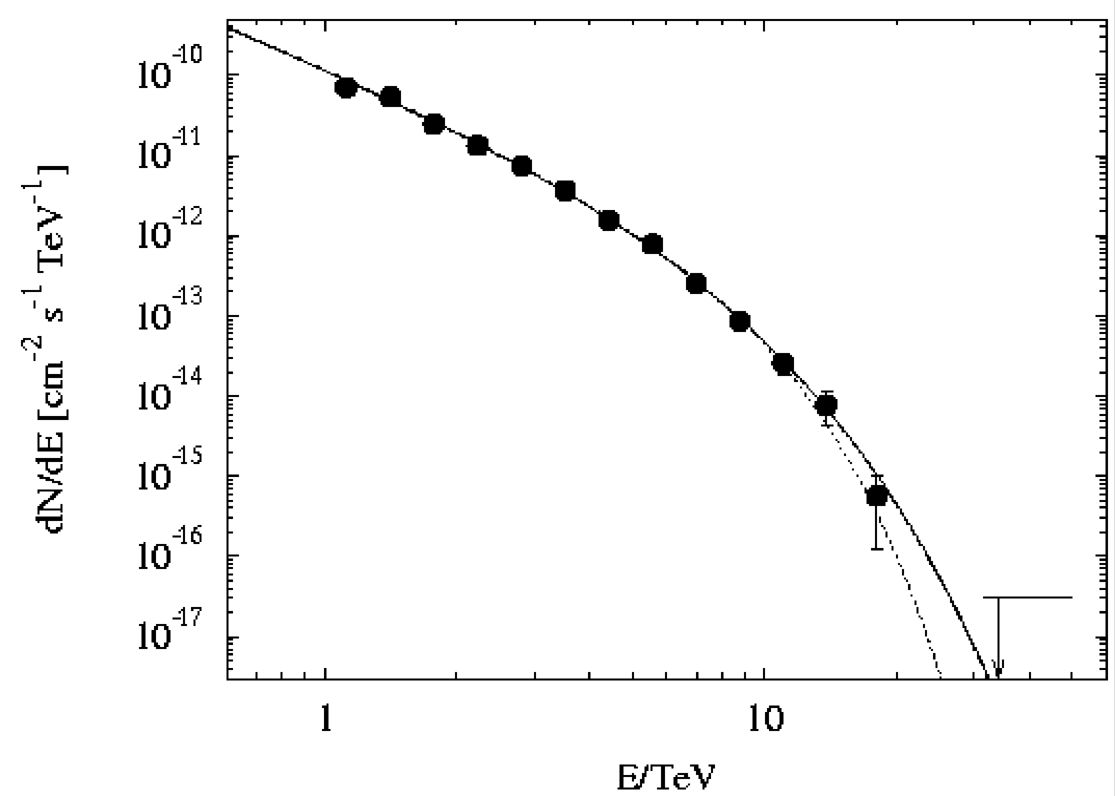

Observations 3 months in '04

Range of zenith angles:
60.3 d < ZA < 65.4 d
Large collection area: 2 km
at 10 TeV energy threshold
High significance:
7000 photons, 100 sigma

$\Gamma = 2.1 \pm 0.1_{\mathrm{stat}} \pm 0.3_{\mathrm{sys}}$ $E_c = 3.1(+0.5 - 0.4)_{\mathrm{stat}} \pm 0.9_{\mathrm{sys}}$ TeV

Curved spectra (Power-law with exponential cutoff):

Mrk 421 II (Variability)

Variability on all time-scales (ksec – months).
Power-law index and cut-off correlated in nighly averages
Spectral variability prohibits integrating long enough
Flux correlates with cut-off energy (hardness?)
SED monitoring (X-rays, MAGIC?)

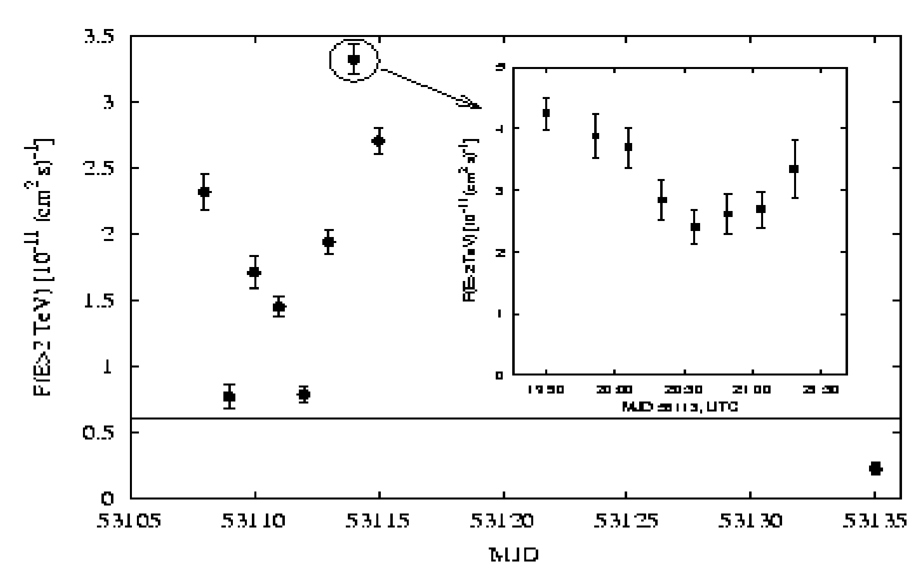

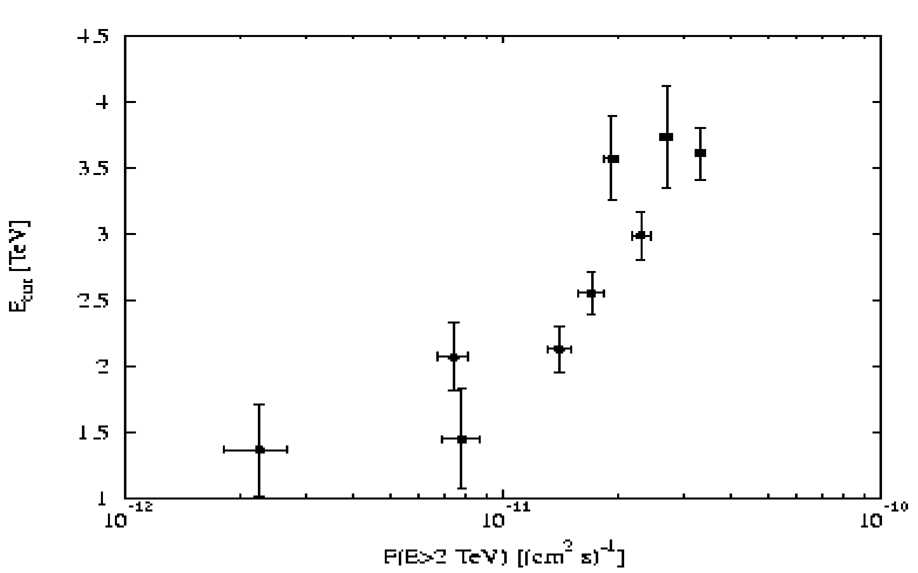

A clue to studying spectral evolution with full temporal resolution

High Energy Blazars

What are the duty cycles/SF/PDF in XBLs?
(quiescent level?, mapping temporal properties to spectra)
How compact are emission zones?
(what happens at low energies? Diffusion time scales, RISS?)
Role of hadrons? What are the seed fields?
(self-consistent modelling of temporal evolution of SED)
Interactions with magnetized large scale flow?
(large-scale speed, dv/dr, jet bending and rigidity)
What are the acceleration mechanisms?
(what is the low-energy cutoff?, where? How; jet launching)
What is the total power?
(unified models, the role of selection effects & Blazar sequence)

Correlations

we want | we get | we need

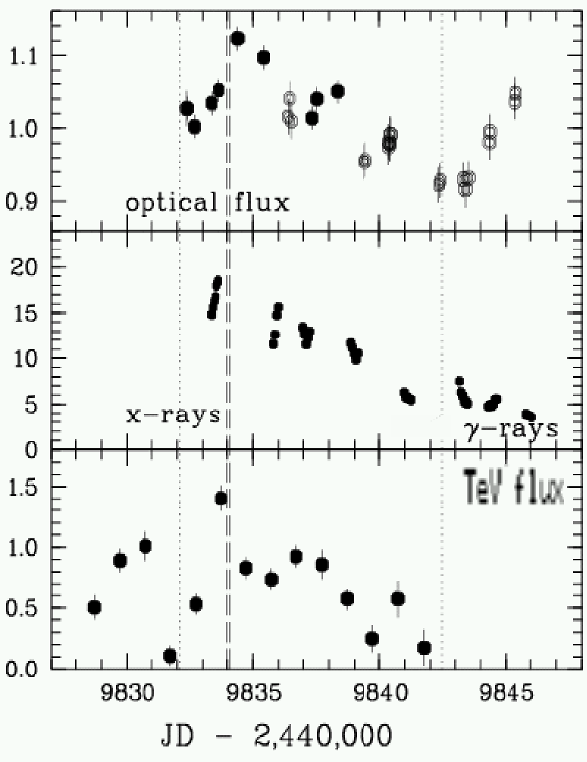

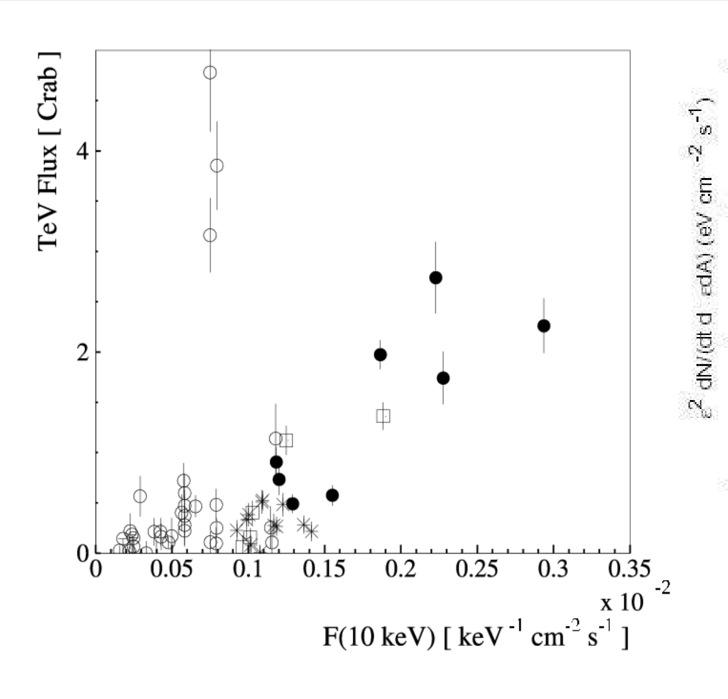

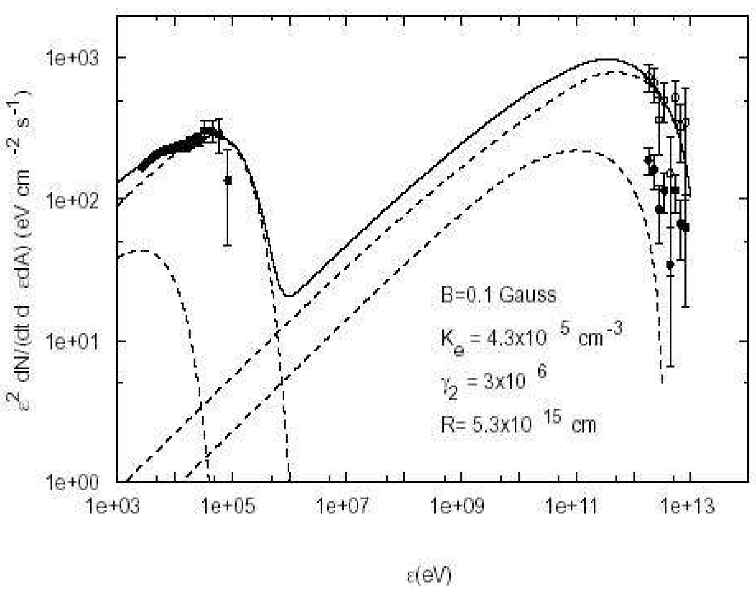

Wagner & Takahashi, 1995

Krawczynski et al., 2003

Bicknell & Wagner, 2003

Possible reason

spectral lags within
one passband
e.g. Mrk 501:
(Wagner & Lamer, 1999, 2001)

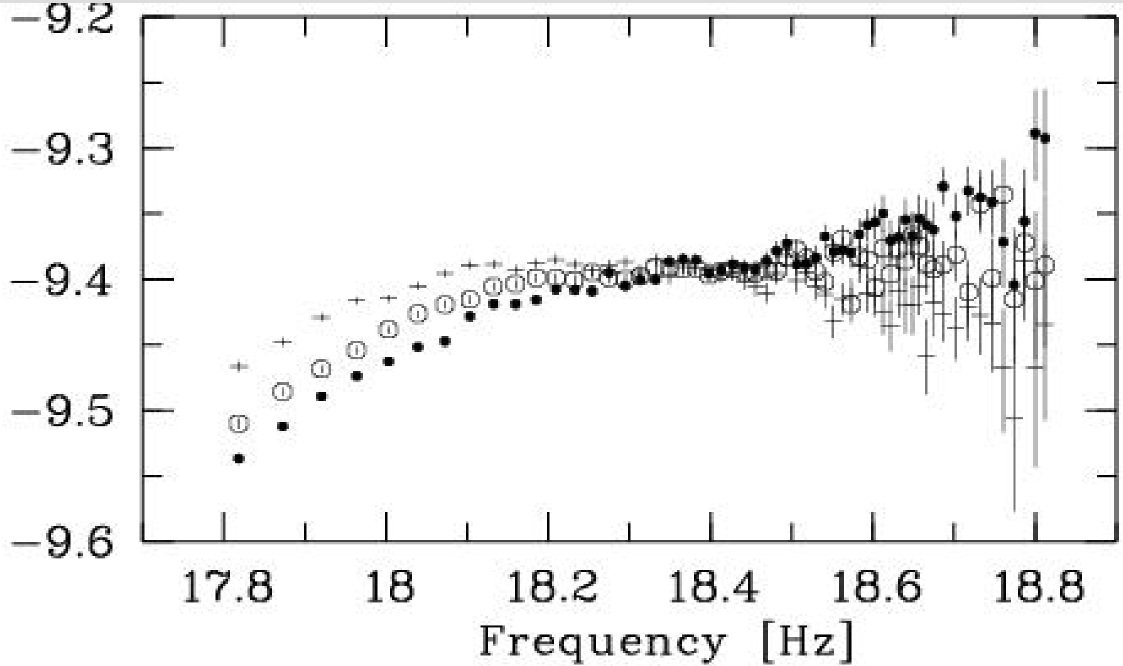

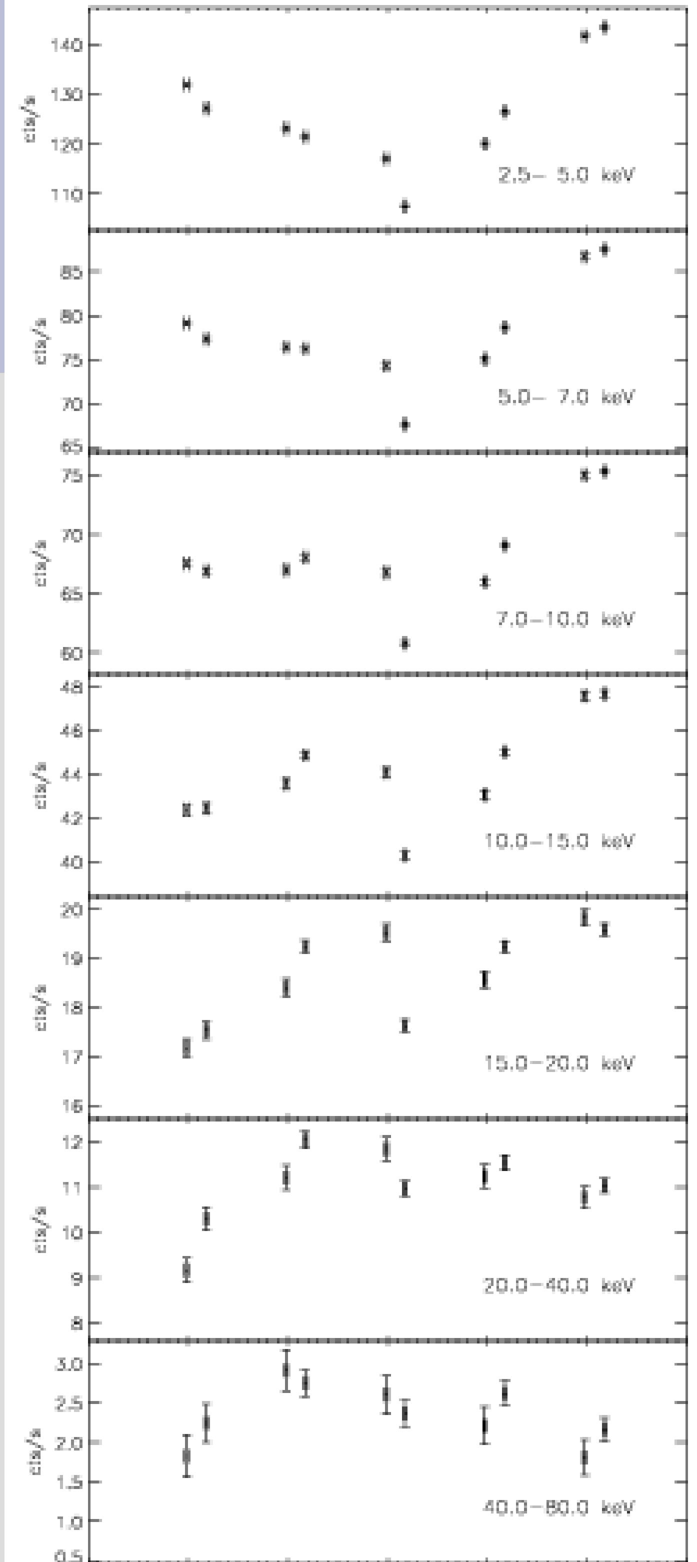

High Energy Blazars

What are the duty cycles/SF/PDF in XBLs?
(task 1)
How compact are emission zones?
(task 2)
Role of hadrons? What are the seed fields?
(task 3)
Interactions with magnetized large scale flow?
(task 4)
What are the acceleration mechanisms?
(task 5)
What is the total power?
(task 6)

High-Energy γ-ray Emission in M 87 Radio Galaxy (and Cen A Radio Galaxy)

Łukasz Stawarz

Landessternwarte Heidelberg, Heidelberg, Germany

Max-Planck-Institut für Kernphysik, Heidelberg, Germany

Obserwatorium Astronomiczne UJ, Kraków, Poland

Collaborators

Felix A. Aharonian *(MPIfK, Heidelberg, Germany)*

Jun Kataoka *(TIT, Tokyo, Japan)*

Michał Ostrowski *(OA UJ, Kraków, Poland)*

Aneta Siemiginowska *(CfA, Cambridge, USA)*

Marek Sikora *(CAMK, Warszawa, Poland)*

Stefan Wagner *(LSW, Heidelberg, Germany*

Large-Scale Radio Structure of M 87

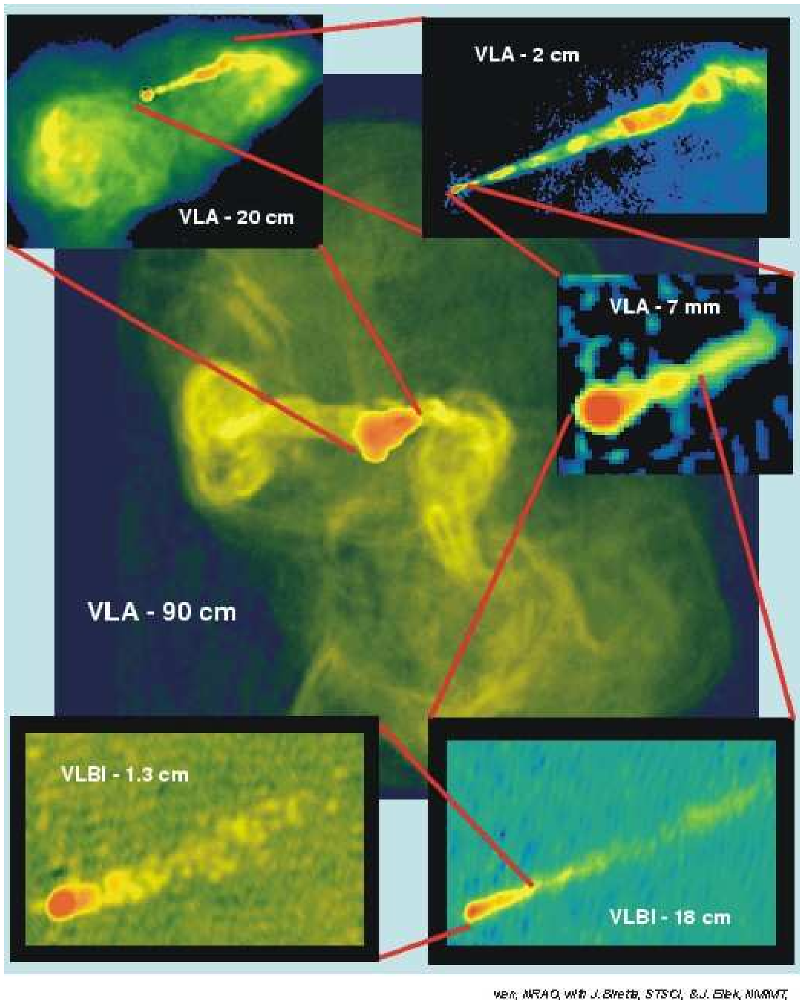

Amorphous large-scale radio structure of M 87 (*Owen et al. 2000, ApJ, 543*).

"buoyant bubbles of cosmic rays (inflated by an earlier nuclear active phase of the galaxy) rise through the cooling gas (...); bubbles uplift relatively cool X-ray-emitting gas from the central regions of the cooling flow to larger distances." (*Churazov et al. 2001, ApJ, 554*)

"the jet disrupts very close to the galactic core, but the plasma flow appears to continue in a much less ordered fashion, forming giant 'bubble' which has partly mixed with the ambient thermal plasma." (*Eilek et al. 2002, New AR, 46*)

X-ray Cluster Gas Around M 87

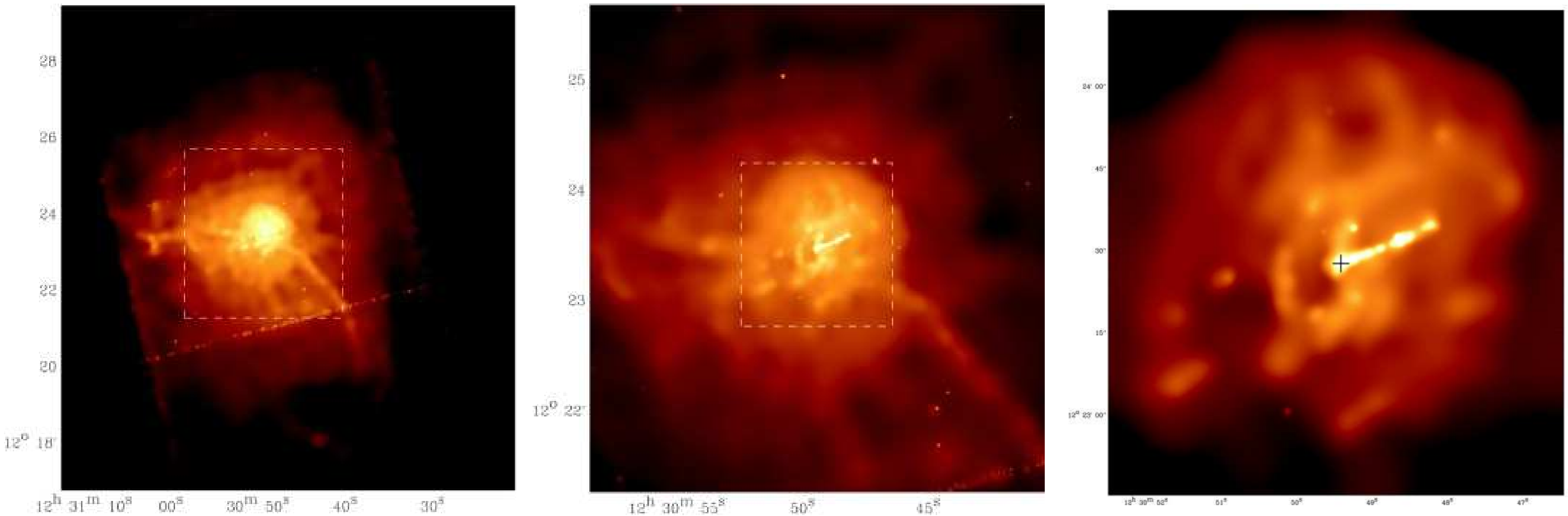

Cluster gas surrounding M 87 as observed in X-rays by the *Chandra X-ray Observatory*:

"The inner radio lobes are aligned with depressions in the X-ray surface brightness, and there is no evidence of shock heating in the X-ray emission immediately surrounding the inner radio lobes, suggesting that the radio plasma has gently pushed aside the X-ray emitting gas. (...) On larger scales the most striking feature is the X-ray arc running from the east, across the central regions of M87, and off to the southwest. The gas in the arc has at least two temperatures, is probably overpressured with respect to, and somewhat more metal-rich than, the ambient intracluster medium" (Young et al. 2002, ApJ, 579; see also Di Matteo et al. 2003, ApJ, 582; Feng et al. 2004, ApJ, 607.)

Synchrotron Emission of the M 87 Jet

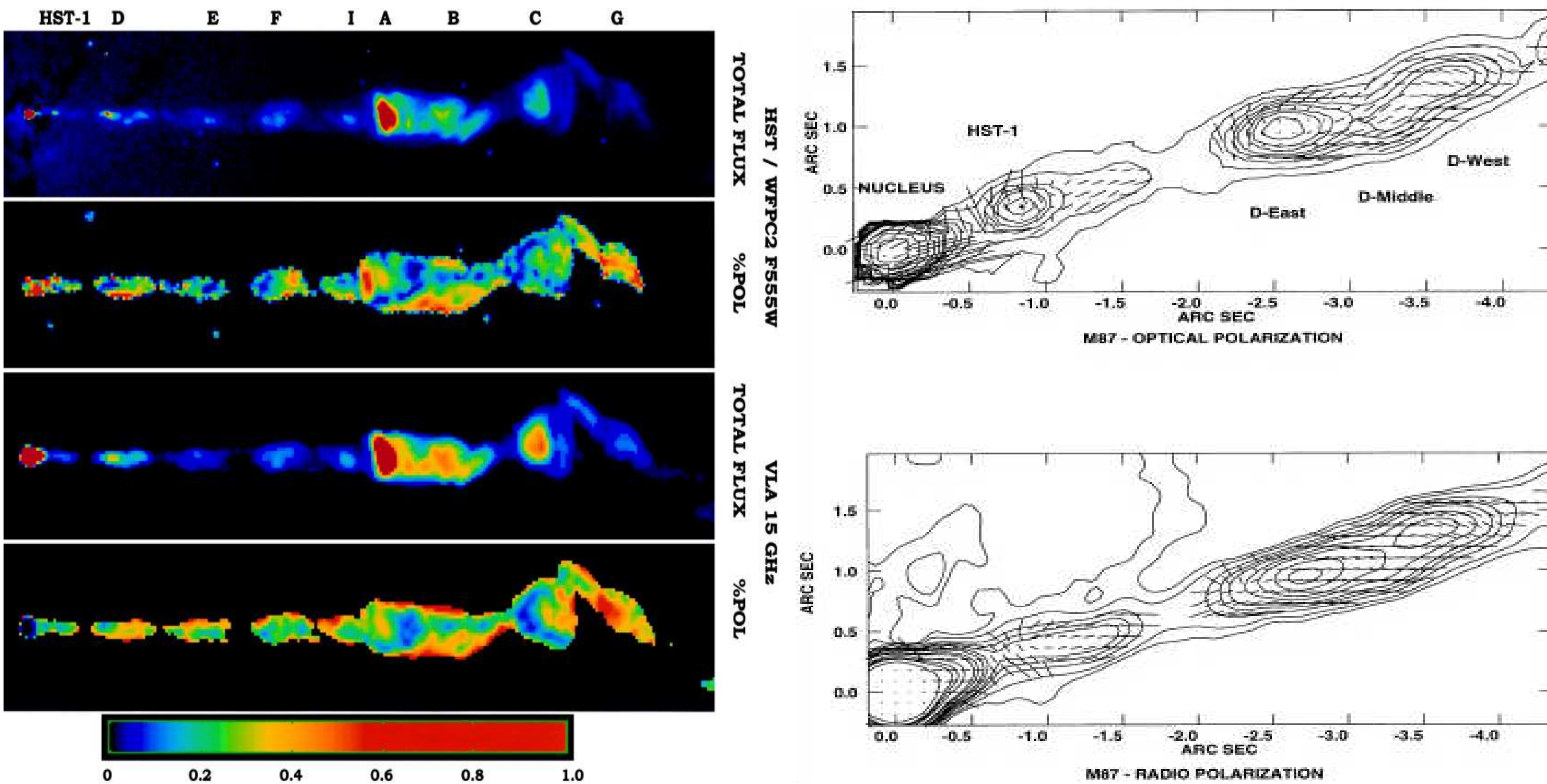

Radio and optical synchrotron emission of 2-kpc-long M 87 jet (*Perlman et al. 1999, AJ, 117*).

VHE Electrons in the M 87 Jet

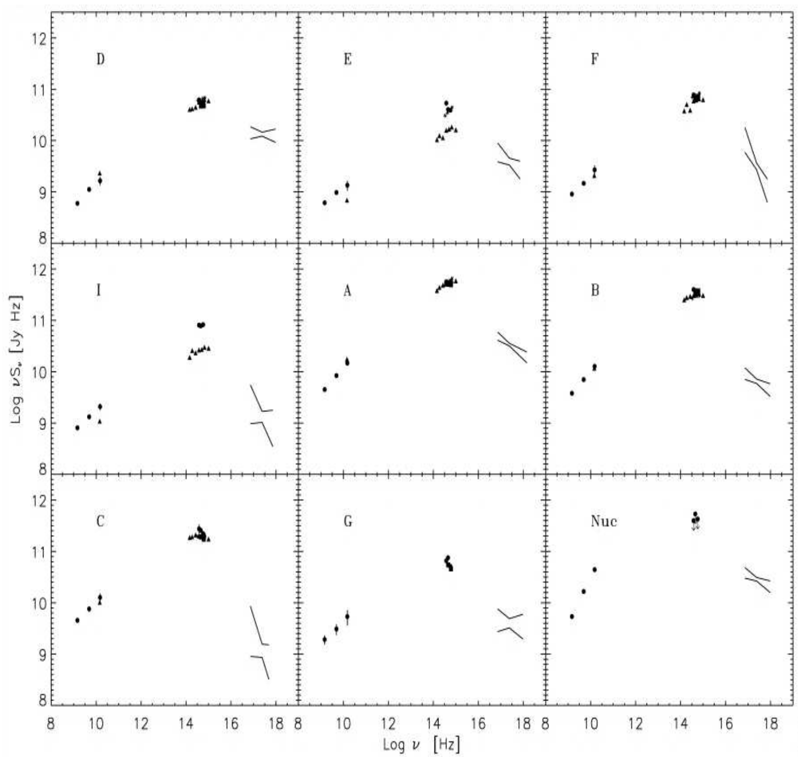

Biretta et al. 1991, AJ, 101; Meisenheimer et al. 1996, A&A, 307; Sparks et al. 1996, ApJ, 473; Perlman et al. 2001, ApJ, 551; Marshall et al. 2002, ApJ, 564; Wilson & Yang 2002, ApJ, 568; Waters & Zepf 2005, ApJ, 624; Perlman & Wilson 2005,ApJ, 627.

Let us reconctruct the comoving energy distribution of the electrons contributing to the observed emission of the brightest knot A (located ~ 1 kpc from the active center), $n'_{\rm e} \equiv \int n'_{\rm e}(\gamma)\, d\gamma$, from the well-constrained synchrotron continuum, and find the expected inverse-Compton emission as a function of free parameters:

- the jet magnetic field B,
- the bulk Lorentz factor Γ,
- the jet viewing angle θ

Dominant Starlight Photon Field

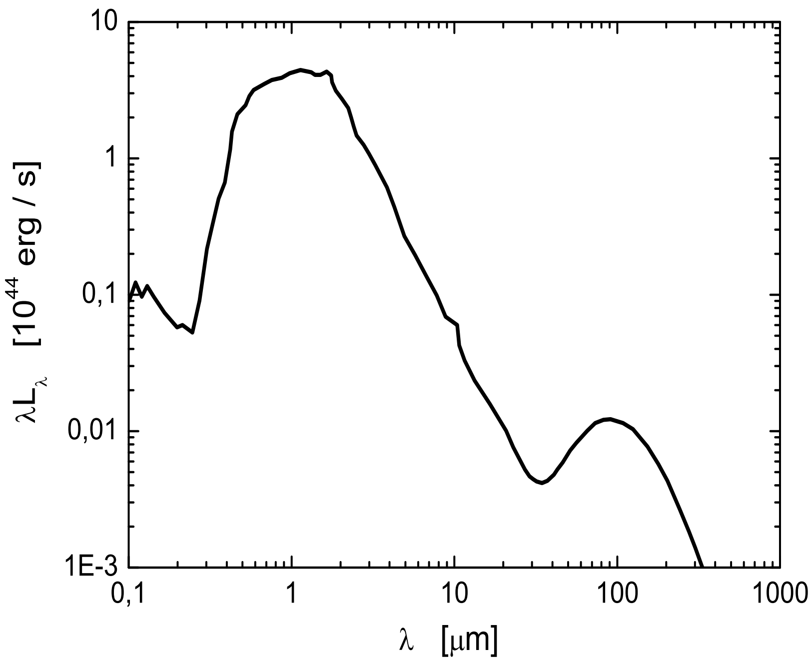

A template SED of a giant elliptical galaxy (*Silva et al. 1998, ApJ, 509*).

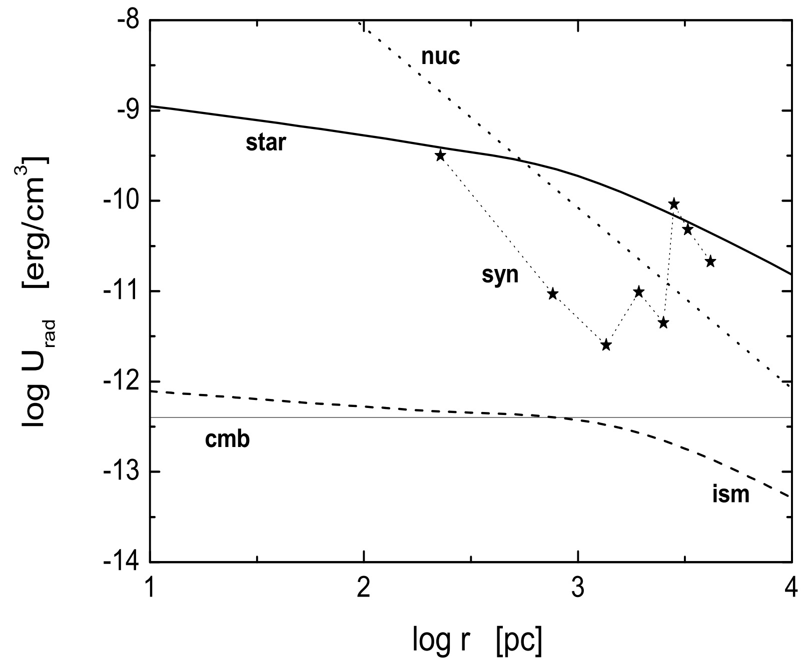

Radiation fields in M87 host galaxy along the jet (as measured by a stationary observer). *Stawarz et al. 2006, MNRAS, 370*

VHE γ-Rays from knot A?

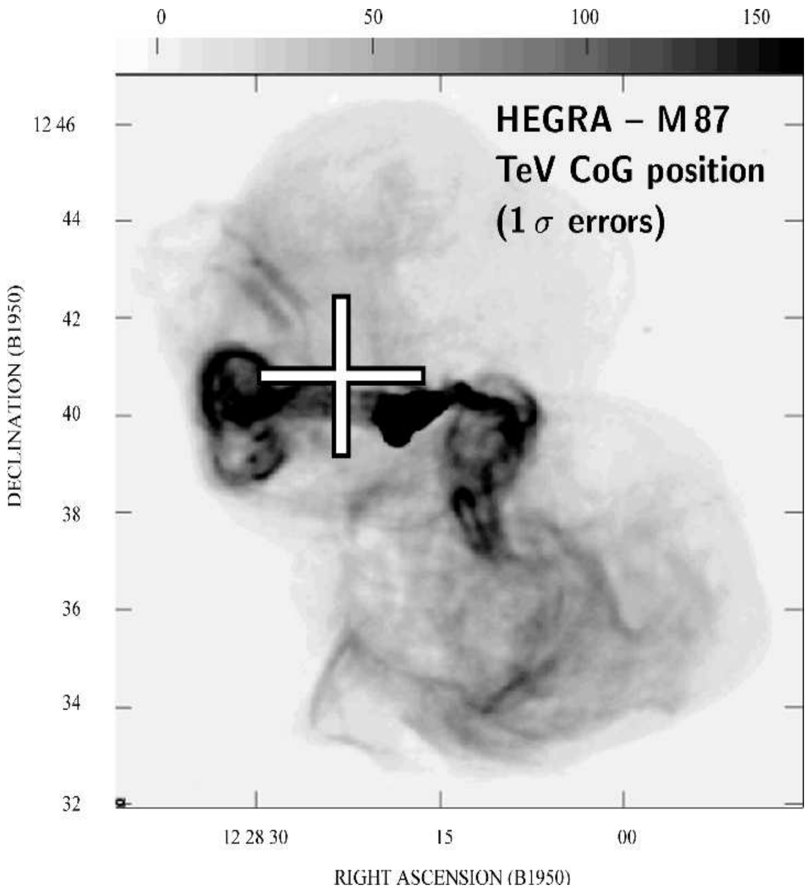

HEGRA detection of M 87 system (*Aharonian et al. 2003, A&A, 403*).

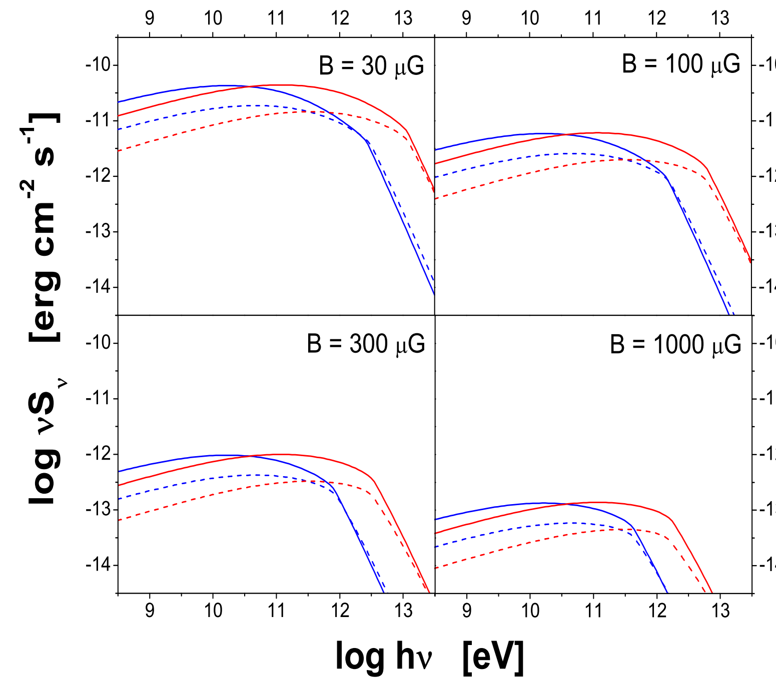

Stawarz et al. 2005, ApJ, 626: IC/STAR emission of knot A: for $\theta = 30^0$ and 20^0 (blue and red), $\Gamma = 5$ and 3 (solid and dashed).

Knot A in the M 87 Jet — Strong Magnetic Field

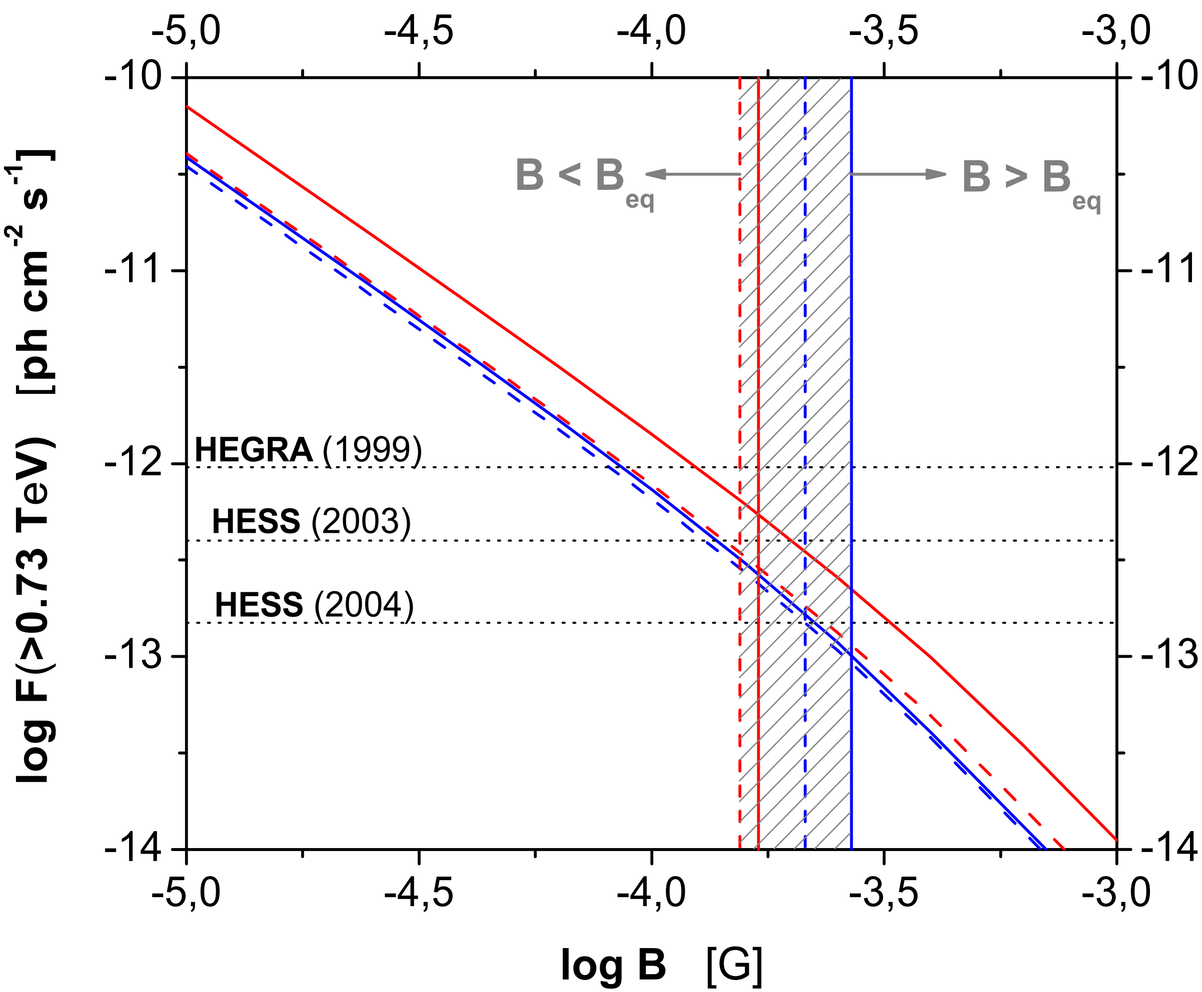

Variable VHE γ-Ray Emission of M 87

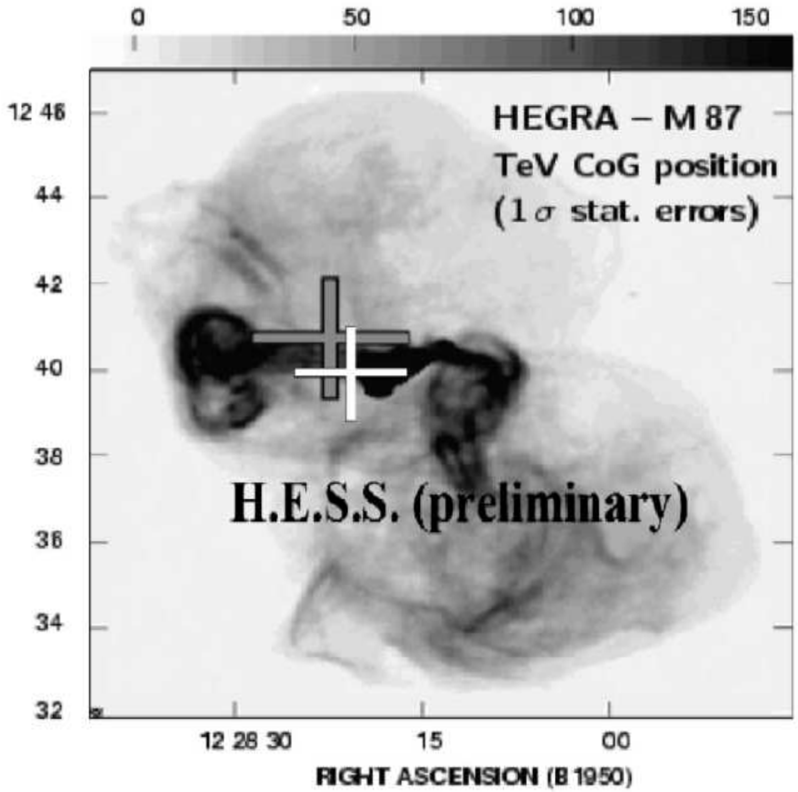

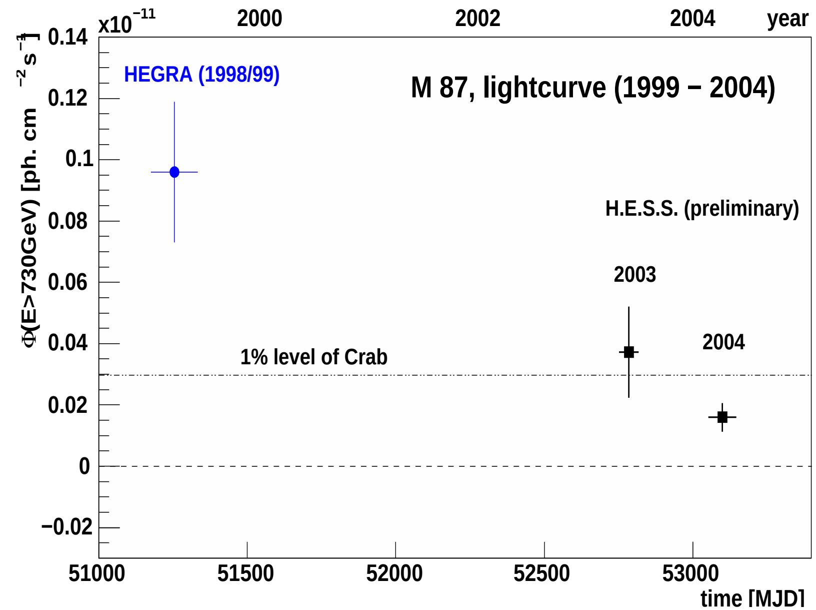

Detection of variable TeV emission of M 87 system by the *H.E.S.S.* Cherenkov Telescopes (*Beilicke et al. 2005, XXII Texas Symposium*).

Misaligned Proton Blazar?

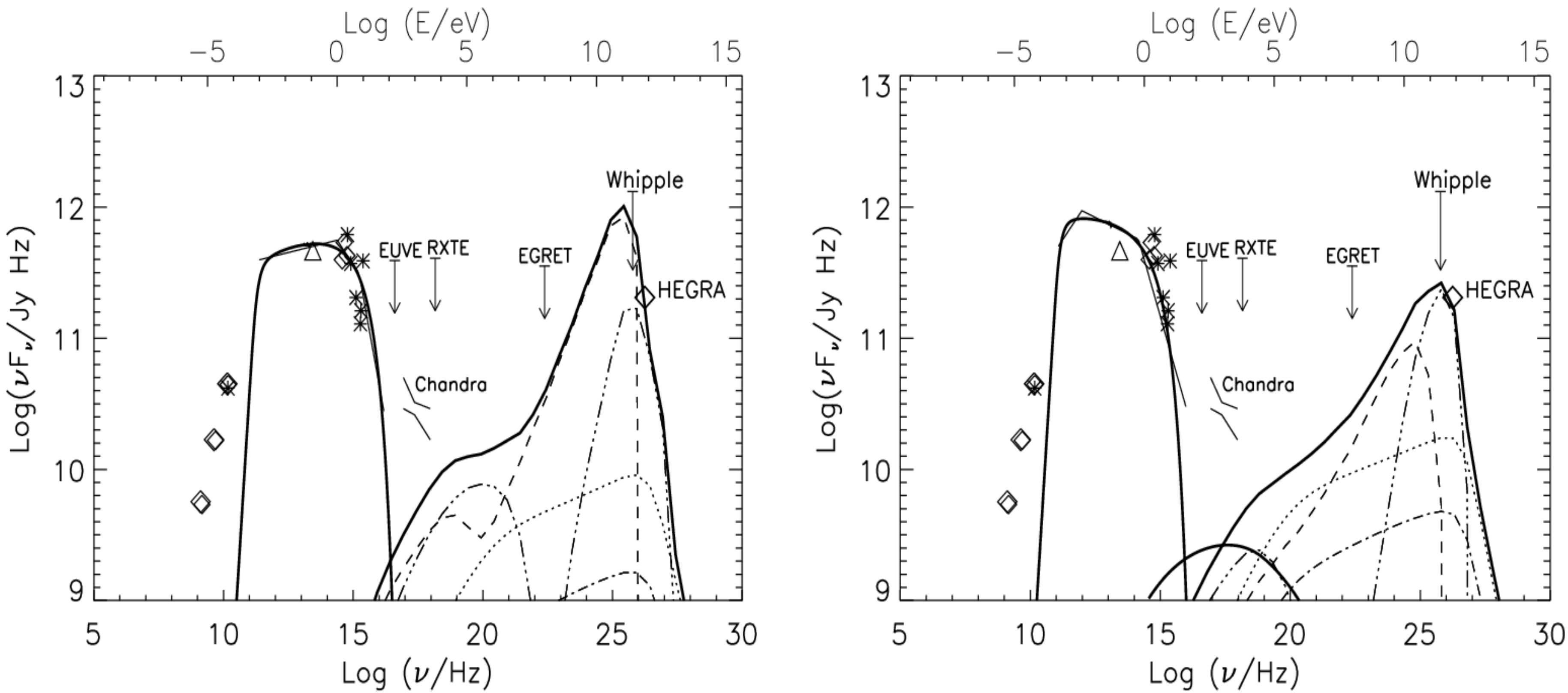

Hadronic processes in the inner portion of the jet (*Reimer et al. 2004, A&A, 419*).

Structured Inner Jet?

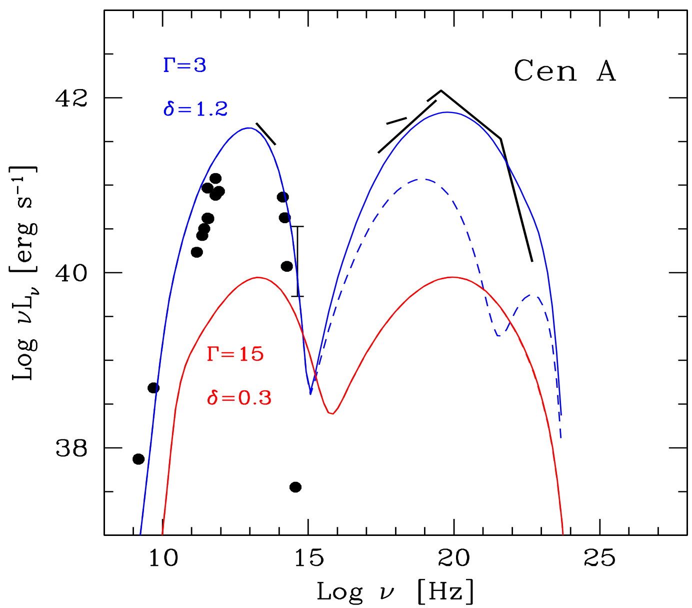

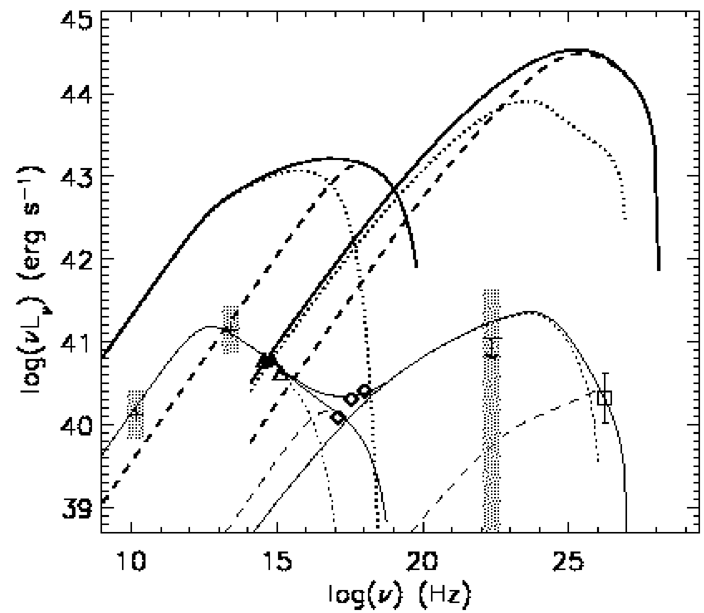

Relative enhancement of the radiation fields produced in the fast spine and the slower layer of the inner jet (*Ghisellini et al. 2005, A&A, 432*).

Crucial issue: jet velocity structure

Relative enhancement of the radiation fields produced in a different parts of the deccelerating flow (*Georganopoulos et al. 2005, ApJ, 634*).

Crucial issue: jet velocity structure

The Most Inner Portions of the M 87 Jet

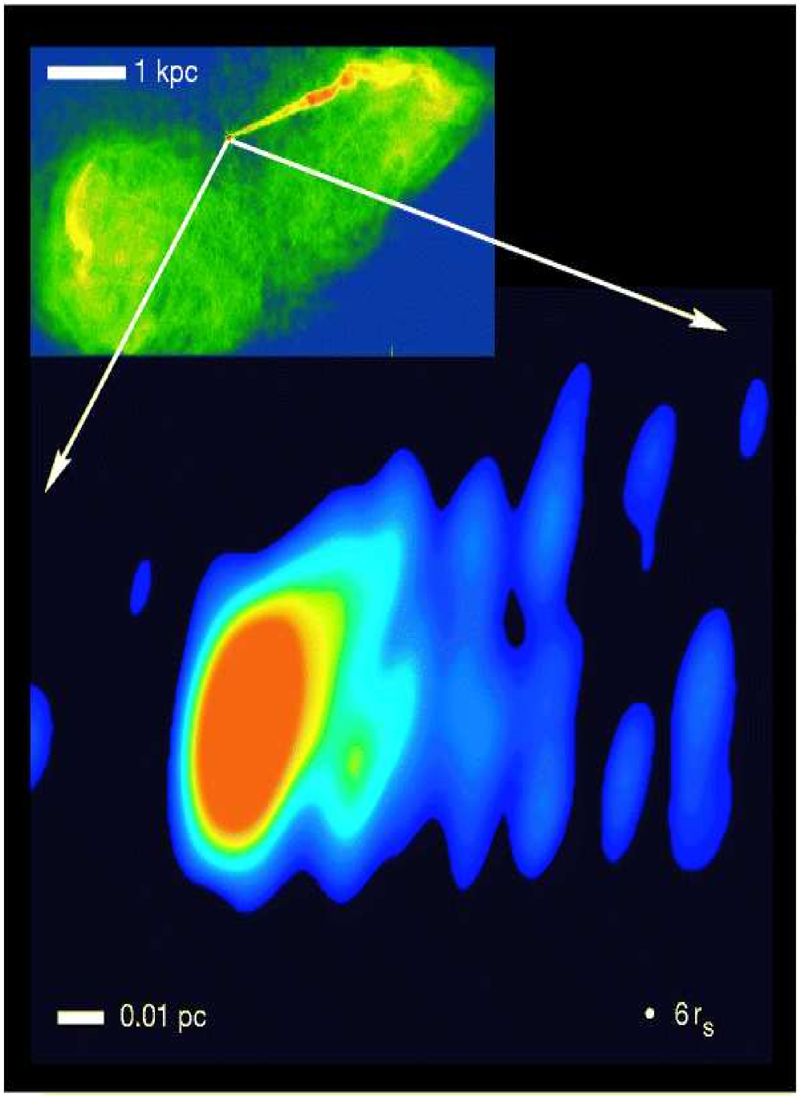

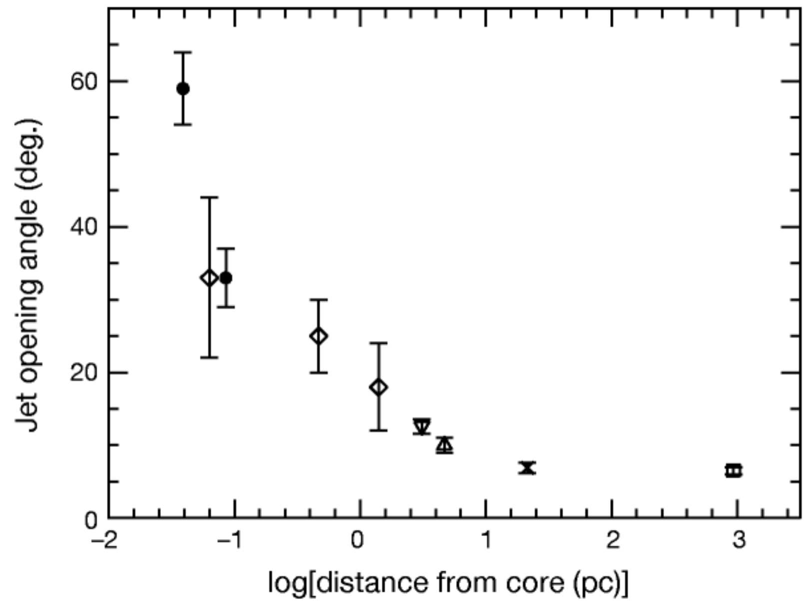

A very broad limb-brightened outflow on the scales < 0.5 mas; strong collimation at $\sim 100\ r_{\rm g} \approx 30$ mpc, continuing out to $\sim 3 \times 10^4\ r_{\rm g} \approx 10$ pc (*Junor et al. 1999, Nature, 401*).

conversion:

$$r_{\rm g} = 3.85\ \mu\text{arcsec} = 0.3\ \text{mpc}$$

Elusive HST-1 knot of the M 87 Jet

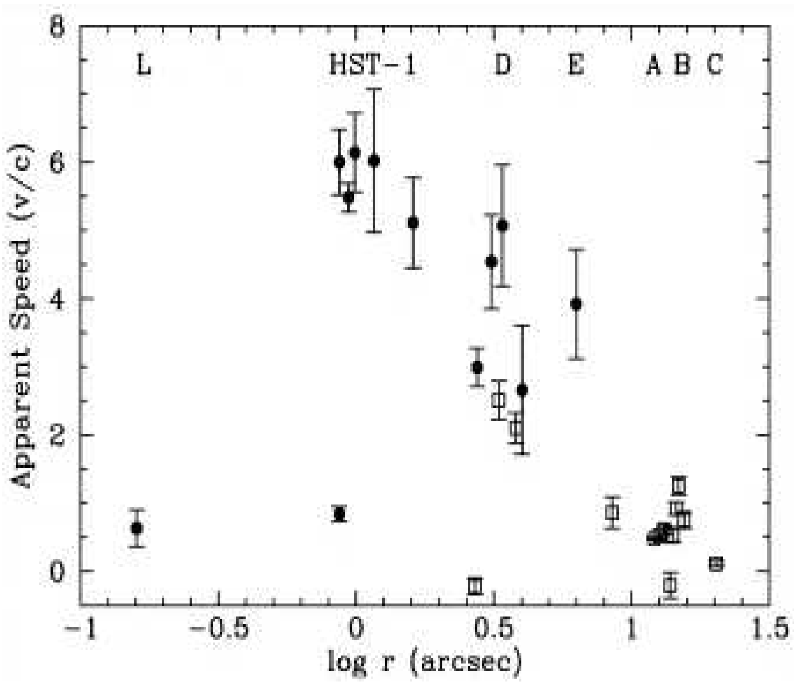

Apparent velocities in M 87 jet (*Biretta et al. 1999, ApJ, 520* and references therein).

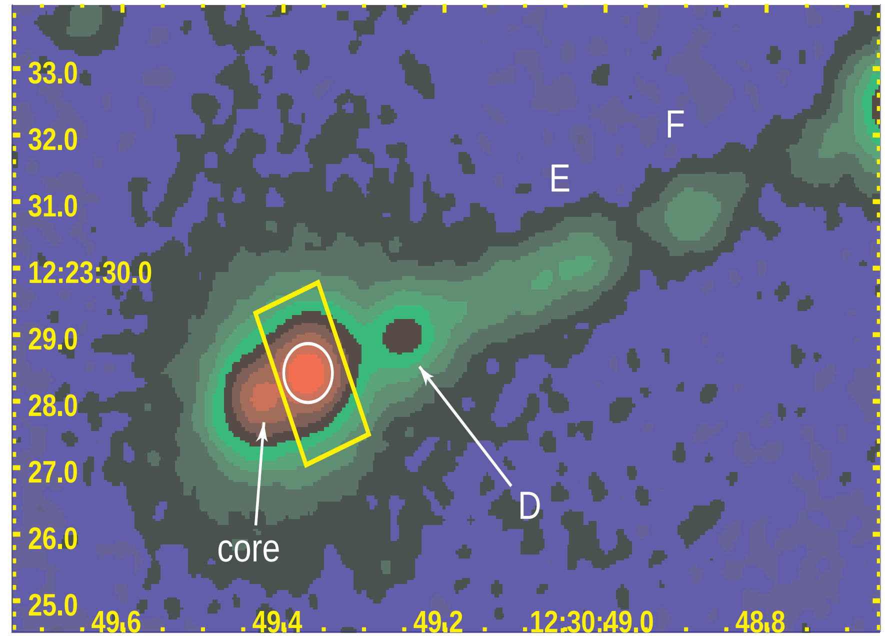

Unusual broad-band outburst of HST-1 knot in M 87 jet

(*Harris et al., 2003, ApJ, 586; Perlman et al. 2003, ApJ, 599; Harris et al. 2006, ApJ, 640*).

Above: X-ray picture A.D. 2005.

Broad-Band Variability of the HST-1 Flaring Point

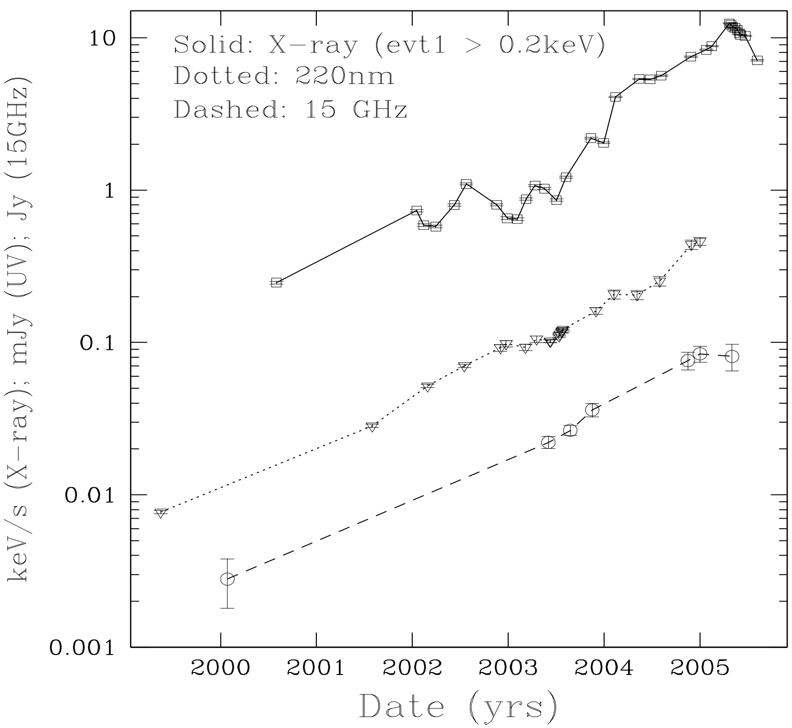

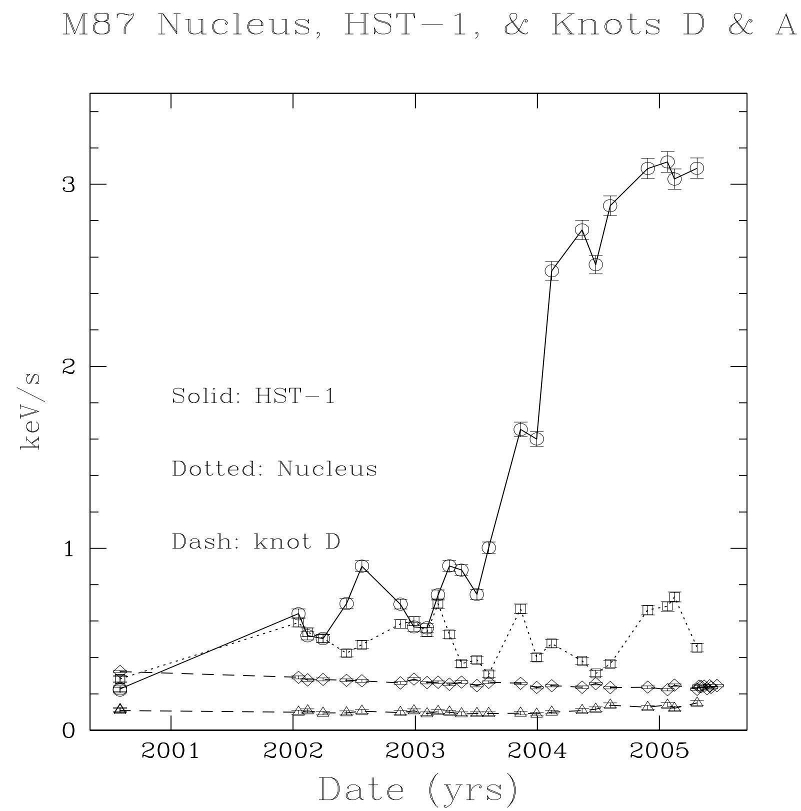

HST-1 lightcurve 2000-2005 (*Harris et al., 2003, ApJ, 586; Perlman et al. 2003, ApJ, 599; Harris et al. 2006, ApJ, 640*)...

... compared with the lightcurve of the core and outer jet (*Harris, priv. com.*).

Host Galaxy Profiles — X-rays

The observed thermal X-ray surface brightness:

(1) $$\mu_{\rm X}(r) \propto \left[1 + \left(\frac{r}{r_{\rm K}}\right)^2\right]^{-3\,\beta+0.5} \propto r^{-0.7} \quad \text{for} \quad r > r_{\rm K} \approx 18'' = 1.4\,\text{kpc}$$

with $\beta = 0.4$, $r_{\rm K} = 18'' = 1.4$ kpc, and $kT_{\rm G} \lesssim 1.5$ keV for $r < 60''$ (*Boehringer et al. 2001, A&A, 365; Young et al. 2002, ApJ, 579; Di Matteo et al. 2003, ApJ, 582*).

The implied density profile of the X-ray emitting hot gas:

(2) $$\rho_{\rm G}(r) \propto \left[1 + \left(\frac{r}{r_{\rm K}}\right)^2\right]^{-3\,\beta/2} \propto r^{-1.2} \quad \text{for} \quad r > r_{\rm K} \approx 18'' = 1.4\,\text{kpc}$$

(for example, $n_{\rm e} \sim 0.15$ cm^{-3} for $r \sim 30''$ and $n_{\rm e} \sim 0.03$ cm^{-3} for $r \sim 100''$, consistently with other ellipticals).

$$\underline{\rho_{\rm G}(r) \propto const \quad \text{for} \quad r < 18'' \quad ?}$$

Host Galaxy Profiles — Optical

The observed starlight surface brightness:

(3) $$\mu_{\rm O}(r) \propto r^{-b} \quad \text{with} \quad b = \begin{cases} 0.25 & \text{for} \quad r < r_{\rm B} \approx 3'' = 234\,\text{pc} \\ 1.3 & \text{for} \quad r > r_{\rm C} \approx 7'' = 546\,\text{pc} \end{cases} ,$$

(*Young et al. 1978, ApJ, 221; Lauer et al. 1992, AJ, 103*). The implied stellar density profile $\rho_{\rm O}(r) \propto r^{-(b+1)}$. A general property of the elliptical galaxies:

(4) $$\mu_{\rm O}(r) \propto \mu_{\rm X}(r) \quad \Rightarrow \quad \rho_{\rm S}(r) \propto \rho_{\rm G}^2(r)$$

Hence, one can reconstruct the pressure of the ambient thermal medium in M 87 host galaxy as:

(5) $$p_{\rm G}(r) = p_0 \times \begin{cases} (r/r_{\rm B})^{-0.6} & \text{for} \quad r < r_{\rm B} \approx 3'' = 234\,\text{pc} \\ 1 & \text{for} \quad r_{\rm B} < r < r_{\rm K} \\ (r/r_{\rm K})^{-1.2} & \text{for} \quad r > r_{\rm K} \approx 18'' = 1,4\,\text{kpc} \end{cases} ,$$

$p_0 = 1.5 \times 10^{-9}$ dyn cm^{-2}.

Pressure Balance

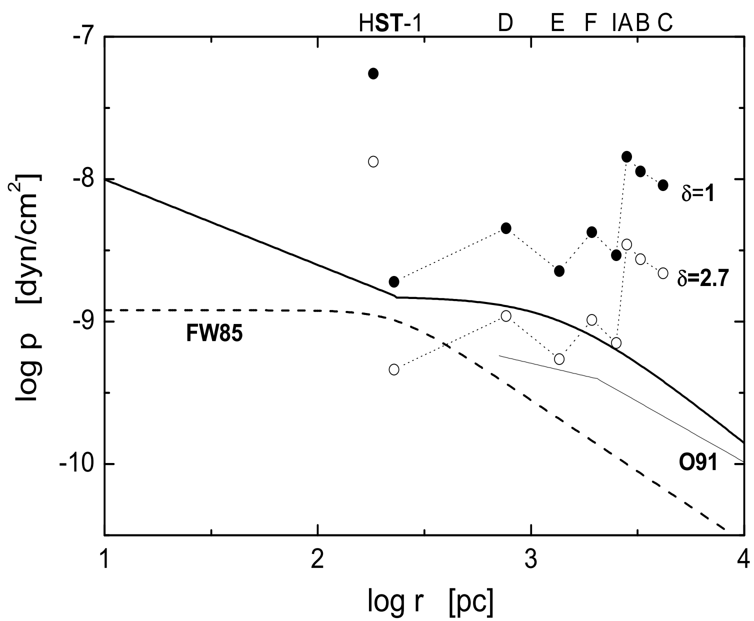

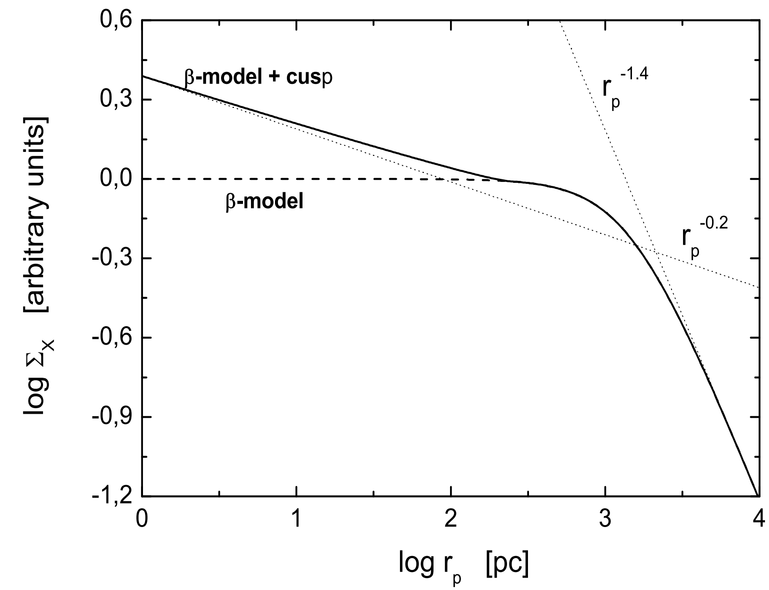

Different profiles of the hot gas pressure in M 87 host galaxy. Circles indicate $p_{\min}$ in jet knots, for $\delta = 1$ (filled ones), and $\delta = 2.7$ (open ones).

Normalized X-ray surface brightness (Σ_X) profiles of the M 87 host galaxy due to emission of the hot gas (*Stawarz et al. 2006, MNRAS, 370*).

Dynamics of M 87 Jet

ASSUMPTION1 : Gradual collimation of the broad innermost jet in M 87 is due to dynamically dominating magnetic field (see, e.g., *Gracia et al. 2005, A&A, 442*).

ASSUMPTION2 : Conversion to the particle flux occurs further out, e.g. at $\sim\ 10^3\ r_{\rm g}$ (see *Giannios & Spruit 2006, A&A, in press, astro-ph/0601172*). Thereby the jet starts to expand freely.

In a free particle dominated jet, gas pressure decreases very rapidly. For example, $p_{\rm j}(r) \propto r^{-2\,\hat{\gamma}} = r^{-8/3}$ for a cold plasma, and $p_{\rm j}(r) \propto r^{-2}$ in the case of ultrarelativistic gas. The ambient gas pressure in M 87 decreases as $p_{\rm G}(r) \propto r^{-\eta}$ with $\eta = 0.6$. Hence, as $\eta < 2\,\hat{\gamma}$ and $\eta < 2$, the initially free jet in M 87 certainly

- will become reconfined at some point r_0,
- will develop a reconfinement shock, and
- the reconfinement shock will reach the jet axis at some further point along the jet, $r_{\rm cr}$, where the jet itself will come to the pressure equilibrium with the external gas

(*Komissarov & Falle 1997, MNRAS, 288*).

Reconfinement Shocks

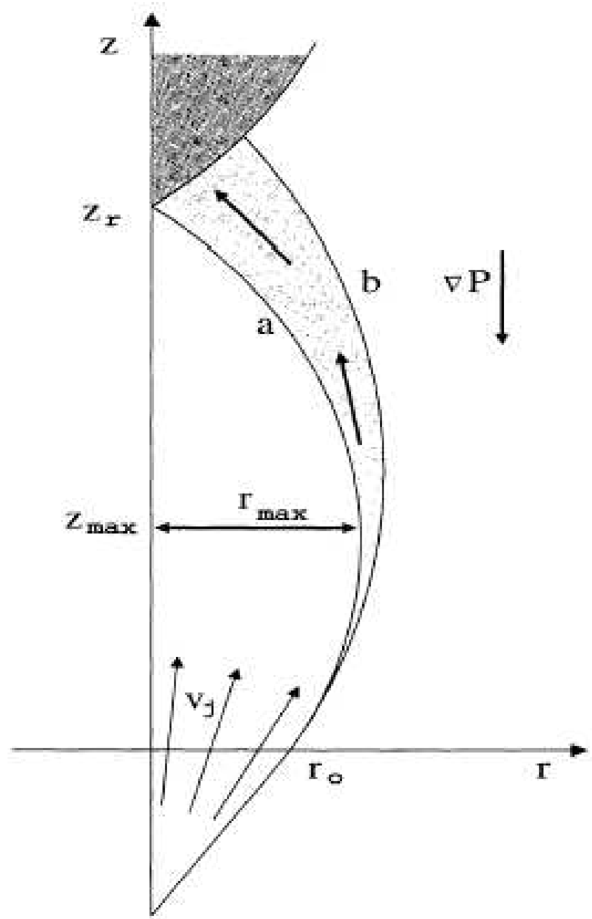

Figure 3. Reconfinement of hypersonic conical jet. (a) is the reconfinement shock, (b) is the jet boundary.

Reconfinement Shock in M 87 Jet

For a free relativistic jet dominated by the ultrarelativistic gas, jet kinetic power is

(6) $$L_{\rm j} = 4\, p_{\rm j}\, \Gamma_{\rm j}^2\, \beta_{\rm j}\, c\pi\, r^2\ \tan^2\Phi \quad ,$$

where the opening angle

(7) $$\tan\Phi = \frac{3\sqrt{2}}{\Gamma_{\rm j}\beta_{\rm j}} \quad .$$

With the pressure profile as given above for the M 87 host, one therefore obtains

(8) $$r_{\rm cr} \approx \left[\frac{0.1\, L_{\rm j}}{c\, p_0\, r_{\rm B}^{0.6}}\right]^{0.7}$$

and hence $r_{\rm cr}/r_0 \sim 10$.

We identify $r_0 \approx 0.05'' - 0.1'' \sim 4 - 8$ pc (*Reid et al. 1989, ApJ, 336*).
This gives $r_{\rm cr} \approx 0.5'' - 1.0''$ (projected).
The projected location of the HST-1 flaring point: $0.8''$.

HST-1 Knot as the Reconfinement Point

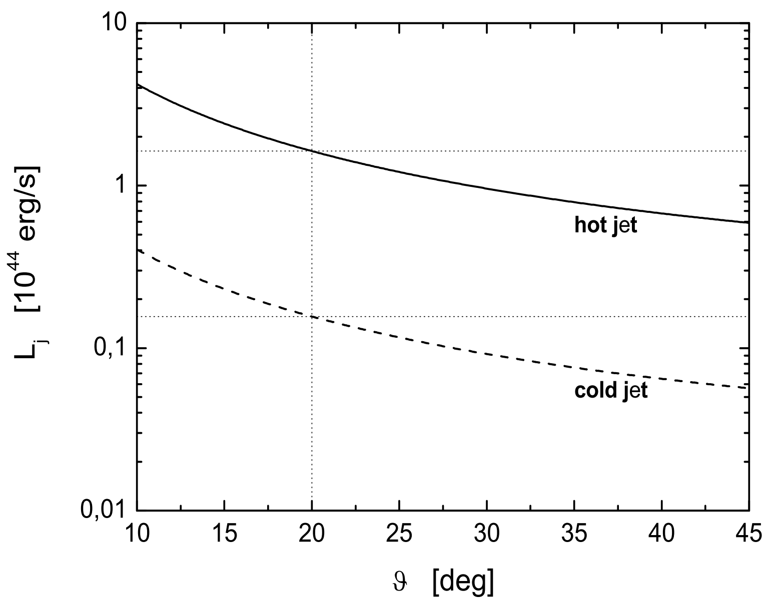

A total kinetic power of the M87 jet as a function of the jet viewing angle θ, implied by the proposed model (*Stawarz et al. 2006, MNRAS, 370*).

We propose that the extremely compact, stationary and overpressured HST-1 flaring point, present at the upstream edge of the HST-1 complex, is placed at $\sim r_{\rm cr}$, while the outer subcomponents of the HST-1 knot — superluminal features characterized by the minimum pressure in rough equilibrium with the surrounding medium — can be identified with the region occupied by a diverging reflected shock further away from $r_{\rm cr}$.

For the jet viewing angle $\theta = 20^0$, the jet luminosity implied by the model, $L_{\rm j} \approx 10^{44}$ erg s^{-1}, is consistent with the jet power required to feed radio lobes (*Bicknell & Begelman 1996, ApJ, 467; Owen et al. 2000, ApJ 543*).

HST-1 Knot as a TeV Source?

Although the reconfinement/reflected shock structure is stationary in the observer's rest frame, variations and changes in the central engine lead inevitably to flaring of this part of the outflow, in particular when the excess particles and photons emitted by the active nucleus in its high-activity epoch and traveling down the jet arrive after some time to the reconfinement nozzle. In a framework of this scenario, one should expect firstly high-energy γ-ray flare due to comptonization of the photons from the nuclear outburst, and then, after some delay

$$\Delta t \approx \frac{r}{c\,\beta_{\rm nuc}} - \frac{r}{c} \approx \frac{r_{\rm p}}{2c\,\Gamma_{\rm nuc}^2\,\sin\theta} \sim 100\,(\sin\theta)^{-1}\,\Gamma_{\rm nuc}^{-2} \quad {\rm yr} \tag{9}$$

(where $r_{\rm p} = r\,\sin\theta = 62.4$ pc is a projected distance of the HST-1 flaring region from the core), synchrotron flare due to excess nuclear particles shocked at the nozzle. This delayed synchrotron flare could be accompanied by the subsequent inverse-Compton brightening due to upscattering of the ambient radiation fields by the increased population of the ultrarelativistic particles.

For example, $\Delta t \sim 6$ yr between presumable maximum of the TeV emission (1998/1999) and the observed maximum of the synchrotron emission of the HST-1 knot (2005) is consistent with $\theta \sim 20^0$ and $\Gamma_{\rm nuc} \sim 7$.

The Expected TeV Fluxes

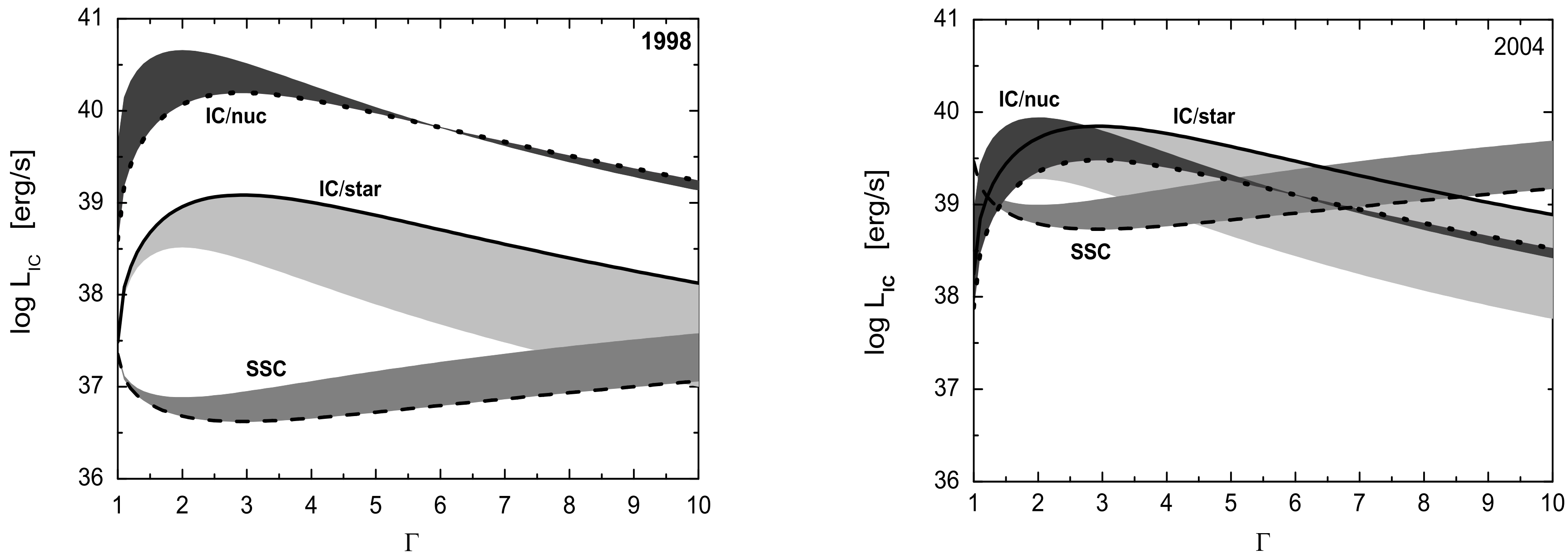

Expected TeV emission of the HST-1 flaring region in 1998 and 2004, for $\theta = 20^0$ and different bulk velocities of the emitting plasma. Shaded regions indicate the appropriate luminosity ranges for $\theta = 20^0 - 30^0$.

The expected fluxes (assuming energy equipartition between radiating electrons and the jet manetic field) are consistent with observations (*Stawarz et al. 2006, MNRAS, 370*).

Conclusions on M 87

- Outer portions of FR I jets (≥ 100 pc) can be sources of very high energy γ-ray emission.
- Such an emission can be detected by modern Cherenkov Telescopes (HESS, MAGIC, CANGAROO-III, VERITAS) in the cases of several nearby FR I radio galaxies.
- Even upper limits for such an emission can be meaningful.
- HEGRA and HESS observations of M 87 radio galaxy indicates that the magnetic field cannot be smaller than the equipartition value for the kpc-scale portion of the jet (brightest knot A placed ~ 1 kpc from the center).
- The detected variable TeV signal from M 87 may by due to HST-1 knot (~ 100 pc from the center), being an unusual echo of the nuclear outburst within the converging and stationary reconfinement shock.

Large-Scale Radio Structure of Cen A

© American Astronomical Society • Provided by the NASA Astrophysics Data System

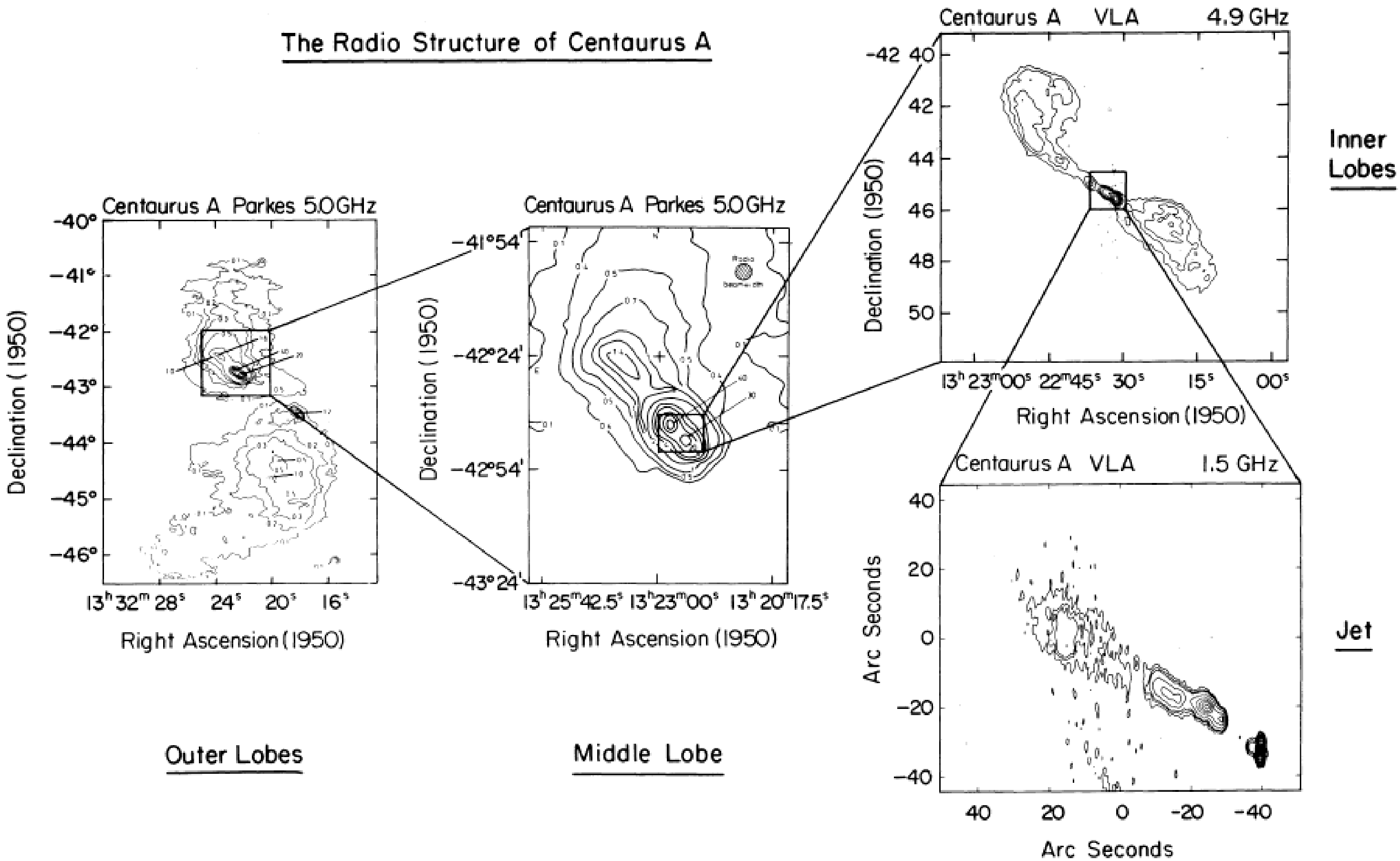

FIG. 11.—An illustration of the different scale sizes of radio structure in Cen A. The Parkes maps of the outer lobes and middle lobe were kindly provided by R. Ekers from a paper by Haynes, Cannon, and Ekers (1982). The inner lobes map is reproduced from Fig. 2, and the jet map is reproduced from Fig. 3.

Merger History of Cen A

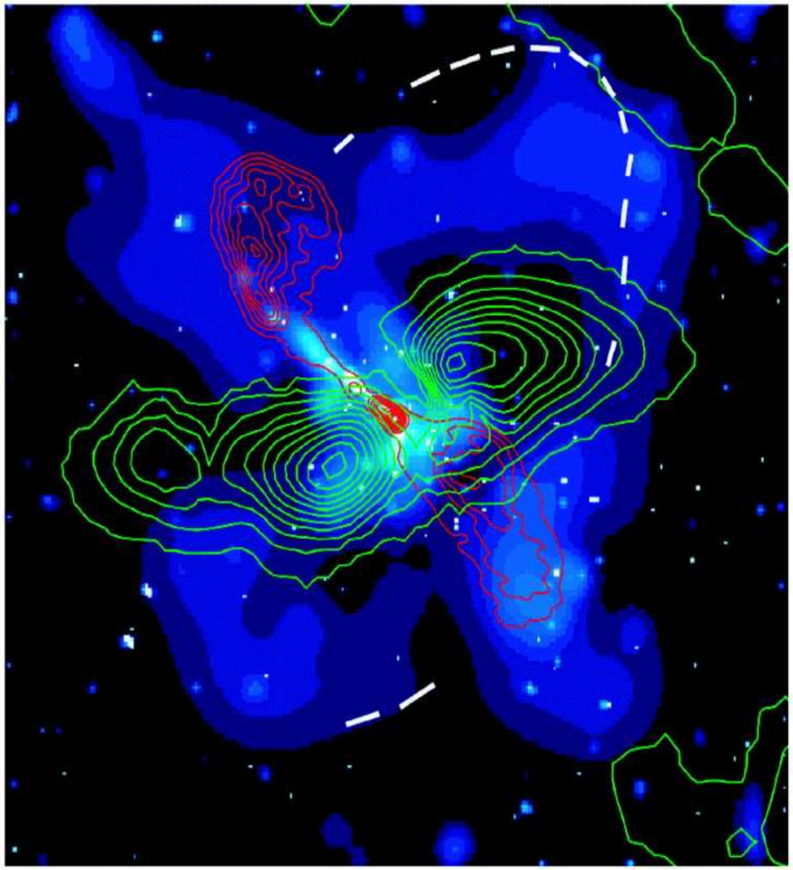

X-rays (blue), 21 cm radio continuum (red contours), 21 cm line H I (green contours) (*Karovska et al. 2002, ApJ, 577*).

$d = 3.4$ Mpc, for which 1$''$ corresponds to 16 pc, and 1$'$ to 0.96 kpc.

Famous 'dark lane' pronounced within the host elliptical body, being in fact an edge-on disk of rotating metal-rich stars, nebulae, dust clouds, H II regions, OB associations, and supernova remnants, is most probably remnant of the merger with spiral galaxy, which happened some $10^8 - 10^9$ *years ago (see Israel 1998, ARA&A, 8).*

Radio and X-ray synchrotron jet in Cen A: a very complex jet morphology with filaments and diffuse sub-structured knots; limb-brightened radio and X-ray profiles; projected magnetic field parallel to the jet axis (see Schreier et al. 1979, 1981; Burns et al. 1983, Clarke et al. 1986, 1992; Kraft et al. 2002; Hardcastle et al. 2003).

Starlight Photon Field I

Starlight surface brightness in elliptical galaxies are typicaly well fitted by a Nuker law

(10) $$I(r) = I_{\rm b}\, 2^{(b-d)/a} \left(\frac{r}{r_{\rm b}}\right)^{-d} \left[1 + \left(\frac{r}{r_{\rm b}}\right)^{a}\right]^{-(b-d)/a} ,$$

where r is the distance from the galactic nucleus. This gives $I(r) \propto r^{-d}$ for $r < r_{\rm b}$, and $I(r) \propto r^{-b}$ at larger distances. For Cen A host galaxy, Capetti & Balmaverde (2005) gives $a = 1.68$, $b = 1.3$, $d = 0.1$, and the break radius $r_{\rm b} = 2.56'' = 41$ pc. This allows to approximate the starlight emissivity, $j(r) \propto r^{-1}\, I(r)$, as

(11) $$\epsilon j_{\epsilon}(\xi) = j_{\rm V}\, g(\epsilon)\, h(\xi) \, ,$$

where $\xi \equiv r/r_{\rm b}$. Here $\epsilon \equiv \varepsilon/m_{\rm e}c^2$ is the starlight photon energy ε in $m_{\rm e}c^2$ units, $j_{\rm V}$ is the total V-band galactic emissivity, $g(\epsilon)$ describes the V-band normalized spectral distribution of the stellar photon field, and the radial depedance function

(12) $$h(\xi) = \left(\frac{r}{r_{\rm b}}\right)^{-1} \frac{I(r)}{I_{\rm b}} = 1.64\; \xi^{-1.1} \, \left(1 + \xi^{1.68}\right)^{-0.7143}$$

We take $\xi_{\rm t} \equiv r_{\rm t}/r_{\rm b} = 375$ (*Stawarz et al. 2006, MNRAS, in press, astro-ph/0605721*).

Starlight Photon Field II

For the spectral distribution of the NGC 5128 starlight, we assume the template spectrum of powerful elliptical galaxy as provided by Silva et al. (1998), restricted to the photon energy range between $\epsilon_{\min} = 10^{-7}$ and $\epsilon_{\max} = 10^{-5}$. This restriction implies that we consider only the direct stellar emission of the evolved red giants (constituting the main body of the elliptical host) and their winds, but not the far infrared emission resulting from the reprocession of the starlight photons by the cold galactic dust. The apparent V-band magnitude of NGC 5128 is $m_{\rm V} = 6.98$. This gives the monochromatic V-band galactic luminosity

(13) $$\log\left(\frac{L_{\rm V}}{\rm erg/s}\right) = 50.078 + 2\,\log\left(\frac{d_{\rm L}}{\rm Mpc}\right) - 0.4\,(m_{\rm V} - A_{\rm V}) - c_{\rm V} = 43.82 \quad ,$$

where the Cen A distance is $d_{\rm L} = 3.4$ Mpc, the extinction is $A_{\rm V} = 0.381$, and $c_{\rm V} = 4.68$. Since, by the definition,

(14) $$L_{\rm V} = 4\pi \int_{\mathcal{V}} [\epsilon j_\epsilon(\xi)]_{\rm V}\; d\mathcal{V} \quad ,$$

one obtains $j_{\rm V} = 1.42 \times 10^{-21}$ cgs. The differential photon number density, $n(\epsilon, \Omega)$, is

(15) $$n(\epsilon, \Omega) = \frac{\epsilon^{-2}}{m_{\rm e} c^3} \int [\epsilon j_\epsilon(\xi)]\; dl \quad .$$

Photon-Photon Annihilation I

Optical depth for photon-photon annihilation, computed for the case of monodirectional beam of γ-ray photons with dimensionless energy ϵ_γ, propagating through the stellar photon field of the host galaxy from the active center up to the terminal distance $r_{\rm t}$, is

$$\tau(\epsilon_\gamma) = \int_0^{r_{\rm t}} dr \int dn\,(1-\varpi)\,\sigma_{\gamma\gamma} \quad , \tag{16}$$

where ϖ is the cos function of the angle between the γ-ray photon and the incident starlight photon, $dn = n(\epsilon,\Omega)\,d\epsilon\,d\Omega$ is the differential starlight photon number density, and

$$\sigma_{\gamma\gamma}(\epsilon_\gamma,\epsilon,\varpi) = \frac{3\sigma_{\rm T}}{16}\,(1-\beta^2)\,\left[(3-\beta^4)\,\ln\left(\frac{1+\beta}{1-\beta}\right) - 2\beta\,(2-\beta^2)\right] \tag{17}$$

is the photon-photon annihilation cross section, where

$$\beta \equiv \left(1 - \frac{2}{\epsilon_\gamma\epsilon\,(1-\varpi)}\right)^{1/2} \quad , \tag{18}$$

is the velocity of the created electron/positron.

Photon-Photon Annihilation II

By choosing $d\Omega = d\phi\, d\varpi$, the differential starlight photon number density reads as

(19) $$n(\epsilon, \Omega) = \frac{\epsilon^{-2}\, r_{\rm b}}{m_{\rm e} c^3} \int_0^{\eta_{\rm max}} [\epsilon j_\epsilon(\zeta)]\; d\eta \quad ,$$

where $\eta \equiv l/r_{\rm b}$, $\zeta = \sqrt{\xi^2 + \eta^2 - 2\xi\eta\varpi}$, and the integration upper limit is $\eta_{\rm max} = \xi\varpi + \sqrt{\xi^2\varpi^2 - \xi^2 + \xi_{\rm t}^2}$. This gives finaly

$$\tau(\epsilon_\gamma) = \frac{2\pi\, j_{\rm V}\, r_{\rm b}^2}{m_{\rm e}\, c^3} \int_{-1}^{+1} d\varpi\,(1-\varpi) \int_{\epsilon_{\rm low}}^{\epsilon_{\rm max}} d\epsilon\, \sigma_{\gamma\gamma}(\epsilon_\gamma, \epsilon, \varpi)\, \frac{g(\epsilon)}{\epsilon^2} \int_0^{\xi_{\rm t}} d\xi \int_0^{\eta_{\rm max}} d\eta\, h(\zeta)\,,$$
(20)

where $\epsilon_{\rm low} = \max(\epsilon_{\rm min}, \epsilon_{\rm tres})$, and the treshold energy is $\epsilon_{\rm tres} = 2/\epsilon_\gamma\,(1-\varpi)$. The bolometric energy density profile for the starlight emission is

(21) $$U_{\rm rad}(\xi) = f_{\rm bol}\, [\nu U_\nu]_{\rm V} = f_{\rm bol}\, \frac{2\pi\, r_{\rm b}\, j_{\rm V}}{c} \int_{-1}^{+1} d\varpi \int_0^{\eta_{\rm max}} d\eta\; h(\zeta) \quad ,$$

where $f_{\rm bol} = 2.5$ is the V-band bolometric correction for the adopted here stellar spectrum.

Optical Depth

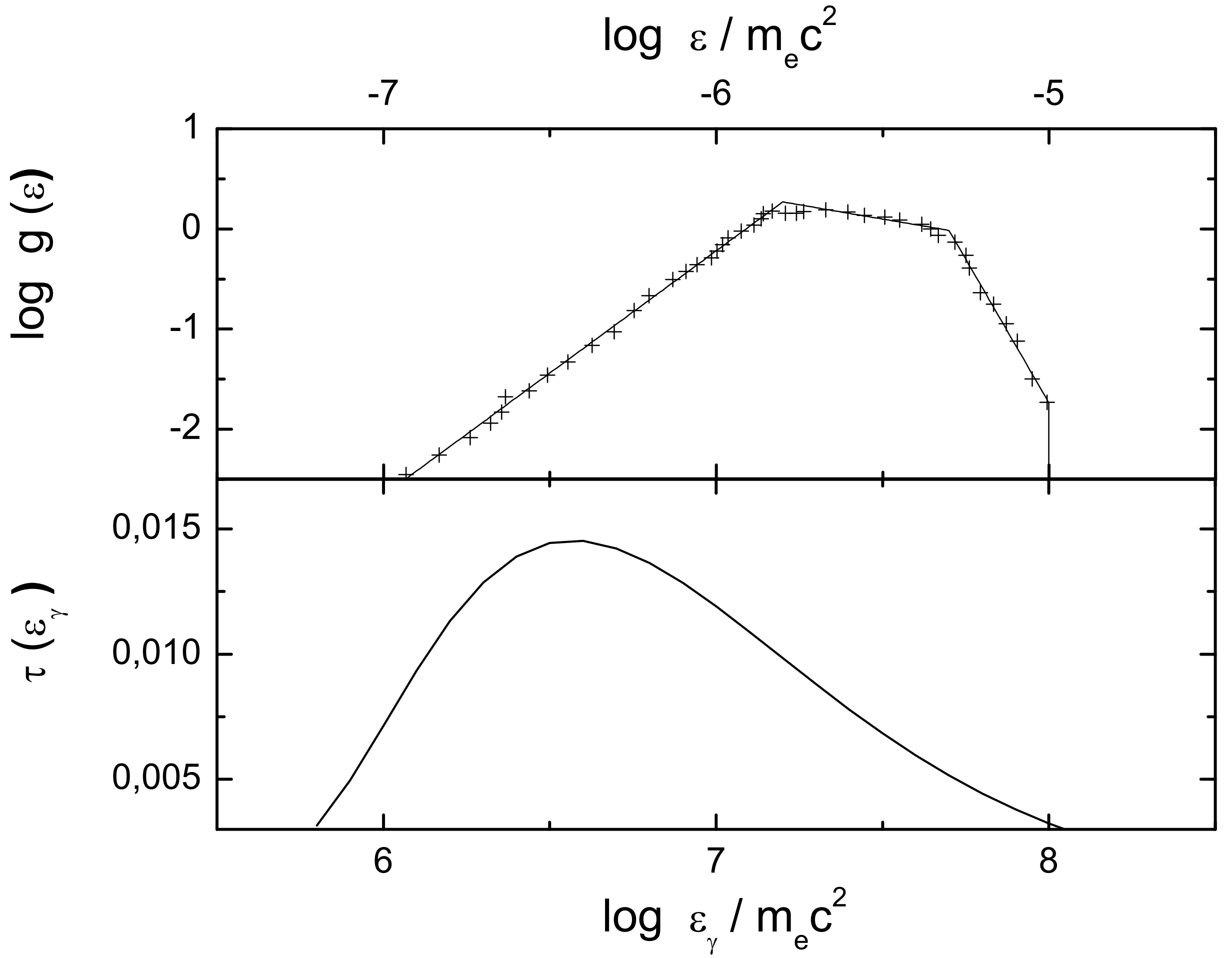

Profiles

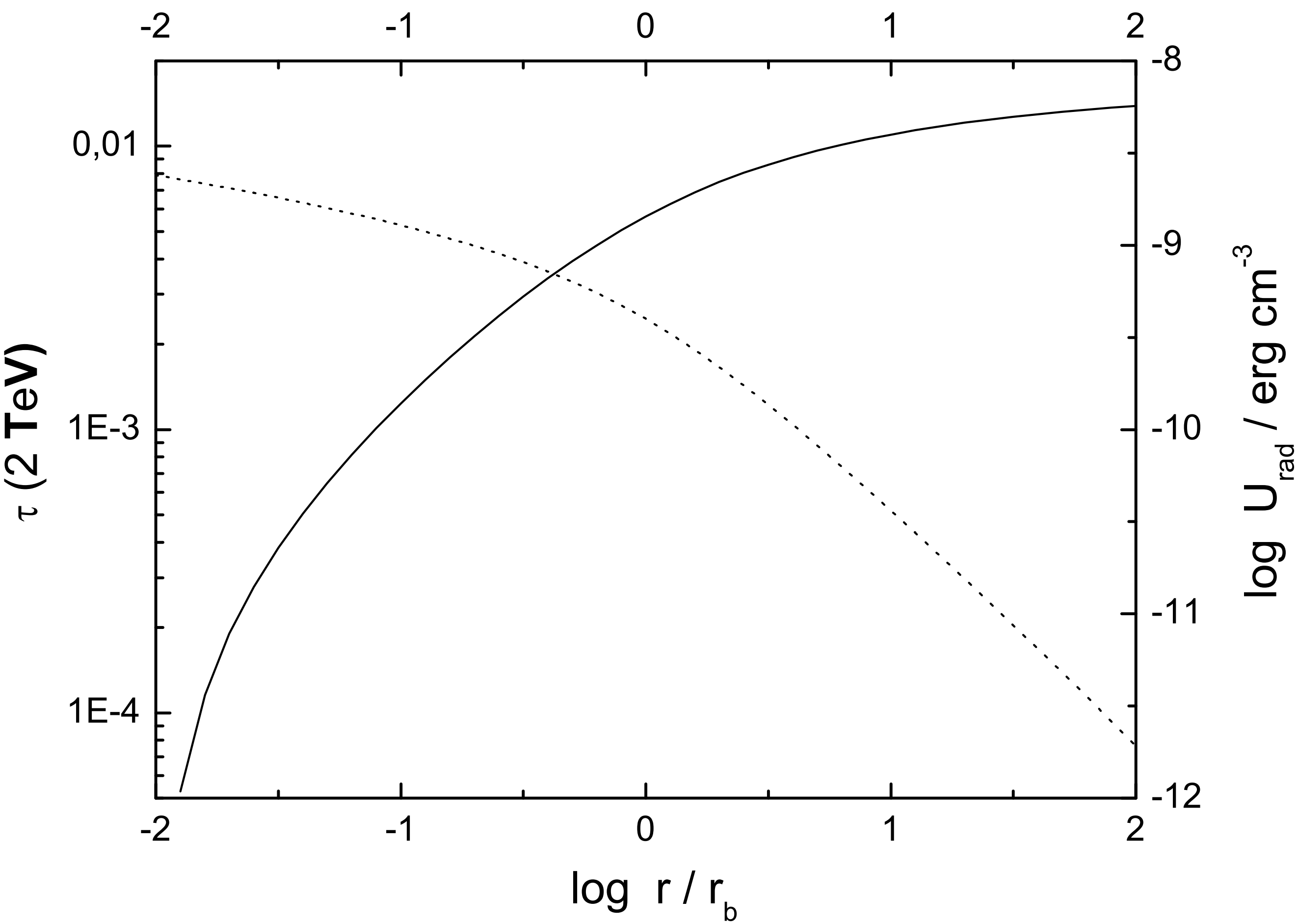

-2
-1
0
1
2
-8
0,01
-9
1E-3
-10
-11
1E-4
-12
-2
-1
0
1
2
τ (2 TeV)
log U_rad / erg cm^-3
log r / r_b

Energetics I

We are interested in the total, time-averaged and angle-averaged (i.e., 'calorimetric') flux of TeV photons produced by the active nucleus and 'injected' into the host galaxy. Assuming quite standard apectral index $\alpha_\gamma = 1$, the relation between the integrated photon flux and the monochromatic flux energy density at any photon energy $\varepsilon \geq \varepsilon_0$ is simply $[\varepsilon S_\varepsilon] = [\varepsilon_0 \, F(> \varepsilon_0)]$. This flux is related to the emitting fluid (jet) intrinsic monochromatic power (assumed to be isotropic in the jet comoving frame) radiated in a given direction, $\partial L' / \partial \Omega' = L' / 4\pi$, by the expression

(22) $$[\nu S_\nu] = \frac{1}{d_{\rm L}^2} \, \frac{\delta_{\rm nuc}^3}{\Gamma_{\rm nuc}} \, \frac{\partial L'}{\partial \Omega'} = \frac{1}{d_{\rm L}^2} \, \frac{\delta_{\rm nuc}^3}{\Gamma_{\rm nuc}} \, \frac{L'}{4\pi} \quad ,$$

where $\Gamma_{\rm nuc}$ and $\delta_{\rm nuc} = \Gamma_{\rm nuc}^{-1} \left(1 - \sqrt{1 - \Gamma_{\rm nuc}^{-2}} \cos\theta\right)^{-1}$ are, respectively, Lorentz and Doppler factors of the nuclear portion of the jet, and θ is the jet viewing angle. On the other hand, the total power radiated into the ambient medium, being of interest here, is

(23) $$L_{\rm inj} = \oint \frac{\delta_{\rm nuc}^3}{\Gamma_{\rm nuc}} \, \frac{\partial L'}{\partial \Omega'} \, d\Omega = \frac{1}{2} \, L' \, \Gamma_{\rm nuc}^{-1} \int_0^\pi \delta_{\rm nuc}^{-3} \, \sin\theta \, d\theta = L' \quad .$$

Hence, $L_{\rm inj} = 4\pi \, d_{\rm L}^2 \, \Gamma_{\rm nuc} \delta_{\rm nuc}^{-3} \, [\varepsilon_0 \, F(> \varepsilon_0)]$.

Energetics II

With the HESS photon flux $F(> 0.19\,\mathrm{TeV}) < 5.68 \times 10^{-12}$ ph cm^{-2} s^{-1} (corresponding to the few-arcmin-integration area centered on the Cen A nucleus) one obtains the upper limit for the total injected monochromatic power $L_{\rm inj} < 2.4 \times 10^{39}\,\Gamma_{\rm nuc}\delta_{\rm nuc}^{-3}$ erg s^{-1}. With the prefered values $\theta \sim 50\,\mathrm{deg} - 80\,\mathrm{deg}$ inferred from the VLBI radio observations, and $\Gamma_{\rm nuc} \sim 10$ widely considered as a typical value for the bulk Lorentz factor of sub-parsec scale AGN jets, this reads as

$$L_{\rm inj} < 10^{42} - 10^{43} \quad \mathrm{erg\,s^{-1}} \quad . \tag{24}$$

The postulated here nuclear γ-ray emission is expected to be Doppler-boosted within the narrow cone characterized by the opening angle $\Gamma_{\rm nuc}^{-1} \lesssim 6\,\mathrm{deg}$. Therefore, when viewed from $\theta \geq 50\,\mathrm{deg}$, it is strongly Doppler hidden. If the observer would be located however within the beaming cone of this emission, then he would detect the flux corresponding to the isotropic luminosity

$$L(0) = (\delta^3_{{\rm nuc},\,\theta=0}/\Gamma_{\rm nuc})\,L' \approx \Gamma^2_{\rm nuc}\,L' < 10^{44} - 10^{45} \quad \mathrm{erg\,s^{-1}} \quad . \tag{25}$$

Such values are not in conflict with luminosities observed from the TeV-detected BL Lac objects.

Pair Production Rate

The pair production rate for small values of the optical depth can be estimated as

(26) $$Q(\gamma, r) \propto \left\{ n_\gamma(\epsilon_\gamma) \times \frac{d\tau(\epsilon_\gamma)}{dr} \right\} \Bigg|_{\epsilon_\gamma = 2\,\gamma} \quad ,$$

where γ is the Lorentz factor of the created particles, and $n_\gamma(\epsilon_\gamma)$ is the photon spectrum of the primary γ-ray photons. For the later we assume power-law form $n_\gamma(\epsilon_\gamma) \propto \epsilon_\gamma^{-\Gamma_\gamma}$, where $\Gamma_\gamma = \alpha_\gamma + 1$ is the photon index. When averaged over the galactic radius,

(27) $$Q(\gamma) \propto \gamma^{-\Gamma_\gamma}\, \tau\,(2\,\gamma) \quad .$$

It can be approxmated by a broken power-law: $Q(\gamma) \propto const$ for $\gamma_0 \equiv 10^5 \leq \gamma \leq \gamma_{\rm br} \equiv 10^6$, and $Q(\gamma) \propto \gamma^{-2.5}$ for $\gamma > \gamma_{\rm br}$. When normalized to the monochromatic 1 TeV power $L_{\rm inj}$, it reads as

(28) $$Q(\gamma) = \frac{\tau\, L_{\rm inj}\, \mathcal{I}(\gamma)}{\gamma_{\rm br}^2\, m_{\rm e} c^2\, \mathcal{V}_{\rm gal}} \quad \text{where} \quad \mathcal{I}(\gamma) = \begin{cases} 1 & \text{for} \quad \gamma_0 \leq \gamma \leq \gamma_{\rm br} \\ (\gamma_{\rm br}/\gamma)^{2.5} & \text{for} \quad \gamma > \gamma_{\rm br} \end{cases} \quad .$$

Here $\tau \equiv \tau(\epsilon_\gamma = 1\,\mathrm{TeV}) \approx 0.01$, and $\mathcal{V}_{\rm gal}$ is the injection volume.

Injected Electrons

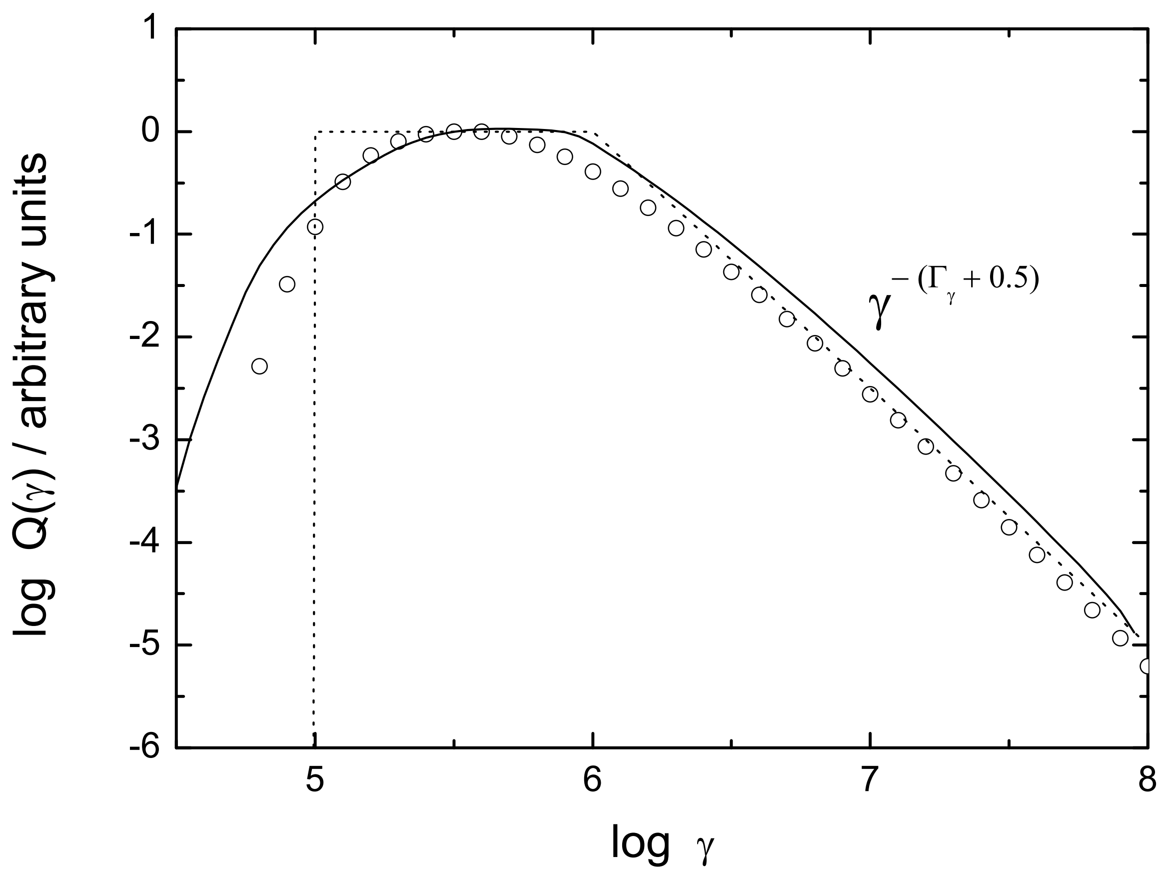

Pairs in the Elliptical Host

We take the characteristic values for the NGC 5128 elliptical host's magnetic field $B_{\rm gal} \approx 3 - 10\ \mu$G, assuming that it consists solely of the (Alfvénic) turbulent component with the maximum wavelength $\lambda_{\max} \sim 100$ pc and Kolmogorov energy spectrum $W(k) \propto k^{-q}$, where $q = 5/3$ (Moss & Shukurov 1996). With these interstellar medium parameters, the mean free path of the created electron-positron pairs for resonant interactions with the turbulent Alfvèn modes, is

$$\lambda_{\rm e} \approx r_{\rm g} \left(\frac{\lambda_{\max}}{r_{\rm g}} \right)^{q-1} = r_{\rm g}^{1/3}\, \lambda_{\max}^{2/3} \sim 0.82 \times \gamma_6^{1/3}\, B_{-5}^{-1/3}\, {\rm pc} \quad , \tag{29}$$

where $\gamma_6 \equiv \gamma/10^6$, $r_{\rm g} \equiv \gamma\, m_{\rm e} c^2 / e B_{\rm gal} \sim 5.5 \times 10^{-5}\ \gamma_6\, B_{-5}^{-1}$ pc is the electrons' gyroradius, and $B_{-5} \equiv B_{\rm gal}/10\ \mu$G. This leads to $t_{\rm iso} \sim 3\, \lambda_{\rm e}/c \sim 8\, \gamma_6^{1/3}\, B_{-5}^{-1/3}$ yrs, $t_{\rm esc} \sim 3\, R^2/\lambda_{\rm e}\, c \sim 2 \times 10^8\, \gamma_6^{-1/3}\, B_{-5}^{1/3}$ yrs, $t_{\rm acc} \sim \beta_{\rm A}^{-2}\, t_{\rm iso} \sim 4.5 \times 10^6\, \gamma_6^{1/3}\, B_{-5}^{-7/3}$ yrs (for the Alfvén velocity $v_{\rm A} \equiv \beta_{\rm A}\, c \approx B_{\rm gal}\, (4\pi\, m_{\rm p}\, n_{\rm gas})^{-1/2} \sim 10^{-3}\, B_{-5}\, c$ with $n_{\rm gas} \sim 3 \times 10^{-3}$ cm^{-3}). Thus, one can conclude that the TeV energy electrons injected to the interstellar medium (via annihilation of the γ-ray emission of the active center) are effectively confined to the elliptical body and quickly isotropized thereby by the galactic magnetic field, and therefore radiate there all their energy by inverse-Compton upscattering of the starlight photons and the synchrotron process, before being re-accelerated by the turbulent processes.

Time Scales

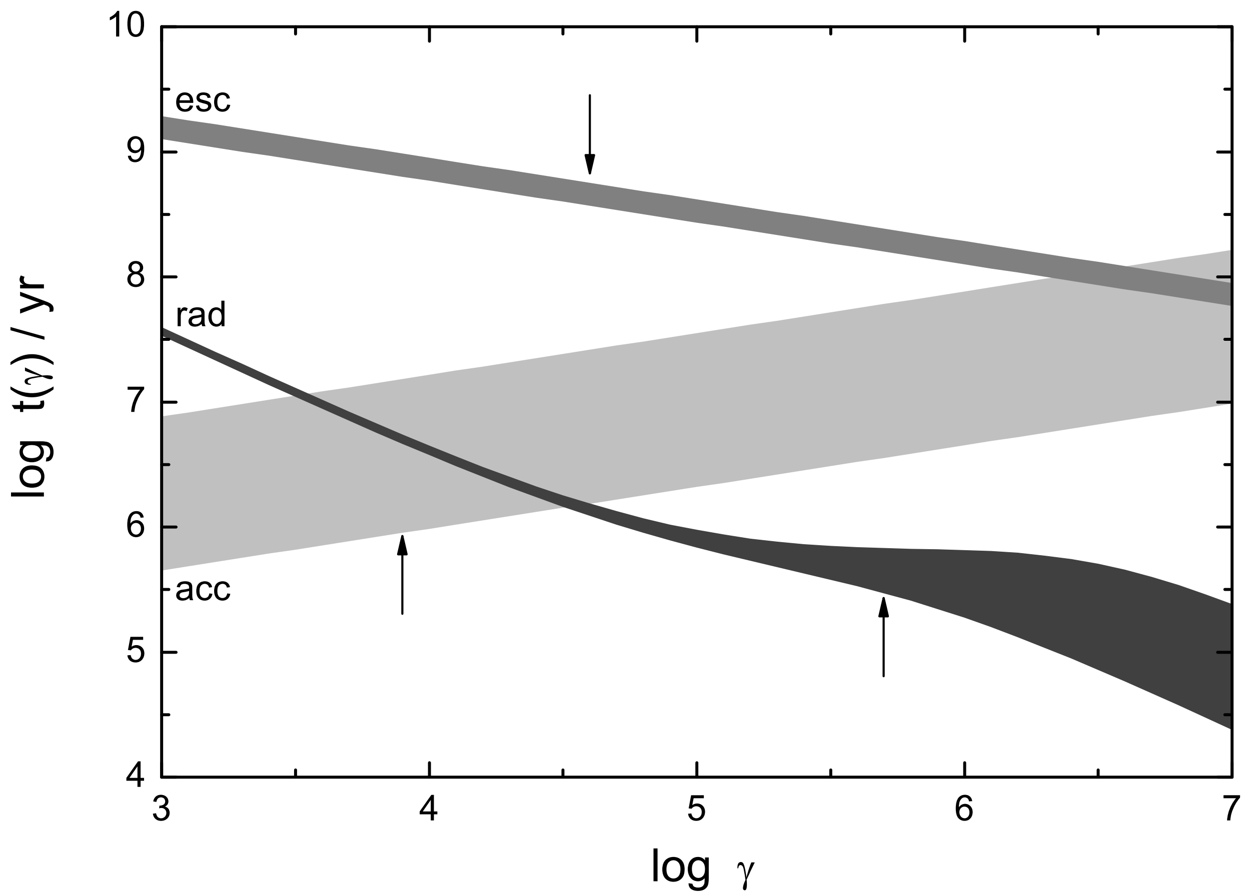

Electrons' Evolution

The resulting electron energy distribution, $n_{\rm e}(\gamma)$, ignoring re-acceleration and escape effects, can be found from the continuity equation

(30) $$\frac{\partial n_{\rm e}(\gamma)}{\partial t} = \frac{\partial}{\partial \gamma} \left\{ |\dot{\gamma}|_{\rm cool}\, n_{\rm e}(\gamma) \right\} + Q(\gamma) \quad ,$$

where $Q(\gamma)$ denotes injection of high-energy electrons through photon-photon annihilation, and $|\dot{\gamma}|_{\rm cool} = |\dot{\gamma}|_{\rm syn} + |\dot{\gamma}|_{\rm ic}$ is the total rate of the radiative cooling.

(31) $$|\dot{\gamma}|_{\rm syn} = \frac{4\, c\sigma_{\rm T}}{3\, m_{\rm e} c^2}\, U_{\rm B}\, \gamma^2 \quad , \quad \text{and} \quad |\dot{\gamma}|_{\rm ic} = \frac{4\, c\sigma_{\rm T}}{3\, m_{\rm e} c^2}\, U_{\rm B}\, \gamma^2\, q\, F_{\rm KN} \quad ,$$

where $q \equiv \langle U_{\rm rad} \rangle / U_{\rm B} \approx 7\, B_{-5}^{-2}$, and $F_{\rm KN} = \frac{1}{\langle U_{\rm rad} \rangle} \int \frac{U_\epsilon}{(1+4\,\gamma\,\epsilon)^{1.5}}\, d\epsilon$. The steady-state solution is then

(32) $$n_{\rm e}(\gamma) = \frac{3\, m_{\rm e} c}{4\, \sigma_{\rm T}}\, \frac{\int_\gamma d\gamma'\, Q(\gamma')}{\gamma^2\, U_{\rm B}\, (1 + q\, F_{\rm KN})} = \frac{3\, \tau\, L_{\rm inj}}{4\, c\, \sigma_{\rm T}\, \gamma_{\rm br}^2\, \mathcal{V}_{\rm gal}}\, \frac{\int_\gamma d\gamma'\, \mathcal{I}(\gamma')}{\gamma^2\, U_{\rm B}\, (1 + q\, F_{\rm KN})} \quad .$$

Electrons' Energy Spectra

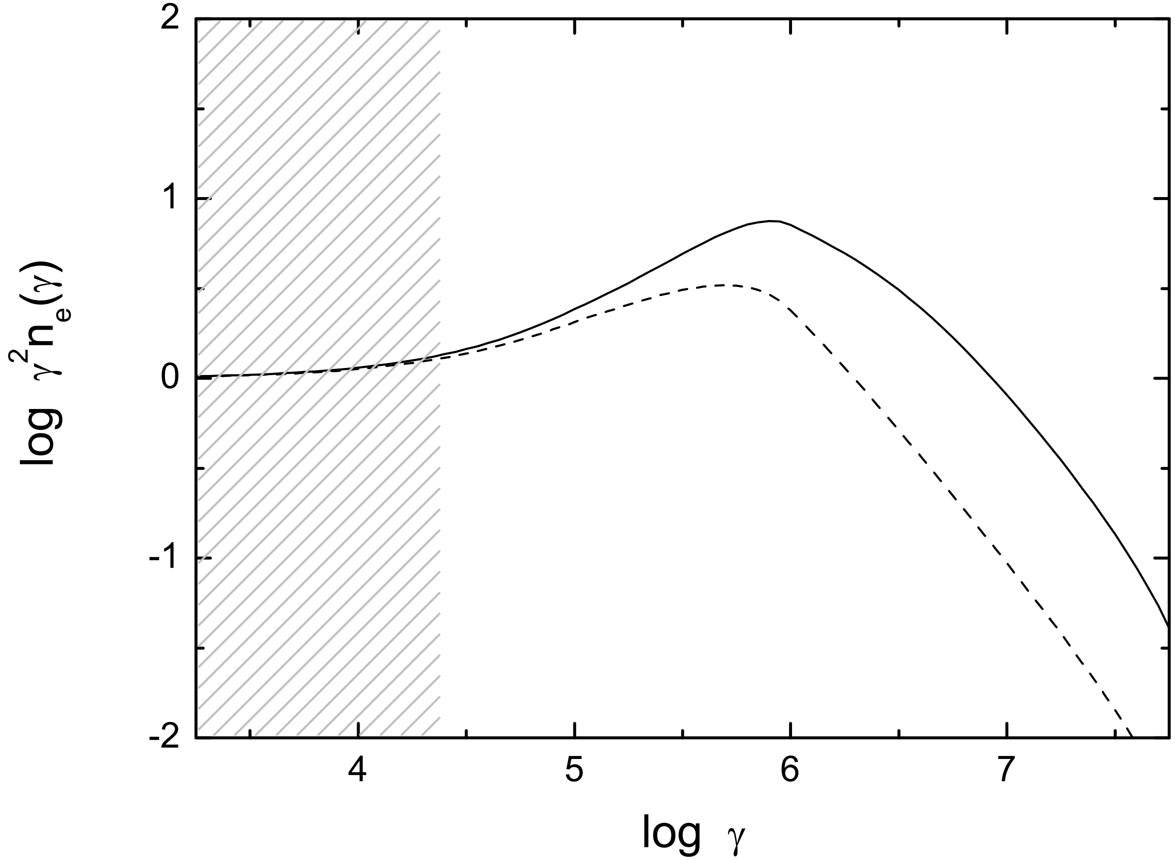

Synchrotron and Inverse-Compton Emission

The synchrotron and inverse-Compton luminosities can be found as

(33) $$[\epsilon L_\epsilon]_{\rm syn} = \frac{\tau\, L_{\rm inj}}{2\, \gamma_{\rm br}^2} \; \frac{\gamma \int_\gamma d\gamma'\, \mathcal{I}(\gamma')}{1 + q\, F_{\rm KN}} \Bigg|_{\gamma = \sqrt{(3/4)\, \epsilon_{\rm syn}\, (B_{\rm cr}/B)}} \quad ,$$

and

(34) $$[\epsilon L_\epsilon]_{\rm ic} = \frac{9\, q\, \tau\, L_{\rm inj}}{16\, f_{\rm bol}\, \gamma_{\rm br}^2} \; \epsilon_{\rm ic}^2 \int d\gamma \int_{\max(\epsilon_{\min}, \epsilon_{\rm low})}^{\min(\epsilon_{\max}, \epsilon_{\rm up})} d\epsilon \; \frac{\mathcal{F}_{\rm iso}(\gamma, \epsilon, \epsilon_{\rm ic})\, g(\epsilon)}{\epsilon^3\, \gamma^4\, (1 + q\, F_{\rm KN})} \int_\gamma d\gamma'\, \mathcal{I}(\gamma') \quad ,$$

where $\epsilon_{\rm low} \equiv \epsilon_{\rm ic}/4\gamma\,(\gamma - \epsilon_{\rm ic})$, and $\epsilon_{\rm up} \equiv \epsilon_{\rm ic}\gamma/(\gamma - \epsilon_{\rm ic})$.
Almost all the energy injected to the elliptical host via annihilation of the nuclear γ-ray emission on the starlight photon field is re-emitted via the synchrotron emission at $\sim 10^{13} - 10^{14}$ Hz frequencies, and via the inverse-Compton emission at $\gtrsim 0.1$ TeV photon energies. Unfortunately, the secondary synchrotron photons have almost the same energy as the target starlight photons, and at the same time much lower total luminosity, and therefore are not likely to be directly observed. However, the secondary γ-ray emission, although also relatively weak, is more promising for the detection.

Emission Spectra

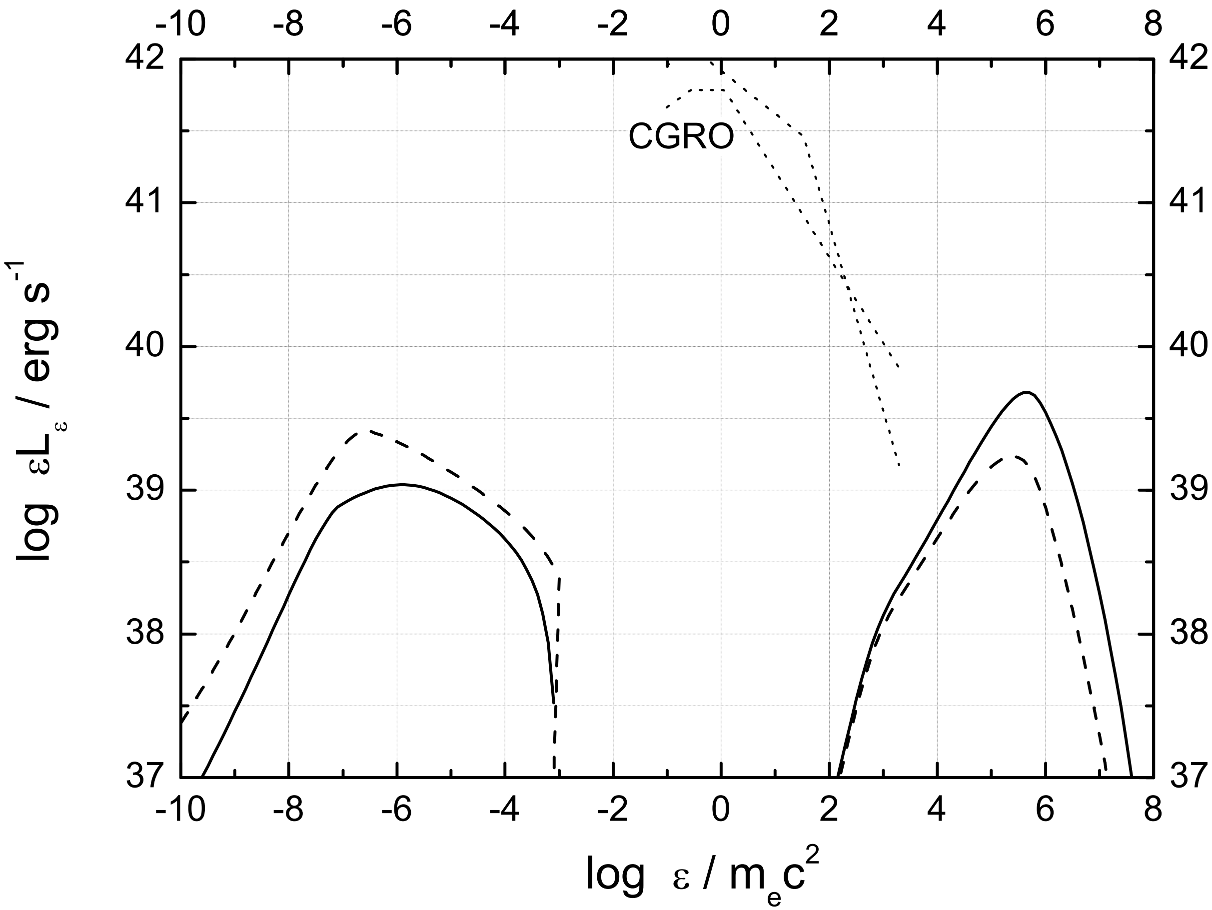

Meaningful Upper Limits

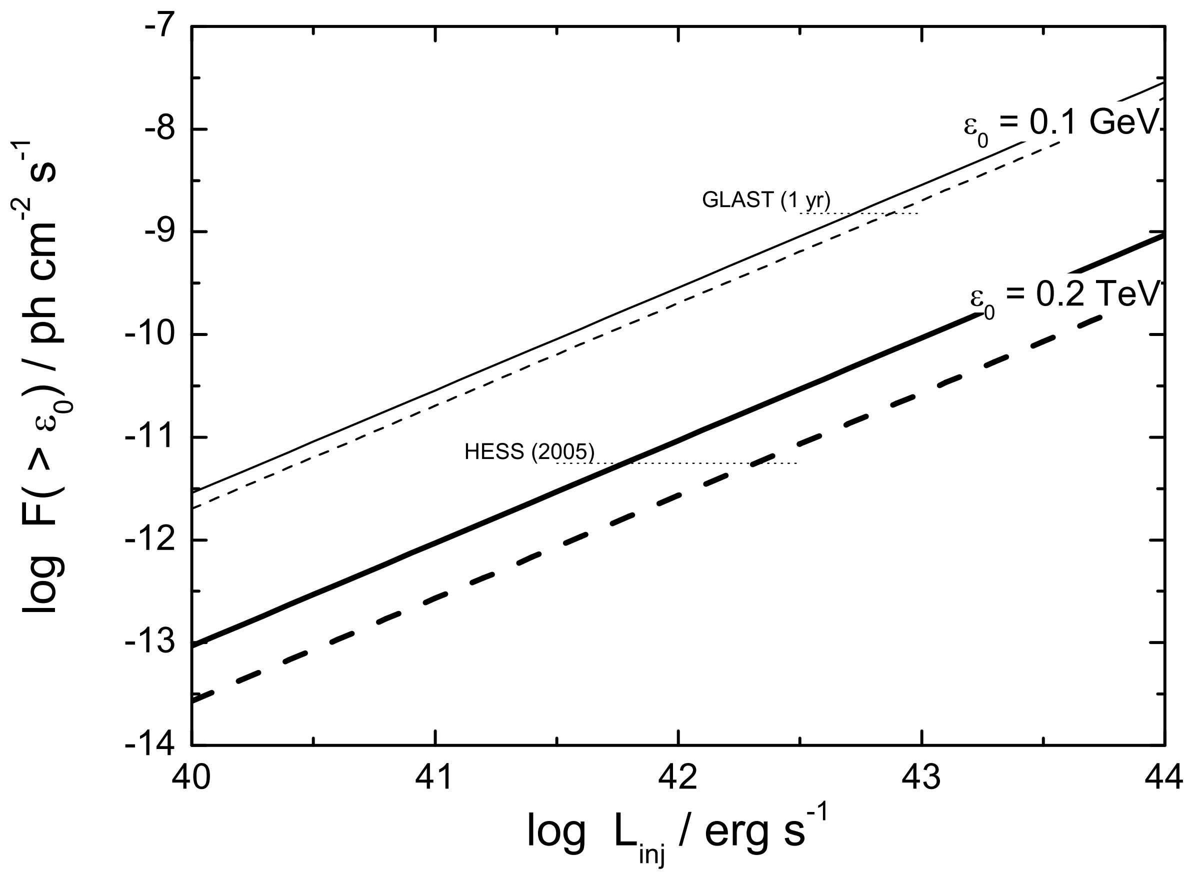

Conclusions on Cen A

- Several BL Lac objects are confirmed sources of variable and strongly Doppler-boosted TeV emission produced in the nuclear portions of their relativistic jets. It is more than probable, that also many of the FR I radio galaxies, believed to be the parent population of BL Lacs, are TeV sources, for which Doppler-hidden nuclear γ-ray radiation may be only to weak to be directly observed.
- About one percent of the total, time-averaged TeV radiation produced by the active nuclei of low-power FR I radio sources is inevitably absorbed and re-processed by the photon-photon annihilation on the starlight photon field, and the following emission of the created and quickly isotropized electron-positron pairs.
- In the case of Cen A radio galaxy, we found that the discussed mechanism can give distinctive observable feature due to the reprocessed isotropic γ-ray emission of the electron-positron pairs injected by the absorption process to the interstellar medium of the inner parts of the elliptical host, and inverse-Compton upscattering thereby starligh radiation mainly to the GeV$-$TeV photon energy range.
- The resulting γ-ray halo is expected to possess characteristic spectrum peaked at ~ 0.1 TeV photon energies, and the photon flux promisingly strong enough to be detected by modern Cherenkov Telescopes and, in a future, by GLAST.
- These findings should apply as well to the other nearby FR I sources.

The synchrotron boiler and the high energy emission of the low-energy peaked BL Lac object

Krzysztof Katarzyński

Osservatorio Astronomico di Brera – Italy,
Nicolaus Copernicus University – Poland,
European Network for the Investigation of Galactic nuclei through Multifrequency Analysis (ENIGMA)

Outline

- self-absorption in a synchrotron source
- synchrotron boiler - particle heating through the self-absorption of photons
- synchrotron self-Compton emission vs external Compton scattering - HBL objects vs LBL sources
- the boiler in the LBL sources (?)

synchrotron source

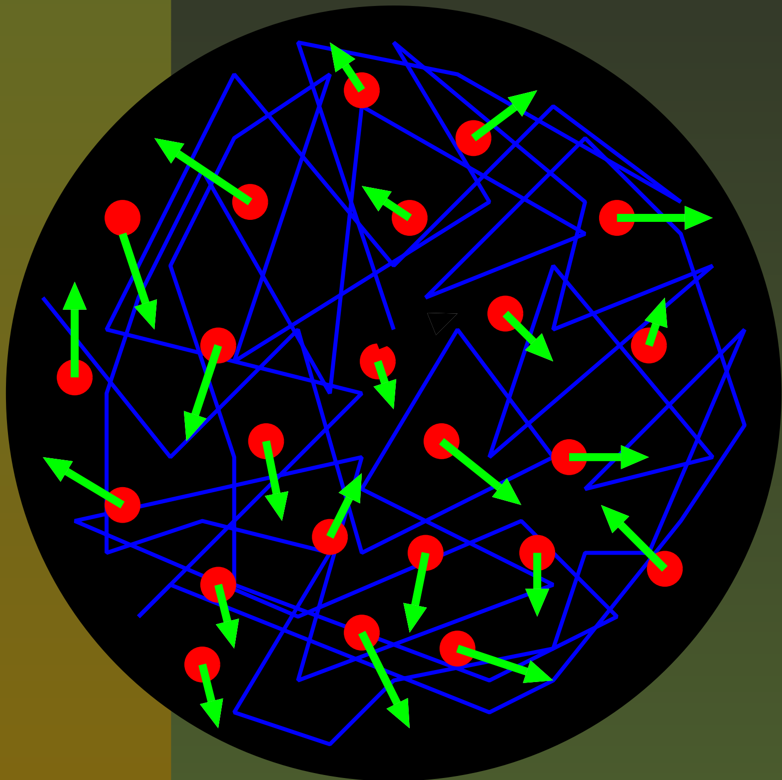

Spherical blob filled up by tangled magnetic field 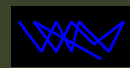 and relativistic electrons . The electrons spinning around the magnetic field lines are producing synchrotron emission 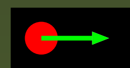.

spectrum of the synchrotron emission

$$N(\gamma) \sim \gamma^{-n} \;\rightarrow\; \alpha = (n-1)/2 \;\rightarrow\; F(\nu) \sim \nu^{-\alpha}$$

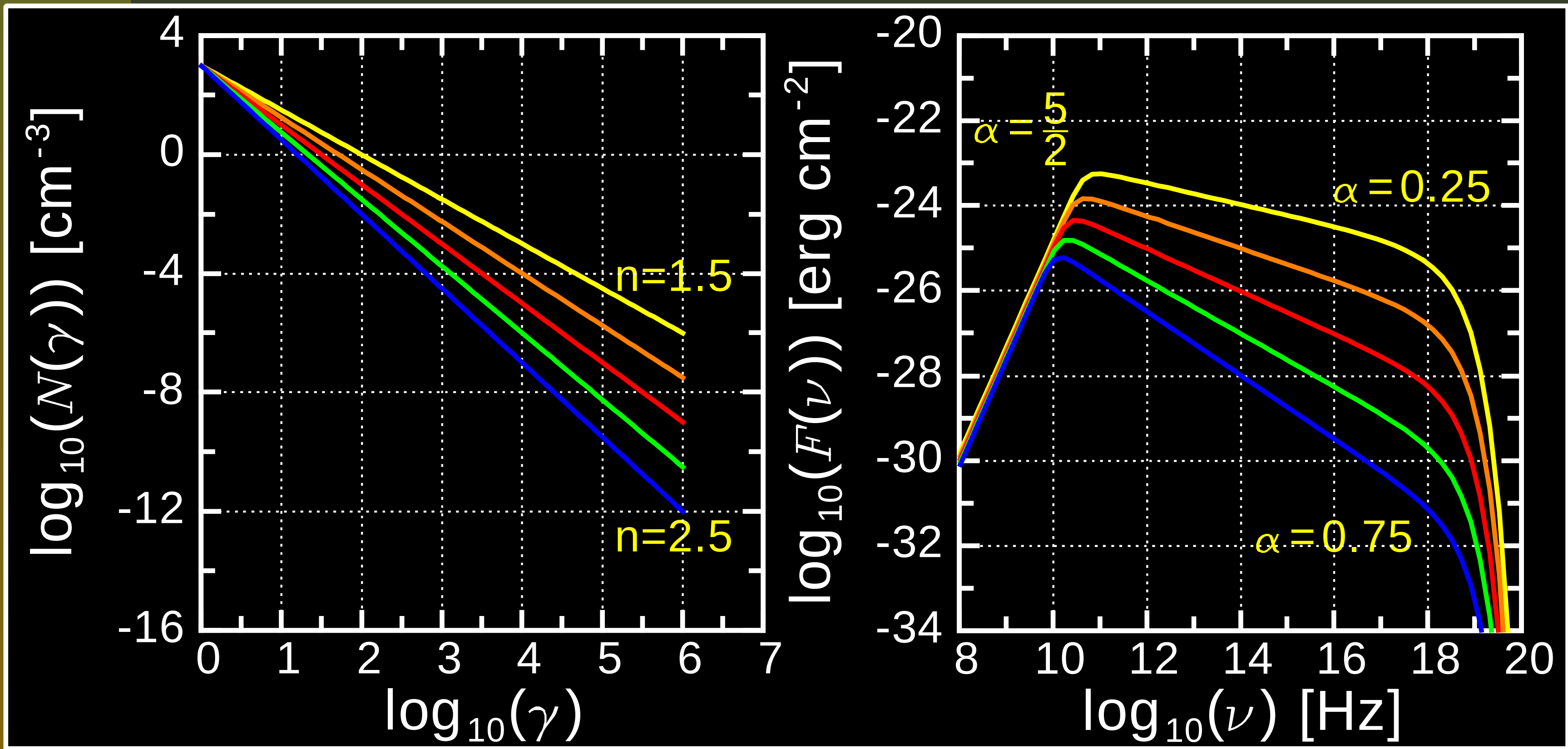

kinetic equation

$$\frac{\partial N(\gamma,t)}{\partial \gamma} = \frac{\partial}{\partial \gamma}\left[\alpha(\gamma)N(\gamma,t) + \beta(\gamma)\gamma p \frac{\partial}{\partial \gamma}\left(\frac{N(\gamma,t)}{\gamma p}\right)\right]$$

$$+S(N,\gamma,t)$$

- $N(\gamma,t)$ - electron energy distribution
- $\alpha(\gamma) = \frac{1}{m_e c^2}\int_0^\infty j(\nu,\gamma)d\gamma$ - cooling term
- $\beta(\gamma) = \frac{1}{2m_e^2 c^2}\int_0^\infty \frac{I(\nu)}{\nu^2} j(\nu,\gamma)d\nu$ - heating term
- $S(N,\gamma,t)$ - possible sources and sinks of electrons
- $j(\nu,\gamma)$ - synchrotron or cyclo-synchrotron emissivity
- $I(\nu)$ - intensity of the emission

thermalization of the spectrum - $N(p)$

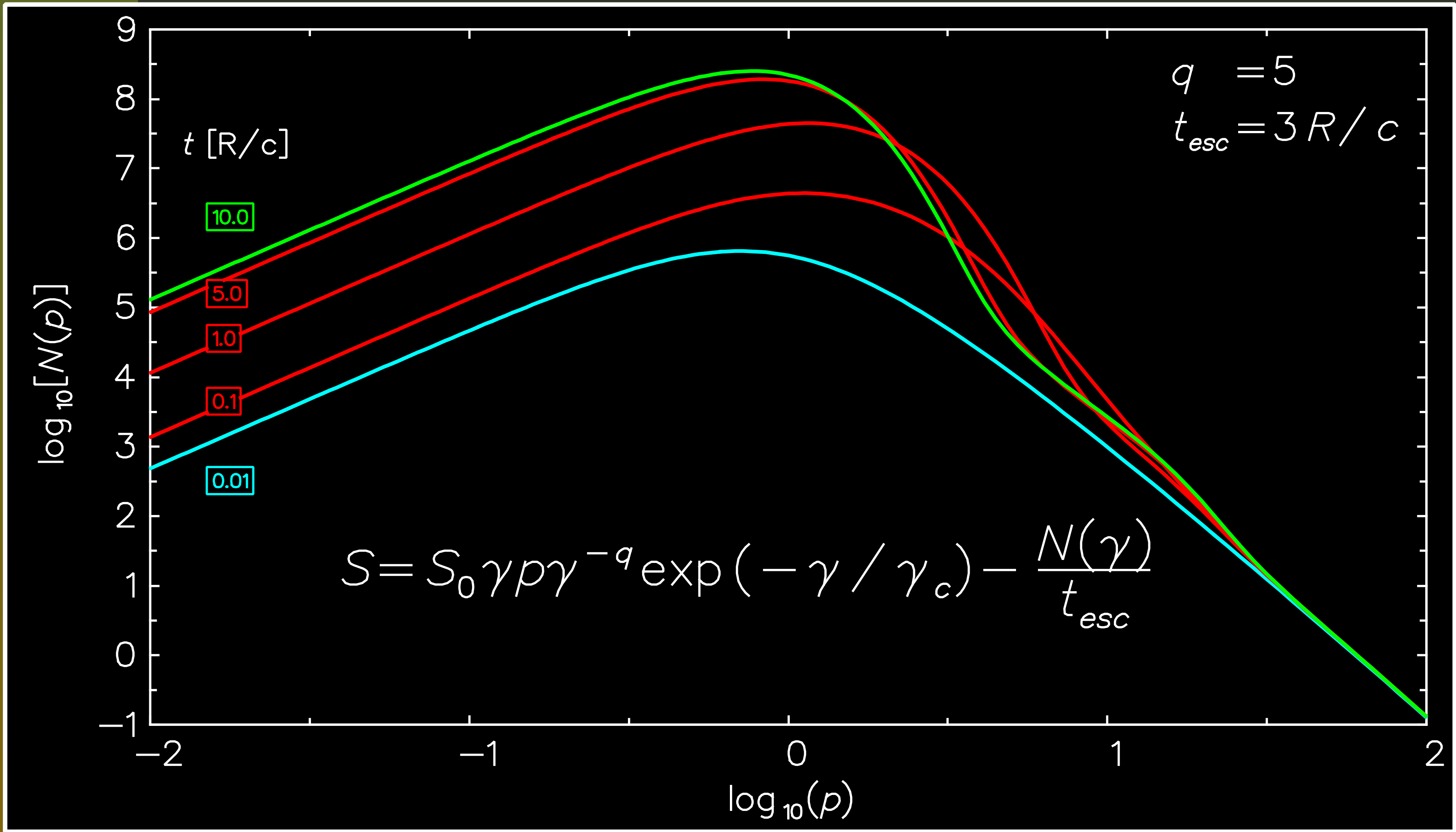

(Ghisellini , Guilbert & Svensson 1988)

thermalization of the spectrum - $N(\gamma)$

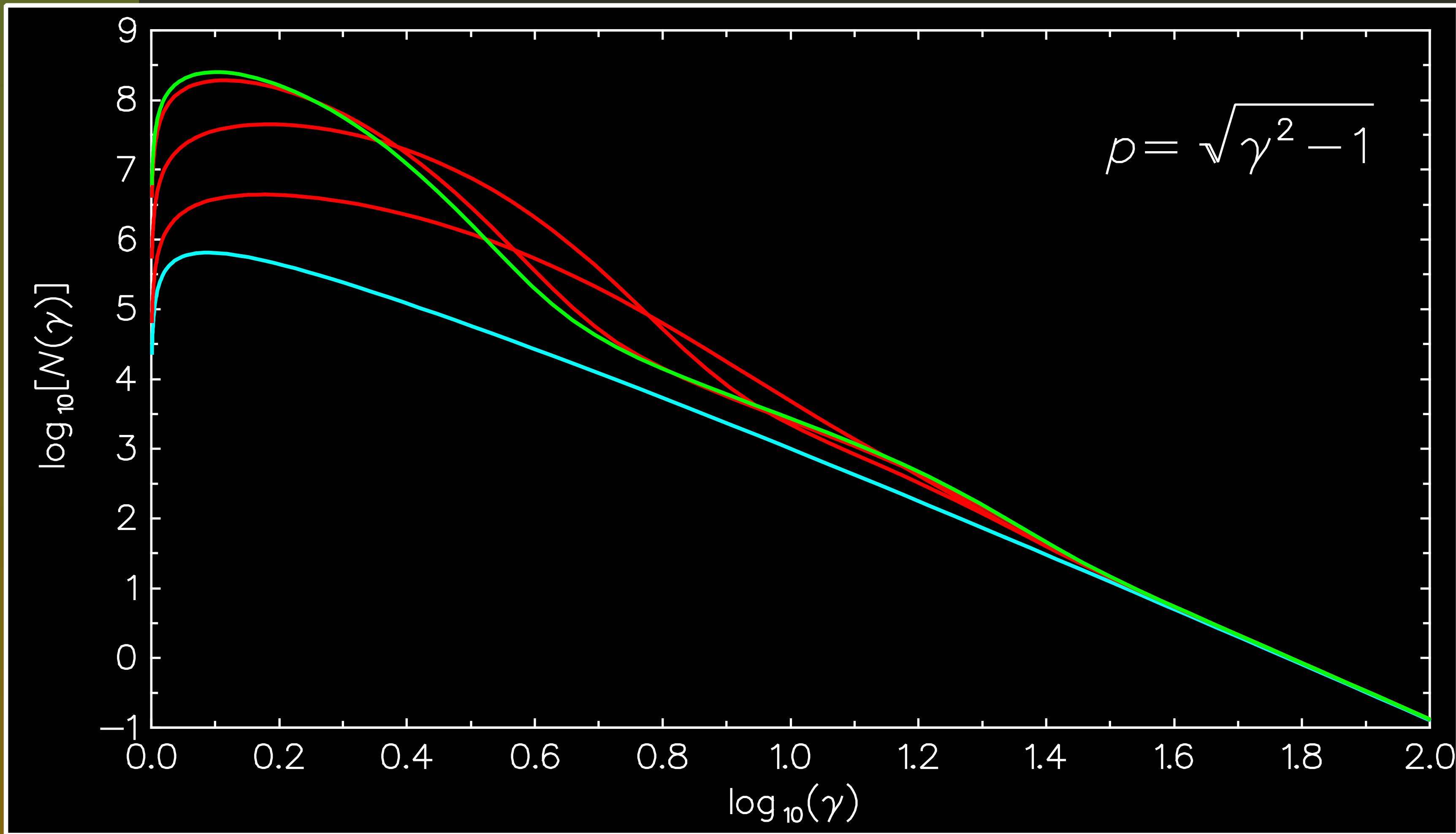

switching off the heating - $N(p)$

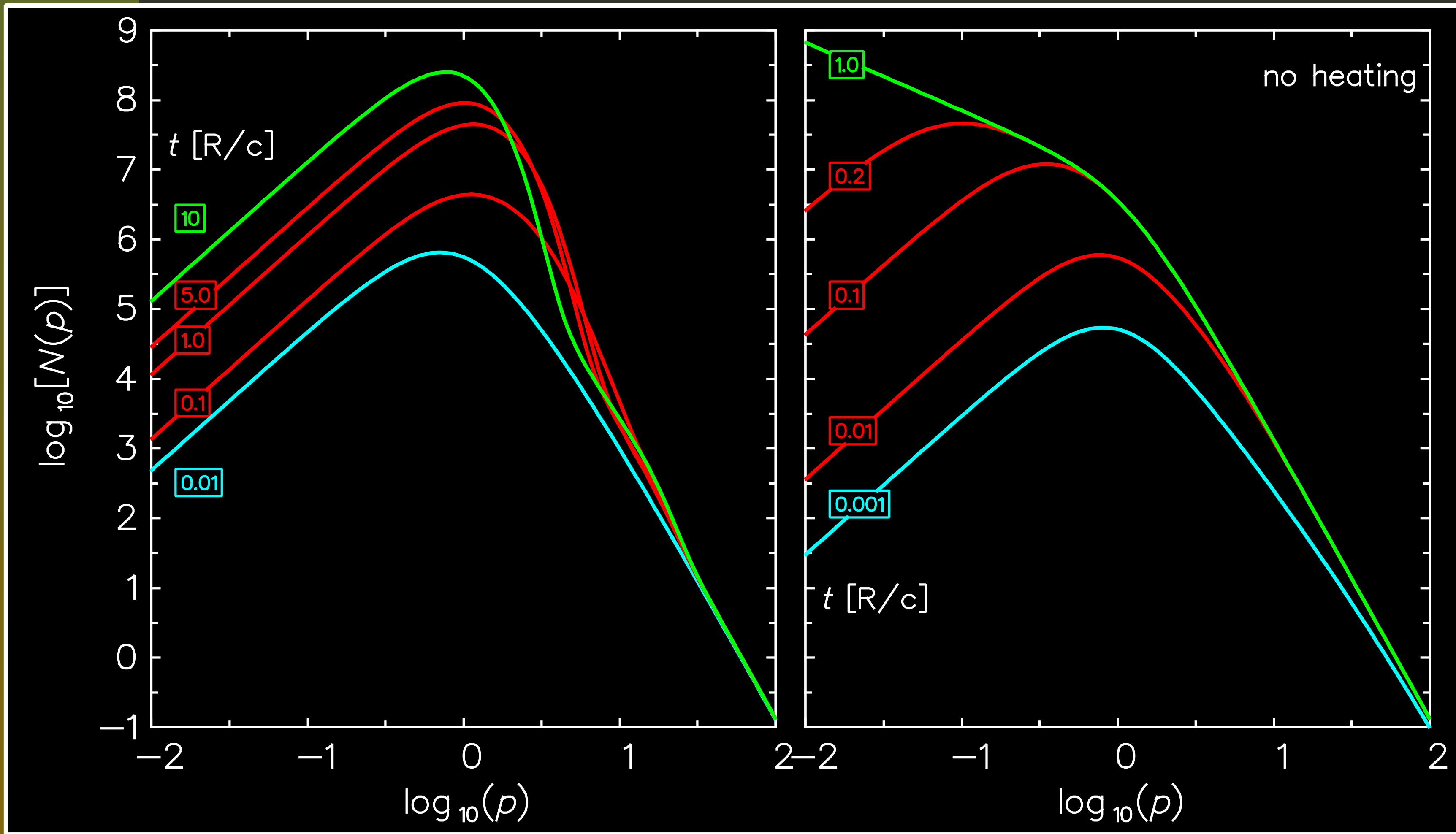

switching off the heating - $N(\gamma)$

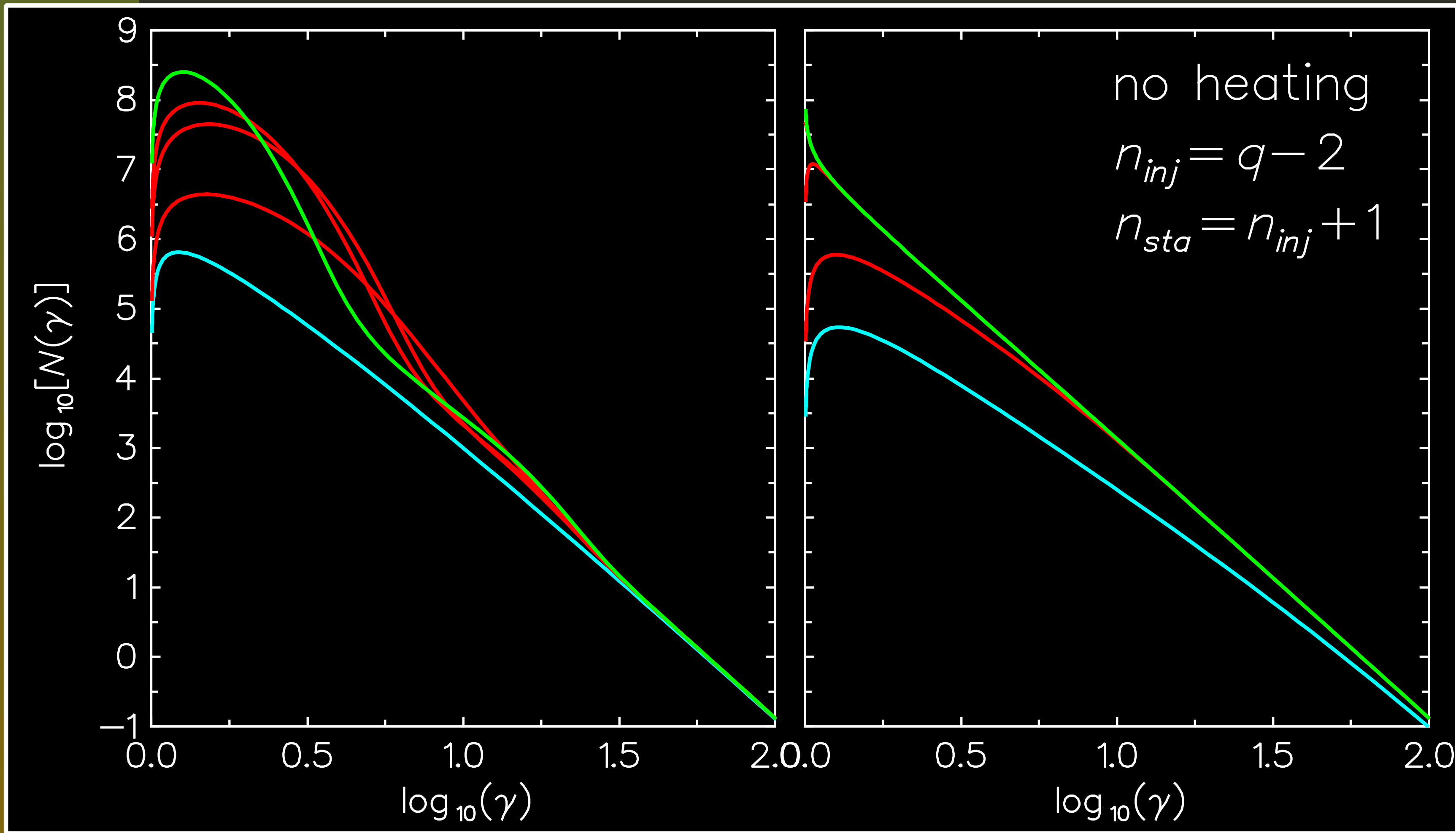

the blazar sequence

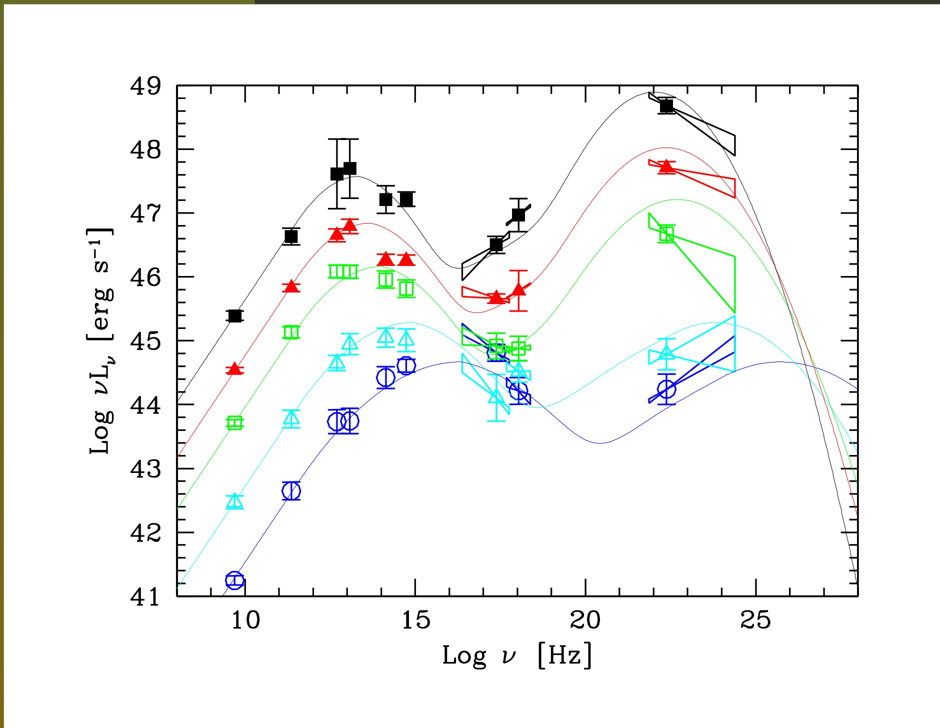

(Fossati et al. 1998)

- HBL - high energy peak BL - Lac objects, $B \lesssim 1$ [G]
- LBL - low energy peak BL - Lac objects, $1 \lesssim B \lesssim 10$ [G]

3C 279 - synchrotron emission

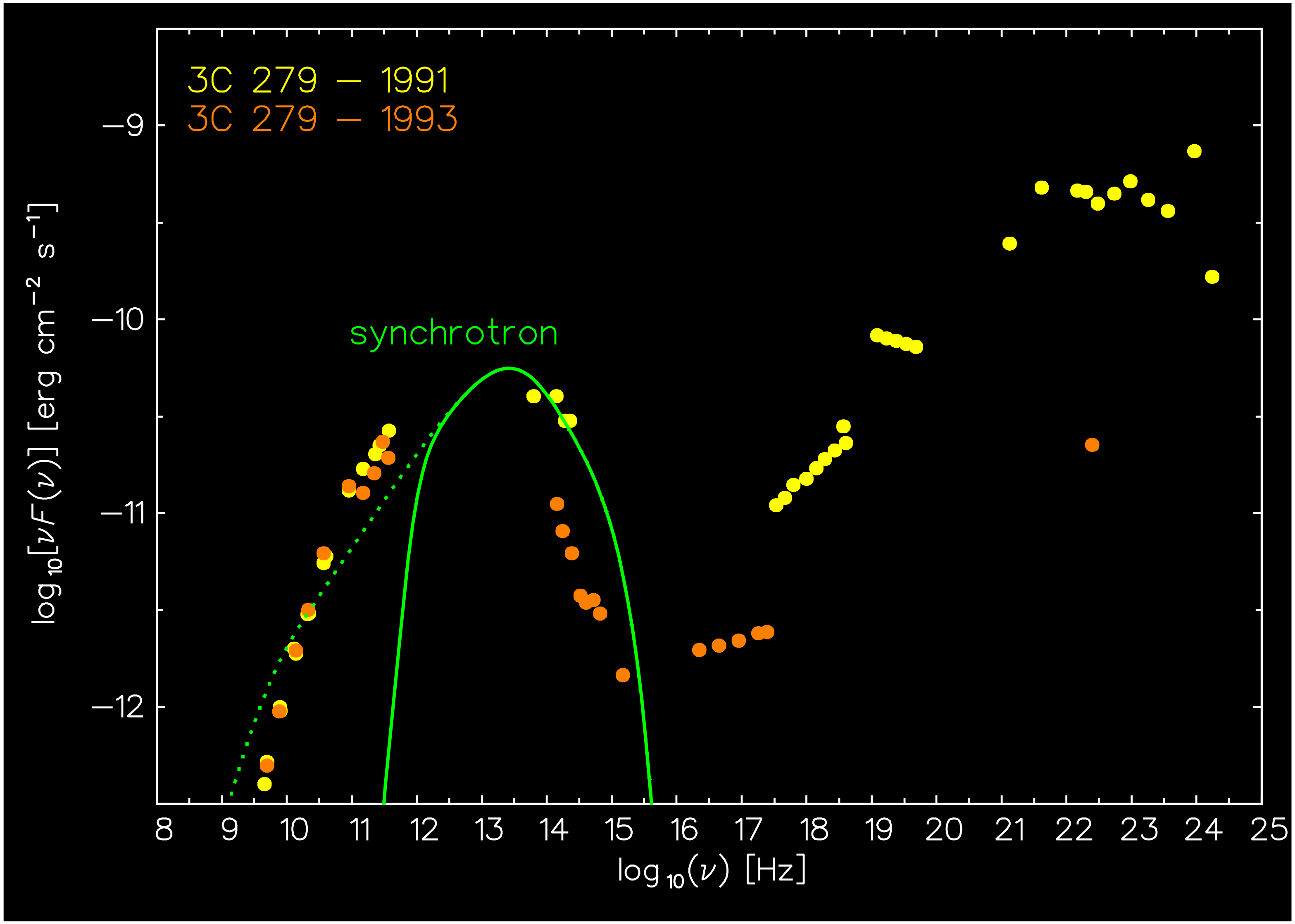

synchrotron self-Compton emission

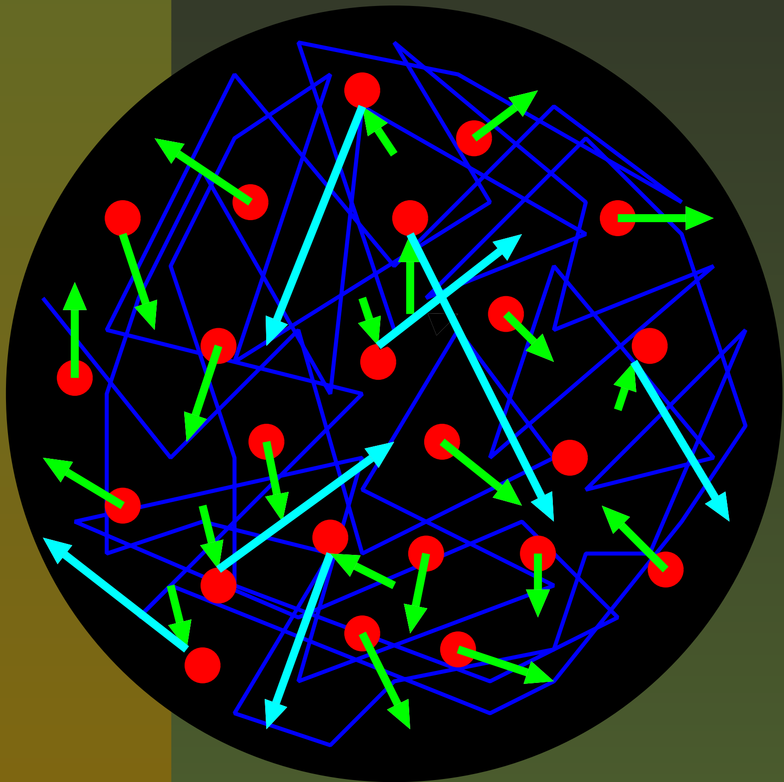

A blob filled up by tangled magnetic field and relativistic electrons. The electrons generate synchrotron emission and up-scatter the synchrotron radiation field (inverse-Compton radiation).

3C 279 - synchrotron + SSC

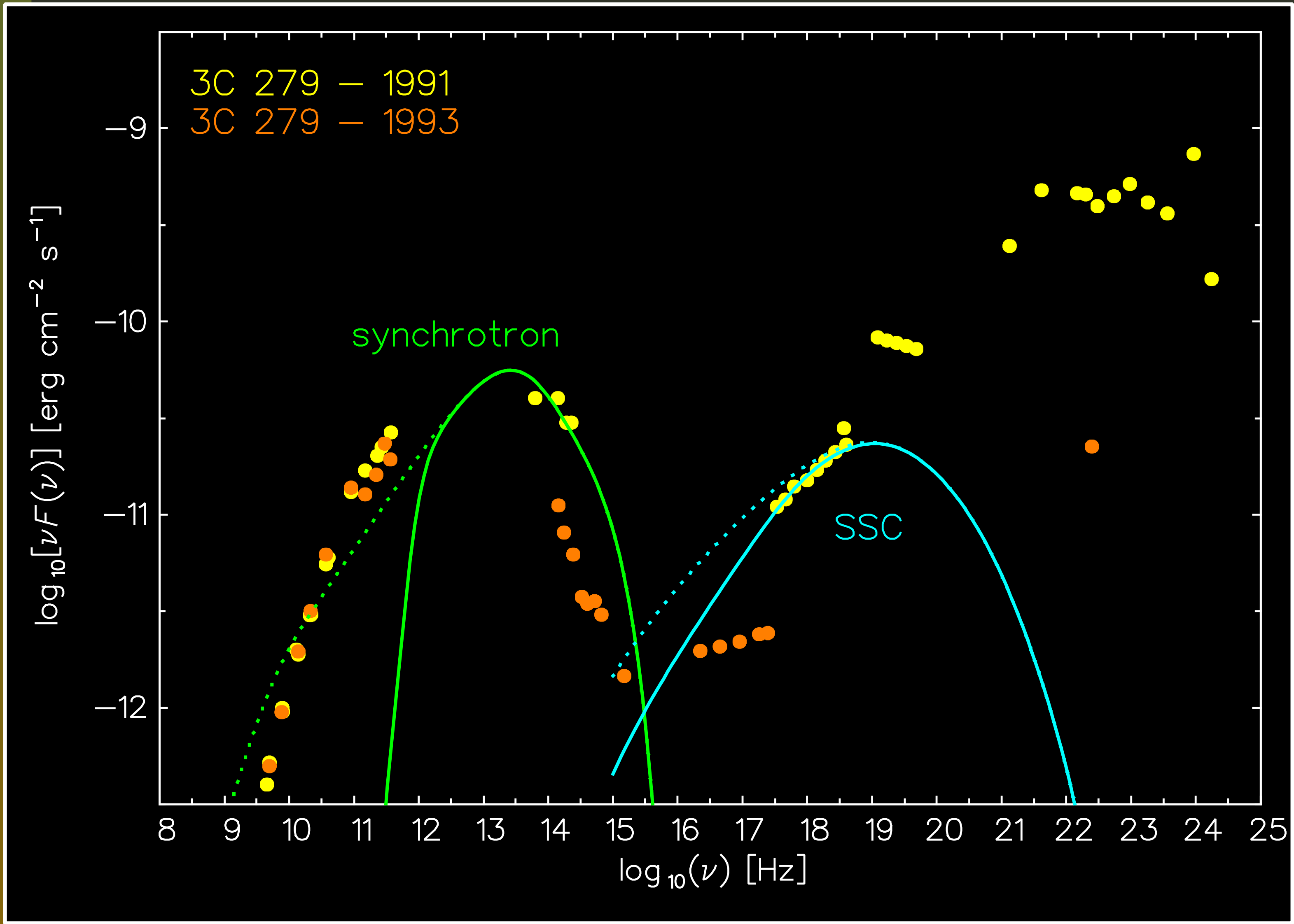

external inverse-Compton scattering

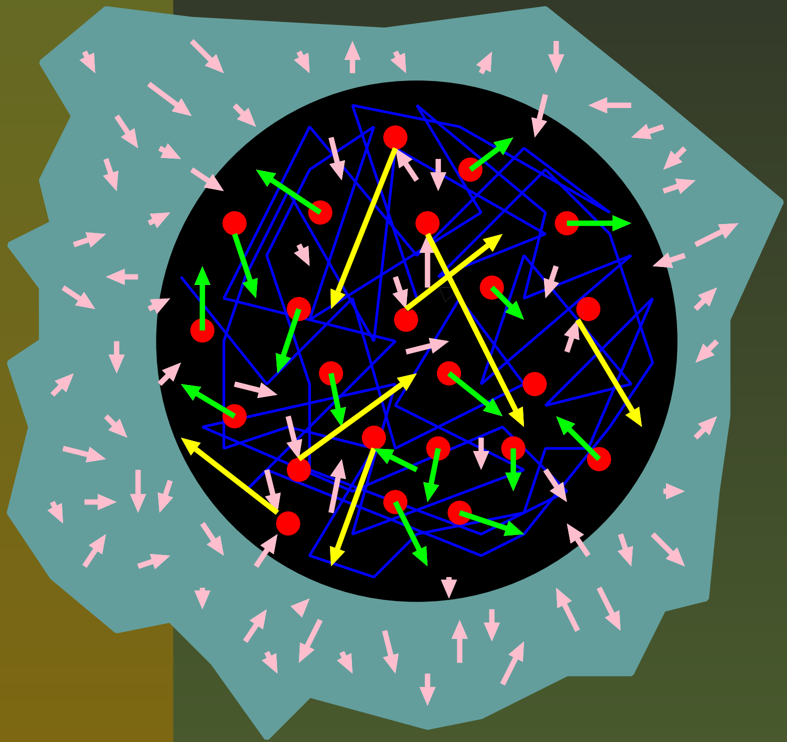

In a case where the blob is surrounded by radiating medium  the relativistic electrons  may up-scatter the external radiation field 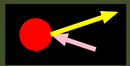 (external inverse-Compton radiation).

3C 279 - synchrotron + SSC + EC

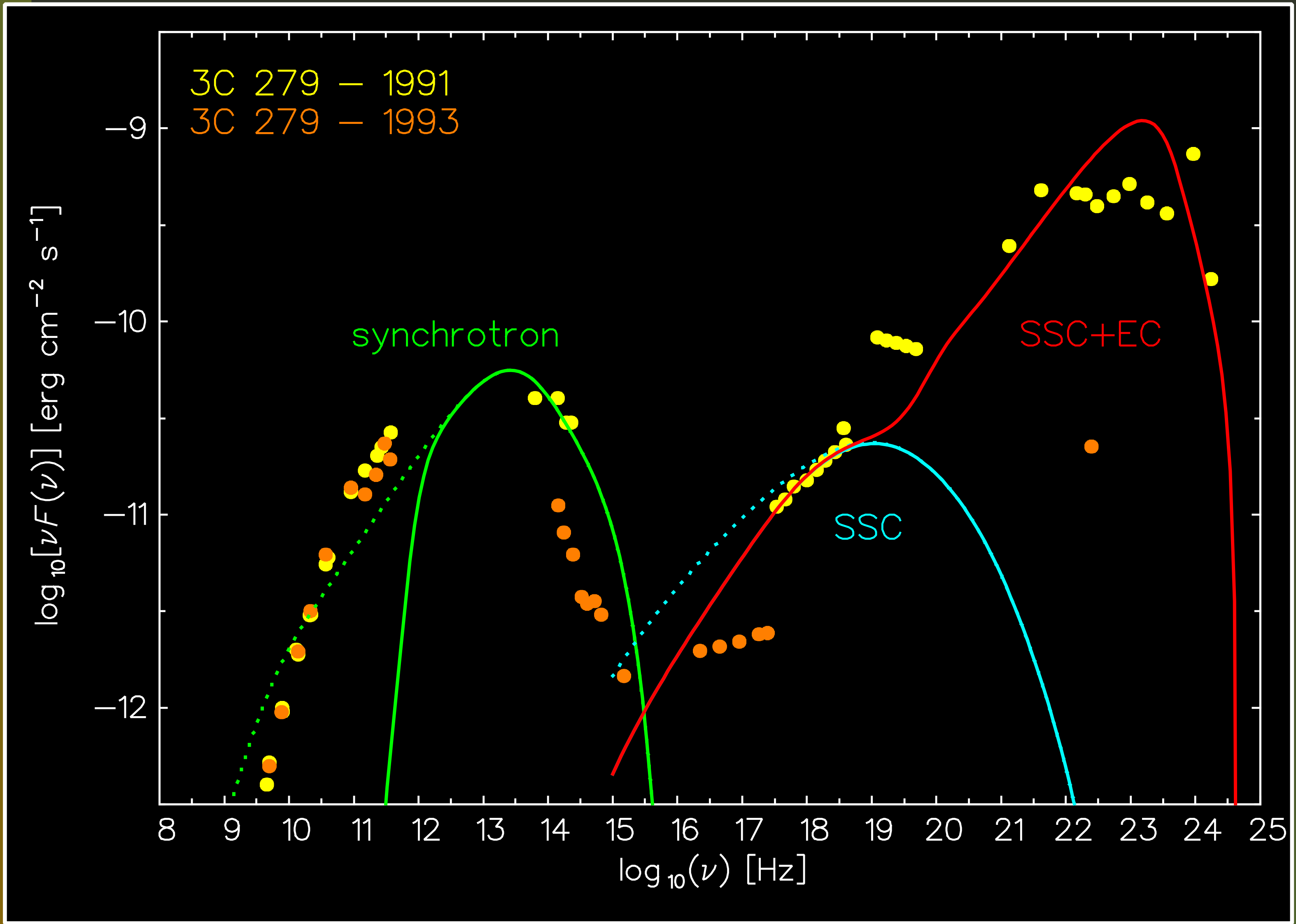

3C 279 - boiler in the low state ?

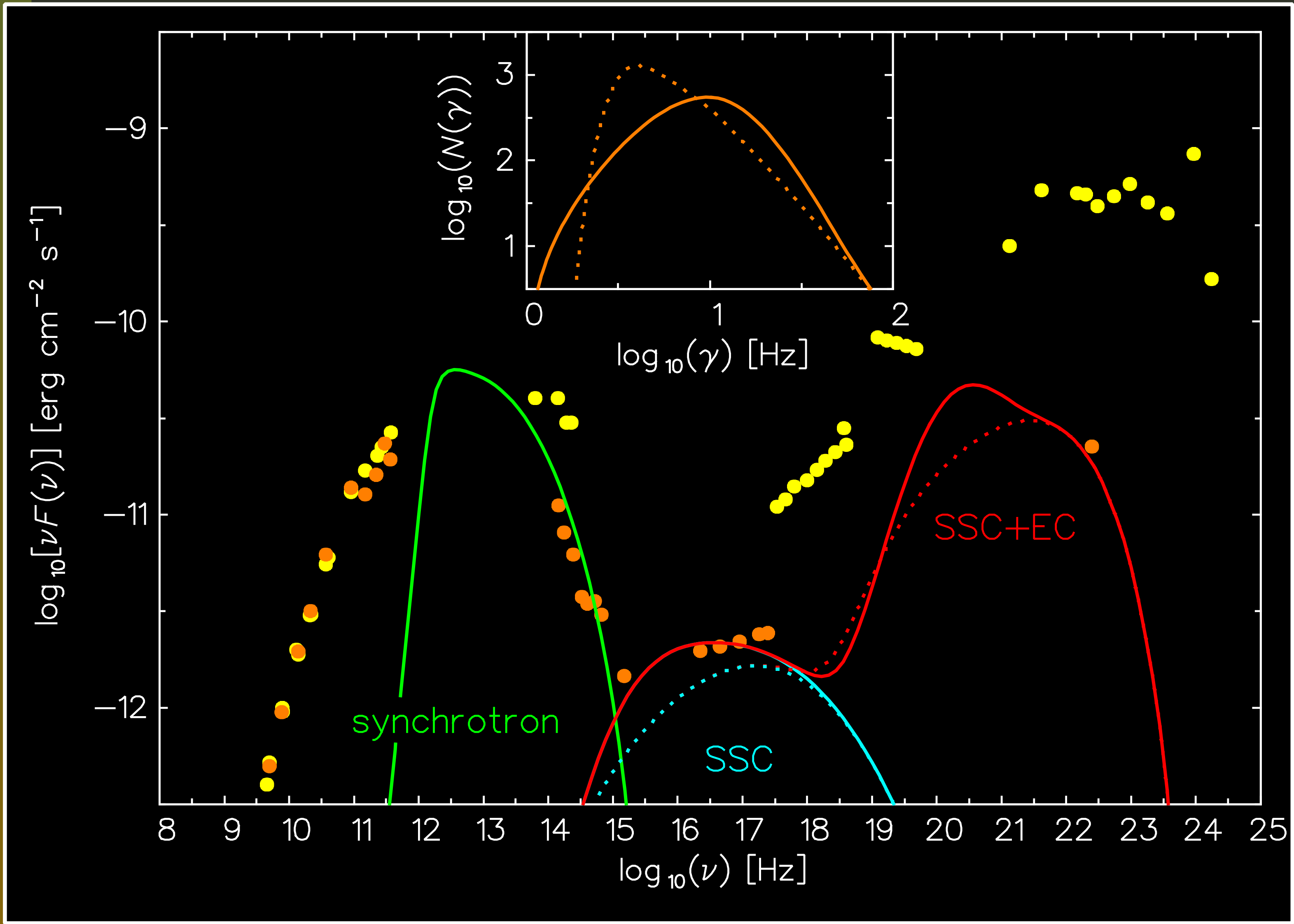

3C 279 in a very low state

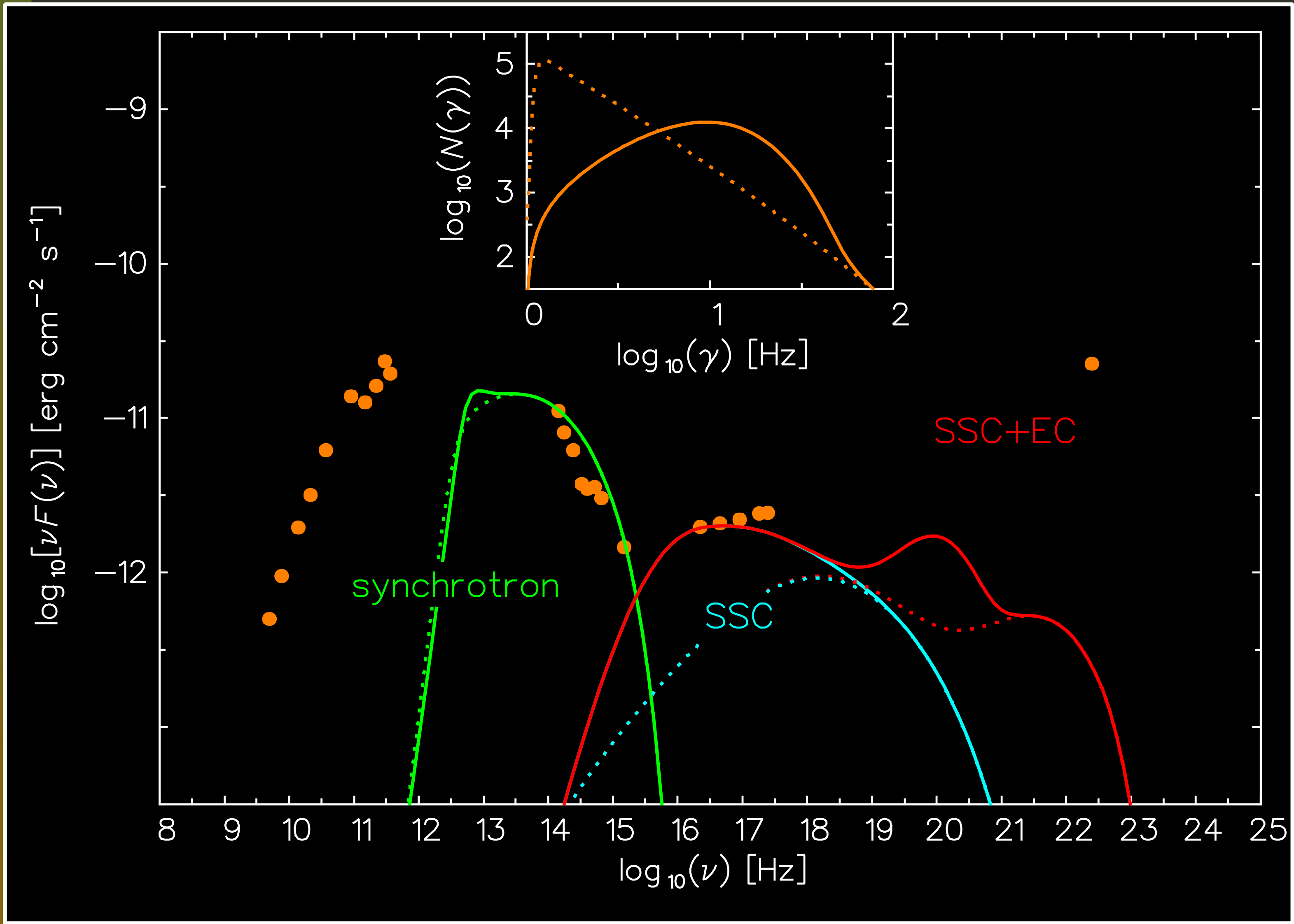

Conclusions

- The particle heating through the self-absorption of the synchrotron photons (boiler) is an important heating process that my thermalize any particle energy distribution. However, to modify significantly the particle spectrum, this process requires magnetically dominated sources where particles are cooled mostly through the synchrotron emission.
- Our simulations show that favourable physical conditions for the boiler may exist in the low energy peak blazars. However, the conditions may be good only in a low state of the emission, when the particle cooling due to external inverse-Compton scattering is less important than the synchrotron cooling.

References

Fossati, G., Maraschi, L., Celotti, A. et al. 1998, MNRAS, 299, 433

Ghisellini, G., Guilbert, P., & Svensson, R., 1988, ApJ, 334, L5

Ghisellini, G., Celotti, A., Fossati, G., et al. 1998, MNRAS, 301, 451

Sikora, M., Begelman, M. C., & Rees, M., 1993, ApJ, 421, 153

My contribution to the network

- “Correlation between the TeV and X-ray emission in high-energy peaked BL Lac objects”, K. Katarzyński, G. Ghisellini, F. Tavecchio, L. Maraschi, G. Fossati, A. Mastichiadis,

  A&A, 433, 479, 2005 - presented in Lapland

- “The correlation between the synchrotron peak frequency and the synchrotron peak flux in TeV blazars”, K. Katarzyński, G. Ghisellini, F. Tavecchio, L. Maraschi, G. Fossati, A. Mastichiadis,

  submitted to A&A, - presented in Perugia

- “Stochastic particle acceleration and synchrotron self-Compton radiation in TeV blazars”, K. Katarzyński, G. Ghisellini, A. Mastichiadis, F. Tavecchio, L. Maraschi,

  accepted for A&A (astro-ph/0603362) - presented in Neubrandenburg

- “The cyclo-synchrotron processes and particle heating through absorption of photons” K. Katarzyński, G. Ghisellini, R. Swensson, J. Gracia,

  accepted for A&A (astro-ph/0602183) - presented in Kinsail

- “Hard TeV spectra of blazars and the constraints to the IR intergalactic background” K. Katarzyński, G. Ghisellini, F. Tavecchio, J. Gracia, L. Maraschi,

  MNRAS 2006, 368L, 52 - presented in Kinsail (Jose)

Aperture photometry and host galaxies

K. Nilsson, M. Pasanen, E. Lindfors, L. O. Takalo, A. Berdyugin and S. Ciprini

Tuorla Observatory

NOT images of nearby BL Lacs

Mrk 501 (z=0.034)

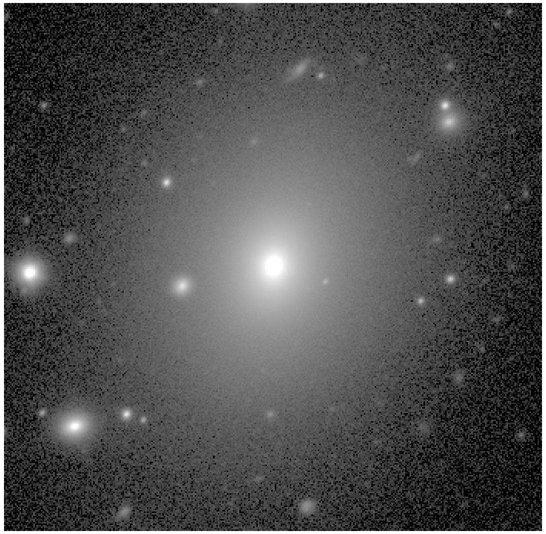

123”

Mrk 180 (z=0.045)

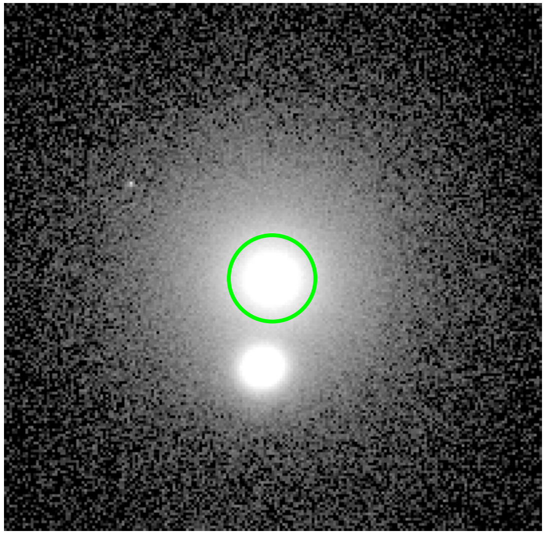

38”

1ES 1959+650 (z=0.047)

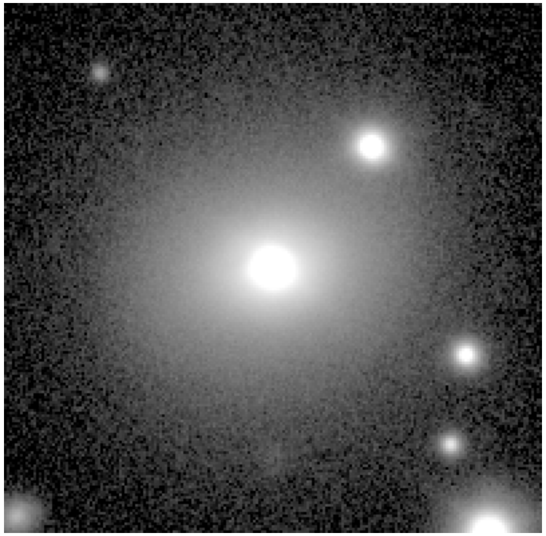

35”

Mrk 501 monitoring, Tuorla & KVA

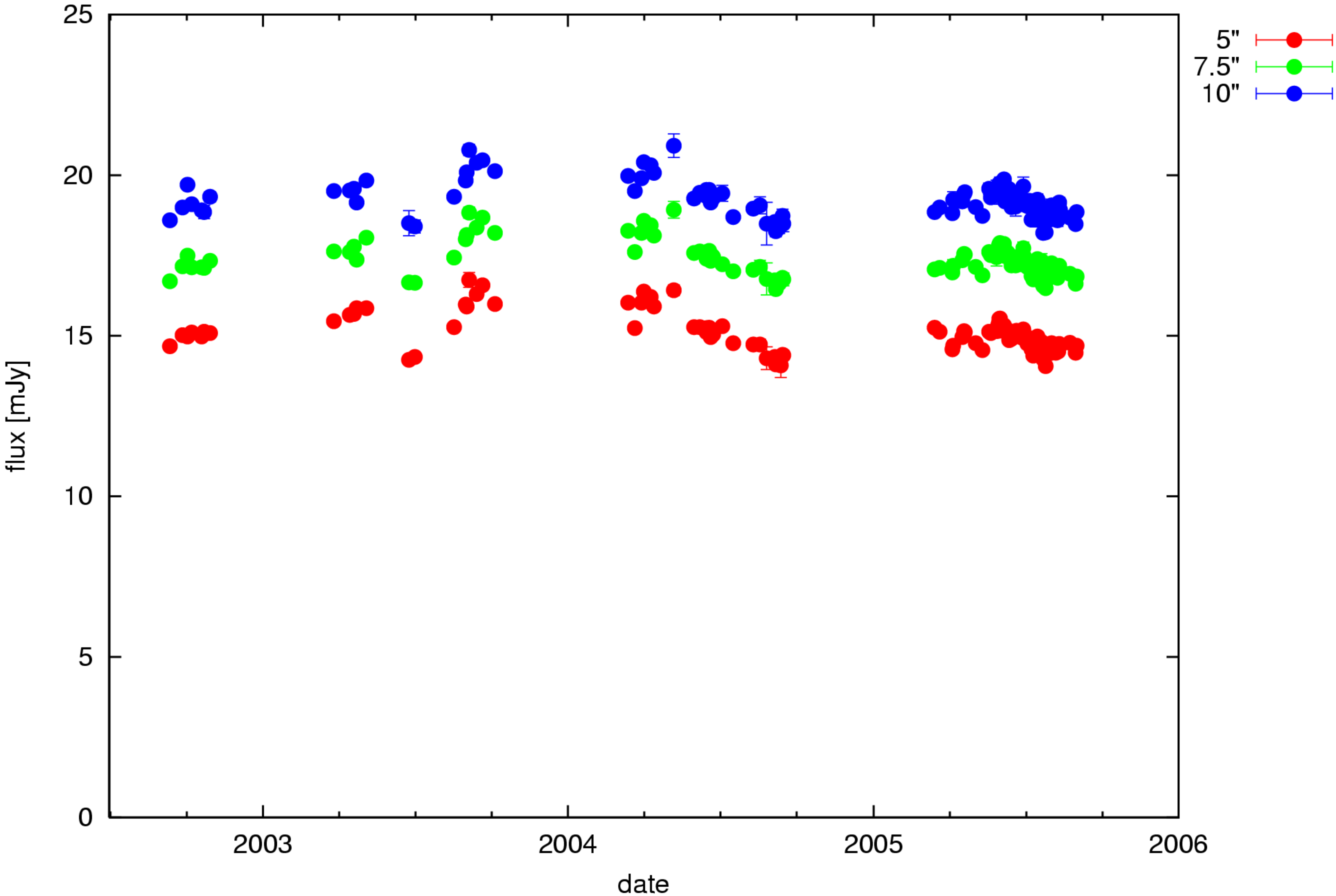

Aims of the study

- Find a method to subtract the host galaxy flux from optical monitoring data.
- Estimate the accuracy of the method.

The method

- Obtain high-resolution images of your monitoring targets.
- Fit a two-dimensional photometric model (nucleus+host galaxy) to the targets → separation of nuclear and host galaxy flux.
- Subtract the nuclear light from the photometric model.
- Repeat over a range of aperture sizes and seeing values:
  - Convolve the photometric model to the desired seeing value.
  - Measure the flux using differential aperture photometry.
- Subtract the host galaxy flux from the monitoring data using the computed correction table.

The test sample

16 BL Lacs from Costamante & Ghisellini (2002):

Object	z	Object	z
1ES 0033+595	-	1ES 1218+304	0.182
1ES 0120+340	0.272	RGB 1417+257	0.237
RGB 0214+517	0.049	1ES 1544+820	-
1ES 0806+524	0.138	Mrk 501	0.034
1ES 1011+496	0.200	OT 546	0.055
Mrk 421	0.031	1ES 1959+650	0.047
Mrk 180	0.045	BL Lac	0.069
RGB 1135+676	0.135	1ES 2344+514	0.044

Imaging

- 11 objects imaged at the NOT during previous projects.
- 2 new images in September 2005.
- 3 images provided by R. Falomo.

Model fitting

- 2-dim. nucleus + host galaxy model, convolved with the PSF.

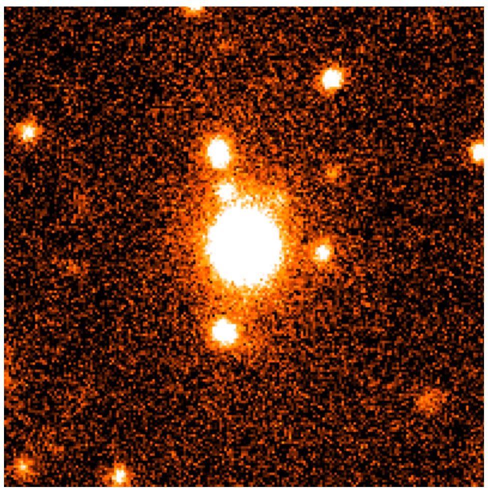

=

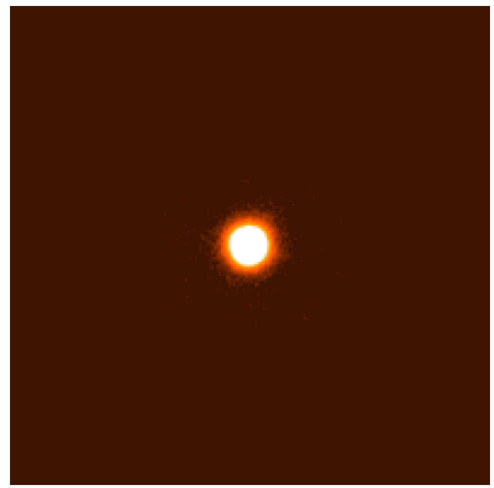

x_c, y_c, m_c

+

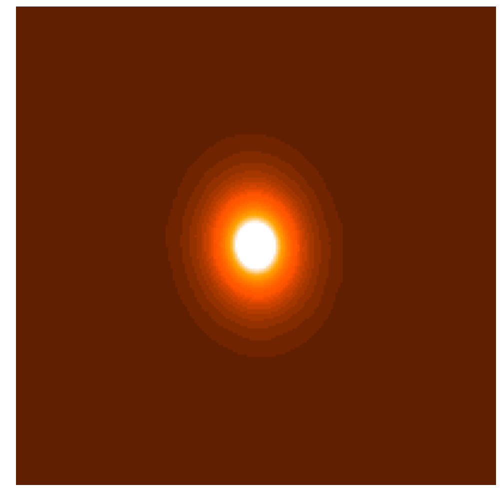

$x_g, y_g, m_g, r_e, \varepsilon, PA, \beta$

Host galaxy: $$I(r) = I(r_e) dex \left\{ -b_\beta [(\frac{r}{r_e})^\beta - 1] \right\}$$

Photometric modeling

Observed → Modeled

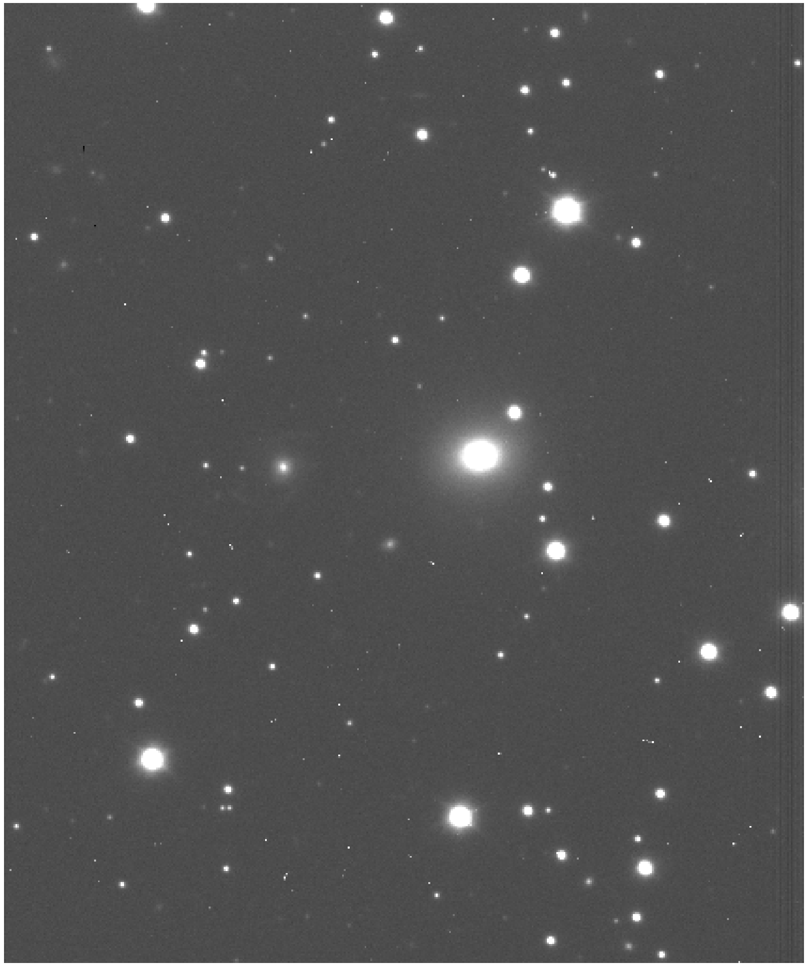

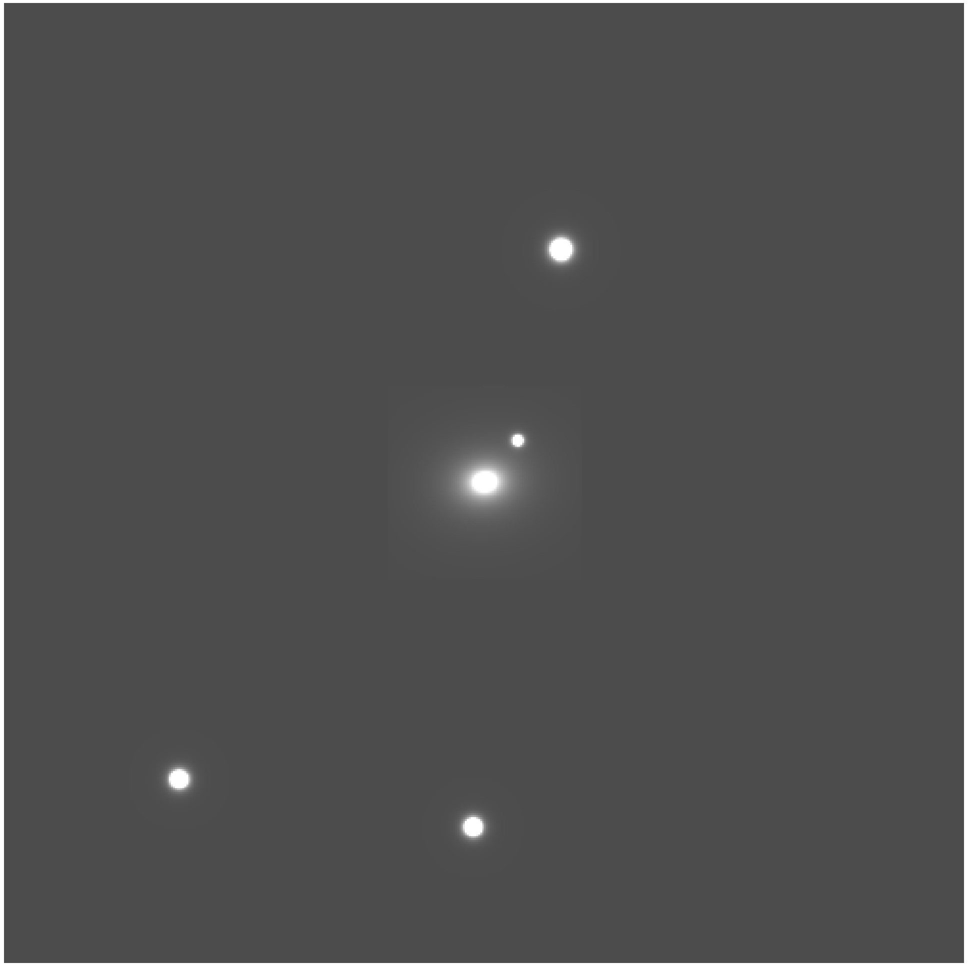

Convolution kernel: Moffat profile (β = 2.0, 2.5 and 3.0)

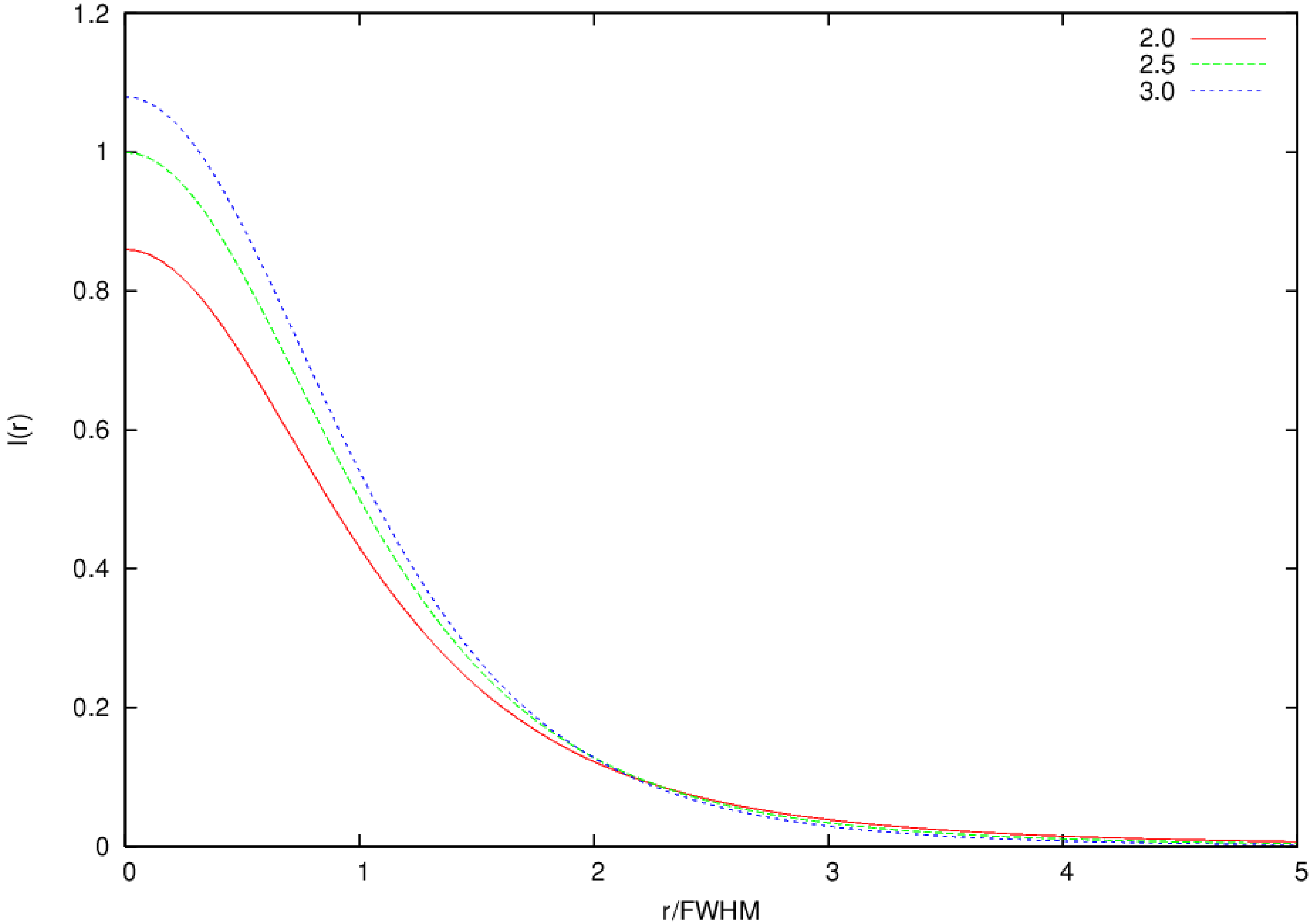

Correction curves

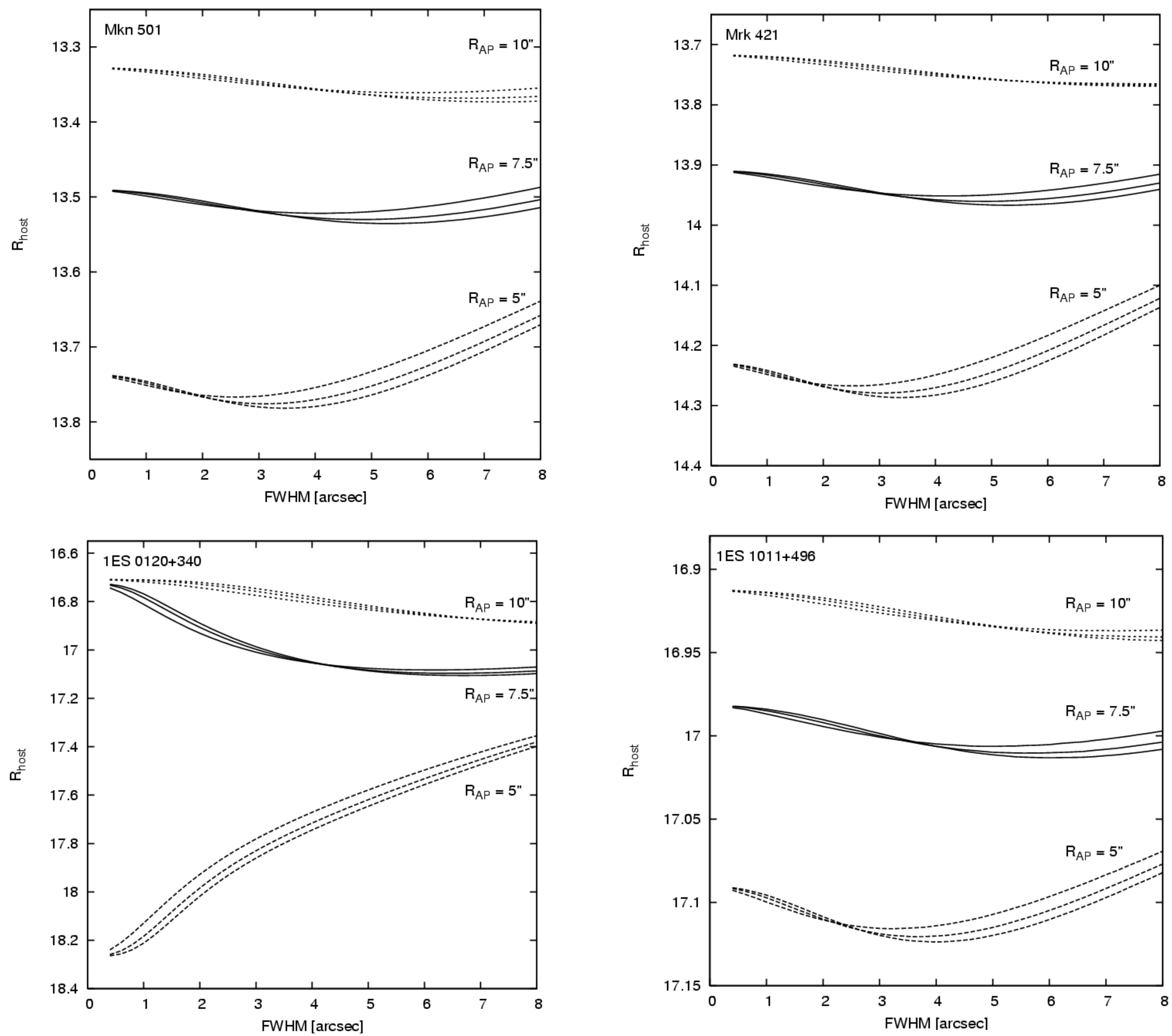

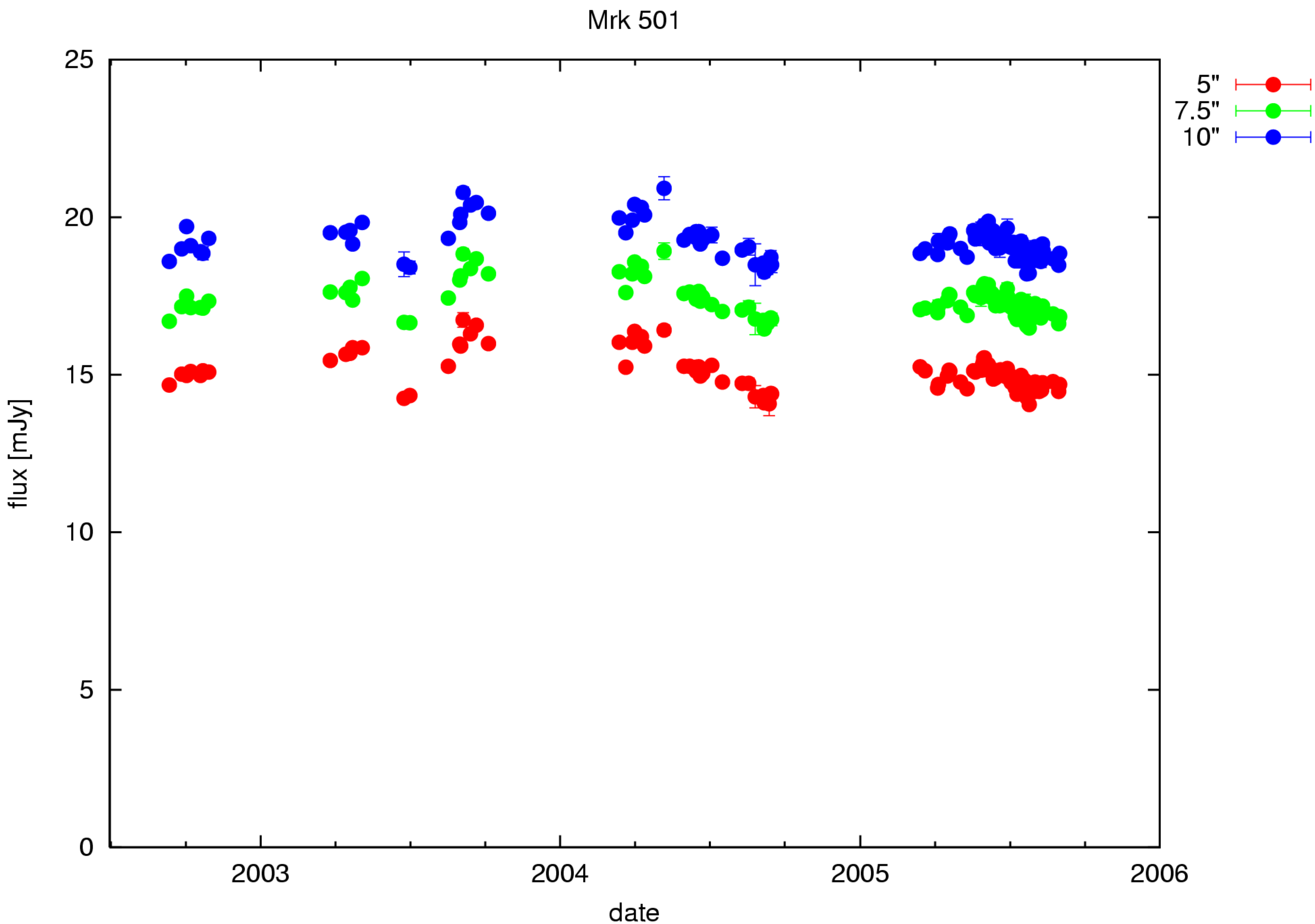
Mrk 501
5"
7.5"
10"
flux [mJy]
date
25
20
15
10
5
0
2003
2004
2005
2006

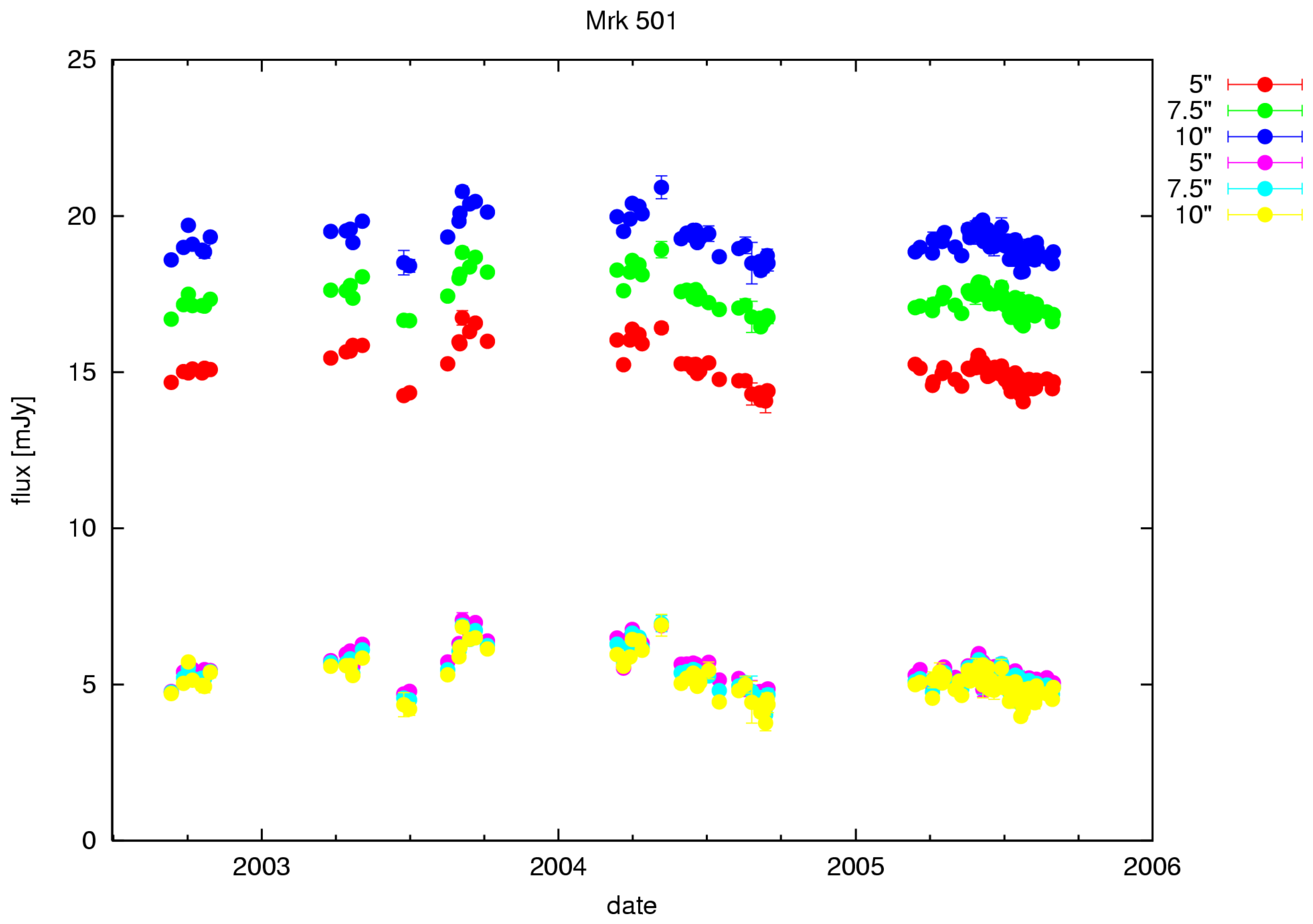

Mrk 501
25
20
15
10
5
0
2003
2004
2005
2006
date
flux [mJy]
5"
7.5"
10"
5"
7.5"
10"

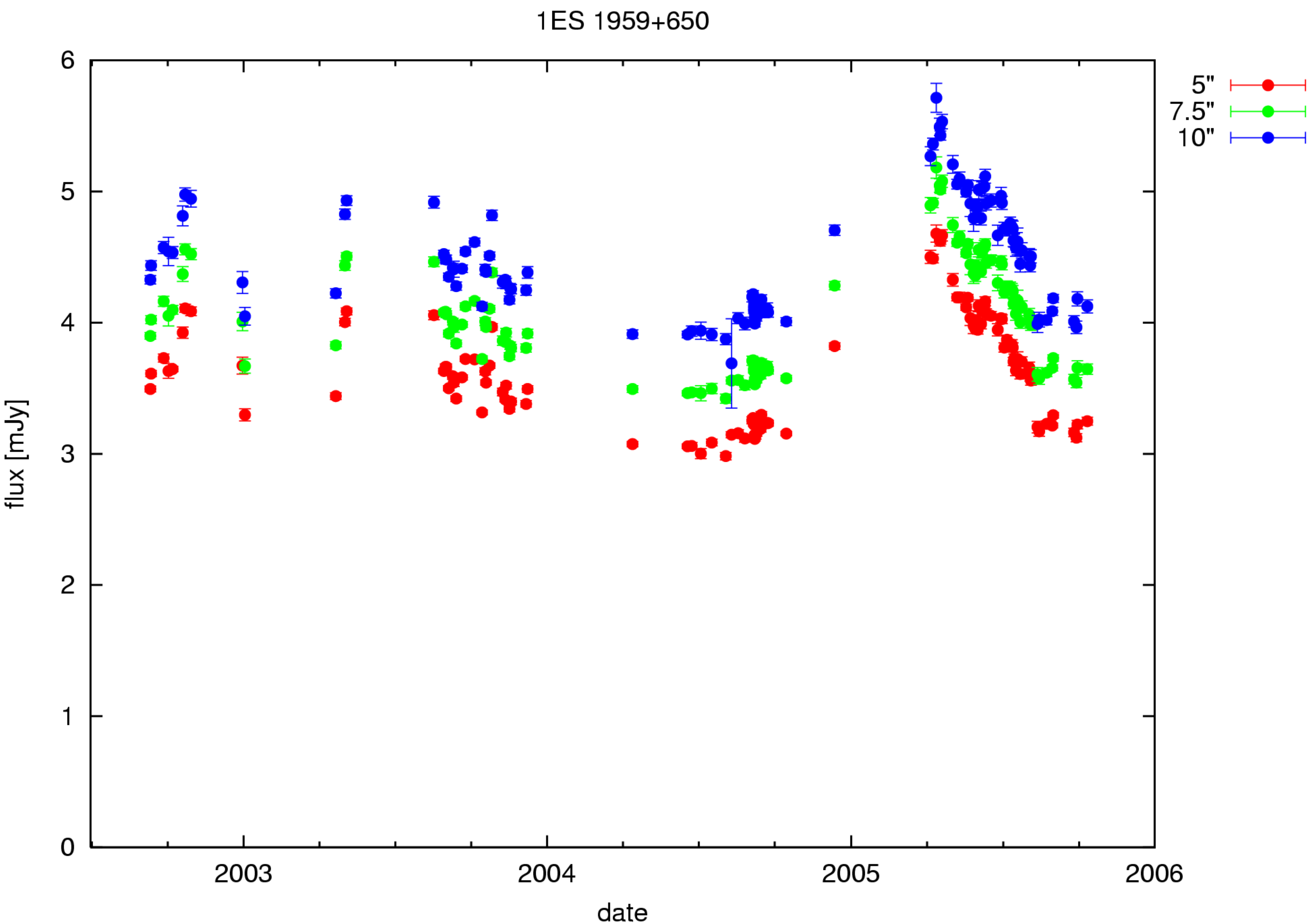
1ES 1959+650
flux [mJy]
date
0
1
2
3
4
5
6
2003
2004
2005
2006
5"
7.5"
10"

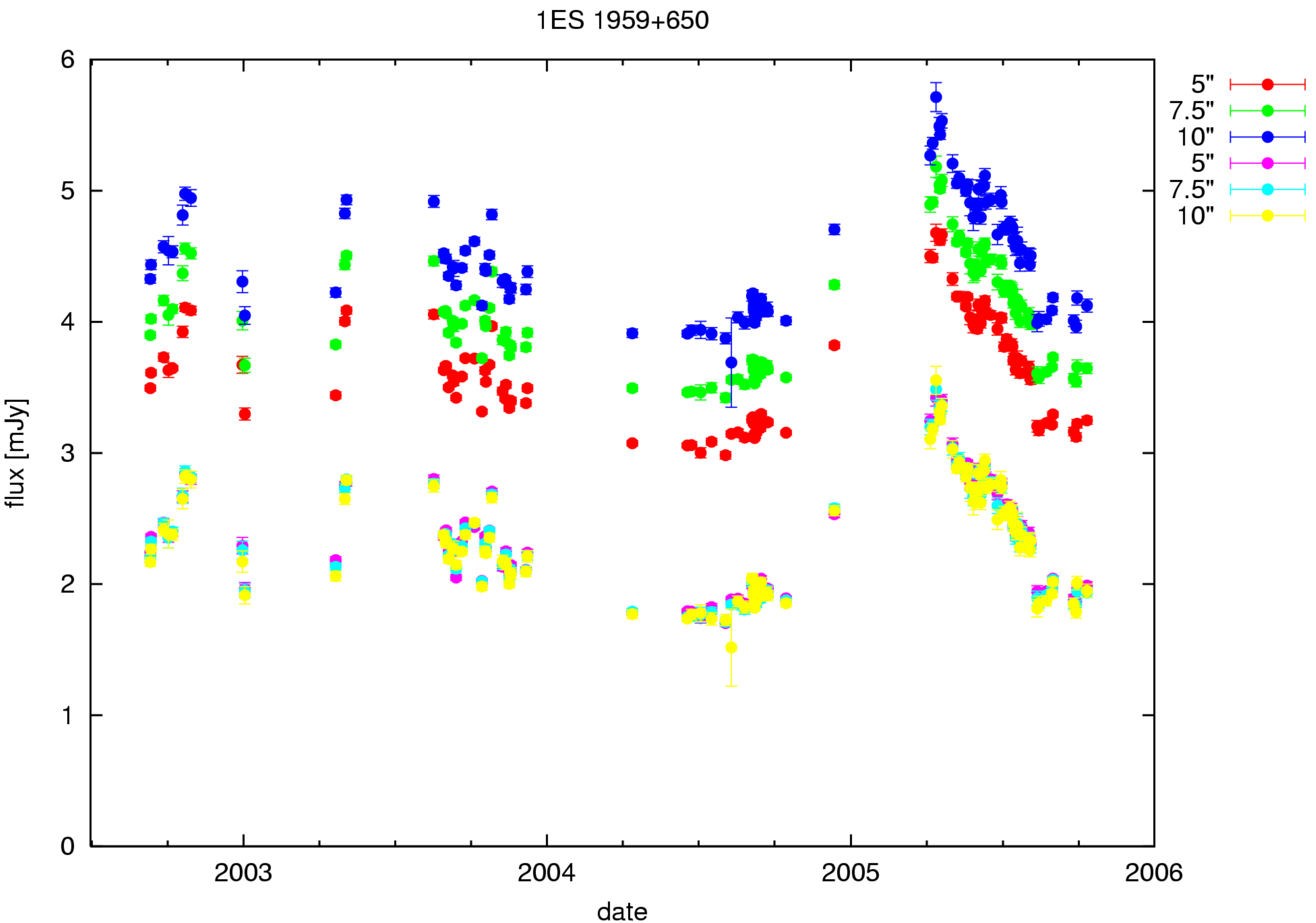

1ES 1959+650
flux [mJy]
date
0
1
2
3
4
5
6
2003
2004
2005
2006
5"
7.5"
10"
5"
7.5"
10"

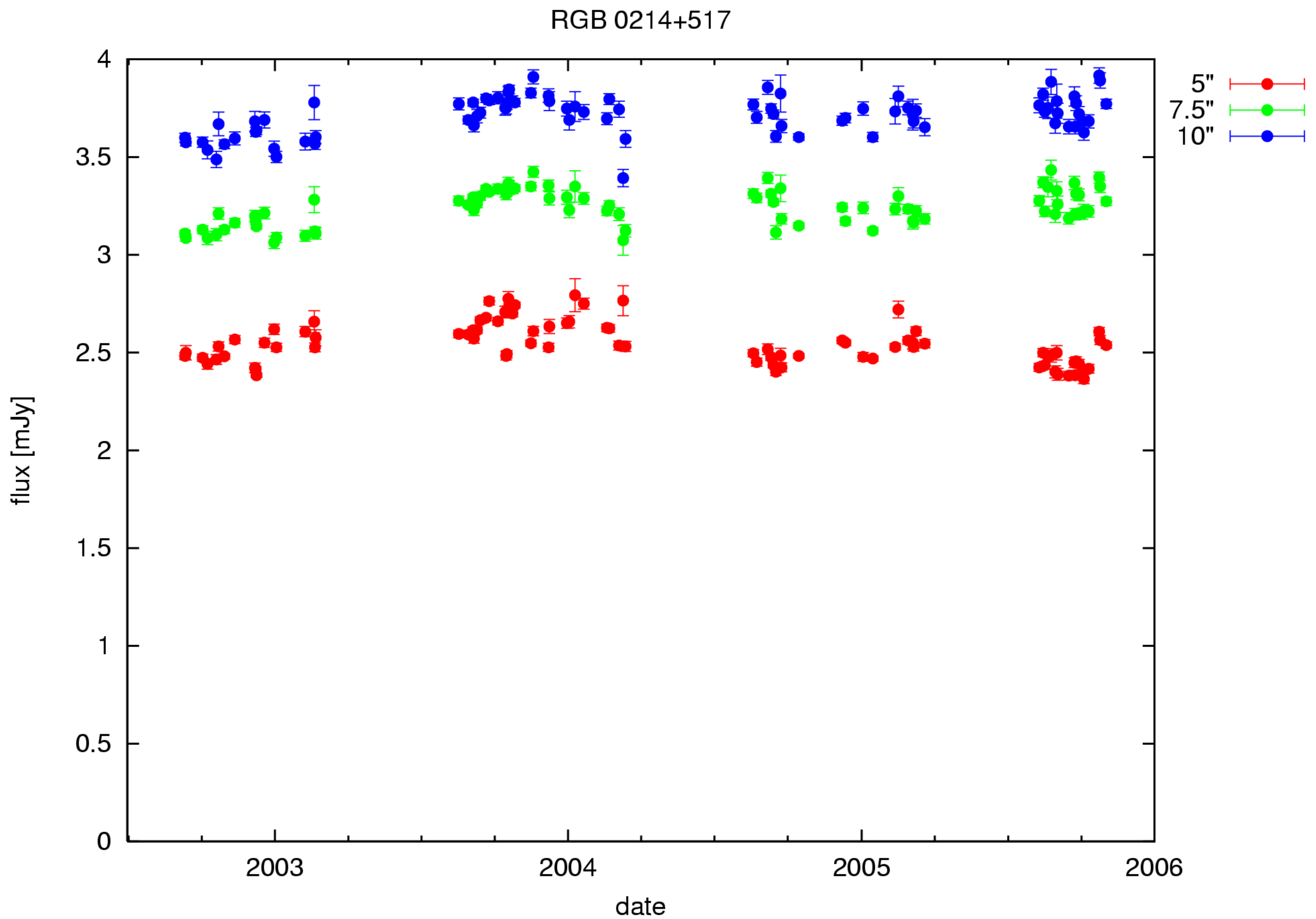
RGB 0214+517
flux [mJy]
date
0
0.5
1
1.5
2
2.5
3
3.5
4
2003
2004
2005
2006
5"
7.5"
10"

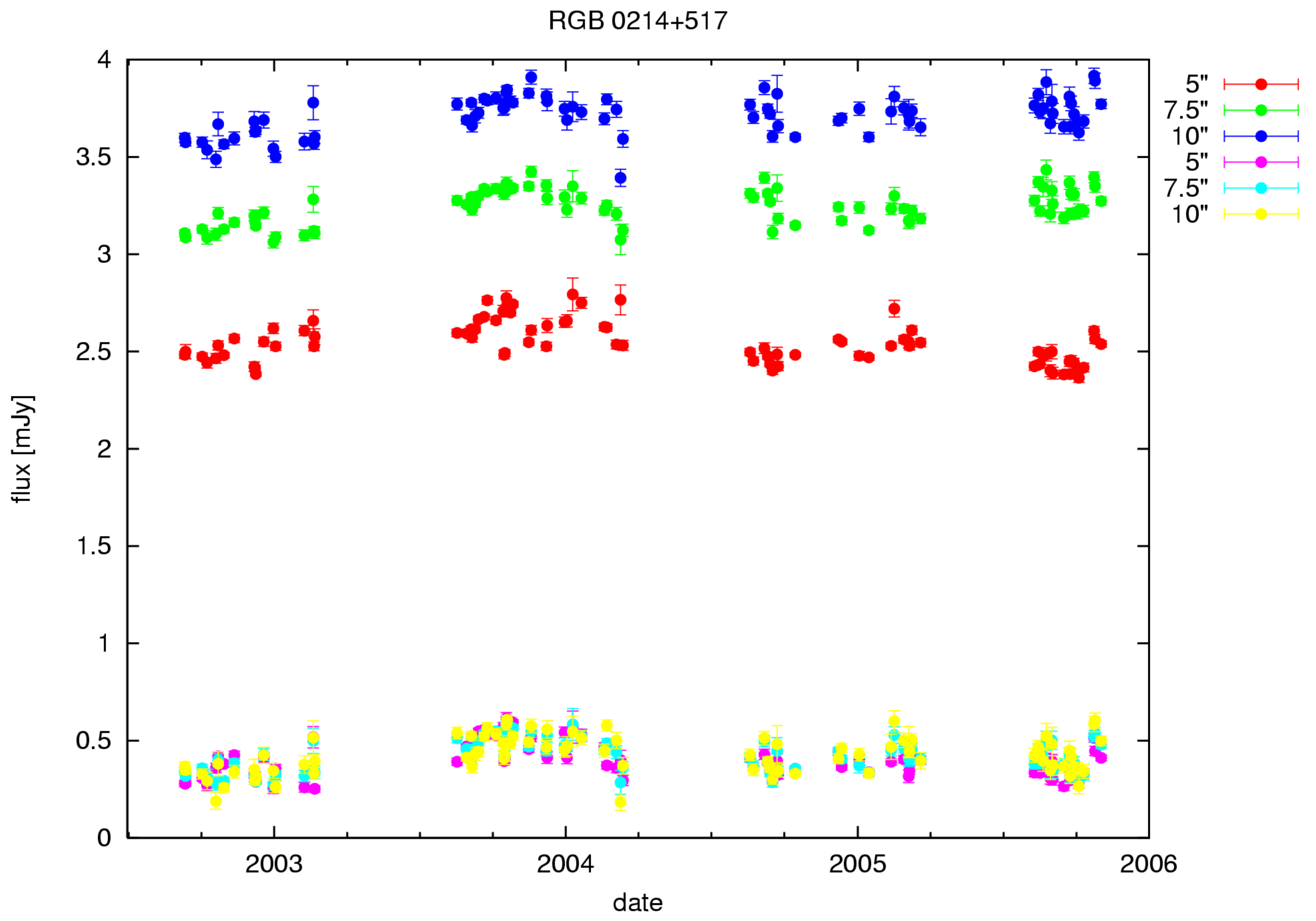

RGB 0214+517
flux [mJy]
date
0
0.5
1
1.5
2
2.5
3
3.5
4
2003
2004
2005
2006
5"
7.5"
10"
5"
7.5"
10"

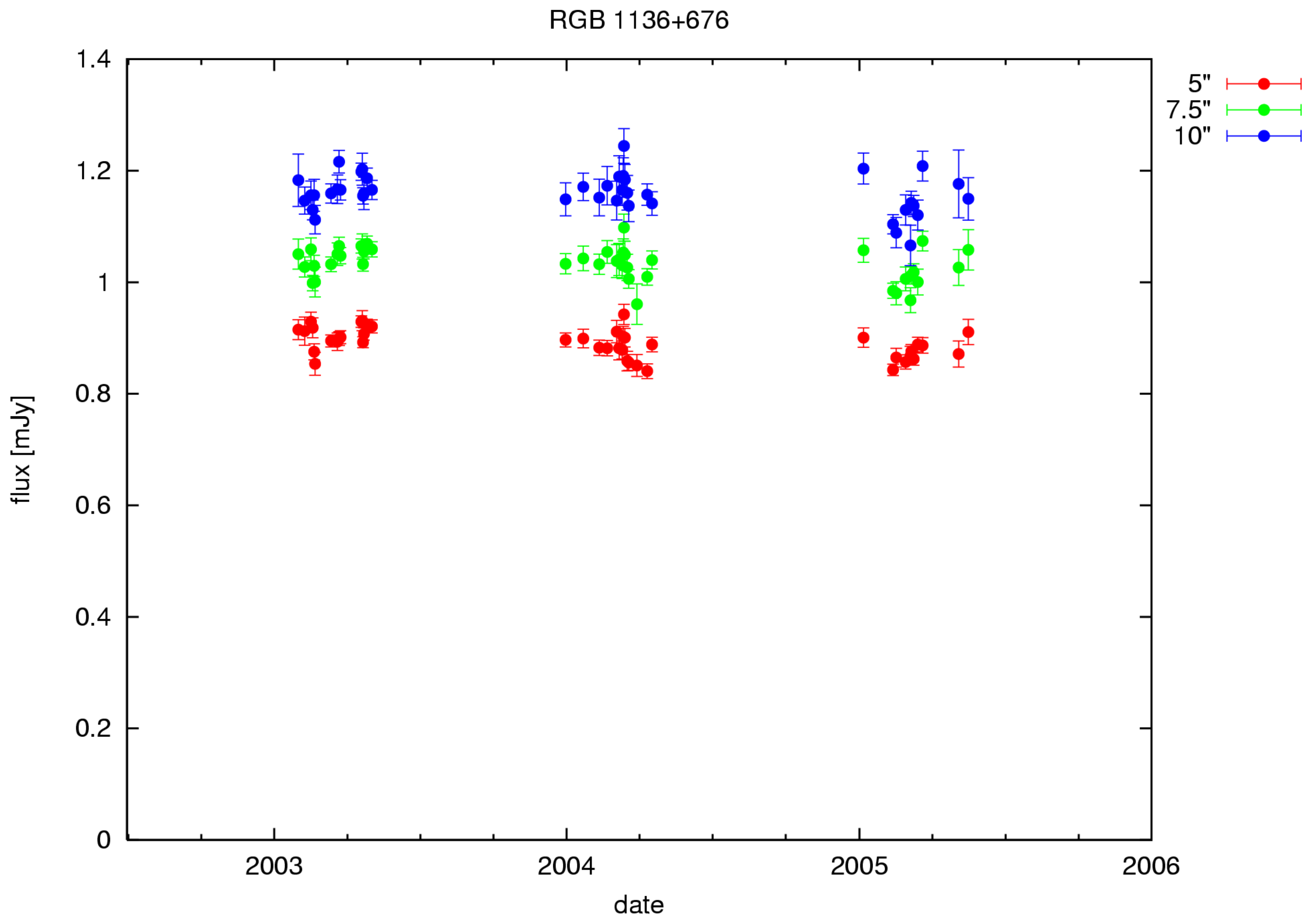
RGB 1136+676
flux [mJy]
date
5"
7.5"
10"
0
0.2
0.4
0.6
0.8
1
1.2
1.4
2003
2004
2005
2006

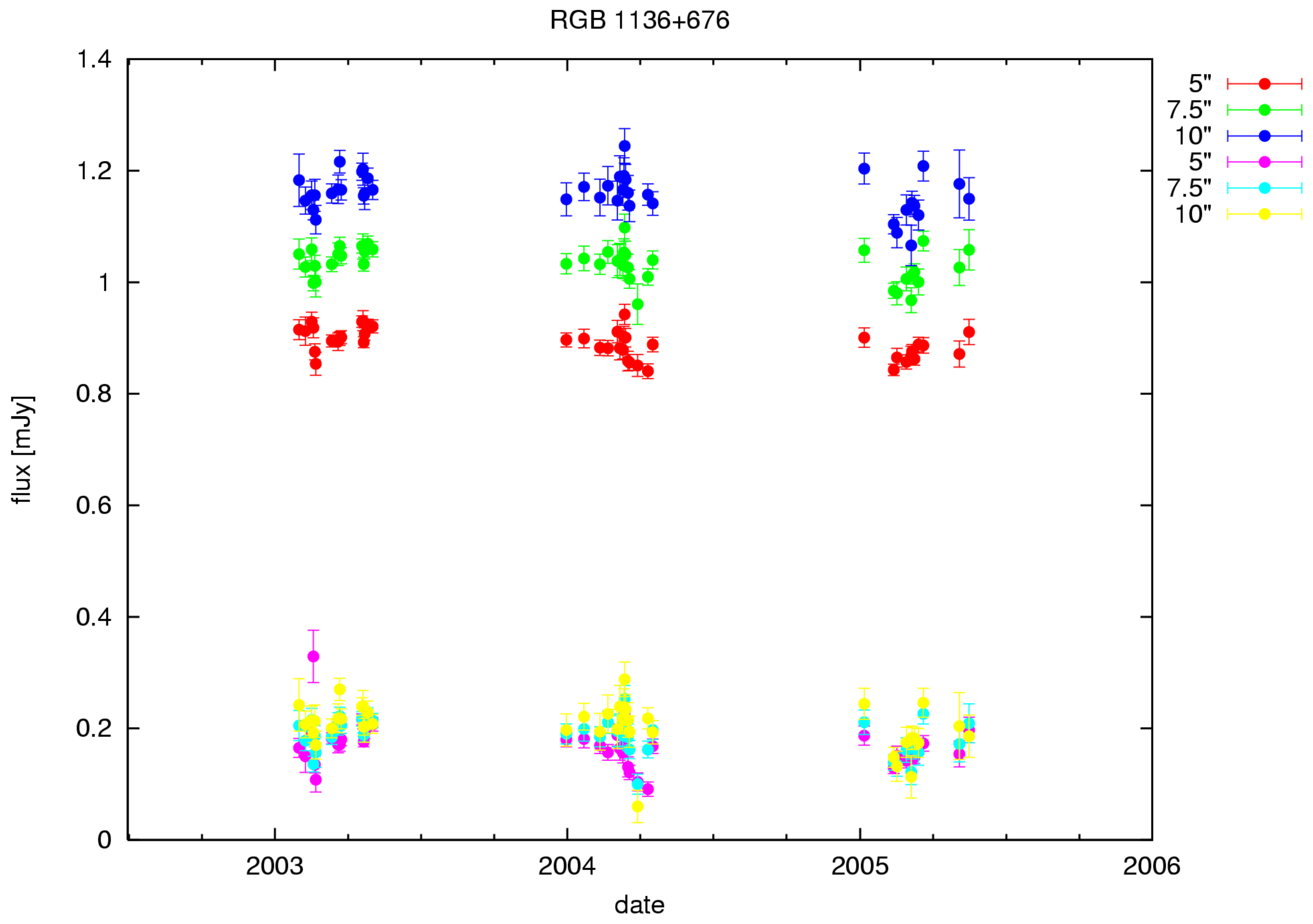

RGB 1136+676
flux [mJy]
date
0
0.2
0.4
0.6
0.8
1
1.2
1.4
2003
2004
2005
2006
5"
7.5"
10"
5"
7.5"
10"

Accuracy of the method

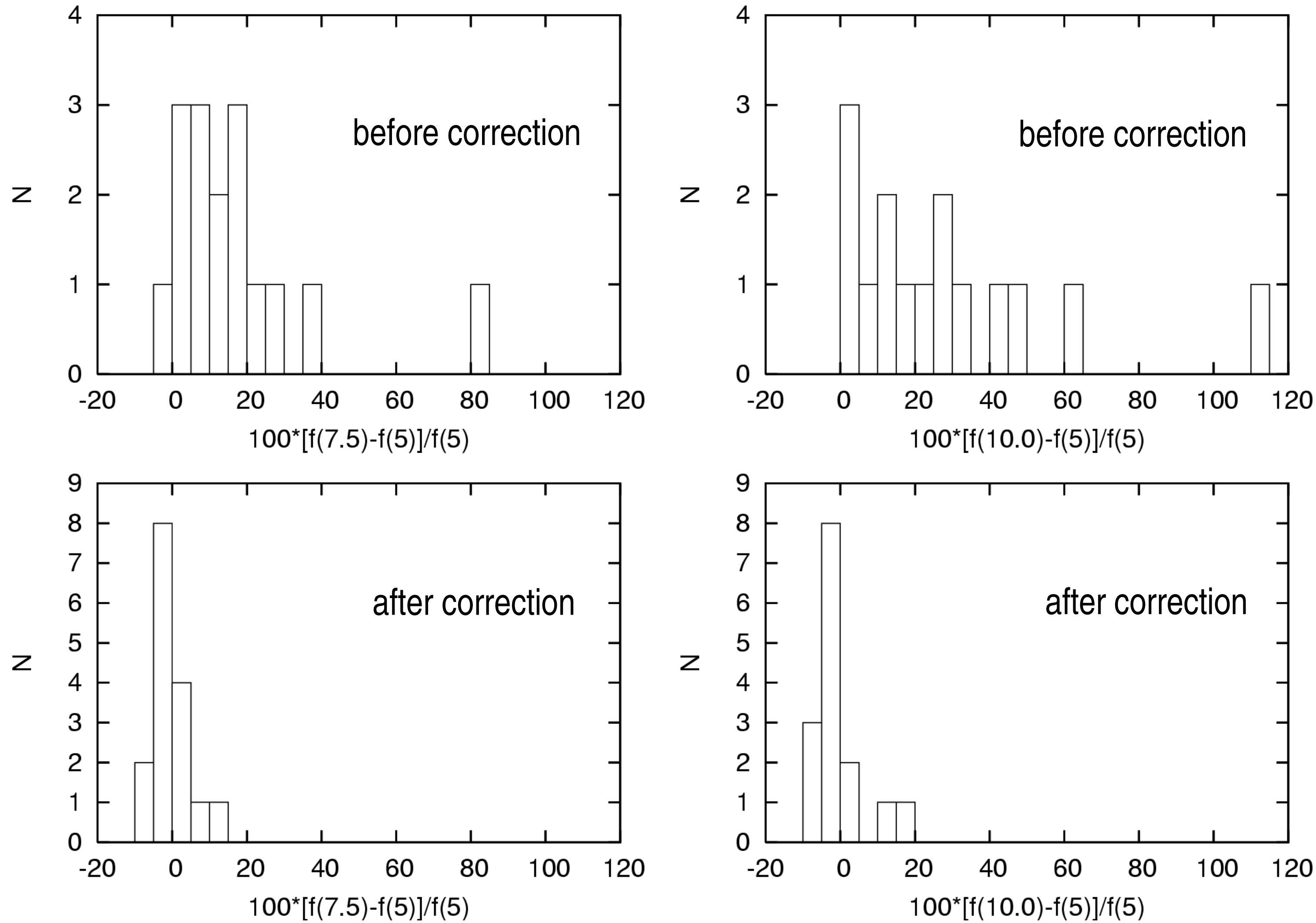

Summary

- The problem of host galaxy subtraction has been investigated using two-dimensional modeling of 16 BL Lacs and their nearby environment.
- Varying aperture size has a major effect to the measured magnitude, whereas the effect of the seeing is, with a few exceptions, fairly small.
- Measurements made with different aperture sizes can be corrected to the same base level (= pure nuclear flux) with an accuracy of 5-7% (but depends on the relative strength of the nucleus).

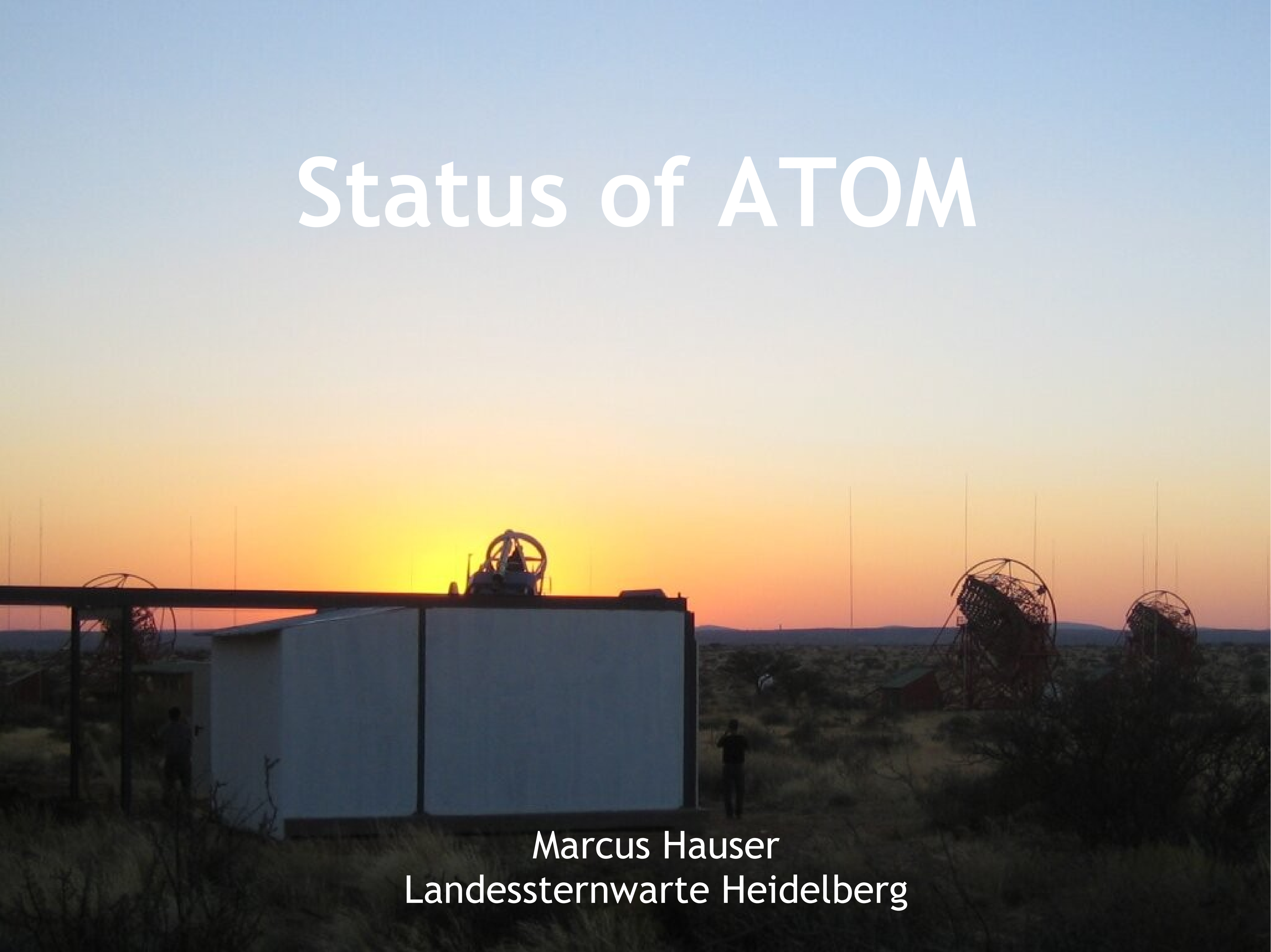

Status of ATOM

Marcus Hauser
Landessternwarte Heidelberg

ATOM

Automatic Telescope for Optical Monitoring

- an automatic optical monitor of variable gamma-ray sources
- an automatic optical monitor of potential H.E.S.S. targets
- a transmission monitor $\rightarrow$ provide extinction measurements for the H.E.S.S data analysis

ATOM fact sheet

Optics

- Ritchey-Chrétien optical system with 75 cm main mirror
- f/8
- image scale ~30 µm/arcsec

Dimensions

- 5m height, 2.2m width
- weight of 4300kg

History

- built by Zeiss as prototype of azimuthal telescope mounting in late 70s
- used at LSW for about 20 years

timeline overview

• April 2004	telescope moved to Hamburg observatory for electronics upgrade
• Jan – April 2005	tests at Hamburg observatory
• June 2005	ATOM shipped to Namibia
• July/August 2005	assembly at H.E.S.S. site
• August, 1st	“first-light” with CCD camera
• 1-8 August 05	pointing and tracking tests
• November 05	integration of new guiding camera, system tests, first observations
• April 06	delivery of main camera to HD, but sent back to manufacturer after some tests - characteristics were worse than specified.

Location

23°16'18" S
16°30'00" E
1800 m asl

Location

23°16'18" S
16°30'00" E
1800 m asl

ATOM enclosure

- 2 movable parts
- mirror cell at same level than rails
- no shadowing for elevation > 14º
- large open part minimizes cooling time


Assembly
22.7.2005

base frame
(m = 1200kg)

turning platform
(m = 1800kg)

telescope tube
(m = 1200kg)

Pointing

- using pointing model of ideal AltAz telescope (misaligned telescope main axes, encoder offset, bending of tube).

  Non-straight axle or bad bearings are not included.

- fitting result:

	normal mode	reverse mode
#grid points	110	61
averag. correction [arcmin]		
Azimuth	0.16	0.2
Elevation	0.07	0.1

Note: FOV of test camera was 5x3 arcmin,

final camera has a FOV of 8x8 arcmin!

tracking accuracy: [actual - nominal] encoder values on main axes

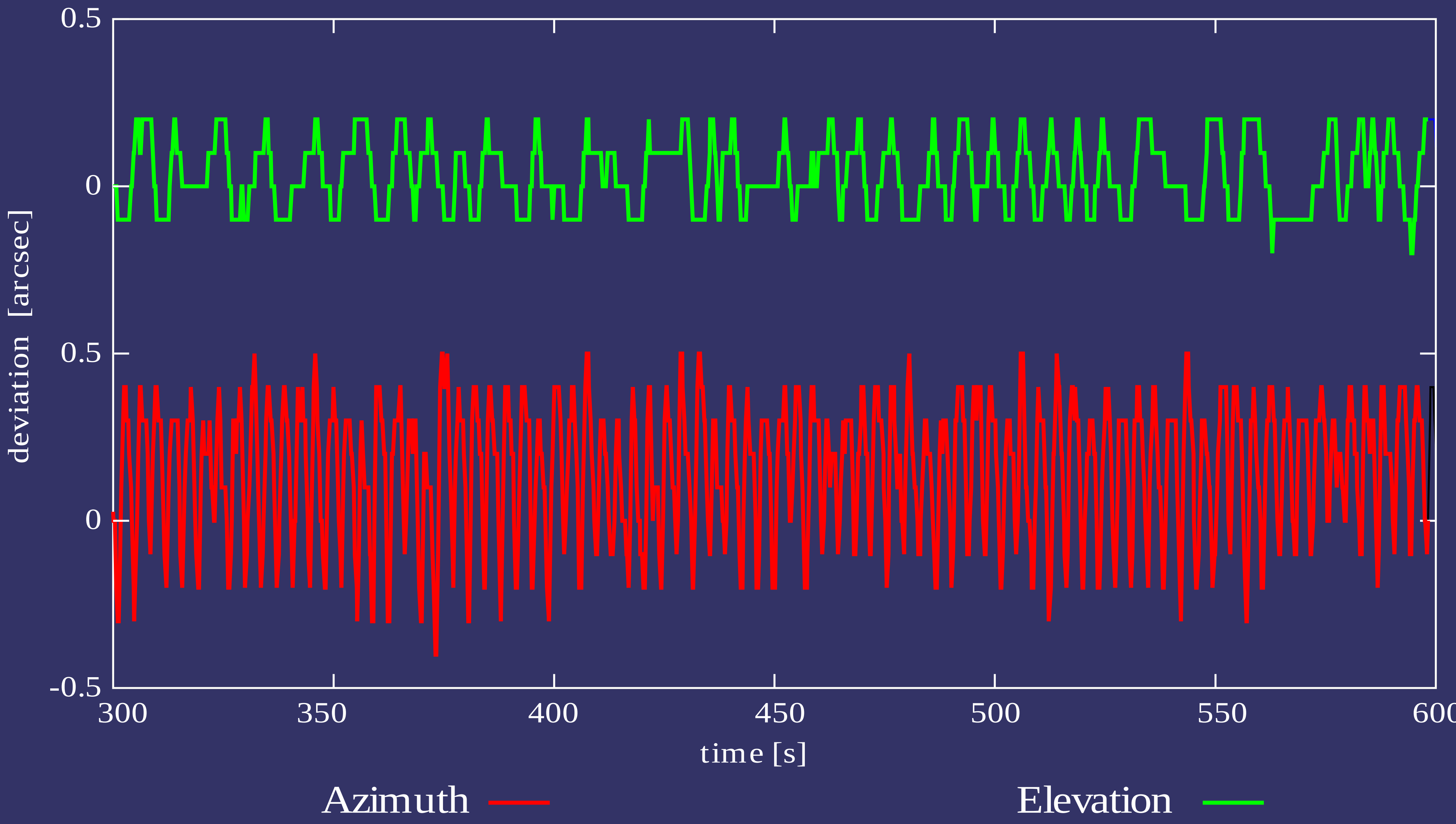

→ motors, gears, encoders and control software are working very well together!

Telescope Control System

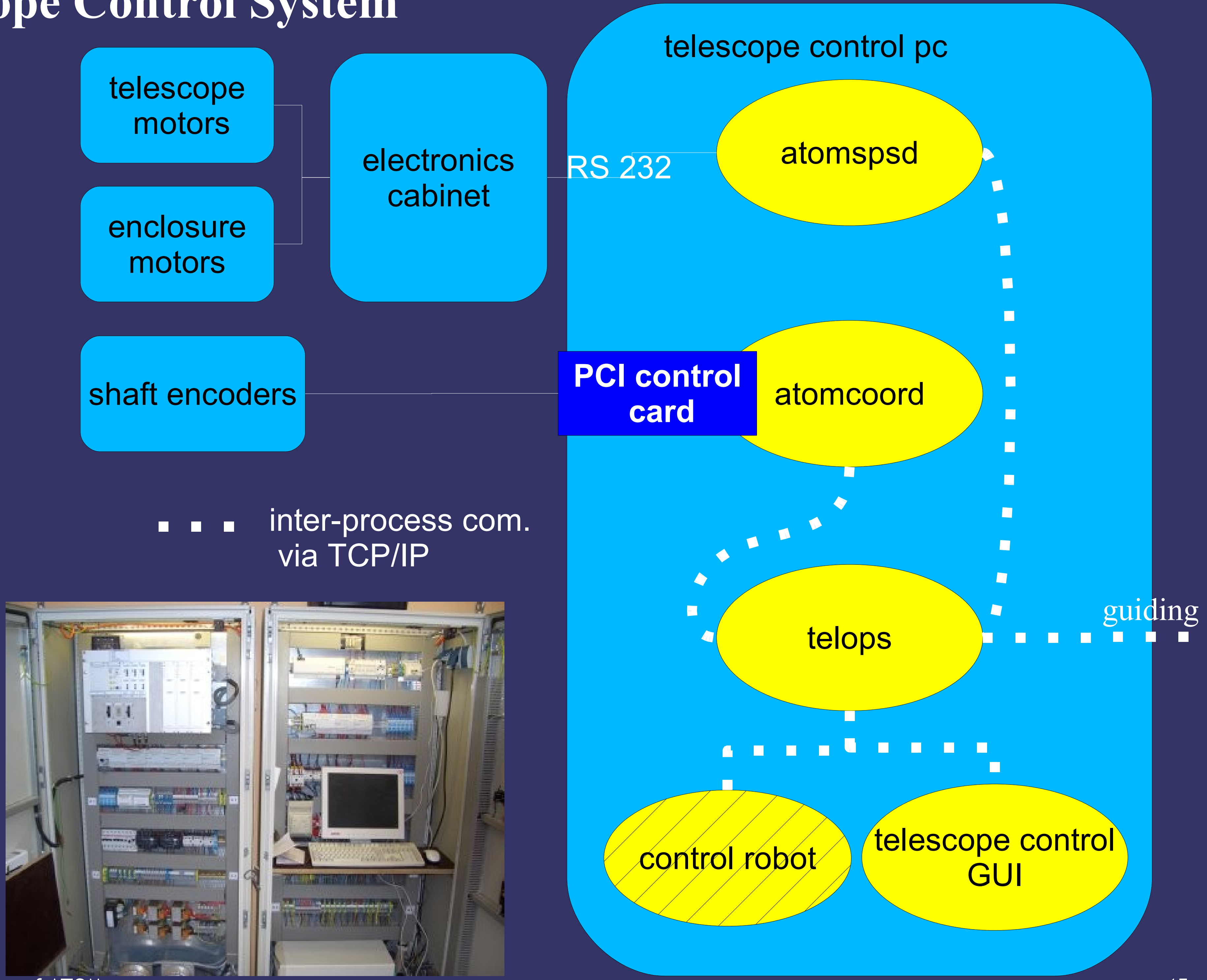

Instrument control system

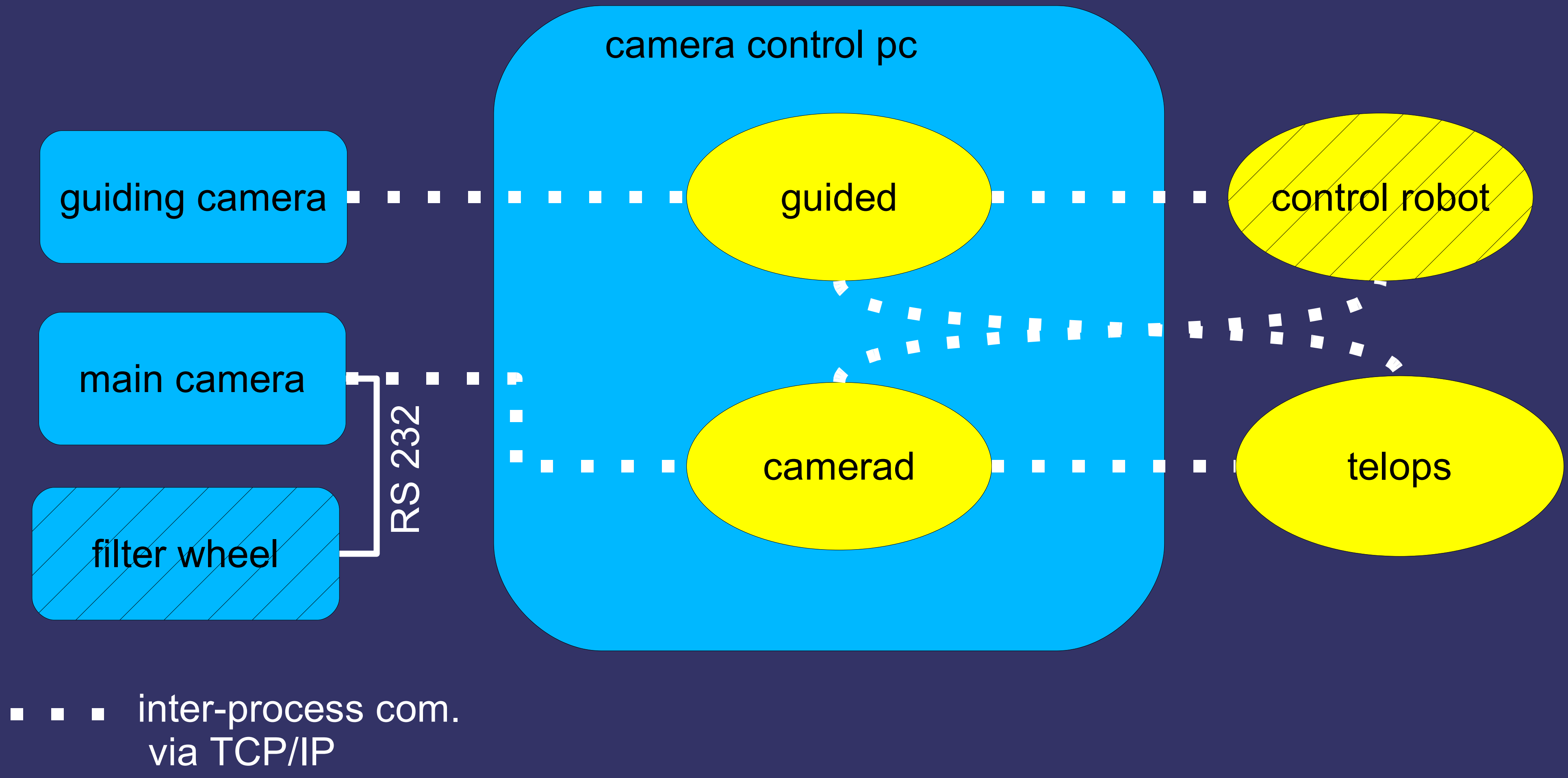

Data reduction pipeline

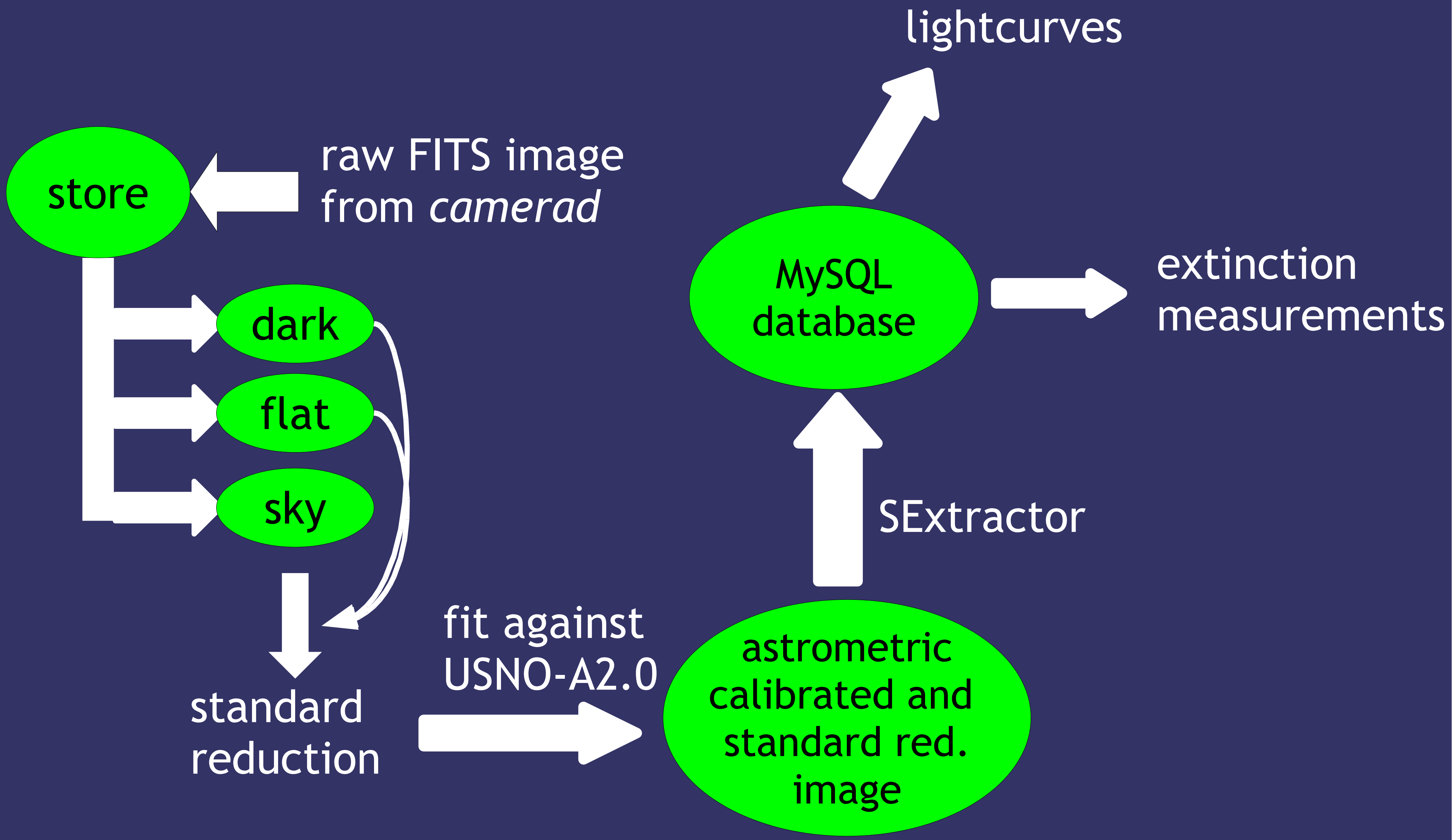

Quality of astrometric fit

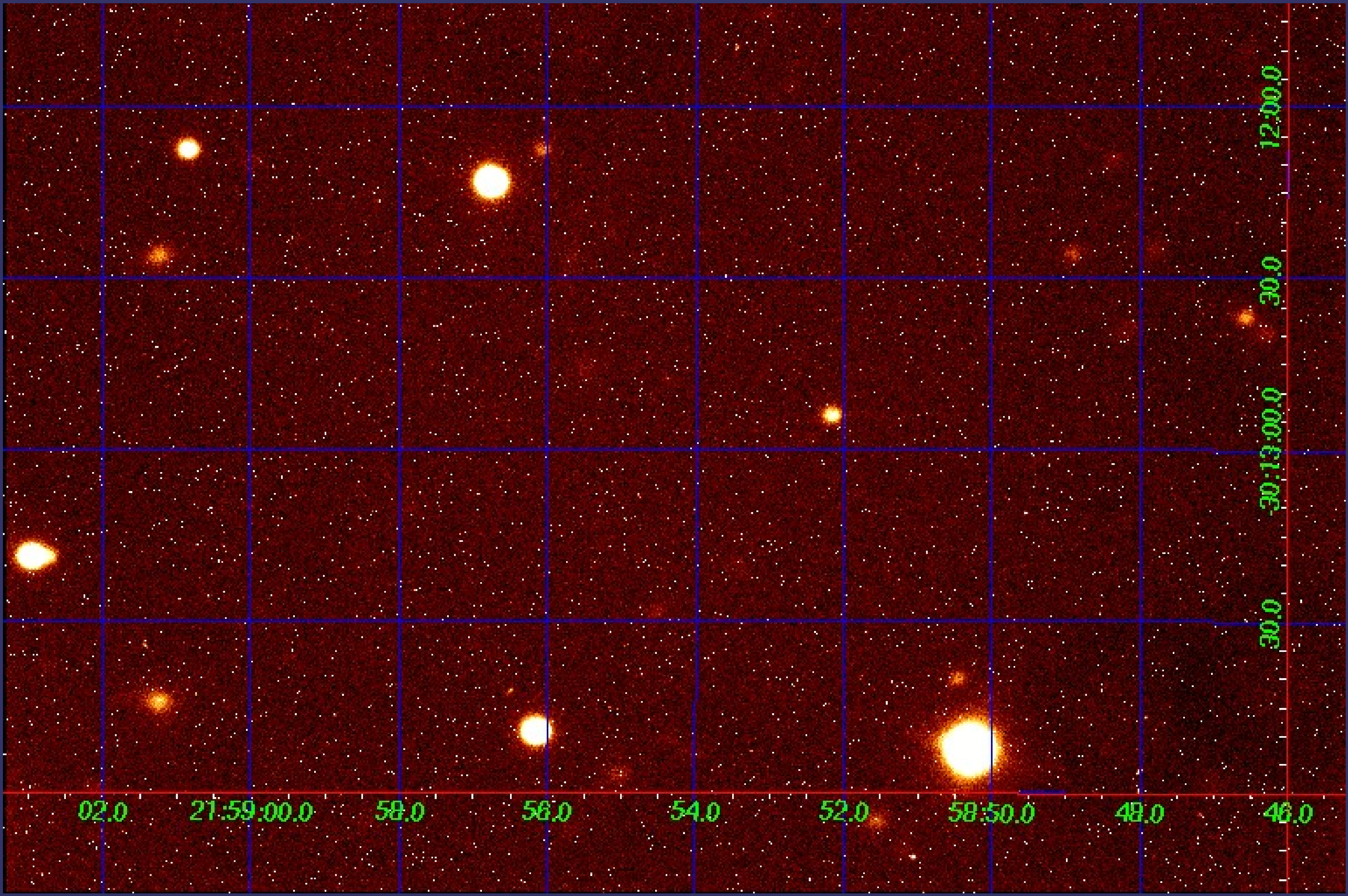

Quality of astrometric fit

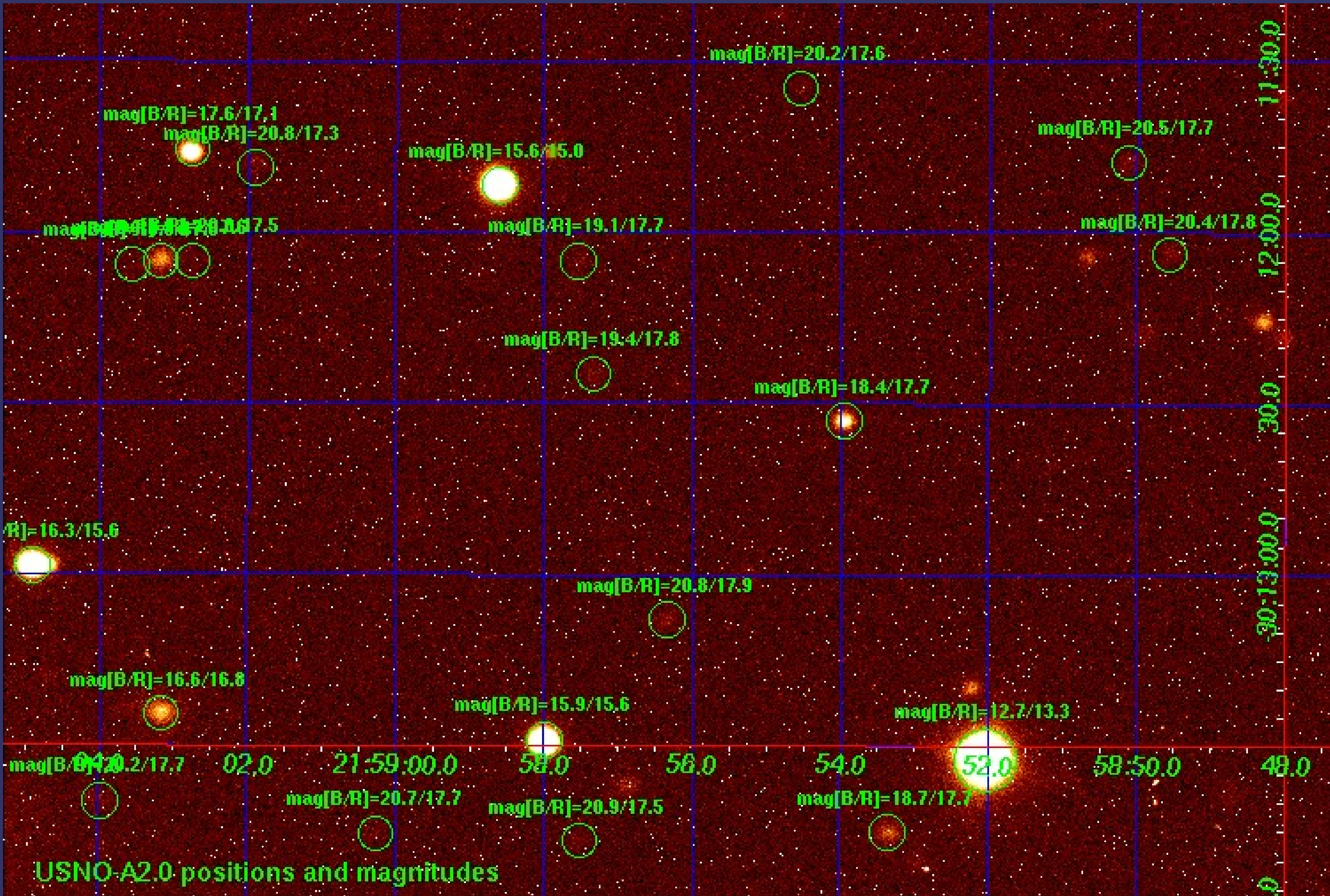

data handling

- expected data rate: 250 MB / night uncompressed
- no good network connection to telescope site (64 kbit/sec)
  => impossible to transfer image data via internet, only results can be sent.
- either include data into H.E.S.S. data transfer via tape
  or ship 1..2 DVDs once per month

for more information see **http://atom.uni-hd.de**